

This is a preprint submitted to EarthArXiv. It corresponds to the resubmitted manuscript following the first round of peer-review.

---

This manuscript has been submitted for publication in REMOTE SENSING OF ENVIRONMENT. Please note the manuscript has yet to be formally accepted for publication. Subsequent versions of this manuscript may have slightly different content. If accepted, the final version of this manuscript will be available via the 'Peer-reviewed Publication DOI' link on the right-hand side of this webpage. Please feel free to contact any of the authors; we welcome feedback.

---

1   **Testing the accuracy and transferability of remotely sensed biomass models across**  
2   **heterogeneous grasslands**

3

4   Jan Schweizer<sup>1,2\*</sup>, Leon T. Hauser<sup>1,2</sup>, Hamed Gholizadeh<sup>3</sup>, Anna K. Schweiger<sup>4</sup>, Christian  
5   Rossi<sup>1,2,3</sup>

6

7   <sup>1</sup>Department of Geoinformation, Swiss National Park, Runatsch 124, 7530 Zernez, CH

8   <sup>2</sup>Department of Geography, University of Zurich, Winterthurerstrasse 190, 8057 Zurich, CH

9   <sup>3</sup>Department of Geography, Oklahoma State University, 318 Social Sciences & Humanities,  
10   74078 Stillwater, OK, USA

11   <sup>4</sup>Department of Land Resources & Environmental Sciences, Montana State University, 334  
12   Leon Johnson Hall, 59717 Bozeman, MT, USA

13   \*Author to whom correspondence should be addressed

14

15   **Keywords**

16   Model comparison, Empirical models, Physically-based models, Hybrid retrieval, Active  
17   Learning, Sentinel-2, LUT inversion, PROSAIL, Gaussian process regression

18    **Abstract**

19    Grassland aboveground biomass provides key insights into ecological processes such as carbon  
20    sequestration, animal movement patterns, and agricultural management practices. Different  
21    model types have been developed to estimate grassland biomass from satellite imagery.  
22    However, differences in model performance across sites with different management regimes  
23    remain largely understudied. In this study, we compared accuracy and transferability of  
24    empirical, physically-based, and hybrid models to estimate grassland biomass from  
25    multispectral Sentinel-2 data. Based on field data from five study sites in Europe and the United  
26    States, we assessed (1) the accuracy of biomass estimation models per site, (2) model  
27    transferability between sites, (3) the performance of models trained or optimized with data from  
28    multiple study sites, and (4) the relationship between epistemic uncertainty and model  
29    transferability. Our results showed that (1) all models exhibited satisfying and comparable  
30    performance at the site level, (2) physically-based models showed the highest degree of  
31    transferability between sites, (3) no model consistently outperformed all other models when  
32    trained or optimized with field data from multiple sites, and (4) epistemic uncertainty was not  
33    necessarily a reliable measure of model applicability to unseen data. Our findings demonstrate  
34    the challenges of developing models applicable across grasslands subject to varying ecological  
35    conditions and management regimes, further highlighting that model transferability should be  
36    considered an integral part of performance assessment when building scalable satellite-based  
37    grassland monitoring systems. As next steps we suggest investigating the degree to which  
38    adding variables such as climate data or multi-sensor approaches would improve model  
39    performance across ecosystems.

40      **1. Introduction**

41      Grasslands cover up to 40% of Earth's terrestrial surface (White et al., 2000) and two-thirds of  
42      the Earth's agricultural land area (O'Mara, 2012). With their extensive land coverage,  
43      grasslands store around a third of the global terrestrial carbon (Bai and Cotrufo, 2022) and host  
44      many endemic species (Hobohm and Bruchmann, 2009). At the same time, grasslands provide  
45      essential ecosystem services (Lemaire et al., 2011; Zhao et al., 2020) including global food  
46      production (Bengtsson et al., 2019; O'Mara, 2012). Given their ecological, cultural, and  
47      economic importance, accurate monitoring of grasslands is imperative to counteract declines in  
48      biodiversity and ecosystem services (Bardgett et al., 2021).

49      Within the overall objective of grassland monitoring, the accurate and reliable estimation of  
50      aboveground biomass (hereafter referred to as biomass) is critical for quantifying numerous  
51      ecological processes and effects of human disturbances. Biomass is an important parameter for  
52      Earth System Models (e.g., Lawrence et al., 2019) and for estimating the contribution of  
53      grasslands to the global carbon cycle (Erb et al., 2018). Grassland biomass is also a key driver  
54      of animal movement and grazing patterns (Bailey et al., 1996; Rempfle et al., 2024; Schweiger  
55      et al., 2015b), and provides information about management practices such as mowing (De  
56      Vroey et al., 2022), whose timing and frequency are linked to biodiversity (Socher et al., 2012;  
57      Van Vooren et al., 2018) and productivity (Zhang et al., 2023).

58      For large-scale grassland biomass estimation, spaceborne remote sensing enables repeated  
59      observations across large spatial domains. Optical sensors measuring surface reflectance, such  
60      as those onboard the European Space Agency's (ESA) Sentinel-2 and the National Aeronautics  
61      and Space Administration's (NASA)/United States Geological Survey's (USGS) Landsat  
62      satellites, are widely used to examine vegetation dynamics of grasslands (Reinermann et al.,  
63      2020). These studies are promoted by open data policies, including the availability of many  
64      years of archived data (Gascon et al., 2017; Masek et al., 2020; Roy et al., 2014). For example,

65 the spectral layout of Sentinel-2 has shown to hold viable information to estimate foliar  
66 properties and canopy structure used to infer biomass (de Sá et al., 2021; Guerini Filho et al.,  
67 2020; Hauser et al., 2021a; Rossi et al., 2020). However, many grasslands are subject to high  
68 levels of spectral complexity arising from several factors, including effects of non-  
69 photosynthetically active vegetation (NPV; Xu et al., 2014), co-occurring plant functional types  
70 (Dixon et al., 2014), and management regimes affecting grassland phenology and species  
71 composition (Ali et al., 2016; Rossi et al., 2024).

72 This complexity led to the emergence of different model types to estimate biomass, including  
73 the use of vegetation indices (VIs), empirical, physical, and hybrid models. Each of these model  
74 types has its specific trade-offs regarding required field data, model complexity, specificity,  
75 and transferability. Vegetation indices (VIs), such as the Normalized Difference Vegetation  
76 Index (NDVI; Guerini Filho et al., 2020; Li et al., 2016; Wang et al., 2019), are found to  
77 correlate to various vegetation properties at both the leaf and canopy level. They are  
78 straightforward to use, but can saturate with high amounts of biomass (Huete et al., 2002; Zeng  
79 et al., 2023). Empirical models are statistical models trained and validated using field data.  
80 Deriving relationships from the training data, they do not rely on prior knowledge about the  
81 relationship between input and output variables, and are generally well-equipped to handle non-  
82 linearity and noise often present in remote sensing data (Verrelst et al., 2015). Numerous  
83 empirical machine and deep learning models such as Random Forest regression (RFR), Support  
84 Vector regression (SVR), Extreme Gradient boosting (XGB), Gaussian process regression  
85 (GPR) and Deep Neural Networks (DNN) have been successfully used to estimate grassland  
86 biomass and vegetation traits from optical Sentinel-2 and Sentinel-1 synthetic aperture radar  
87 (SAR) data (Li et al., 2021; Muro et al., 2022; Raab et al., 2020; Schwieder et al., 2020; Verrelst  
88 et al., 2012). Physically-based Radiative Transfer Models (RTMs) simulate the interactions  
89 between light and matter at leaf- and canopy-scales reducing reliance on field data and

improving transferability by leveraging universal physical principles (He et al., 2019; Wang et al., 2023). RTM inversion can be achieved by using a look-up table (LUT) approach (Verrelst et al., 2014), which connects simulated or measured spectra with trait combinations linked to those spectra. For example, the PROSAIL RTM (Jacquemoud et al., 2009) can be inverted to estimate grassland biomass derived by multiplying leaf dry matter content with leaf area index (LAI; see e.g., He et al. (2019)). However, the PROSAIL RTM is based on certain assumptions, such as uniformly distributed leaf constituents and geometrically homogeneous canopies (Jacquemoud and Baret, 1990; Verhoef et al., 2007), that are never met in reality. Hybrid models combine RTM-simulated canopy spectra with machine learning models for model inversion (Verrelst et al., 2015). Active Learning (AL) is often used in combination with hybrid models to select the most informative training samples (Verrelst et al., 2016) to perform the RTM inversion which is inherently ill-posed (Combal et al., 2003), coming however at the potential cost of model transferability (Berger et al., 2021b; Tagliabue et al., 2022). Hybrid models have been successfully used for estimating vegetation properties in croplands (Berger et al., 2021a, 2020; Ranghetti et al., 2022; Tagliabue et al., 2022; Verrelst et al., 2021; Woher et al., 2022) and forests (Binh et al., 2022; Brown et al., 2019; Hauser et al., 2021a; Yuan et al., 2015). However, the findings from these previous studies cannot be simply extended to grasslands, since grasslands are more chemically and structurally diverse compared to croplands and differ in plant size and canopy characteristics from forests (Habel et al., 2013; Wellstein et al., 2013). Grasslands also tend to violate the assumption of geometrically homogeneous canopies of one-dimensional RTMs (Berger et al., 2018; Rossi et al., 2020), complicating the selection of the most appropriate model for a given application.

In this paper, we aim to compare empirical, physically-based, and hybrid models to estimate biomass across grassland sites with different management regimes, altitude and climate, and determine model performance by assessing their local accuracy, transferability, and epistemic

115 uncertainty (= model uncertainty referring to the confidence of a model about its prediction)  
116 sensu Martínez-Ferrer et al. (2022). Our goals are to develop adequate grassland biomass  
117 estimation models for each site and to identify key considerations for model transferability.

118 **2. Methods**119 **2.1. Study sites and data acquisition**

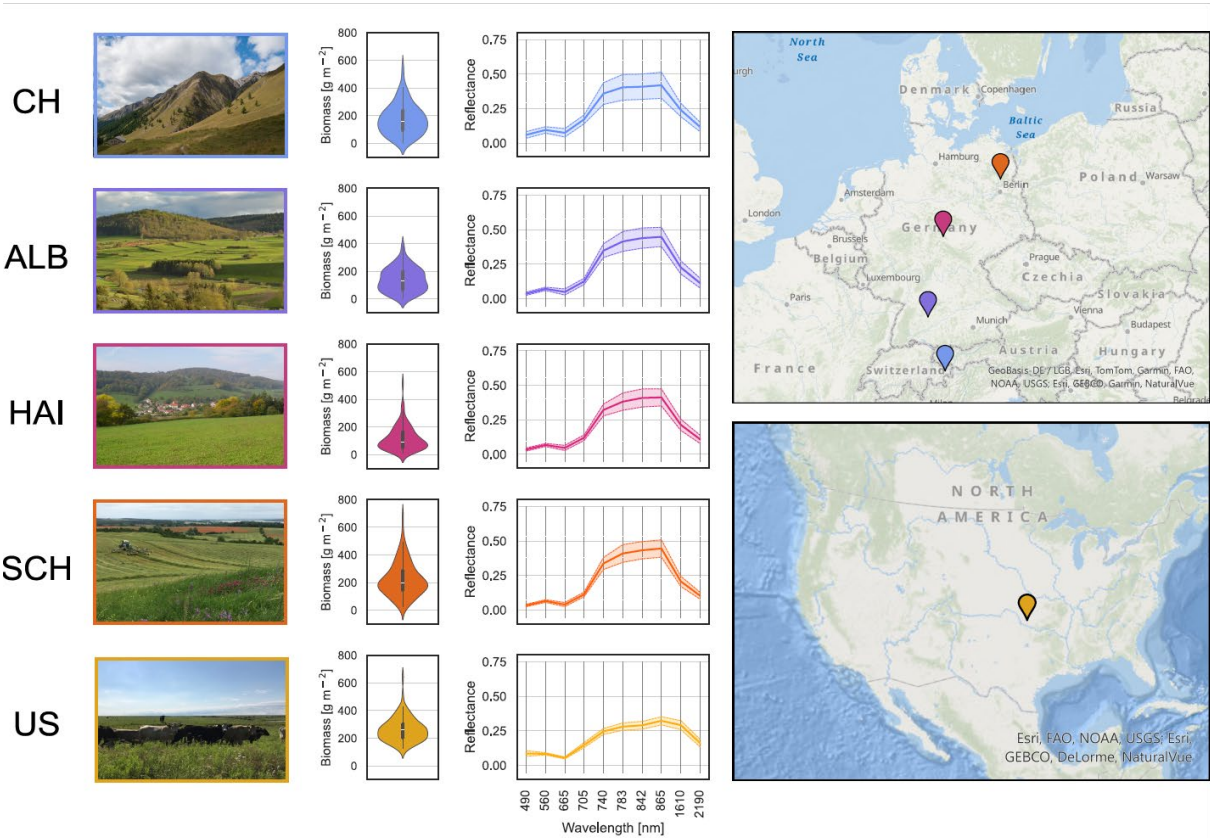
120 We used field and remote sensing data from five study sites: one in Switzerland, three in  
 121 Germany, and one in the United States differing in environmental characteristics, including  
 122 altitude, climate, and management practices (Table 1, Figure 1). These differences make our  
 123 compiled dataset particularly valuable for assessing model transferability. The number of  
 124 samples per study site ranged from 100 to 429, but we based all our models on 100 samples to  
 125 keep them comparable. For sample selection we used Latin hypercube sampling (LHS) as  
 126 implemented in the `clhs` package *v0.9.0* (Roudier, 2021) in R *v4.2.1* (R Core Team, 2021).

127 *Table 1: Overview of the characteristics of the five study sites covering a wide range of topographic and climate, and*  
 128 *management practices. Remote sensing data were acquired with the Airborne Prism Experiment (APEX) and Sentinel-2*  
 129 *between 2010 and 2020. The Köppen-Geiger climate classification is following Beck et al. (2018) for period 1991-2020.*  
 130 *Dominant species are provided for Switzerland by the Swiss National Park's long-term permanent grassland monitoring*  
 131 *project, for Germany by Bolliger et al. (2020), and for the United States by Gholizadeh et al. (2022). m.a.s.l.: meters above sea*  
 132 *level, MAT: mean annual air temperature, MAP: mean annual precipitation.*

Country	Switzerland		Germany			United States
Site code	CH		ALB	HAI	SCH	US
Site	Swiss National Park	Lower Engadine, Val Müstair	Schwäbische Alb	Hainich-Dün	Schorfheide-Chorin	The Nature Conservancy's Tallgrass Prairie Preserve (Pawhuska, OK)
Elevation [m.a.s.l.]	1,400 – 2,500		460 – 860	285 – 550	3 – 140	252 - 365
MAT [°C]	1 (at 2,000 m.a.s.l.)		6 – 7	6.5 – 8	8 – 8.5	17.4
MAP [mm/a]	800		700 – 1,000	500 – 800	500 – 600	960
Köppen-Geiger climate class	Cold, no dry season, cold summer (Dfc)		Cold, no dry season, warm summer (Dfb)	Mostly Cfb, small areas Dfb	Temperate, no dry season, warm summer (Cfb)	Temperate, no dry season, hot summer (Cfa)

<b>Dominant species</b>	<i>Erica carnea, Nardus stricta, Carex sempervirens, Festuca rubra</i>	<i>Alopecurus pratensis,</i> <i>Taraxacum sp.,</i> <i>Festuca rubra</i> aggr., <i>Bromus erectus</i>	<i>Poa pratensis</i> aggr., <i>Taraxacum sp.,</i> <i>Lolium perenne,</i> <i>Alopecurus pratensis</i>	<i>Poa pratensis</i> aggr., <i>Lolium perenne, Poa trivialis, Elymus repens</i>	<i>Schizachyrium scoparium,</i> <i>Andropogon gerardii,</i> <i>Sorghastrum nutans, Panicum virgatum</i>
<b>Management</b>	Strict protection	Grazing, mowing, fertilizing			Grazing, burning
<b>Sensor</b>	Resampled APEX	Sentinel-2			
<b>Years</b>	2010 - 2013	2016 - 2017	2017 - 2020		2022
<b>Number of available samples</b>	407	22	194	185	146
<b>Number of selected samples</b>	78	22	100	100	100

133



134

135 *Figure 1: Overview of the five study sites. Violin plots show dried aboveground biomass for the 100 selected samples per site.*  
136 *Line plots show the mean spectra ( $\pm 1$  standard deviation) per site for Sentinel-2 or resampled APEX data. CH: Switzerland,*  
137 *image credits: Swiss National Park/Hans Lozza. ALB: Schwäbische Alb, image credits: Biodiversity Exploratories Information*  
138 *System (BExIS)/Martin Fellendorf. HAI: Hainich-Dün, image credits: BExIS/Steffen Both. SCH: Schorfheide-Chorin, image*  
139 *credits: BExIS/Ulrike Garbe. US: United States, image credits: Nicholas McMillan.*

#### 140 2.1.1. Switzerland

141 The Swiss study site (site code CH) encompasses the Lower Engadine and the Val Müstair in  
142 the Canton of Grisons in southeast Switzerland. Plots located in the Swiss National Park (SNP),  
143 an IUCN (International Union for the Conservation of Nature) category Ia nature reserve  
144 (highest protection level – strict nature reserve), are unmanaged. Plots in the Lower Engadine  
145 and the Val Müstair adjacent to the SNP are fertilized, mown, and grazed to varying degrees  
146 (Rossi et al., 2020).

147 At the CH site, biomass sampling took place on the day of remote sensing data acquisition  
148 in late June to early July of 2010 – 2013 and 2016 – 2017, respectively. Biomass was clipped

149 approximately 1 cm above the ground in 1 m<sup>2</sup> plots representative for a homogeneous area of 6  
150 × 6 m, and dried at 65° for 48 h for 429 samples (Rossi et al., 2020; Schweiger et al., 2017,  
151 2015b, 2015a). From 2010 to 2013 (before the launch of Sentinel-2), remote sensing data were  
152 acquired with the Airborne Prism Experiment (APEX) imaging spectrometer (Jehle et al., 2010;  
153 Schaepman et al., 2015). APEX data were resampled to 2 m pixel size using nearest neighbor  
154 interpolation and the parametric geocoding procedure PARGE (Schläpfer and Richter, 2002)  
155 and the airborne atmospheric and topographic correction model ATCOR-4 (Richter and  
156 Schläpfer, 2002) were used for geometric and atmospheric correction, respectively (Schweiger  
157 et al., 2015b). APEX data were resampled to Sentinel-2 bands (Appendix A Section A.1) using  
158 the prospectR R package v0.2.6 (Stevens and Ramirez-Lopez, 2022) in R v4.2.1, and can be  
159 considered comparable with Sentinel-2 (Helfenstein et al., 2022). In 2016 and 2017, Sentinel-  
160 2 Level-1C (top of atmosphere) images were downloaded from the Copernicus Open Access  
161 Hub (<https://scihub.copernicus.eu/dhus/>) and processed to Level-2A (surface reflectance) using  
162 Sen2Cor v2.3 (Müller-Wilm et al., 2013) and the SRTM 90 m digital elevation model (Reuter  
163 et al., 2007). The 10 m bands (B2, B3, B4, B8) were aggregated to a spatial resolution of 20 m  
164 using the arithmetic mean and bidirectional reflectance distribution function (BRDF) correction  
165 was applied following Poortinga et al. (2019). No cloud masking was required. For each plot,  
166 the spectral reflectance was sampled in the respective Sentinel-2 image by calculating the  
167 weighted mean on 20 m resolution around the plot center coordinate.

### 168 2.1.2. Germany

169 The three German study sites (site codes ALB, HAI, SCH) are part of the *Biodiversity*  
170 *Exploratories* (<https://www.biodiversity-exploratories.de/en/>). At each site, 50 grassland plots  
171 with different management regimes have been closely monitored since 2009 (Fischer et al.,  
172 2010; Hinderling et al., 2023; Ostrowski et al., 2020). Management intensity varies from

173 extensive to moderately intensive, e.g., from no mowing or fertilization to three mowing events  
174 per year plus fertilization (Blüthgen et al., 2012; Fischer et al., 2010).

175 Biomass was harvested between late April and mid-July from 2017 to 2020 by clipping biomass  
176 approximately 4 cm above the ground on an area of 2 m<sup>2</sup> in plots representative of a  
177 homogeneous area of 50 × 50 m and subsequent drying at 80° for 48 h, resulting in 600 samples  
178 (Hinderling et al., 2023). We linearly scaled the dry biomass content to 1 m<sup>2</sup> for consistency  
179 with the other study sites. Sentinel-2 Level-2A data closest to the day of biomass harvest were  
180 acquired through the Google Earth Engine (GEE, Gorelick et al., 2017) using the “Harmonized  
181 Sentinel-2 MSI: MultiSpectral Instrument, Level-2A” collection. The s2cloudless algorithm  
182 was used to mask out clouds and cloud shadows with the cloud probability threshold set to 10%  
183 (Zupanc, 2017). Again, the 10 m bands were aggregated to 20 m using the function  
184 *reduceResolution* in GEE and BRDF correction was applied. Sampling of the spectral  
185 reflectance for each plot follows the protocol for the CH site. An NDVI threshold was applied  
186 to prevent the inclusion of plots influenced by artifacts such as remaining cloud shadows or  
187 inhomogeneous vegetation cover (Appendix A Section A.2) with 525 samples remaining (Table  
188 1).

189 2.1.3. United States

190 The study site in the United States (site code US) is located near Pawhuska, Oklahoma, and  
191 falls within The Nature Conservancy’s Tallgrass Prairie Reserve (TGPP), encompassing an area  
192 of approximately 160 km<sup>2</sup> mostly covered by tallgrass prairie with some oak woodland  
193 (Hamilton, 2007; The Nature Conservancy, 2023). The TGPP is managed by cattle or bison  
194 grazing, and patch burning (Sherrill, 2019). This creates a “*shifting mosaic*” (Fuhlendorf and  
195 Engle, 2004) of patches with varying grazing pressure, as bison and cattle tend to primarily  
196 graze in recently burned areas with high nutrient availability (Anderson et al., 2006; Fuhlendorf  
197 and Engle, 2001).

198 Biomass sampling was conducted between July and August 2022 across 100 plots of  $30 \times 30$   
199 m, each containing nine  $1 \text{ m}^2$  quadrats (Gholizadeh et al., 2024). Biomass was clipped in 80 of  
200 the 900  $1 \text{ m}^2$  quadrats at approximately 2.54 cm (1 inch) above ground and dried at  $65^\circ$  for 144  
201 h. In the remaining quadrats, biomass was determined using the digital obstruction method  
202 using the 80 samples for calibration (Limb et al., 2007). For each of the 100 plots, biomass was  
203 calculated as the mean biomass across the nine quadrats. Sentinel-2 Level-2A data for each plot  
204 were acquired following the same protocol as for the German study sites.

205 2.2. Model types

206 We assessed the accuracy and transferability of three different model types (i.e., empirical,  
207 physically-based, and hybrid; Figure 2). Field data were partitioned into training (for the  
208 empirical models) or optimization (for the physically-based and hybrid models) and external  
209 testing sets using an 80:20% split using LHS (Figure 2A). We used scikit-learn v1.5.2  
210 (Pedregosa et al., 2012) and xgboost v2.1.2 (Chen and Guestrin, 2016) in Python 3.13 for model  
211 training, optimization, and validation.

212 2.2.1. Empirical models

213 A wide variety of algorithms can be used to train empirical models (Figure 2B). We used  
214 Random Forest regression (RFR), Support Vector regression (SVR), Extreme Gradient  
215 boosting regression (XGB), and Gaussian process regression (GPR) models to represent both  
216 tree-based and kernel-based methods. These algorithms all have been successfully used to  
217 estimate grassland biomass (Li et al., 2021; Muro et al., 2022; Raab et al., 2020; Schwieder et  
218 al., 2020; Verrelst et al., 2015, 2012). RFR uses an ensemble of decision trees, where each tree  
219 is trained on a random subset of samples and features and the final prediction is obtained by  
220 averaging the predictions of all trees (Breiman, 2001). SVR was originally introduced by  
221 Vapnik et al. (1997) and uses support vectors to fit hyperplanes in the data within a specified

222 margin of tolerance. XGB is based on the concept of gradient boosting of regression trees  
 223 introduced by Friedman (2001) and incorporates regularization to mitigate overfitting (Chen  
 224 and Guestrin, 2016). Lastly, GPR uses a prior belief about the latent function describing the  
 225 relationship between input and output variables, and training data to form the posterior  
 226 distribution (Rasmussen and Williams, 2006). The advantages of using GPR include automatic  
 227 hyperparameter optimization during model training and the provision of epistemic uncertainty  
 228 (Verrelst et al., 2013a). To predict a data point, the model returns the mean of the posterior  
 229 distribution as the estimated value and the predictive standard deviation (SD) as a measure of  
 230 epistemic uncertainty.

231 A 5-fold cross-validation (CV) scheme with negative RMSE for scoring was used to identify  
 232 the optimal model parametrization from all possible combinations of parameters listed in Table  
 233 2.

234 *Table 2: Parameter values used for cross-validation of empirical Random Forest regression (RF), Support Vector regression*  
 235 *(SVR), Extreme Gradient Boosting regression (XGB), and Gaussian process regression (GPR) models. Nomenclature of*  
 236 *parameter names for RFR, SVR, and GPR according to Pedregosa et al. (2012), for XGB according to Chen and Guestrin (2016).*

Model	Parameter function	Parameter name	Values
RF	Number of trees	n_estimators	100, 200, 500
	Maximum tree depth	max_depth	None, 5, 10, 15
	Minimum number of samples required to be at a leaf node	min_samples_leaf	1, 2, 5
	Number of features	max_features	'sqrt', 'log2', 10
	Maximum number of leaf nodes	max_leaf_nodes	10, 20, None
SVR	Kernel type	kernel	'rbf', 'linear'
	Kernel coefficient	gamma	'scale', 'auto', 0.01, 0.1, 1
	Regularization parameter	C	0.1, 1, 10, 100
	Epsilon-tube	epsilon	0.01, 0.1, 0.5, 1
XGB	Number of gradient boosted trees	n_estimators	100, 200, 300
	Maximum tree depth	max_depth	3, 5, 7, 9
	Boosting learning rate	learning_rate	0.01, 0.1, 0.2
	Subsample ratio of training instance	subsample	0.8, 1

	Subsample ratio of columns when constructing each tree	subsample_bytree	0.8, 1
	Minimum loss reduction	gamma	0, 0.1, 0.2
GPR	Kernel	kernel	ConstantKernel() * RBF()
	Length scale bounds of RBF kernel	length_scale_bounds	(-100, 100)

237

238        2.2.2. Physically-based model

239        Here we used the PROSAIL RTM (Jacquemoud et al., 2009), which combines the PROSPECT-  
 240        D (Féret et al., 2017) and 4SAIL (Verhoef et al., 2007) RTMs, to simulate grassland canopy  
 241        reflectance (Figure 2C). PROSPECT-D simulates leaf level reflectance by considering leaf  
 242        properties such as chlorophyll content (CHL), leaf mass per area (LMA) and the angle of  
 243        incoming solar radiation (Féret et al., 2008). Subsequently, 4SAIL computes the bidirectional  
 244        reflectance at the canopy level, employing canopy properties such as LAI and sun-target-sensor  
 245        geometry. We used the prosail R package *v1.1.1* (Féret and de Boissieu, 2022) in R *v4.2.1* to  
 246        create a single LUT for all study sites containing 10,000 simulated canopy reflectance spectra  
 247        with input parameters selected by means of LHS within their respective value ranges (Table 3)  
 248        derived from satellite image metadata, prior knowledge, and literature (He et al., 2019; Rossi  
 249        et al., 2020; Verrelst et al., 2021). The value ranges and size of the LUT were consistent with  
 250        other studies (Darvishzadeh et al., 2011; Hauser et al., 2021a; Locherer et al., 2015; Punalekar  
 251        et al., 2018; Rivera et al., 2013; Rossi et al., 2020). We used the psoil parameter as weighting  
 252        factor for the built-in dry and wet soil spectra of the prosail R package with psoil = 0  
 253        corresponding to completely dry soil conditions and psoil = 1 corresponding to completely wet  
 254        soil conditions, respectively. The simulated reflectance spectra were resampled to Sentinel-2  
 255        bands using the prospectR R package and their corresponding biomass content was calculated  
 256        following Quan et al. (2017, Equation 1).

257                   $\text{biomass } [g \text{ m}^{-2}] = \text{LMA } [g \text{ cm}^{-2}] * \text{LAI} * 10,000$                   (1)

Table 3: Value ranges and distributions of PROSAIL input parameters used in this study.

Parameter	Variable	Unit	Minimum value	Maximum value	Distribution
Leaf structure parameter	N	[ $\cdot$ ]	1.5	1.9	uniform
Chlorophyll content	CHL	[ $\mu\text{g cm}^{-2}$ ]	5	75	uniform
Carotenoid content	CAR	[ $\mu\text{g cm}^{-2}$ ]	2	60	uniform
Anthocyanin content	ANT	[ $\mu\text{g cm}^{-2}$ ]	0	2	uniform
Brown pigment content	BROWN	[ $\cdot$ ]	0	1	uniform
Equivalent water thickness	EWT	[cm]	0.001	0.04	uniform
Leaf mass per area	LMA	[ $\text{g cm}^{-2}$ ]	0.002	0.015	uniform
Angle for incident light at leaf surface	alpha	[ $^\circ$ ]	40	40	fixed
Leaf inclination distribution function	TypeLidf	[ $\cdot$ ]	2	2	fixed
Average leaf angle	LIDFa	[ $^\circ$ ]	40	70	uniform
Leaf area index	LAI	[ $\cdot$ ]	0.1	4	uniform
Hot spot parameter	q	[ $\cdot$ ]	0.01	0.1	uniform
Sun zenith angle	tts	[ $^\circ$ ]	25	75	uniform
Observer zenith angle	tto	[ $^\circ$ ]	0	0	fixed
Relative azimuth angle	psi	[ $^\circ$ ]	50	180	uniform
Dry/wet soil factor	psoil	[ $\cdot$ ]	0	1	uniform

260 Two parameters must be determined for the inversion of the generated LUT: the cost function  
 261 and the number of spectra with the lowest cost to consider (hereafter referred to as percentage  
 262 of solutions). We tested 17 commonly used cost functions listed by Rivera et al. (2013) and  
 263 different percentages of solutions, namely 0.01% (= 1 solution), 1%, 2%, 5%, and 10%  
 264 (Punalekar et al., 2018; Rivera et al., 2013; Rossi et al., 2020) to optimize parameter choice.  
 265 The predicted biomass value was calculated as the mean value of the selected solutions, with  
 266 the corresponding SD being indicative of epistemic uncertainty (Locherer et al., 2015; Rivera  
 267 et al., 2013).

268       2.2.3. Hybrid model

269 For the hybrid model, we created a LUT containing 1,000 simulations (Tagliabue et al., 2022;  
 270 Verrelst et al., 2021) as described above. But in this case, the simulated canopy reflectance

271 spectra were used to train a regression algorithm for RTM inversion (Figure 2D). Here we used  
272 a GPR model (see Section 2.2.1 for further details) with the parameters indicated in Table 2 for  
273 the regression task. We used AL to avoid biophysically unrealistic variable combinations and  
274 redundant information, and select the most informative simulations from the LUT (Verrelst et  
275 al., 2016). Using the AL-selected subset of simulations for GPR training can help to mitigate  
276 the ill-posedness inherent to RTM inversion as different variable combinations can lead to  
277 similar spectra (Combal et al., 2003), and increase computational efficiency (Berger et al.,  
278 2021b). AL selects a predefined percentage of simulations from the LUT as an initial training  
279 dataset. Subsequently, the GPR model is trained using this initial training set, and its predictive  
280 training accuracy is assessed via the root-mean-square error (RMSE) computed with the  
281 optimization set. By employing a selection heuristic, such as Euclidean distance-based diversity  
282 (EBD), a simulation from the remaining LUT is selected, temporarily added to the training set,  
283 and only permanently kept if the updated training set leads to an improved RMSE. This  
284 optimization process continues until all simulations are evaluated. Finally, the validation  
285 accuracy of the GPR model trained with the optimal training set is determined.

286 In line with previous studies, we used 2% of the data as initial training data (Tagliabue et al.,  
287 2022; Wocher et al., 2022). Hybrid models without the use of AL did not lead to meaningful  
288 results in the context of this study (Appendix A Section A.3) and were therefore not further  
289 analyzed.

## 290 2.3. Model comparisons

291 We conducted three model comparisons to investigate model accuracy and assess model  
292 transferability (Figure 3). First, models were trained (empirical) or optimized (physically-based  
293 and hybrid) and validated individually for each study site (hereafter referred to as local models,  
294 Figure 3A). This setting corresponds to that of most local to regional scale studies in which  
295 field data of a specific area of interest are available. Second, the local models were applied to

296 the field data of the other study sites to assess their transferability (hereafter referred to as  
297 transferred models, Figure 3B), simulating the case where a model trained or optimized for one  
298 area is applied to another area where no field data are available. Third, models were trained or  
299 optimized with field data from four study sites and validated using the field data of the  
300 remaining site to examine any improvement in transferability (hereafter referred to as global  
301 models, Figure 3C). This mimics the case in which a diverse set of field data are available, for  
302 example from a compiled database, and used to make predictions for an area not covered by the  
303 database. In addition, we compared epistemic uncertainties with model accuracies for all model  
304 comparisons where available – namely empirical GPR, physically-based, and hybrid models.

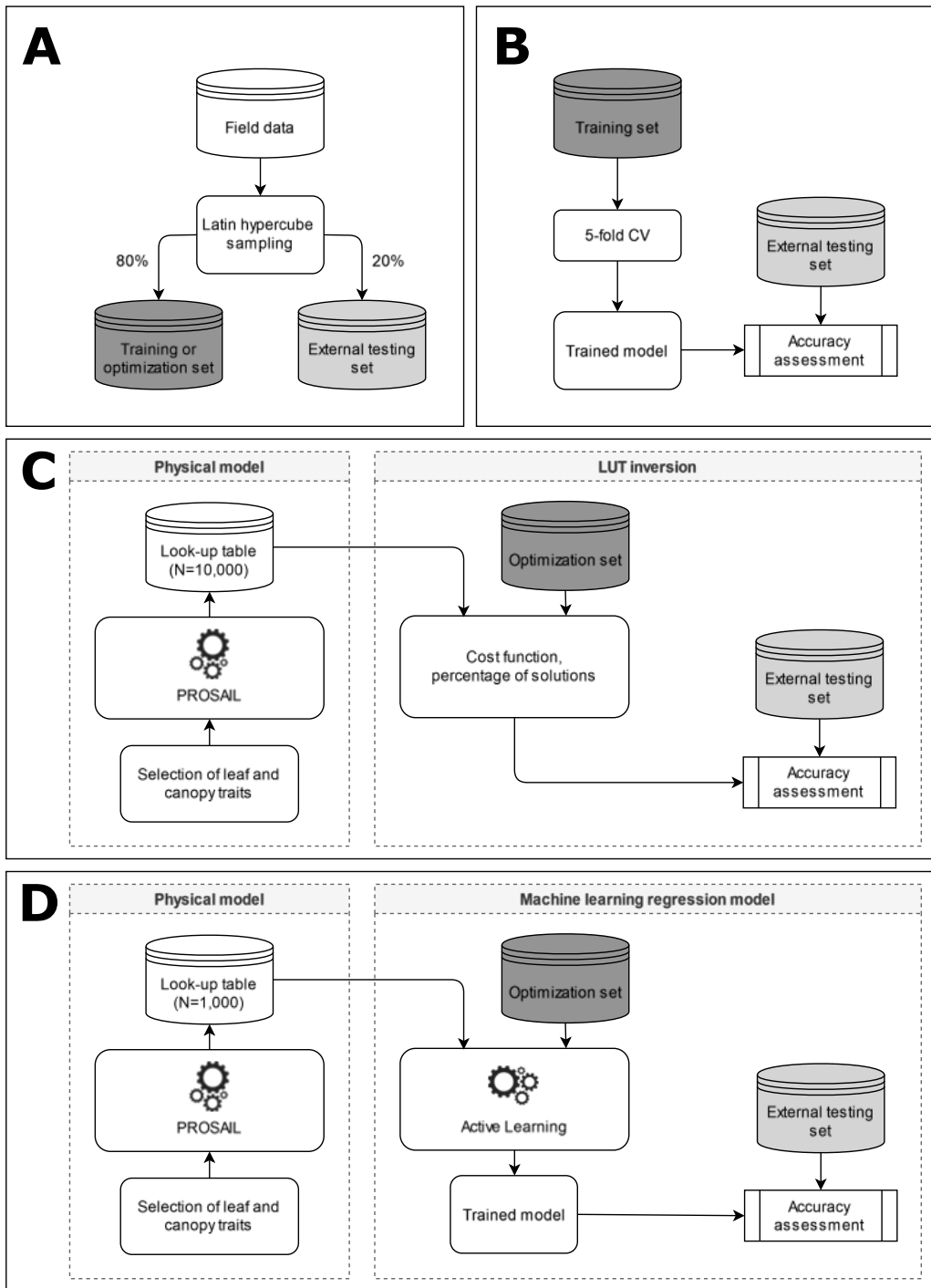
305 Model performance was assessed by coefficient of determination ( $R^2$ ), relative root-mean-  
306 square errors (RRMSE) calculated as the RMSE divided by the mean value of the external  
307 testing set (Richter et al., 2012), and mean bias error (MBE) using the external testing set. In  
308 all cases, we used the ten Sentinel-2 bands in the visible and near-infrared (B2 – B8A) and the  
309 short-wave infrared regions (B11 – B12) as predictor variables with reflectance values being  
310 standardized for empirical and hybrid models and normalized, i.e., treating the spectra as  
311 probability distributions summing up to 1, for physically-based models (Rivera et al., 2013),  
312 respectively.

313 We note that due to comparatively small sample size, partitioning of the data into training or  
314 calibration and external testing set was repeated 10 times for the local and transferred models  
315 to account for stochastic effects (Muro et al., 2022). Correspondingly, local and transferred  
316 model performance of all model types were assessed by calculating both mean and SD for  $R^2$ ,  
317 RRMSE, and MBE.

318 For the empirical models, the best-performing method was selected to be presented in the results  
319 as the focus lied on the comparison of model types and not different empirical models.

320 Comprehensive cross-validation and testing performances for all models including additional  
321 performance metrics are enclosed in Appendix A Sections A.4 to A.16.

322 Lastly, the epistemic uncertainty of the local, transferred, and global models was compared to  
323 the absolute difference between measured and predicted biomass of the external testing set to  
324 test if epistemic uncertainty could potentially be used as an indicator of model transferability  
325 for heterogeneous grasslands. Further information about said relation for all models, including  
326 the individual repetitions of local and transferred models, is included in Appendix A Section  
327 A.17. We tested the relationship between absolute difference and epistemic uncertainty since it  
328 has been demonstrated that epistemic uncertainty of GPR models can serve as a *quality*  
329 *indicator* to identify reliable and unreliable predictions of transferred models for croplands,  
330 even when applied across spatial scales (Verrelst et al., 2013b, 2013a, 2012).

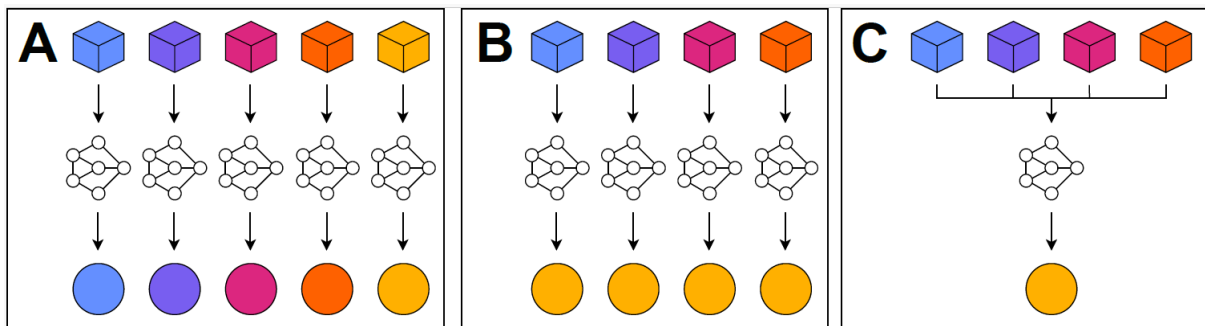


331

332 *Figure 2: Functioning of the models used in this study. A: As a prerequisite for all models, the field data need to be split into*  
 333 *training (in the case of empirical models) or optimization set (in case of physically-based and hybrid models; colored in dark*  
 334 *grey) and external testing set (colored in light grey) using Latin hypercube sampling. B: Empirical models are data-driven and*  
 335 *learn data-specific relationships between predictor variables. The 5-fold cross-validation (CV) was performed with each*  
 336 *possible combination of parameters listed in Table 2. C: Physically-based models use a radiative transfer model (RTM) such as*  
 337 *PROSAIL to simulate canopy reflectance spectra and a cost function is used to find a predefined number of best matches*  
 338 *between each field data point and the simulated spectra, a process commonly referred to as look-up table (LUT) inversion. D:*

339 Hybrid models are trained with a set of RTM-simulated spectra, which are optionally optimized using Active Learning.

340 Subsequently, a machine learning regression model is used to perform the LUT inversion.



341

342 Figure 3: The three model comparisons conducted in this study. Cubes represent data used for training (of empirical models)  
343 or optimization (of physically-based and hybrid models). Circles represent data used for model validation. Colors represent  
344 data from different study sites. A: Local models with training/optimization and validation data from the same study site. B:  
345 Transferred models with training/optimization and validation data from different study site (only one of five cases shown). C:  
346 Global models with training/optimization data from four sites and validation data from the remaining site (only one of five  
347 cases shown).

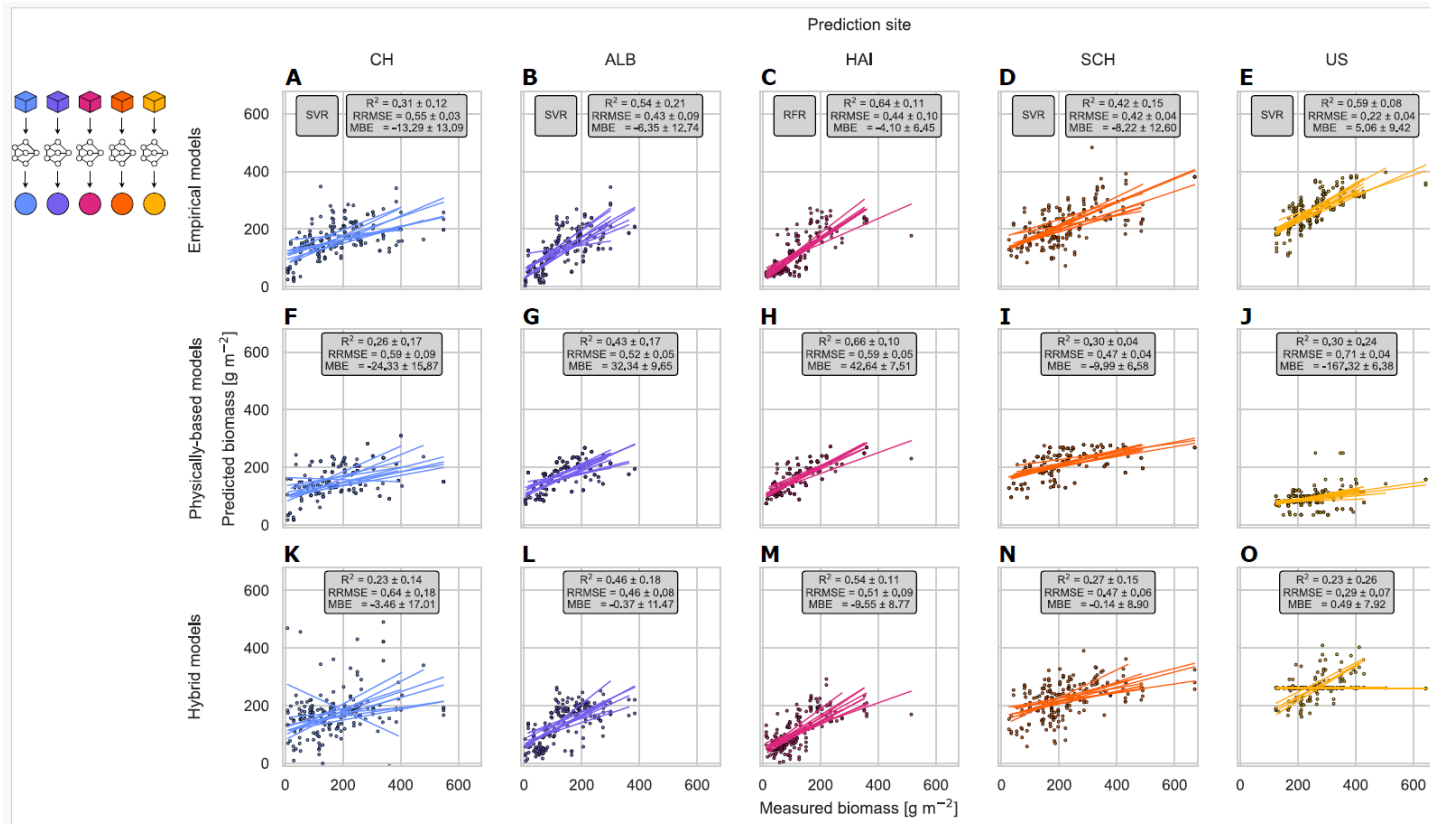
348       **3. Results**

349        3.1. Local models

350       The accuracy of all models varied with the study sites (Figure 4). For empirical models (Figure  
351       4A-E), mean  $R^2$  ranged from 0.31 to 0.64 (CH and HAI, respectively) and mean RRMSE from  
352       0.22 to 0.55 (US and CH, respectively). Mean MBE indicated a systematic underestimation for  
353       all sites between -4.1 and -13.29 g/m<sup>2</sup> (HAI and CH, respectively) except for the US, for which  
354       a mean overestimation of 5.06 g/m<sup>2</sup> was observed. SVR outperformed the other empirical  
355       models for most sites, only the HAI site was best predicted by RFR.

356       For physically-based models (Figure 4F-J), mean  $R^2$  ranged from 0.26 to 0.66 (CH and HAI,  
357       respectively) and mean RRMSE from 0.47 to 0.71 (SCH and US, respectively). For the ALB  
358       and HAI sites, a mean MBE of up to 42.64 g/m<sup>2</sup> was observed while on average, biomass was  
359       underestimated for CH and SCH. For the US model, a severe underestimation of -167.32 g/m<sup>2</sup>  
360       was reported. Compared to empirical models, model accuracy slightly decreased for most sites;  
361       for the US site it decreased substantially.

362       For hybrid models (Figure 4K-O), mean  $R^2$  ranged from 0.23 to 0.54 (US and HAI,  
363       respectively) while mean RRMSE ranged from 0.29 to 0.64 (US and CH, respectively). Except  
364       for the US site, a slight underestimation in terms of MBE could be observed. Model accuracy  
365       across sites resembled those of empirical models, although they were again slightly lower.



368 *Figure 4: Scatterplots of measured versus predicted biomass for the local empirical (A-E), physically-based (F-J), and hybrid models (L-O). Textboxes show mean coefficient of determination ( $R^2$ ),*  
 369 *relative root-mean-square error (RRMSE) and mean bias error (MBE) ± 1 standard deviation across 10 repetitions for each model type. For empirical models, only the best-performing model in terms*  
 370 *of lowest RRMSE is shown with the corresponding model name added in a separate textbox. CH: Switzerland (A, F, K), ALB: Schwäbische Alb (B, G, L), HAI: Hainich-Dün (C, H, M), SCH:*  
 371 *Schorfheide-Chorin (D, I, N), US: United States (E, J, O), RFR: Random Forest regression, SVR: Support Vector regression.*

372

373       3.2. Transferred models

374       In general, model accuracy decreased when local models were applied to other sites, although  
375       physical models sustained their predictive power the best (Table 4).

376       Out of all transferred empirical models, the accuracy of the CH models transferred to the SCH  
377       site (mean  $R^2 = 0.33$ , mean RRMSE = 0.49) and models transferred among the three German  
378       sites came closest to that of the local models, e.g., the ALB models predicting the HAI site  
379       (mean  $R^2 = 0.49$ , mean RRMSE = 0.54) or the HAI and SCH models predicting the ALB site  
380       (mean  $R^2 = 0.30$ , mean RRMSE = 0.53 and mean  $R^2 = 0.49$ , mean RRMSE = 0.64,  
381       respectively). For the CH site, only a mean  $R^2$  of 0.15 with an associated mean RRMSE of 0.65  
382       could be achieved by the transferred empirical model trained at the SCH site. For the US site,  
383       all transferred empirical models exhibited a systematic underestimation of the present biomass  
384       while the US models themselves overestimated biomass at other sites, e.g., with a mean MBE  
385       of 146.09 g/m<sup>2</sup> when predicting the HAI site.

386       Regarding physically-based models, transferability diverged less strongly between  
387       combinations of optimization and prediction sites, with the performance being best for the ALB,  
388       HAI, and SCH sites. Overall, variability between the 10 repetitions was comparatively low, as  
389       identical combinations of cost function and percentage of solutions were selected for the  
390       German sites (Appendix A Section A.5). Best results were achieved for the ALB site with the  
391       HAI models having performed similarly to the local models (mean  $R^2 = 0.43$ , mean RRMSE =  
392       0.51). A slight decline in performance could be observed for the HAI site, although the ALB  
393       model still achieved a mean  $R^2$  of 0.53 and a mean RRMSE of 0.66, with the decline for the  
394       SCH site being more pronounced. For the CH site, the models showed a lower mean  $R^2$ , but  
395       only a slightly higher mean RRMSE. For the US site, in contrast, a direct comparison with the  
396       local models was difficult; generally, a higher mean  $R^2$  was achieved, but mean RRMSE and

397 systematic underestimation also increased. Moreover, the US models consistently performed  
398 worst for all other prediction sites. In comparison with transferred empirical models, the  
399 transferability of physically-based models was higher for the CH, ALB, and HAI sites.  
  
400 The transferability of hybrid models also varied among different combinations of optimization  
401 and validation sites with best results for combinations of the German study sites such as the  
402 ALB models for the HAI site (mean  $R^2 = 0.32$ , mean RRMSE = 0.63) and vice versa (mean  $R^2$   
403 = 0.34, mean RRMSE = 0.52). The ALB models for the SCH site showed comparatively good  
404 values for mean  $R^2$  and RRMSE, but with increased systematic underestimation. For the CH  
405 and US sites, no satisfactory performance could be achieved. Overall, the transferred hybrid  
406 models exhibited similar patterns to the empirical models, although their performance was  
407 somewhat lower. Particularly notable was the comparatively good performance among the  
408 German study sites and the systematic underestimation of biomass for the US site.

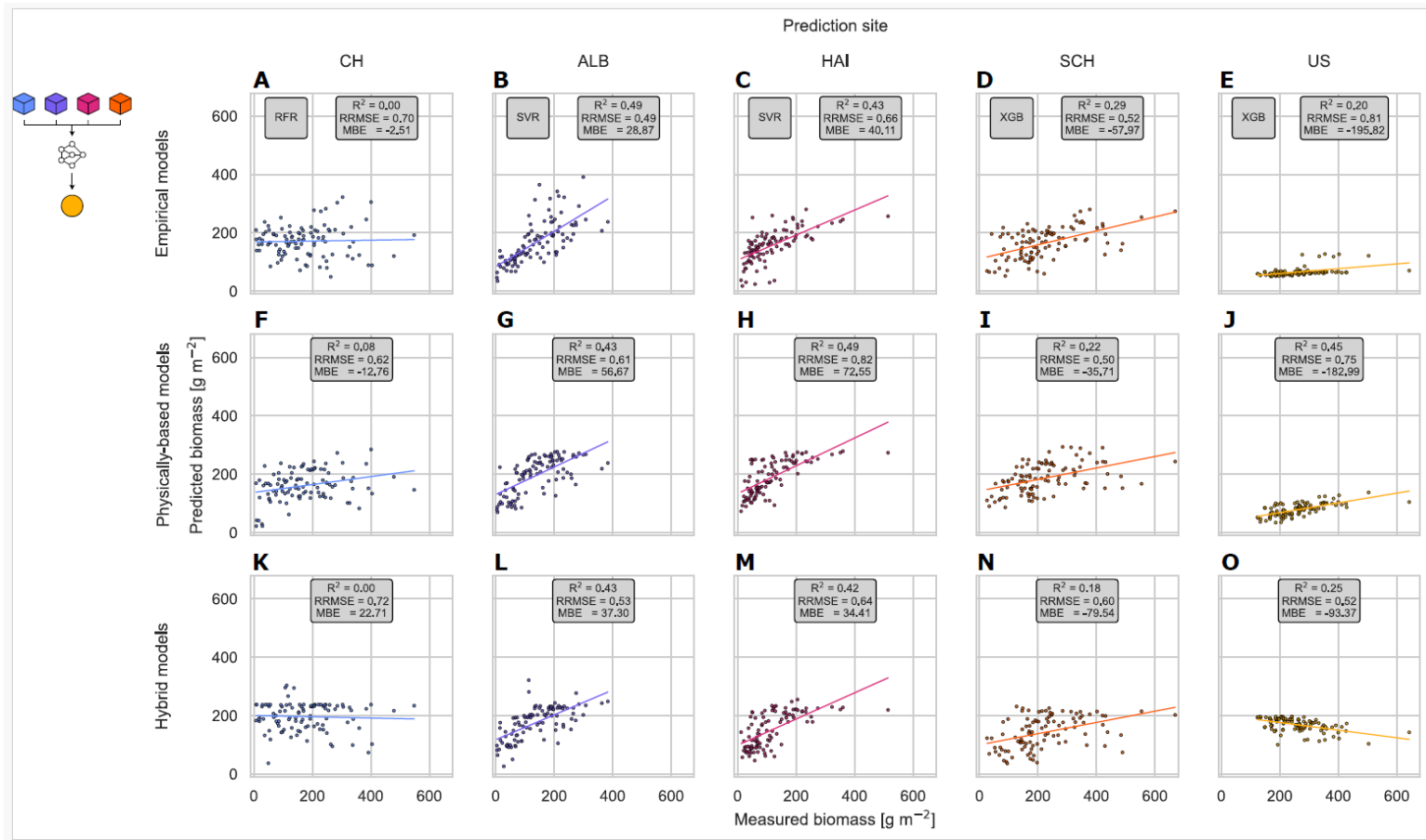
409 *Table 4: Mean coefficient of determination ( $R^2$ ), relative root-mean-square error (RRMSE), and mean bias error (MBE) for  $\pm 1$  standard deviation across 10 repetitions for the transferred empirical,*  
 410 *physically-based, and hybrid models. To facilitate an estimation of model transferability, the metrics of the local models were included (in italic). For empirical models, only the best-performing model*  
 411 *in terms of lowest RRMSE is shown with the corresponding model name added in brackets. CH: Switzerland, ALB: Schwäbische Alb, HAI: Hainich-Dün, SCH: Schorfheide-Chorin, US: United States, RFR:*  
 412 *Random Forest regression, SVR: Support Vector regression, XGB: Extreme Gradient Boosting regression, GPR: Gaussian Process regression.*

		Prediction site														
		CH			ALB			HAI			SCH			US		
Model type	Training/optimization site	$R^2$	RRMSE	MBE	$R^2$	RRMSE	MBE	$R^2$	RRMSE	MBE	$R^2$	RRMSE	MBE	$R^2$	RRMSE	MBE
Empirical	CH	$0.31 \pm 0.12$ (SVR)	$0.55 \pm 0.03$ (SVR)	$-13.29 \pm 13.09$ (SVR)	$0.46 \pm 0.12$ (GPR)	$0.70 \pm 0.12$ (GPR)	$67.46 \pm 23.94$ (SVR)	$0.39 \pm 0.04$ (SVR)	$0.92 \pm 0.15$ (SVR)	$77.08 \pm 20.47$ (SVR)	$0.33 \pm 0.08$ (SVR)	$0.49 \pm 0.05$ (SVR)	$-14.42 \pm 23.94$ (SVR)	$0.08 \pm 0.05$ (GPR)	$0.48 \pm 0.00$ (GPR)	$-88.80 \pm 0.88$ (GPR)
	ALB	$0.04 \pm 0.02$ (GPR)	$0.69 \pm 0.00$ (GPR)	$-37.63 \pm 0.98$ (GPR)	$0.54 \pm 0.21$ (SVR)	$0.43 \pm 0.09$ (SVR)	$-6.35 \pm 12.74$ (SVR)	$0.49 \pm 0.05$ (SVR)	$0.54 \pm 0.02$ (SVR)	$-10.15 \pm 5.00$ (XGB)	$0.30 \pm 0.03$ (XGB)	$0.55 \pm 0.01$ (XGB)	$-68.78 \pm 3.22$ (XGB)	$0.04 \pm 0.02$ (GPR)	$0.57 \pm 0.00$ (GPR)	$-123.02 \pm 0.86$ (GPR)
	HAI	$0.00 \pm 0.01$ (GPR)	$0.73 \pm 0.00$ (GPR)	$-62.02 \pm 0.58$ (GPR)	$0.30 \pm 0.03$ (GPR)	$0.53 \pm 0.02$ (GPR)	$-13.74 \pm 3.73$ (RFR)	$0.64 \pm 0.11$ (RFR)	$0.44 \pm 0.10$ (RFR)	$-4.10 \pm 6.45$ (XGB)	$0.16 \pm 0.03$ (XGB)	$0.63 \pm 0.02$ (XGB)	$-83.11 \pm 5.78$ (XGB)	$0.16 \pm 0.04$ (GPR)	$0.65 \pm 0.00$ (GPR)	$-146.93 \pm 0.65$ (GPR)
	SCH	$0.15 \pm 0.02$ (RFR)	$0.65 \pm 0.03$ (RFR)	$22.32 \pm 9.96$ (SVR)	$0.49 \pm 0.04$ (SVR)	$0.64 \pm 0.04$ (SVR)	$64.65 \pm 7.68$ (SVR)	$0.48 \pm 0.05$ (SVR)	$0.76 \pm 0.05$ (SVR)	$62.53 \pm 6.07$ (SVR)	$0.42 \pm 0.15$ (SVR)	$0.42 \pm 0.04$ (SVR)	$-8.22 \pm 12.60$ (SVR)	$0.09 \pm 0.03$ (GPR)	$0.36 \pm 0.00$ (GPR)	$-39.81 \pm 1.23$ (GPR)
	US	$0.01 \pm 0.00$ (GPR)	$0.81 \pm 0.00$ (GPR)	$87.98 \pm 1.09$ (GPR)	$0.03 \pm 0.01$ (GPR)	$1.07 \pm 0.01$ (GPR)	$122.53 \pm 1.11$ (GPR)	$0.02 \pm 0.00$ (GPR)	$1.46 \pm 0.01$ (GPR)	$146.09 \pm 1.31$ (GPR)	$0.01 \pm 0.00$ (GPR)	$0.57 \pm 0.00$ (GPR)	$39.83 \pm 1.14$ (GPR)	$0.59 \pm 0.08$ (SVR)	$0.22 \pm 0.04$ (SVR)	$5.06 \pm 9.42$ (SVR)
Physically-based	CH	$0.26 \pm 0.17$	$0.59 \pm 0.09$	$-24.33 \pm 15.87$	$0.41 \pm 0.00$	$0.53 \pm 0.00$	$34.97 \pm 0.37$	$0.53 \pm 0.00$	$0.69 \pm 0.00$	$51.81 \pm 0.23$	$0.21 \pm 0.00$	$0.51 \pm 0.00$	$-40.07 \pm 0.25$	$0.45 \pm 0.00$	$0.75 \pm 0.01$	$-182.43 \pm 1.66$
	ALB	$0.14 \pm 0.00$	$0.61 \pm 0.00$	$-24.61 \pm 0.00$	$0.43 \pm 0.17$	$0.52 \pm 0.05$	$32.34 \pm 9.65$	$0.53 \pm 0.00$	$0.66 \pm 0.00$	$45.83 \pm 0.00$	$0.20 \pm 0.00$	$0.53 \pm 0.00$	$-45.64 \pm 0.00$	$0.44 \pm 0.00$	$0.75 \pm 0.00$	$-182.09 \pm 0.00$
	HAI	$0.14 \pm 0.00$	$0.61 \pm 0.00$	$-24.61 \pm 0.00$	$0.43 \pm 0.00$	$0.51 \pm 0.00$	$29.33 \pm 0.00$	$0.66 \pm 0.10$	$0.59 \pm 0.05$	$42.64 \pm 7.51$	$0.20 \pm 0.00$	$0.53 \pm 0.00$	$-45.64 \pm 0.00$	$0.44 \pm 0.00$	$0.75 \pm 0.00$	$-182.09 \pm 0.00$
	SCH	$0.12 \pm 0.00$	$0.60 \pm 0.00$	$-3.44 \pm 0.00$	$0.45 \pm 0.00$	$0.63 \pm 0.00$	$60.49 \pm 0.00$	$0.50 \pm 0.00$	$0.85 \pm 0.00$	$77.44 \pm 0.00$	$0.30 \pm 0.04$	$0.47 \pm 0.04$	$-9.99 \pm 6.58$	$0.43 \pm 0.00$	$0.71 \pm 0.00$	$-170.48 \pm 0.00$
	US	$0.13 \pm 0.00$	$0.64 \pm 0.04$	$-18.58 \pm 7.28$	$0.22 \pm 0.21$	$0.68 \pm 0.07$	$19.05 \pm 37.63$	$0.26 \pm 0.23$	$0.84 \pm 0.02$	$41.44 \pm 31.11$	$0.12 \pm 0.12$	$0.60 \pm 0.13$	$-45.40 \pm 31.62$	$0.30 \pm 0.24$	$0.71 \pm 0.04$	$-167.32 \pm 6.38$
Hybrid	CH	$0.23 \pm 0.14$	$0.64 \pm 0.18$	$-3.46 \pm 17.01$	$0.07 \pm 0.07$	$0.88 \pm 0.06$	$55.91 \pm 19.27$	$0.03 \pm 0.03$	$1.13 \pm 0.11$	$70.71 \pm 24.06$	$0.02 \pm 0.02$	$0.64 \pm 0.06$	$-44.35 \pm 27.74$	$0.13 \pm 0.10$	$0.70 \pm 0.10$	$-148.09 \pm 28.52$
	ALB	$0.02 \pm 0.02$	$0.73 \pm 0.05$	$-31.66 \pm 21.59$	$0.46 \pm 0.18$	$0.46 \pm 0.08$	$-0.37 \pm 11.47$	$0.32 \pm 0.04$	$0.63 \pm 0.01$	$0.42 \pm 12.18$	$0.23 \pm 0.04$	$0.58 \pm 0.04$	$-75.77 \pm 12.38$	$0.12 \pm 0.10$	$0.62 \pm 0.15$	$-132.65 \pm 46.57$
	HAI	$0.02 \pm 0.03$	$0.72 \pm 0.06$	$-36.42 \pm 18.12$	$0.34 \pm 0.07$	$0.52 \pm 0.03$	$-19.74 \pm 5.34$	$0.54 \pm 0.11$	$0.51 \pm 0.09$	$-9.55 \pm 8.77$	$0.17 \pm 0.07$	$0.65 \pm 0.03$	$-94.74 \pm 5.45$	$0.14 \pm 0.11$	$0.59 \pm 0.04$	$-120.22 \pm 12.54$
	SCH	$0.03 \pm 0.03$	$0.79 \pm 0.07$	$36.96 \pm 48.54$	$0.41 \pm 0.09$	$0.77 \pm 0.06$	$83.55 \pm 6.82$	$0.25 \pm 0.06$	$0.95 \pm 0.04$	$78.01 \pm 6.21$	$0.27 \pm 0.15$	$0.47 \pm 0.06$	$-0.14 \pm 8.90$	$0.19 \pm 0.05$	$0.45 \pm 0.09$	$-48.41 \pm 44.96$
	US	$0.01 \pm 0.01$	$0.94 \pm 0.20$	$93.61 \pm 20.14$	$0.03 \pm 0.02$	$1.14 \pm 0.20$	$117.33 \pm 42.37$	$0.02 \pm 0.03$	$1.55 \pm 0.27$	$146.89 \pm 38.34$	$0.02 \pm 0.03$	$0.65 \pm 0.12$	$39.24 \pm 43.46$	$0.23 \pm 0.26$	$0.29 \pm 0.07$	$0.49 \pm 7.92$

413

414        3.3. Global models

415        For empirical models, accuracy was generally low (Figure 5A-E). It was highest for the ALB  
416        site, followed by the HAI and SCH sites, but accompanied by a high MBE. For the CH site, the  
417         $R^2$  of the prediction was practically 0.00, while the systematic underestimation for the US site  
418        amounted to -195.82 g/m<sup>2</sup>. Comparatively poor results were also produced by the physically-  
419        based models in most cases (Figure 5F-J). An exception was the US site, for which an  $R^2$  of  
420        0.45 and an RRMSE of 0.75 were achieved. However, the systematic underestimation also  
421        tended to be high with an MBE of -183.99 g/m<sup>2</sup>. Regarding hybrid models (Figure 5K-O), best  
422        results were obtained for the models predicting the ALB, HAI, and SCH sites, although the  
423        MBE indicated substantial over- and underestimations ranging from 37.30 for the ALB model  
424        to -79.07 g/m<sup>2</sup> for the SCH model, respectively. No satisfactory performance was achieved for  
425        the CH and US sites. Overall, the accuracy of global models was lower than for the local models  
426        (with the exception of the physically-based model for the US site, Figure 5K).



427

428 *Figure 5: Scatterplots of measured versus predicted biomass for the global empirical (A-E), physically-based (F-J), and hybrid models (L-O). Textboxes show coefficient of determination ( $R^2$ ), relative*  
 429 *root-mean-square error (RRMSE) and mean bias error (MBE) for each model. For empirical models, only the best-performing model in terms of lowest RRMSE is shown with the corresponding model*  
 430 *name added in a separate textbox. CH: Switzerland (A, F, K), ALB: Schwäbische Alb (B, G, L), HAI: Hainich-Dün (C, H, M), SCH: Schorfheide-Chorin (D, I, N), US: United States (E, J, O), RFR: Random*  
 431 *Forest regression, SVR: Support Vector regression, XGB: Extreme Gradient Boosting regression.*

432

433      3.4. Epistemic uncertainty

434      For none of the comparisons (local, transferred, and global), a systematic relationship between  
435      epistemic uncertainty and absolute differences between measured and predicted biomass values  
436      was observed when considering all predicted data points (10 repetitions of 20 data points for  
437      local and transferred models, 100 data points for global models; Tables 5 and 6). Only isolated  
438      weak correlations were found, e.g., for local and transferred physically-based models predicting  
439      the US site ( $R^2$  up to 0.31) or the global hybrid model predicting the US site ( $R^2 = 0.38$ ).

440      Only for the mean values of epistemic uncertainty and absolute difference, a few patterns could  
441      be identified. Regarding the local empirical and hybrid models, a positive correlation between  
442      mean epistemic uncertainty and mean absolute difference could be observed. The lowest  
443      correlation values were found for the HAI site (for both model types) and the highest values for  
444      the SCH and CH sites (for empirical and hybrid models, respectively). The physically-based  
445      models displayed a negative correlation; the US site exhibited the lowest mean epistemic  
446      uncertainty but the highest mean absolute difference (52.71 and 162.16 g/m<sup>2</sup>, respectively).

447      For the transferred models, a clear pattern between combinations of training or optimization  
448      and prediction site was found. The respective empirical and hybrid models of the ALB and HAI  
449      sites exhibited low values for both mean epistemic uncertainty and absolute difference for  
450      mutual prediction. The highest values for mean epistemic uncertainty and absolute difference  
451      were produced by the CH and US models of both model types. For the transferred physically-  
452      based models, the lowest values for mean epistemic uncertainty were observed for the US site  
453      (38.86 g/m<sup>2</sup> for ALB and HAI models), which did not coincide with the high values for mean  
454      absolute difference (182.09 g/m<sup>2</sup> for ALB and HAI models). For the global models, no  
455      agreement between mean epistemic uncertainty and mean absolute difference was found for  
456      any model type or prediction site.

457 Table 5: Mean difference between predicted and measured grassland biomass and epistemic uncertainty  $\pm$  1 standard deviation and coefficient of determination ( $R^2$ ) for the 10 local (in italic) and  
 458 local transferred models. For the local models, 200 samples (10 predictions of 20 samples each) and for the transferred models, 1000 samples (10 predictions of 100 samples each) were available. If  
 459 the percentage of solutions of a given physically-based model was 0.01%, only 1 solution was used to derive the predicted biomass value and no epistemic uncertainty could be calculated for the  
 460 corresponding predicted samples (see Appendix A Section A.5). The absolute difference was calculated by taking the absolute value after subtracting the measured biomass value from the predicted  
 461 biomass value for each predicted sample. For the empirical and hybrid models, the epistemic uncertainty for a predicted sample corresponds to the predicted standard deviation of the Gaussian  
 462 process regression (GPR) models. For the physically-based models, the epistemic uncertainty corresponds to the standard deviation of all selected solutions. CH: Switzerland, ALB: Schwäbische Alb,  
 463 HAI: Hainich-Dün, SCH: Schorfheide-Chorin, US: United States.

		Prediction site														
		CH			ALB			HAI			SCH			US		
Model type	Training/optimization site	Absolute difference [g m <sup>-2</sup> ]	Epistemic uncertainty [g m <sup>-2</sup> ]	R <sup>2</sup>	Absolute difference [g m <sup>-2</sup> ]	Epistemic uncertainty [g m <sup>-2</sup> ]	R <sup>2</sup>	Absolute difference [g m <sup>-2</sup> ]	Epistemic uncertainty [g m <sup>-2</sup> ]	R <sup>2</sup>	Absolute difference [g m <sup>-2</sup> ]	Epistemic uncertainty [g m <sup>-2</sup> ]	R <sup>2</sup>	Absolute difference [g m <sup>-2</sup> ]	Epistemic uncertainty [g m <sup>-2</sup> ]	R <sup>2</sup>
Empirical	CH	94.67 ± 21.25			108.78 ± 11.78			119.89 ± 10.10			109.00 ± 10.10			111.90 ± 8.79		
	ALB	82.00 ± 3.57	0.10	0.08	55.08 ± 14.89	0.01	0.08	53.80 ± 12.51	0.05	0.08	70.18 ± 12.51	0.05	0.08	69.07 ± 11.85	0.00	0.08
	HAI	87.96 ± 7.87	0.03	0.02	58.07 ± 16.17	0.02	0.02	41.89 ± 17.38	0.03	0.02	57.10 ± 17.38	0.03	0.02	65.59 ± 15.87	0.07	0.02
	SCH	123.63 ± 5.15	0.00	0.00	100.29 ± 14.43	0.05	0.00	105.34 ± 13.54	0.13	0.00	111.95 ± 13.54	0.05	0.00	110.94 ± 14.80	0.02	0.00
	US	100.43 ± 66.40			96.99 ± 7.78			96.99 ± 7.78			105.34 ± 15.39			96.99 ± 7.78		
Physically-based	CH	72.64 ± 28.22	0.02	0.02	64.22 ± 25.47	0.00	0.02	68.23 ± 24.39	0.01	0.02	87.73 ± 24.39	0.01	0.02	95.65 ± 21.07	0.04	0.02
	ALB	71.98 ± 24.64	0.01	0.01	63.10 ± 25.09	0.00	0.01	64.28 ± 24.24	0.02	0.01	84.10 ± 24.24	0.02	0.01	80.90 ± 20.37	0.03	0.01
	HAI	71.98 ± 24.64	0.01	0.01	60.97 ± 25.29	0.00	0.01	59.18 ± 25.56	0.00	0.01	81.59 ± 25.56	0.00	0.01	81.28 ± 20.37	0.03	0.01
	SCH	95.62 ± 24.64	0.01	0.01	76.02 ± 27.38	0.04	0.01	87.85 ± 27.38	0.05	0.01	101.54 ± 24.53	0.05	0.01	109.97 ± 19.35	0.02	0.01
	US	79.70 ± 67.66	0.01	0.01	76.02 ± 27.38	0.04	0.01	100.68 ± 28.68	0.03	0.01	97.41 ± 27.84	0.07	0.01	107.35 ± 23.30	0.03	0.01
Hybrid	CH	168.42 ± 64.24	0.02	0.02	100.74 ± 57.08	0.10	0.02	113.54 ± 47.26	0.00	0.02	84.32 ± 47.26	0.00	0.02	102.34 ± 55.32	0.02	0.02
	ALB	127.65 ± 34.26	0.03	0.03	49.07 ± 38.06	0.00	0.03	100.59 ± 33.13	0.04	0.03	76.32 ± 33.13	0.04	0.03	84.99 ± 36.44	0.06	0.03
	HAI	130.98 ± 27.94	0.03	0.03	52.71 ± 30.03	0.00	0.03	101.47 ± 41.62	0.01	0.03	83.56 ± 29.03	0.01	0.03	89.19 ± 31.22	0.07	0.03
	SCH	138.79 ± 41.65	0.00	0.00	93.55 ± 42.53	0.00	0.00	109.98 ± 43.11	0.05	0.00	87.59 ± 43.11	0.05	0.00	100.39 ± 44.62	0.08	0.00
	US	135.55 ± 47.69	0.01	0.01	135.62 ± 38.63	0.04	0.01	163.14 ± 38.63	0.00	0.01	107.63 ± 33.42	0.00	0.01	112.79 ± 36.61	0.00	0.01

464      Table 6: Mean difference between predicted and measured grassland biomass and epistemic uncertainty  $\pm 1$  standard deviation and coefficient of determination ( $R^2$ ) for global models. For each  
 465      model, 100 samples (1 prediction of 100 samples each) were available. The absolute difference was calculated by taking the absolute value after subtracting the measured biomass value from the  
 466      predicted biomass value for each predicted sample. For the empirical and hybrid models, the epistemic uncertainty for a predicted sample corresponds to the predicted standard deviation of the  
 467      Gaussian process regression (GPR) models. For the physically-based models, the epistemic uncertainty corresponds to the standard deviation of all selected solutions. CH: Switzerland, ALB:  
 468      Schwäbische Alb, HAI: Hainich-Dün, SCH: Schorfheide-Chorin, US: United States.

Model type	Prediction site																
	CH			ALB			HAI			SCH			US				
Absolute difference [g m <sup>-2</sup> ]	Epistemic uncertainty [g m <sup>-2</sup> ]	R <sup>2</sup>	Absolute difference [g m <sup>-2</sup> ]	Epistemic uncertainty [g m <sup>-2</sup> ]	R <sup>2</sup>	Absolute difference [g m <sup>-2</sup> ]	Epistemic uncertainty [g m <sup>-2</sup> ]	R <sup>2</sup>	Absolute difference [g m <sup>-2</sup> ]	Epistemic uncertainty [g m <sup>-2</sup> ]	R <sup>2</sup>	Absolute difference [g m <sup>-2</sup> ]	Epistemic uncertainty [g m <sup>-2</sup> ]	R <sup>2</sup>			
Empirical	112.11 $\pm$ 65.55	0.00	89.36 $\pm$ 65.55	0.00	0.00	115.07 $\pm$ 0.00	0.00	0.00	105.16 $\pm$ 56.70	0.00	0.00	92.12 $\pm$ 90.44	0.00	0.00			
Physically-based	83.49 $\pm$ 27.37	0.00	81.37 $\pm$ 71.47	74.45 $\pm$ 42.24	0.03	100.68 $\pm$ 28.68	0.03	0.07	83.05 $\pm$ 46.07	27.84	0.07	78.35 $\pm$ 79.36	21.91	0.01	102.31 $\pm$ 81.66	108.8 $\pm$ 0.00	0.00
Hybrid	138.74 $\pm$ 25.66	0.01	98.72 $\pm$ 75.78	62.54 $\pm$ 40.14	0.03	138.67 $\pm$ 51.71	57.72 $\pm$ 45.84	0.14	88.45 $\pm$ 24.39	97.38 $\pm$ 92.43	0.11	106.99 $\pm$ 34.61	101.97 $\pm$ 90.03	0.38	132.54 $\pm$ 7.63	182.99 $\pm$ 11.05	0.20

469

470

471      **4. Discussion**

472      Remote sensing has gained traction in its application for monitoring ecosystem functioning,  
473      with spatial (and temporal) scalability often highlighted as a key advantage. When developing  
474      scalable models, model transferability should be an integral part of performance assessment;  
475      however, systematic evaluation often lags behind the ambition for scalability within and across  
476      ecosystems. In this study, we demonstrated the importance of assessing model transferability  
477      when evaluating the performance of remotely sensed grassland biomass estimates and related  
478      model selection considerations. Our model comparisons indicated that in most cases physically-  
479      based models exhibited the highest transferability when applied to unseen grassland sites.  
480      However, no single model consistently outperformed others when trained or optimized with  
481      data from multiple sites. These results underscore the challenges in developing scalable models,  
482      highlight the importance and possible trade-offs of appropriate model selection, and shed light  
483      on the discrepancies between epistemic uncertainty and predictive accuracy.

484      **4.1. Accuracy of local models**

485      All model types performed similarly when predicting biomass locally with accuracies  
486      comparable to those of other studies conducted in alpine and semi-natural grasslands in  
487      Switzerland and Germany (Raab et al., 2020; Schweiger et al., 2015a). Generally, model  
488      accuracy decreased with increasing biomass range and (to a lesser extent) spectral variability  
489      (see also Dehghan-Shoar et al., 2023, and Appendix A Section A.18). Overall, empirical models  
490      performed best at the site level, presumably due to their high flexibility, allowing them to  
491      incorporate site-specific relationships in the data without necessarily relying on physical  
492      principles.

493 For the physical models, we found a large discrepancy between the *in situ* and modeled data  
494 for the US site caused by the employed LUT parametrization. Although the models recognized  
495 the underlying relationship between biomass and spectral information to a certain extent (mean  
496  $R^2 = 0.30$ ), a high RRMSE of 0.71 resulted probably due to a too narrow range of values for  
497 LMA in the LUT since testing an alternative value range with a higher upper bound for LMA  
498 resulted in a mean  $R^2$  of 0.51 and mean RRMSE of 0.33 (Appendix A Section A.19). However,  
499 broadening the trait ranges increased ill-posedness (Combal et al., 2003; Verrelst et al., 2014)  
500 and deteriorated model performance for the other sites; therefore, a site-specific parametrization  
501 of multiple narrowly defined LUTs would be necessary to obtain comparable results to the  
502 empirical models for all sites.

503 The hybrid models performed similarly compared to the empirical models. Selecting training  
504 samples with AL led to substantial improvements in performance as stated in AL theory  
505 (Verrelst et al., 2016). In our case, the use of AL for selecting the most informative optimization  
506 samples was essential because we did not parameterize the LUT *a priori* or excluded  
507 biophysically unrealistic simulations as done by others (see, e.g., Campos-Taberner et al.,  
508 2018). Moreover, the hybrid models did not display the aforementioned imbalance between  $R^2$   
509 and RRMSE for the US site although having been trained on a suboptimally configured LUT,  
510 presumably because the employed GPR kernel was able to scale the predictions by the  
511 magnitude of the employed constant kernel resulting in a lower RRMSE compared to the  
512 physically-based models while keeping comparatively  $R^2$  high (scikit-learn Developers, 2023).

513 4.2. Transferability of local models

514 Several factors possibly hampered model transferability. First, the transferability of empirical  
515 and hybrid models remained limited to combinations of training or optimization and validation  
516 sites sharing similar environmental and management characteristics such as ALB and HAI. This  
517 is consistent with the findings of Muro et al. (2022) who, among the German study sites, found

518 the prediction of SCH to be the most challenging due to an elevated level of soil organic content  
519 and different management compared to ALB and HAI (Busch et al., 2018). At the other  
520 extreme, the US site, which was poorly predicted by transferred models, was sampled during a  
521 very dry summer, and the Sentinel-2 spectra showed a substantial increase in reflectance in the  
522 short-wave infrared region, likely due to low water content confounding the overall spectra  
523 (Jacquemoud et al., 2009; Mesonet, 2024; Appendix A Section A.20). The summer drought  
524 may have also led to early senescence, resulting in a potential underestimation of LAI in  
525 PROSAIL as the latter is predominantly equipped for modelling green vegetation and struggles  
526 to capture NPV (Amin et al., 2021; Delegido et al., 2015; Schiefer et al., 2021; Verrelst et al.,  
527 2023). Second, differences in the abundance of C3 and C4 grasses among sites may have further  
528 limited model transferability from European sites to the US exhibiting a substantially higher  
529 cover fraction of C4 grasses (Kothari and Schweiger, 2022; Shoko et al., 2016; Appendix A  
530 Section A.21). Third, the derivation of biomass values in physically-based and hybrid  
531 approaches via LUT-based LMA and LAI multiplication resulted in numerous parameter  
532 combinations associated with the same biomass values, increasing the prevalent ill-posedness  
533 of the model. Fourth, plot definition and field measurements were handled differently among  
534 the study sites and field campaigns. For example, the plots being monitored by the Biodiversity  
535 Exploratories were selected to be representative of an area of 2,500 m<sup>2</sup> and biomass was cut for  
536 an area of 2 m<sup>2</sup> (Hinderling et al., 2023), whereas the plots in Switzerland were representative  
537 for an area of 36 m<sup>2</sup> and biomass harvesting was limited to 1 m<sup>2</sup> (Schweiger et al., 2015b).  
538 While such discrepancies between monitoring programs are likely to introduce uncertainties,  
539 they are difficult to mitigate when working with already existing field data. Moreover, the *in*  
540 *situ* data collection might not necessarily have been optimized for the pixel grid of the utilized  
541 remote sensing data, e.g., 20 × 20 m grid for Sentinel-2, leading to the problem of diminished  
542 representativeness (Hauser et al., 2021b; Schweiger, 2020) such as in the case of mixed pixels.  
543 Even though standardization of field campaigns could potentially benefit the transferability of

544 model trained with remote sensing data, it might be hardly feasible due to ecological or policy  
545 constraints and the legitimate interest of existing monitoring programs to ensure temporally  
546 consistent measurements.

547 Nevertheless, physically-based models outperformed empirical and hybrid models when  
548 predicting novel study sites which is consistent with the claimed transferability of physically-  
549 based models and the results of previous studies conducted at leaf level (Féret et al., 2019;  
550 Verrelst et al., 2015; Wang et al., 2023). For the hybrid models, we expected a comparatively  
551 high transferability due to the physical foundation of the RTM-simulated training data. In  
552 addition, previous studies have shown the general ability of machine learning regression models  
553 to serve as RTM emulators, i.e., being able to accurately grasp the physical principles of RTMs  
554 during model training (Rivera et al., 2015; Verrelst et al., 2017). However, our results showed  
555 that the transferability of the hybrid models was weakest in most cases, potentially because the  
556 empirical features of hybrid models overrode the physical foundation of the training data by  
557 fitting data-specific single-trait relationships between the AL-selected training set and the  
558 optimization data. To increase the transferability of hybrid models, it has been suggested to  
559 increase the initial training set size (Berger et al., 2021b; Tagliabue et al., 2022), enforcing the  
560 inclusion of more general training data prior to the employment of AL. However, no general  
561 increase in transferability was apparent in our results even when using different initial training  
562 set sizes (Appendix A Section A.22).

563       4.3. Accuracy of global models

564 In this study, global models were defined as models that were trained (empirical) or optimized  
565 (physically-based and hybrid) using field data from multiple sites and applied to an unseen  
566 prediction site. The reasoning behind this model set-up was that model training or optimization  
567 with heterogeneous field data might increase model transferability by allowing the model to  
568 learn from a larger pool of diverse field data motivated by previous studies employing similar

569 approaches (Muro et al., 2022) and the emergence of global plant trait products derived from  
570 remote sensing data using physically-based or machine learning models (Campos-Taberner et  
571 al., 2018; Kovács et al., 2023; Moreno-Martinez et al., 2020) relying on accurate predictions  
572 for unsampled areas. The results of this third model comparison were not conclusive as to which  
573 model performed best at this task.

574 The global physically-based models achieved lower accuracy than the local models for all sites,  
575 indicating a strong influence of the selected combinations of cost function and percentage of  
576 solutions, which differed strongly from those of the local models (Appendix A Sections A.5  
577 and A.8). This seems to contradict the observed higher transferability of the transferred  
578 physically-based models and the eventual conclusion that physically-based models are always  
579 the best choice if no validation data is available (see Section 4.2).

580 One major challenge for global empirical and hybrid models was that different confounding  
581 relationships between biomass and spectral information are possible for various study sites.  
582 This was reflected for the empirical and hybrid models by the increased mean RRMSE of the  
583 US site, whose specific conditions could not be adequately learned by the models without  
584 additional contextual information (in the case of the global physically-based models, the reason  
585 for the high mean RRMSE was most likely the parametrization of the LUT as discussed in 4.1).  
586 Nevertheless, comparatively good results were obtained by the empirical models for the ALB  
587 site ( $R^2 = 0.49$ , RRMSE = 0.49, MBE = 28.87 g/m<sup>2</sup>) and by the hybrid models for the ALB ( $R^2$   
588 = 0.43, RRMSE = 0.53, MBE = 37.30 g/m<sup>2</sup>) and HAI sites ( $R^2 = 0.42$ , RRMSE = 0.64, MBE =  
589 34.41 g/m<sup>2</sup>) which is consistent with the results of Muro et al. (2022) who reported a lower  
590 transferability of models applied to the SCH site due to confounding factors such as soil organic  
591 content and management practices (Busch et al., 2018). Identifying the exact factors  
592 contributing to the divergent performance is challenging within the multi-site training set-up  
593 and limits definitive conclusions to be drawn on model selection and suitability.

594 4.4. Prediction uncertainty as a measure of model applicability to unseen data

595 Value and acceptance of remote sensing products increase with a quantitative specification of  
596 uncertainty (Woodcock, 2002); increased attention to uncertainty is also called for in the context  
597 of machine learning applications (Meyer and Pebesma, 2020). Motivated by the finding that  
598 epistemic uncertainty of GPR models might help to identify reliable and unreliable predictions  
599 for croplands (Verrelst et al., 2013b, 2013a, 2012), we tested if epistemic uncertainty could be  
600 used as proxy for model transferability across heterogeneous grasslands by comparing the  
601 absolute difference between measured and predicted biomass with the epistemic uncertainty  
602 associated with each prediction and found low correspondence between the two (as shown in  
603 Section 3.4).

604 In the case of GPR, epistemic uncertainty is a direct model output in the form of the predictive  
605 SD. According to Rasmussen and Williams (2006), the epistemic uncertainty of GPR models  
606 is determined by the similarity between a data point to be predicted and the training data as well  
607 as the properties of the optimized kernel, e.g., the magnitude of the constant kernel and the  
608 lengthscale of the RBF kernel. Accordingly, it is not surprising that the empirical models for  
609 the mutual prediction of the spectrally more similar ALB and HAI sites showed lower mean  
610 epistemic uncertainty than the US models, whose training data exhibited different spectral  
611 properties, e.g., the high reflectance in the short-wave infrared region for the US site. The fact  
612 that the AL-selected training data of the hybrid models did not differ much among the study  
613 sites (Appendix A Section A.23) led to a consistently lower epistemic uncertainty for the  
614 German sites, for which the spectral properties of the field data were more similar to those of  
615 the AL-selected training data. Correspondingly, a high mean epistemic uncertainty resulted for  
616 the CH and US sites, since these sites exhibited larger spectral heterogeneity (as shown in  
617 Appendix A Section A.18) or contained spectra that were not fully covered by the current  
618 parametrization of the PROSAIL LUT, respectively. Thus, a high epistemic uncertainty

619 indicated that the data points to be predicted are not optimally covered by the training data,  
620 while a low epistemic uncertainty on the contrary did not necessarily indicate a reliable  
621 prediction as suggested by the missing correspondence between low absolute differences and  
622 associated epistemic uncertainty. Hence, using the epistemic uncertainty as a measure of model  
623 applicability to unseen data might be valid only in the case of comparable relationships between  
624 biomass and spectral information – a condition violated in our study. Nevertheless, the GPR  
625 uncertainty still serves as valuable information to optimize field sampling efforts as outlined in  
626 Verrelst et al. (2012).

627 In the case of physically-based models, the SD of the solutions considered in the LUT inversion  
628 process is a comparatively simple approach to express the variability of the candidate solutions  
629 and thus to quantify the diversity of the possible solutions. This diversity was relatively  
630 consistent per prediction site, e.g., mean epistemic uncertainty was between 38.86 and 51.96  
631 g/m<sup>2</sup> for predictions of the US site, suggesting a subordinate influence of the cost functions and  
632 percentages of solutions used for different LUT inversions. Rather, the epistemic uncertainty  
633 appeared to depend primarily on the spectral properties of the predicted data. For example, the  
634 US site had by far the lowest epistemic uncertainty, which was not consistent with the  
635 comparatively high mean RRMSE. In fact, a more accurate prediction of the US site would  
636 have required a modification of the LUT parameterization (as shown in Appendix A Section  
637 A.19), which is obscured by relying solely on the prediction uncertainty. Therefore, in our  
638 study, the epistemic uncertainty expressed as diversity of the possible solutions did not allow a  
639 direct conclusion on the applicability of the models to unseen data.

640       4.5. Possible improvements

641 Regarding the performance of local models, various opportunities for improvement are  
642 conceivable depending on the model type. First, the use of alternative algorithms or cost  
643 functions should be considered. For empirical models, alternative algorithms such as Artificial

644 Neural Networks (ANNs) as employed by Ali et al. (2017) and Muro et al. (2022) could be  
645 tested to determine further improvements in model accuracy. For the physically-based models,  
646 the cost functions discussed by Rivera et al. (2013) were tested but since the choice of the  
647 optimal cost functions varied between study sites, the inclusion of additional cost functions  
648 such as genetic algorithms (Fang et al., 2003) could benefit the accuracy of the LUT inversion.  
649 Second, subsetting the LUT using correlations between PROSAIL input parameters could  
650 reduce solution space (Campos-Taberner et al., 2018). For this, *in situ* data of several PROSAIL  
651 input parameters are necessary whose correlations could be exploited to prevent unrealistic  
652 parameter combinations being included in the LUT (Combal et al., 2003) as done by Schiefer  
653 et al. (2021). Ideally, the *in situ* data should be collected for each study site, since the correlation  
654 between the parameters is subject to environmental gradients such as climatic and soil factors  
655 (Joswig et al., 2021). Third, the inclusion of additional predictor variables could improve model  
656 accuracy and transferability, for example additional biomass-relevant variables such as  
657 vegetation height could lead to improved predictions. However, sampling of additional  
658 variables is time- and labor-intensive and deriving them from remote sensing data is  
659 challenging, highlighting the need for reliable, accurate, and transferable remote sensing  
660 models. For example, the mean average error (MAE) of the estimated canopy height from  
661 spaceborne laser altimeters amounts to at least 2 m (Liu et al., 2021) and the use of Sentinel-1  
662 SAR data has led to mixed results, ranging from improving grassland biomass estimation to  
663 providing little or no added value when combined with optical data (Muro et al., 2022; Raab et  
664 al., 2020; Wang et al., 2019). For hybrid models, it is possible to employ further advanced  
665 models such as multi-output GPR models (MOGPs) if additional *in situ* measured PROSAIL  
666 parameters are available, which allow to predict multiple output variables while preserving the  
667 correlations among the input variables (Liu et al., 2018). The feasibility of employing MOGPs  
668 in the context of biophysical variable estimation has already been demonstrated by Pipia et al.

669 (2019) and Caballero et al. (2023) who predicted LAI and vegetation water content (VWC),  
670 respectively, by combining Sentinel-1 and Sentinel-2 data.

671 To improve the local models' transferability as well as the global models' accuracy, it is  
672 essential to disentangle the site-specific confounded relationships between biomass and spectral  
673 information. First, additional predictor variables could help to distinguish these relationships,  
674 including vegetation height, climate data, land use intensity as continuous proxy for  
675 management information (Blüthgen et al., 2012; Rossi et al., 2024), and the quantification of  
676 NPV. Second, a stratification based on climatic priors for subsequent LUT optimization would  
677 be useful in the context of diverse study sites and resonates with studies making the case for a  
678 stronger embedding of remote sensing data with ancillary data (Aguirre-Gutiérrez et al., 2021;  
679 Cavender-Bares et al., 2022; Moreno-Martinez et al., 2020; Verrelst et al., 2023). Although a  
680 remote sensing-only solution may have been desirable, our results reaffirm, through a new  
681 perspective, the trade-off between a LUT parametrization covering the ecological conditions of  
682 all sites and a degradation of the LUT inversion accuracy. Such a stratification would allow, in  
683 the first step, the data points to be projected into different environmental regimes based on  
684 climate data and in the second step, to use LUTs subsetted based on correlations between  
685 PROSAIL parameters and with optimized parameter ranges for the physically-based or hybrid  
686 models. While coarse-resolution climate data for the first step are freely available over large  
687 spatial scales (e.g., ERA5-Land; Muñoz Sabater, 2019), the second step still places high  
688 demand on the availability of *in situ* data.

689    **Conclusion**

690    In this study, we compared different models for biomass estimation from multispectral  
691    spaceborne remote sensing data across heterogeneous grasslands to assess model assumptions  
692    and facilitate model choice for specific applications. In three model comparisons, we  
693    investigated the accuracy and transferability of empirical, physically-based, and hybrid models  
694    across five study sites regarding (1) their local applicability, (2) their spatial transferability, and  
695    (3) the opportunity to compile field data from multiple study sites to increase transferability.

696    Our results showed that:

697        1) on the local level, all models performed similarly well in terms of RRMSE and  $R^2$ .

698        Further, we found that in the context of hybrid models, employing AL to identify the  
699        most informative training samples was required.

700        2) when transferring local models to a different study site, the physically-based models led

701        to the most promising results for most combinations of training (empirical models) or  
702        optimization (physically-based and hybrid models) and validation sites. Moreover, we  
703        observed a trade-off between LUT specificity and generality, impeding the universal  
704        application of a single physically-based model. The transferability of empirical and  
705        hybrid models was limited to combinations of sites sharing similar ecological and/or  
706        spectral conditions.

707        3) when compiling the field data of four study sites to predict the remaining one, no model

708        clearly outperformed the others. Differences in model performance remained  
709        challenging to explain, highlighting the need to further explore the possibilities and  
710        characterize the trade-offs of developing models applicable on a large spatial scale and  
711        across ecological gradients.

712        4) common epistemic uncertainty implementations were not necessarily reliable measures  
713            of model applicability to unseen data in the case of varying relationships between  
714            biomass and spectral information across study sites.

715        5) model transferability needs to be thoroughly tested when developing remote sensing  
716            applications whose intended applicability goes beyond the local scale.

717        Possibilities for improving local model accuracy and transferability include the testing of  
718            alternative machine and deep learning algorithms and cost functions, hierarchical subsetting of  
719            LUTs based on ecological priors, and the use of multi-output models to preserve correlations  
720            among predictor variables, incorporating additional predictors such as NPV or climate data, and  
721            exploring multi-sensor approaches. To fully exploit the spatio-temporal potential of satellite  
722            observations, evaluating and improving model transferability should be a priority; this requires  
723            datasets that enable rigorous testing across sites and conditions, along with theory-driven  
724            foundations to build models capable of robust prediction when applied to new unseen data.

725 **CRediT authorship contribution statement**

726 **Jan Schweizer:** Conceptualization, Methodology, Software, Investigation, Data Curation,  
727 Writing – Original draft, Visualization. **Leon T. Hauser:** Conceptualization, Methodology,  
728 Investigation, Data Curation, Writing – Original draft, Supervision, Funding Acquisition.  
729 **Anna-Katharina Schweiger:** Data Curation, Writing – Review & Editing. **Hamed  
730 Gholizadeh:** Data Curation, Writing – Review & Editing. **Christian Rossi:** Conceptualization,  
731 Methodology, Investigation, Data Curation, Writing – Original draft, Supervision, Funding  
732 Acquisition.

733

734 **Acknowledgements**

735 This work was conducted under the ‘Biodiv-Watch’ project, funded by the ESA Initial Support  
736 for Innovation (EISI) [Grant Number 4000138090], and with the financial and operational  
737 support of the Swiss National Park (SNP). Hamed Gholizadeh was supported by a NASA NIP  
738 award [80NSSC21K0941]. This work is based on data obtained within the DFG Priority  
739 Program 1374 ‘Infrastructure-Biodiversity-Exploratories’. We thank the staff of the three  
740 exploratories, the BE office and the BExIS team for their work in maintaining the plot and  
741 project infrastructure, and Markus Fischer, the late Elisabeth Kalko, Eduard Linsenmair,  
742 Dominik Hessenmöller, Jens Nieschulze, Daniel Prati, Ingo Schöning, François Buscot, Ernst-  
743 Detlef Schulze and Wolfgang W. Weisser for their role in setting up the Biodiversity  
744 Exploratories project. Field work permits were issued by the responsible state environmental  
745 offices of Baden-Württemberg, Thüringen, and Brandenburg (according to § 72 BbgNatSchG).  
746 The authors thank Antonia Ludwig for her insightful comments on an earlier version of the  
747 manuscript and Matteo Delucchi of the consulting team of the Applied Statistics group at the  
748 Department of Mathematical Modeling and Machine Learning, University of Zurich.

749 **Data availability**

750 This work is based on data elaborated by the BExIS and Botany core projects of the Biodiversity  
751 Exploratories program (DFG Priority Program 1374). The datasets are publicly available in the  
752 Biodiversity Exploratories Information System (<http://doi.org/10.17616/R32P9Q>). The  
753 datasets are listed in the references section. Field data for Switzerland and Oklahoma are  
754 available upon request. Python codes and synthetic mock data are available upon request.

755 **References**

- 756 Aguirre-Gutiérrez, J., Rifai, S., Shenkin, A., Oliveras, I., Bentley, L.P., Svátek, M., Girardin, C.A.J., Both,  
757 S., Riutta, T., Berenguer, E., Kissling, W.D., Bauman, D., Raab, N., Moore, S., Farfan-Rios, W.,  
758 Figueiredo, A.E.S., Reis, S.M., Ndong, J.E., Ondo, F.E., N'ssi Bengone, N., Mihindou, V., Moraes  
759 de Seixas, M.M., Adu-Bredou, S., Abernethy, K., Asner, G.P., Barlow, J., Burslem, D.F.R.P.,  
760 Coomes, D.A., Cernusak, L.A., Dargie, G.C., Enquist, B.J., Ewers, R.M., Ferreira, J., Jeffery, K.J.,  
761 Joly, C.A., Lewis, S.L., Marimon-Junior, B.H., Martin, R.E., Morandi, P.S., Phillips, O.L., Quesada,  
762 C.A., Salinas, N., Schwantes Marimon, B., Silman, M., Teh, Y.A., White, L.J.T., Malhi, Y., 2021.  
763 Pantropical modelling of canopy functional traits using Sentinel-2 remote sensing data. *Remote*  
764 *Sens Environ* 252, 112122. <https://doi.org/10.1016/j.rse.2020.112122>
- 765 Ali, I., Cawkwell, F., Dwyer, E., Barrett, B., Green, S., 2016. Satellite remote sensing of grasslands:  
766 from observation to management. *Journal of Plant Ecology* 9, 649–671.  
767 <https://doi.org/10.1093/jpe/rtw005>
- 768 Ali, I., Cawkwell, F., Dwyer, E., Green, S., 2017. Modeling Managed Grassland Biomass Estimation by  
769 Using Multitemporal Remote Sensing Data—A Machine Learning Approach. *IEEE J Sel Top Appl*  
770 *Earth Obs Remote Sens* 10, 3254–3264. <https://doi.org/10.1109/JSTARS.2016.2561618>
- 771 Amin, E., Verrelst, J., Rivera-Caicedo, J.P., Pipia, L., Ruiz-Verdú, A., Moreno, J., 2021. Prototyping  
772 Sentinel-2 green LAI and brown LAI products for cropland monitoring. *Remote Sens Environ*  
773 255, 112168. <https://doi.org/10.1016/j.rse.2020.112168>
- 774 Anderson, R.H., Fuhlendorf, S.D., Engle, D.M., 2006. Soil Nitrogen Availability in Tallgrass Prairie  
775 Under the Fire–Grazing Interaction. *Rangel Ecol Manag* 59, 625–631.  
776 <https://doi.org/10.2111/05-088R2.1>
- 777 Bai, Y., Cotrufo, M.F., 2022. Grassland soil carbon sequestration: Current understanding, challenges,  
778 and solutions. *Science* (1979) 377, 603–608. <https://doi.org/10.1126/science.abo2380>
- 779 Bailey, D.W., Gross, J.E., Laca, E.A., Rittenhouse, L.R., Coughenour, M.B., Swift, D.M., Sims, P.L., 1996.  
780 Mechanisms That Result in Large Herbivore Grazing Distribution Patterns. *Journal of Range*  
781 *Management* 49, 386. <https://doi.org/10.2307/4002919>
- 782 Bardgett, R.D., Bullock, J.M., Lavorel, S., Manning, P., Schaffner, U., Ostle, N., Chomel, M., Durigan,  
783 G., L. Fry, E., Johnson, D., Lavallee, J.M., Le Provost, G., Luo, S., Png, K., Sankaran, M., Hou, X.,  
784 Zhou, H., Ma, L., Ren, W., Li, X., Ding, Y., Li, Y., Shi, H., 2021. Combatting global grassland  
785 degradation. *Nat Rev Earth Environ* 2, 720–735. <https://doi.org/10.1038/s43017-021-00207-2>
- 786 Beck, H.E., Zimmermann, N.E., McVicar, T.R., Vergopolan, N., Berg, A., Wood, E.F., 2018. Present and  
787 future Köppen-Geiger climate classification maps at 1-km resolution. *Sci Data* 5, 180214.  
788 <https://doi.org/10.1038/sdata.2018.214>
- 789 Bengtsson, J., Bullock, J.M., Ego, B., Everson, C., Everson, T., O'Connor, T., O'Farrell, P.J., Smith, H.G.,  
790 Lindborg, R., 2019. Grasslands—more important for ecosystem services than you might think.  
791 *Ecosphere* 10, e02582. <https://doi.org/10.1002/ecs2.2582>
- 792 Berger, K., Atzberger, C., Danner, M., D'Urso, G., Mauser, W., Vuolo, F., Hank, T., 2018. Evaluation of  
793 the PROSAIL Model Capabilities for Future Hyperspectral Model Environments: A Review Study.  
794 *Remote Sens (Basel)* 10, 85. <https://doi.org/10.3390/rs10010085>

- 795 Berger, K., Hank, T., Halabuk, A., Rivera-Caicedo, J.P., Wocher, M., Mojses, M., Gerhátová, K.,  
796 Tagliabue, G., Dolz, M.M., Venteo, A.B.P., Verrelst, J., 2021a. Assessing Non-Photosynthetic  
797 Cropland Biomass from Spaceborne Hyperspectral Imagery. *Remote Sens (Basel)* 13, 4711.  
798 <https://doi.org/10.3390/rs13224711>
- 799 Berger, K., Rivera Caicedo, J.P., Martino, L., Wocher, M., Hank, T., Verrelst, J., 2021b. A Survey of  
800 Active Learning for Quantifying Vegetation Traits from Terrestrial Earth Observation Data.  
801 *Remote Sens (Basel)* 13, 287. <https://doi.org/10.3390/rs13020287>
- 802 Berger, K., Verrelst, J., Féret, J.-B., Hank, T., Wocher, M., Mauser, W., Camps-Valls, G., 2020. Retrieval  
803 of aboveground crop nitrogen content with a hybrid machine learning method. *International  
804 Journal of Applied Earth Observation and Geoinformation* 92, 102174.  
805 <https://doi.org/10.1016/j.jag.2020.102174>
- 806 Binh, N.A., Hauser, L.T., Viet Hoa, P., Thi Phuong Thao, G., An, N.N., Nhut, H.S., Phuong, T.A., Verrelst,  
807 J., 2022. Quantifying mangrove leaf area index from Sentinel-2 imagery using hybrid models and  
808 active learning. *Int J Remote Sens* 43, 5636–5657.  
809 <https://doi.org/10.1080/01431161.2021.2024912>
- 810 Blüthgen, N., Dormann, C.F., Prati, D., Klaus, V.H., Kleinebecker, T., Hözel, N., Alt, F., Boch, S., Gockel,  
811 S., Hemp, A., Müller, J., Nieschluz, J., Renner, S.C., Schöning, I., Schumacher, U., Socher, S.A.,  
812 Wells, K., Birkhofer, K., Buscot, F., Oelmann, Y., Rothenwörler, C., Scherber, C., Tscharntke, T.,  
813 Weiner, C.N., Fischer, M., Kalko, E.K.V., Linsenmair, K.E., Schulze, E.-D., Weisser, W.W., 2012. A  
814 quantitative index of land-use intensity in grasslands: Integrating mowing, grazing and  
815 fertilization. *Basic Appl Ecol* 13, 207–220. <https://doi.org/10.1016/j.baae.2012.04.001>
- 816 Bolliger, R., Prati, D., Fischer, M., 2020. Vegetation Records for Grassland EPs, 2008 - 2020. Version 2.  
817 Biodiversity Exploratories Information System. Dataset. <https://www.bexis.uni-jena.de/ddm/data>Showdata/27386>. Dataset ID = 27386.
- 819 Breiman, L., 2001. Random forests. *Mach Learn* 45, 5–32.  
820 <https://doi.org/https://doi.org/10.1023/A:1010933404324>
- 821 Brown, L.A., Ogutu, B.O., Dash, J., 2019. Estimating Forest Leaf Area Index and Canopy Chlorophyll  
822 Content with Sentinel-2: An Evaluation of Two Hybrid Retrieval Algorithms. *Remote Sens (Basel)*  
823 11, 1752. <https://doi.org/10.3390/rs11151752>
- 824 Busch, V., Klaus, V.H., Penone, C., Schäfer, D., Boch, S., Prati, D., Müller, J., Socher, S.A., Niinemets,  
825 Ü., Peñuelas, J., Hözel, N., Fischer, M., Kleinebecker, T., 2018. Nutrient stoichiometry and land  
826 use rather than species richness determine plant functional diversity. *Ecol Evol* 8, 601–616.  
827 <https://doi.org/10.1002/ece3.3609>
- 828 Caballero, G., Pezzola, A., Winschel, C., Sanchez Angonova, P., Casella, A., Orden, L., Salinero-  
829 Delgado, M., Reyes-Muñoz, P., Berger, K., Delegido, J., Verrelst, J., 2023. Synergy of Sentinel-1  
830 and Sentinel-2 Time Series for Cloud-Free Vegetation Water Content Mapping with Multi-  
831 Output Gaussian Processes. *Remote Sens (Basel)* 15, 1822. <https://doi.org/10.3390/rs15071822>
- 832 Campos-Taberner, M., Moreno-Martínez, Á., García-Haro, F., Camps-Valls, G., Robinson, N., Kattge,  
833 J., Running, S., 2018. Global Estimation of Biophysical Variables from Google Earth Engine  
834 Platform. *Remote Sens (Basel)* 10, 1167. <https://doi.org/10.3390/rs10081167>
- 835 Cavender-Bares, J., Schneider, F.D., Santos, M.J., Armstrong, A., Carnaval, A., Dahlin, K.M., Fatoyinbo,  
836 L., Hurt, G.C., Schimel, D., Townsend, P.A., Ustin, S.L., Wang, Z., Wilson, A.M., 2022. Integrating

- 837 remote sensing with ecology and evolution to advance biodiversity conservation. *Nat Ecol Evol*  
838 6, 506–519. <https://doi.org/10.1038/s41559-022-01702-5>
- 839 Chen, T., Guestrin, C., 2016. XGBoost: A scalable tree boosting system. *Proceedings of the ACM*  
840 SIGKDD International Conference on Knowledge Discovery and Data Mining 13-17-August-2016,  
841 785–794. <https://doi.org/10.1145/2939672.2939785>
- 842 Combal, B., Baret, F., Weiss, M., Trubuil, A., Macé, D., Pragnère, A., Myneni, R., Knyazikhin, Y., Wang,  
843 L., 2003. Retrieval of canopy biophysical variables from bidirectional reflectance. *Remote Sens*  
844 *Environ* 84, 1–15. [https://doi.org/10.1016/S0034-4257\(02\)00035-4](https://doi.org/10.1016/S0034-4257(02)00035-4)
- 845 Darvishzadeh, R., Atzberger, C., Skidmore, A., Schlerf, M., 2011. Mapping grassland leaf area index  
846 with airborne hyperspectral imagery: A comparison study of statistical approaches and  
847 inversion of radiative transfer models. *ISPRS Journal of Photogrammetry and Remote Sensing*  
848 66, 894–906. <https://doi.org/10.1016/J.ISPRSJPRS.2011.09.013>
- 849 de Sá, N.C., Baratchi, M., Hauser, L.T., van Bodegom, P., 2021. Exploring the Impact of Noise on  
850 Hybrid Inversion of PROSAIL RTM on Sentinel-2 Data. *Remote Sens (Basel)* 13, 648.  
851 <https://doi.org/10.3390/rs13040648>
- 852 De Vroey, M., de Vendictis, L., Zavagli, M., Bontemps, S., Heymans, D., Radoux, J., Koetz, B.,  
853 Defourny, P., 2022. Mowing detection using Sentinel-1 and Sentinel-2 time series for large scale  
854 grassland monitoring. *Remote Sens Environ* 280, 113145.  
855 <https://doi.org/10.1016/j.rse.2022.113145>
- 856 Dehghan-Shoar, M.H., Orsi, A.A., Pullanagari, R.R., Yule, I.J., 2023. A hybrid model to predict nitrogen  
857 concentration in heterogeneous grassland using field spectroscopy. *Remote Sens Environ* 285,  
858 113385. <https://doi.org/10.1016/j.rse.2022.113385>
- 859 Delegido, J., Verrelst, J., Rivera, J.P., Ruiz-Verdú, A., Moreno, J., 2015. Brown and green LAI mapping  
860 through spectral indices. *International Journal of Applied Earth Observation and*  
861 *Geoinformation* 35, 350–358. <https://doi.org/10.1016/j.jag.2014.10.001>
- 862 Dixon, A.P., Faber-Langendoen, D., Josse, C., Morrison, J., Loucks, C.J., 2014. Distribution mapping of  
863 world grassland types. *J Biogeogr* 41, 2003–2019. <https://doi.org/10.1111/jbi.12381>
- 864 Erb, K.-H., Kastner, T., Plutzar, C., Bais, A.L.S., Carvalhais, N., Fetzel, T., Gingrich, S., Haberl, H., Lauk,  
865 C., Niedertscheider, M., Pongratz, J., Thurner, M., Luyssaert, S., 2018. Unexpectedly large  
866 impact of forest management and grazing on global vegetation biomass. *Nature* 553, 73–76.  
867 <https://doi.org/10.1038/nature25138>
- 868 ESA, 2015. Sentinel-2 User Handbook Issue 1 Revision 2. Noordwijk.
- 869 Fang, H., Liang, S., Kuusk, A., 2003. Retrieving leaf area index using a genetic algorithm with a canopy  
870 radiative transfer model. *Remote Sens Environ* 85, 257–270. [https://doi.org/10.1016/S0034-4257\(03\)00005-1](https://doi.org/10.1016/S0034-4257(03)00005-1)
- 872 Féret, J., de Boissieu, F., 2022. prosail: PROSAIL leaf and canopy radiative transfer model and  
873 inversion routines. R package version 1.1.1 [WWW Document]. URL  
874 <https://gitlab.com/jbferet/prosail>
- 875 Féret, J.-B., François, C., Asner, G.P., Gitelson, A.A., Martin, R.E., Bidel, L.P.R., Ustin, S.L., le Maire, G.,  
876 Jacquemoud, S., 2008. PROSPECT-4 and 5: Advances in the leaf optical properties model

- 877 separating photosynthetic pigments. *Remote Sens Environ* 112, 3030–3043.  
878 <https://doi.org/10.1016/j.rse.2008.02.012>
- 879 Féret, J.-B., Gitelson, A.A., Noble, S.D., Jacquemoud, S., 2017. PROSPECT-D: Towards modeling leaf  
880 optical properties through a complete lifecycle. *Remote Sens Environ* 193, 204–215.  
881 <https://doi.org/10.1016/j.rse.2017.03.004>
- 882 Féret, J.-B., le Maire, G., Jay, S., Berveiller, D., Bendoula, R., Hmimina, G., Cheraiet, A., Oliveira, J.C.,  
883 Ponzoni, F.J., Solanki, T., de Boissieu, F., Chave, J., Nouvellon, Y., Porcar-Castell, A., Proisy, C.,  
884 Soudani, K., Gastellu-Etchegorry, J.-P., Lefèvre-Fonollosa, M.-J., 2019. Estimating leaf mass per  
885 area and equivalent water thickness based on leaf optical properties: Potential and limitations  
886 of physical modeling and machine learning. *Remote Sens Environ* 231, 110959.  
887 <https://doi.org/10.1016/j.rse.2018.11.002>
- 888 Fischer, M., Bosdorf, O., Gockel, S., Hänsel, F., Hemp, A., Hessenmöller, D., Korte, G., Nieschulze, J.,  
889 Pfeiffer, S., Prati, D., Renner, S., Schöning, I., Schumacher, U., Wells, K., Buscot, F., Kalko, E.K.V.,  
890 Linsenmair, K.E., Schulze, E.-D., Weisser, W.W., 2010. Implementing large-scale and long-term  
891 functional biodiversity research: The Biodiversity Exploratories. *Basic Appl Ecol* 11, 473–485.  
892 <https://doi.org/10.1016/j.baae.2010.07.009>
- 893 Friedman, J.H., 2001. Greedy function approximation: A gradient boosting machine. *Ann Stat* 29,  
894 1189–1232. <https://doi.org/10.1214/AOS/1013203451>
- 895 Fuhlendorf, S.D., Engle, D.M., 2004. Application of the fire-grazing interaction to restore a shifting  
896 mosaic on tallgrass prairie. *Journal of Applied Ecology* 41, 604–614.  
897 <https://doi.org/10.1111/j.0021-8901.2004.00937.x>
- 898 Fuhlendorf, S.D., Engle, D.M., 2001. Restoring Heterogeneity on Rangelands: Ecosystem Management  
899 Based on Evolutionary Grazing Patterns. *Bioscience* 51, 625–632.  
900 [https://doi.org/https://doi.org/10.1641/0006-3568\(2001\)051\[0625:RHOREM\]2.0.CO;2](https://doi.org/https://doi.org/10.1641/0006-3568(2001)051[0625:RHOREM]2.0.CO;2)
- 901 Gascon, F., Bouzinac, C., Thépaut, O., Jung, M., Francesconi, B., Louis, J., Lonjou, V., Lafrance, B.,  
902 Massera, S., Gaudel-Vacaresse, A., Languille, F., Alhammoud, B., Viallefont, F., Pflug, B., Bieniarz,  
903 J., Clerc, S., Pessiot, L., Trémás, T., Cadau, E., De Bonis, R., Isola, C., Martimort, P., Fernandez, V.,  
904 2017. Copernicus Sentinel-2A Calibration and Products Validation Status. *Remote Sens (Basel)* 9,  
905 584. <https://doi.org/10.3390/rs9060584>
- 906 Gholizadeh, H., Friedman, M.S., McMillan, N.A., Hammond, W.M., Hassani, K., Sams, A. V., Charles,  
907 M.D., Garrett, D.R., Joshi, O., Hamilton, R.G., Fuhlendorf, S.D., Trowbridge, A.M., Adams, H.D.,  
908 2022. Mapping invasive alien species in grassland ecosystems using airborne imaging  
909 spectroscopy and remotely observable vegetation functional traits. *Remote Sens Environ* 271,  
910 112887. <https://doi.org/10.1016/j.rse.2022.112887>
- 911 Gholizadeh, H., Rakotoarivony, M.N.A., Hassani, K., Johnson, K.G., Hamilton, R.G., Fuhlendorf, S.D.,  
912 Schneider, F.D., Bachelot, B., 2024. Advancing our understanding of plant diversity-biological  
913 invasion relationships using imaging spectroscopy. *Remote Sens Environ* 304, 114028.  
914 <https://doi.org/10.1016/j.rse.2024.114028>
- 915 Gorelick, N., Hancher, M., Dixon, M., Ilyushchenko, S., Thau, D., Moore, R., 2017. Google Earth  
916 Engine: Planetary-scale geospatial analysis for everyone. *Remote Sens Environ* 202, 18–27.  
917 <https://doi.org/10.1016/j.rse.2017.06.031>

- 918 Guerini Filho, M., Kuplich, T.M., Quadros, F.L.F. De, 2020. Estimating natural grassland biomass by  
919 vegetation indices using Sentinel 2 remote sensing data. *Int J Remote Sens* 41, 2861–2876.  
920 <https://doi.org/10.1080/01431161.2019.1697004>
- 921 Habel, J.C., Dengler, J., Janišová, M., Török, P., Wellstein, C., Wiezik, M., 2013. European grassland  
922 ecosystems: threatened hotspots of biodiversity. *Biodivers Conserv* 22, 2131–2138.  
923 <https://doi.org/10.1007/s10531-013-0537-x>
- 924 Hamilton, R.G., 2007. Restoring heterogeneity on the Tallgrass Prairie Preserve: applying the fire-  
925 grazing interaction model, in: Masters, R.E., Galley, K.E.M. (Eds.), *Proceedings of the 23rd Tall  
926 Timbers Fire Ecology Conference: Fire in Grassland and Shrubland Ecosystems*. Tall Timbers  
927 Research Station, Tallahassee, FL, pp. 163–169.
- 928 Hauser, L.T., Féret, J.-B., An Binh, N., van der Windt, N., Sil, Â.F., Timmermans, J., Soudzilovskaia,  
929 N.A., van Bodegom, P.M., 2021a. Towards scalable estimation of plant functional diversity from  
930 Sentinel-2: In-situ validation in a heterogeneous (semi-)natural landscape. *Remote Sens Environ*  
931 262, 112505. <https://doi.org/10.1016/j.rse.2021.112505>
- 932 Hauser, L.T., Timmermans, J., van der Windt, N., Sil, Â.F., César de Sá, N., Soudzilovskaia, N.A., van  
933 Bodegom, P.M., 2021b. Explaining discrepancies between spectral and in-situ plant diversity in  
934 multispectral satellite earth observation. *Remote Sens Environ* 265, 112684.  
935 <https://doi.org/10.1016/j.rse.2021.112684>
- 936 He, L., Li, A., Yin, G., Nan, X., Bian, J., 2019. Retrieval of Grassland Aboveground Biomass through  
937 Inversion of the PROSAIL Model with MODIS Imagery. *Remote Sensing* 2019, Vol. 11, Page 1597  
938 11, 1597. <https://doi.org/10.3390/RS11131597>
- 939 Helfenstein, I.S., Schneider, F.D., Schaepman, M.E., Morsdorf, F., 2022. Assessing biodiversity from  
940 space: Impact of spatial and spectral resolution on trait-based functional diversity. *Remote Sens  
941 Environ* 275, 113024. <https://doi.org/10.1016/j.rse.2022.113024>
- 942 Hinderling, J., Penone, C., Fischer, M., Prati, D., Hoelzel, N., 2023. Biomass data for grassland EPs,  
943 2009 - 2022. Version 8. Biodiversity Exploratories Information System. Dataset.  
944 <https://www.bexis.uni-jena.de/ddm/data>Showdata/31448>. Dataset ID = 31448.
- 945 Hobohm, C., Bruchmann, I., 2009. Endemische Gefäßpflanzen und ihre Habitate in Europa - Plädoyer  
946 für den Schutz der Grasland-Ökosysteme. *Berichte der Reinhold-Tüxen-Gesellschaft* 21, 142–  
947 161.
- 948 Huete, A., Didan, K., Miura, T., Rodriguez, E.P., Gao, X., Ferreira, L.G., 2002. Overview of the  
949 radiometric and biophysical performance of the MODIS vegetation indices. *Remote Sens  
950 Environ* 83, 195–213. [https://doi.org/10.1016/S0034-4257\(02\)00096-2](https://doi.org/10.1016/S0034-4257(02)00096-2)
- 951 Jacquemoud, S., Baret, F., 1990. PROSPECT: A model of leaf optical properties spectra. *Remote Sens  
952 Environ* 34, 75–91. [https://doi.org/10.1016/0034-4257\(90\)90100-Z](https://doi.org/10.1016/0034-4257(90)90100-Z)
- 953 Jacquemoud, S., Verhoef, W., Baret, F., Bacour, C., Zarco-Tejada, P.J., Asner, G.P., François, C., Ustin,  
954 S.L., 2009. PROSPECT + SAIL models: A review of use for vegetation characterization. *Remote  
955 Sens Environ* 113, S56–S66. <https://doi.org/10.1016/J.RSE.2008.01.026>
- 956 Jehle, M., Hueni, A., Damm, A., D'Odorico, P., Weyermann, J., Kneubühler, M., Schlapfer, D.,  
957 Schaepman, M.E., Meuleman, K., 2010. APEX - current status, performance and validation  
958 concept, in: 2010 IEEE Sensors. IEEE, pp. 533–537.  
959 <https://doi.org/10.1109/ICSENS.2010.5690122>

- 960 Joswig, J.S., Wirth, C., Schuman, M.C., Kattge, J., Reu, B., Wright, I.J., Sippel, S.D., Rüger, N., Richter,  
961 R., Schaepman, M.E., van Bodegom, P.M., Cornelissen, J.H.C., Díaz, S., Hattingh, W.N., Kramer,  
962 K., Lens, F., Niinemets, Ü., Reich, P.B., Reichstein, M., Römermann, C., Schrodt, F., Anand, M.,  
963 Bahn, M., Byun, C., Campetella, G., Cerabolini, B.E.L., Craine, J.M., Gonzalez-Melo, A., Gutiérrez,  
964 A.G., He, T., Higuchi, P., Jactel, H., Kraft, N.J.B., Minden, V., Onipchenko, V., Peñuelas, J., Pillar,  
965 V.D., Sosinski, Ė., Soudzilovskaia, N.A., Weiher, E., Mahecha, M.D., 2021. Climatic and soil  
966 factors explain the two-dimensional spectrum of global plant trait variation. *Nat Ecol Evol* 6, 36–  
967 50. <https://doi.org/10.1038/s41559-021-01616-8>
- 968 Kothari, S., Schweiger, A.K., 2022. Plant spectra as integrative measures of plant phenotypes. *Journal  
969 of Ecology* 110, 2536–2554. <https://doi.org/10.1111/1365-2745.13972>
- 970 Kovács, D.D., Reyes-Muñoz, P., Salinero-Delgado, M., Mészáros, V.I., Berger, K., Verrelst, J., 2023.  
971 Cloud-Free Global Maps of Essential Vegetation Traits Processed from the TOA Sentinel-3  
972 Catalogue in Google Earth Engine. *Remote Sens (Basel)* 15, 3404.  
973 <https://doi.org/10.3390/rs15133404>
- 974 Lawrence, D.M., Fisher, R.A., Koven, C.D., Oleson, K.W., Swenson, S.C., Bonan, G., Collier, N., Ghimire,  
975 B., van Kampenhout, L., Kennedy, D., Kluzek, E., Lawrence, P.J., Li, F., Li, H., Lombardozzi, D.,  
976 Riley, W.J., Sacks, W.J., Shi, M., Vertenstein, M., Wieder, W.R., Xu, C., Ali, A.A., Badger, A.M.,  
977 Bisht, G., van den Broeke, M., Brunke, M.A., Burns, S.P., Buzan, J., Clark, M., Craig, A., Dahlin, K.,  
978 Drewniak, B., Fisher, J.B., Flanner, M., Fox, A.M., Gentine, P., Hoffman, F., Keppel-Aleks, G.,  
979 Knox, R., Kumar, S., Lenaerts, J., Leung, L.R., Lipscomb, W.H., Lu, Y., Pandey, A., Pelletier, J.D.,  
980 Perket, J., Randerson, J.T., Ricciuto, D.M., Sanderson, B.M., Slater, A., Subin, Z.M., Tang, J.,  
981 Thomas, R.Q., Val Martin, M., Zeng, X., 2019. The Community Land Model Version 5:  
982 Description of New Features, Benchmarking, and Impact of Forcing Uncertainty. *J Adv Model  
983 Earth Syst* 11, 4245–4287. <https://doi.org/10.1029/2018MS001583>
- 984 Lemaire, G., Hodgson, J., Chabbi, A. (Eds.), 2011. Grassland productivity and ecosystem services. CAB  
985 International, Wallingford.
- 986 Li, C., Zhou, L., Xu, W., 2021. Estimating Aboveground Biomass Using Sentinel-2 MSI Data and  
987 Ensemble Algorithms for Grassland in the Shengjin Lake Wetland, China. *Remote Sensing* 2021,  
988 Vol. 13, Page 1595 13, 1595. <https://doi.org/10.3390/RS13081595>
- 989 Li, F., Zeng, Y., Luo, J., Ma, R., Wu, B., 2016. Modeling grassland aboveground biomass using a pure  
990 vegetation index. *Ecol Indic* 62, 279–288. <https://doi.org/10.1016/j.ecolind.2015.11.005>
- 991 Limb, R.F., Hickman, K.R., Engle, D.M., Norland, J.E., Fuhlendorf, S.D., 2007. Digital Photography:  
992 Reduced Investigator Variation in Visual Obstruction Measurements for Southern Tallgrass  
993 Prairie. *Rangel Ecol Manag* 60, 548–552. [https://doi.org/https://doi.org/10.2111/1551-5028\(2007\)60\[548:DPRIVI\]2.0.CO;2](https://doi.org/https://doi.org/10.2111/1551-5028(2007)60[548:DPRIVI]2.0.CO;2)
- 995 Liu, A., Cheng, X., Chen, Z., 2021. Performance evaluation of GEDI and ICESat-2 laser altimeter data  
996 for terrain and canopy height retrievals. *Remote Sens Environ* 264, 112571.  
997 <https://doi.org/10.1016/j.rse.2021.112571>
- 998 Liu, H., Cai, J., Ong, Y.-S., 2018. Remarks on multi-output Gaussian process regression. *Knowl Based  
999 Syst* 144, 102–121. <https://doi.org/10.1016/j.knosys.2017.12.034>
- 1000 Locherer, M., Hank, T., Danner, M., Mauser, W., 2015. Retrieval of Seasonal Leaf Area Index from  
1001 Simulated EnMAP Data through Optimized LUT-Based Inversion of the PROSAIL Model. *Remote  
1002 Sens (Basel)* 7, 10321–10346. <https://doi.org/10.3390/rs70810321>

- 1003 Louis, J., Debaecker, V., Pflug, B., Main-Knorn, M., Bieniarz, J., Mueller-Wilm, U., Cadau, E., Gascon,  
1004 F., 2016. Sentinel-2 SEN2COR: L2A processor for users, in: Ouwehand, L. (Ed.), Proceedings  
1005 Living Planet Symposium 2016. Prague, pp. 1–8.
- 1006 Martínez-Ferrer, L., Moreno-Martínez, Á., Campos-Taberner, M., García-Haro, F.J., Muñoz-Marí, J.,  
1007 Running, S.W., Kimball, J., Clinton, N., Camps-Valls, G., 2022. Quantifying uncertainty in high  
1008 resolution biophysical variable retrieval with machine learning. *Remote Sens Environ* 280,  
1009 113199. <https://doi.org/10.1016/J.RSE.2022.113199>
- 1010 Masek, J.G., Wulder, M.A., Markham, B., McCorkel, J., Crawford, C.J., Storey, J., Jenstrom, D.T., 2020.  
1011 Landsat 9: Empowering open science and applications through continuity. *Remote Sens Environ*  
1012 248, 111968. <https://doi.org/10.1016/j.rse.2020.111968>
- 1013 Mesonet, 2024. Monthly Rainfall Table: Norman (NRMN) Monthly Actual Oklahoma Mesonet Rainfall  
1014 Table (in inches) [WWW Document]. URL <https://www.mesonet.org/weather/rainfall/monthly->  
1015 rainfall-table?ref=1210 (accessed 1.4.24).
- 1016 MeteoSwiss, 2022. Data portal for teaching and research (IDAweb) [WWW Document]. URL  
1017 <https://www.meteoswiss.admin.ch/services-and-publications/service/weather-and-climate->  
1018 products/data-portal-for-teaching-and-research.html (accessed 11.21.23).
- 1019 Meyer, H., Pebesma, E., 2020. Predicting into unknown space? Estimating the area of applicability of  
1020 spatial prediction models. *Methods Ecol Evol* 12, 1620–1633. <https://doi.org/10.1111/2041->  
1021 210X.13650
- 1022 Moreno-Martinez, A., Camps-Valls, G., Kattge, J., Robinson, N., Reichstein, M., van Bodegom, P.,  
1023 Kramer, K., Cornelissen, J.H.C., Reich, P., Bahn, M., Niinemets, Ülo, Peñuelas, J., Craine, J.,  
1024 Cerabolini, B.E.L., Minden, V., Laughlin, D.C., Sack, L., Allred, B., Baraloto, C., Byun, C.,  
1025 Soudzilovskaia, N.A., Running, S.W., 2020. A Methodology to Derive Global Maps of Leaf Traits  
1026 Using Remote Sensing and Climate Data. *Remote Sens Environ* 218, 69–88.  
1027 <https://doi.org/10.1016/j.rse.2018.09.006>
- 1028 Müller-Wilm, U., Louis, J., Richter, R., Gascon, F., Niezette, M., 2013. Sentinel-2 level 2A prototype  
1029 processor: architecture, algorithms and first results, in: Proceedings of the ESA Living Planet  
1030 Symposium. Edinburgh, UK, pp. 9–13.
- 1031 Muñoz Sabater, J., 2019. ERA5-Land hourly data from 1950 to present. Copernicus Climate Change  
1032 Service (C3S) Climate Data Store. <https://doi.org/10.24381/cds.e2161bac>
- 1033 Muro, J., Linstädter, A., Magdon, P., Wöllauer, S., Männer, F.A., Schwarz, L.-M., Ghazaryan, G.,  
1034 Schultz, J., Malenovský, Z., Dubovýk, O., 2022. Predicting plant biomass and species richness in  
1035 temperate grasslands across regions, time, and land management with remote sensing and  
1036 deep learning. *Remote Sens Environ* 282, 113262. <https://doi.org/10.1016/j.rse.2022.113262>
- 1037 O'Mara, F.P., 2012. The role of grasslands in food security and climate change. *Ann Bot* 110, 1263–  
1038 1270. <https://doi.org/10.1093/aob/mcs209>
- 1039 Ostrowski, A., Nieschulze, J., Schulze, E.D., König-Ries, B., 2020. Coordinates and Inventory Overview  
1040 of all Grid Plots (GPs). Version 6. Biodiversity Exploratories Information System. Dataset.  
1041 <https://www.bexis.uni-jena.de>. Dataset ID = 20907.
- 1042 Pedregosa, F., Varoquaux, G., Gramfort, A., Michel, V., Thirion, B., Grisel, O., Blondel, M., Müller, A.,  
1043 Nothman, J., Louppe, G., Prettenhofer, P., Weiss, R., Dubourg, V., Vanderplas, J., Passos, A.,

- 1044 Cournapeau, D., Brucher, M., Perrot, M., Duchesnay, É., 2012. Scikit-learn: Machine Learning in  
1045 Python. *Journal of Machine Learning Research* 12, 2825–2830.
- 1046 Pipia, L., Muñoz-Marí, J., Amin, E., Belda, S., Camps-Valls, G., Verrelst, J., 2019. Fusing optical and SAR  
1047 time series for LAI gap filling with multioutput Gaussian processes. *Remote Sens Environ* 235,  
1048 111452. <https://doi.org/10.1016/j.rse.2019.111452>
- 1049 Poortinga, A., Tenneson, K., Shapiro, A., Nquyen, Q., San Aung, K., Chishtie, F., Saah, D., 2019.  
1050 Mapping Plantations in Myanmar by Fusing Landsat-8, Sentinel-2 and Sentinel-1 Data along  
1051 with Systematic Error Quantification. *Remote Sens (Basel)* 11, 831.  
1052 <https://doi.org/10.3390/rs11070831>
- 1053 Punalekar, S.M., Verhoef, A., Quaife, T.L., Humphries, D., Bermingham, L., Reynolds, C.K., 2018.  
1054 Application of Sentinel-2A data for pasture biomass monitoring using a physically based  
1055 radiative transfer model. *Remote Sens Environ* 218, 207–220.  
1056 <https://doi.org/10.1016/j.rse.2018.09.028>
- 1057 Quan, X., He, B., Yebra, M., Yin, C., Liao, Z., Zhang, X., Li, X., 2017. A radiative transfer model-based  
1058 method for the estimation of grassland aboveground biomass. *International Journal of Applied  
1059 Earth Observation and Geoinformation* 54, 159–168.  
1060 <https://doi.org/10.1016/J.JAG.2016.10.002>
- 1061 R Core Team, 2021. R: A Language and Environment for Statistical Computing. Vienna.
- 1062 Raab, C., Riesch, F., Tonn, B., Barrett, B., Meißner, M., Balkenhol, N., Isselstein, J., 2020. Target-  
1063 oriented habitat and wildlife management: estimating forage quantity and quality of semi-  
1064 natural grasslands with Sentinel-1 and Sentinel-2 data. *Remote Sens Ecol Conserv* 6, 381–398.  
1065 <https://doi.org/10.1002/rse2.149>
- 1066 Ranghetti, M., Boschetti, M., Ranghetti, L., Tagliabue, G., Panigada, C., Gianinetto, M., Verrelst, J.,  
1067 Candiani, G., 2022. Assessment of maize nitrogen uptake from PRISMA hyperspectral data  
1068 through hybrid modelling. *Eur J Remote Sens.* <https://doi.org/10.1080/22797254.2022.2117650>
- 1069 Rasmussen, C.E., Williams, C.K.I., 2006. Gaussian Processes for Machine Learning. MIT Press,  
1070 Cambridge, MA.
- 1071 Reinermann, S., Asam, S., Kuenzer, C., 2020. Remote Sensing of Grassland Production and  
1072 Management—A Review. *Remote Sens (Basel)* 12, 1949. <https://doi.org/10.3390/rs12121949>
- 1073 Rempfler, T., Rossi, C., Schweizer, J., Peters, W., Signer, C., Filli, F., Jenny, H., Hackländer, K.,  
1074 Buchmann, S., Anderwald, P., 2024. Remote sensing reveals the role of forage quality and  
1075 quantity for summer habitat use in red deer. *Mov Ecol* 12, 80. <https://doi.org/10.1186/s40462-024-00521-6>
- 1077 Reuter, H.I., Nelson, A., Jarvis, A., 2007. An evaluation of void-filling interpolation methods for SRTM  
1078 data. *International Journal of Geographical Information Science* 21, 983–1008.  
1079 <https://doi.org/10.1080/13658810601169899>
- 1080 Richter, K., Atzberger, C., Hank, T.B., Mauser, W., 2012. Derivation of biophysical variables from Earth  
1081 observation data: validation and statistical measures. *J Appl Remote Sens* 6, 063557–1.  
1082 <https://doi.org/10.1117/1.JRS.6.063557>

- 1083 Richter, R., Schläpfer, D., 2002. Geo-atmospheric processing of airborne imaging spectrometry data.  
1084 Part 2: Atmospheric/topographic correction. *Int J Remote Sens* 23, 2631–2649.  
1085 <https://doi.org/10.1080/01431160110115834>
- 1086 Rivera, J., Verrelst, J., Gómez-Dans, J., Muñoz-Marí, J., Moreno, J., Camps-Valls, G., 2015. An Emulator  
1087 Toolbox to Approximate Radiative Transfer Models with Statistical Learning. *Remote Sens*  
1088 (*Basel*) 7, 9347–9370. <https://doi.org/10.3390/rs70709347>
- 1089 Rivera, J., Verrelst, J., Leonenko, G., Moreno, J., 2013. Multiple Cost Functions and Regularization  
1090 Options for Improved Retrieval of Leaf Chlorophyll Content and LAI through Inversion of the  
1091 PROSAIL Model. *Remote Sens* (*Basel*) 5, 3280–3304. <https://doi.org/10.3390/rs5073280>
- 1092 Rossi, C., Kneubühler, M., Schütz, M., Schaepman, M.E., Haller, R.M., Risch, A.C., 2020. From local to  
1093 regional: Functional diversity in differently managed alpine grasslands. *Remote Sens Environ*  
1094 236, 111415. <https://doi.org/10.1016/j.rse.2019.111415>
- 1095 Rossi, C., McMillan, N.A., Schweizer, J.M., Gholizadeh, H., Groen, M., Ioannidis, N., Hauser, L.T., 2024.  
1096 Parcel level temporal variance of remotely sensed spectral reflectance predicts plant diversity.  
1097 *Environmental Research Letters* 19, 074023. <https://doi.org/10.1088/1748-9326/ad545a>
- 1098 Roudier, P., 2021. Introduction to conditioned Latin hypercube sampling with the clhs package  
1099 [WWW Document]. URL <https://CRAN.R-project.org/package=clhs>
- 1100 Roy, D.P., Wulder, M.A., Loveland, T.R., C.E., W., Allen, R.G., Anderson, M.C., Helder, D., Irons, J.R.,  
1101 Johnson, D.M., Kennedy, R., Scambos, T.A., Schaaf, C.B., Schott, J.R., Sheng, Y., Vermote, E.F.,  
1102 Belward, A.S., Bindschadler, R., Cohen, W.B., Gao, F., Hippel, J.D., Hostert, P., Huntington, J.,  
1103 Justice, C.O., Kilic, A., Kovalskyy, V., Lee, Z.P., Lymburner, L., Masek, J.G., McCorkel, J., Shuai, Y.,  
1104 Trezza, R., Vogelmann, J., Wynne, R.H., Zhu, Z., 2014. Landsat-8: Science and product vision for  
1105 terrestrial global change research. *Remote Sens Environ* 145, 154–172.  
1106 <https://doi.org/10.1016/j.rse.2014.02.001>
- 1107 Schaepman, M.E., Jehle, M., Hueni, A., D'Odorico, P., Damm, A., Weyermann, J., Schneider, F.D.,  
1108 Laurent, V., Popp, C., Seidel, F.C., Lenhard, K., Gege, P., Küchler, C., Brazile, J., Kohler, P., De Vos,  
1109 L., Meuleman, K., Meynart, R., Schläpfer, D., Kneubühler, M., Itten, K.I., 2015. Advanced  
1110 radiometry measurements and Earth science applications with the Airborne Prism Experiment  
1111 (APEX). *Remote Sens Environ* 158, 207–219. <https://doi.org/10.1016/j.rse.2014.11.014>
- 1112 Schiefer, F., Schmidlein, S., Kattenborn, T., 2021. The retrieval of plant functional traits from canopy  
1113 spectra through RTM-inversions and statistical models are both critically affected by plant  
1114 phenology. *Ecol Indic* 121, 107062. <https://doi.org/10.1016/j.ecolind.2020.107062>
- 1115 Schläpfer, D., Richter, R., 2002. Geo-atmospheric processing of airborne imaging spectrometry data.  
1116 Part 1: Parametric orthorectification. *Int J Remote Sens* 23, 2609–2630.  
1117 <https://doi.org/10.1080/01431160110115825>
- 1118 Schweiger, A.K., 2020. Spectral Field Campaigns: Planning and Data Collection, in: *Remote Sensing of*  
1119 *Plant Biodiversity*. Springer International Publishing, Cham, pp. 385–423.  
1120 [https://doi.org/10.1007/978-3-030-33157-3\\_15](https://doi.org/10.1007/978-3-030-33157-3_15)
- 1121 Schweiger, A.K., Risch, A.C., Damm, A., Kneubühler, M., Haller, R., Schaepman, M.E., Schütz, M.,  
1122 2015a. Using imaging spectroscopy to predict above-ground plant biomass in alpine grasslands  
1123 grazed by large ungulates. *Journal of Vegetation Science* 26, 175–190.  
1124 <https://doi.org/10.1111/jvs.12214>

- 1125 Schweiger, A.K., Schütz, M., Anderwald, P., Schaepman, M.E., Kneubühler, M., Haller, R., Risch, A.C.,  
1126 2015b. Foraging ecology of three sympatric ungulate species – Behavioural and resource maps  
1127 indicate differences between chamois, ibex and red deer. *Mov Ecol* 3, 6.  
1128 <https://doi.org/10.1186/s40462-015-0033-x>
- 1129 Schweiger, A.K., Schütz, M., Risch, A.C., Kneubühler, M., Haller, R., Schaepman, M.E., 2017. How to  
1130 predict plant functional types using imaging spectroscopy: linking vegetation community traits,  
1131 plant functional types and spectral response. *Methods Ecol Evol* 8, 86–95.  
1132 <https://doi.org/10.1111/2041-210X.12642>
- 1133 Schwieder, M., Buddeberg, M., Kowalski, K., Pföch, K., Bartsch, J., Bach, H., Pickert, J., Hostert, P.,  
1134 2020. Estimating Grassland Parameters from Sentinel-2: A Model Comparison Study. *PFG –*  
1135 *Journal of Photogrammetry, Remote Sensing and Geoinformation Science* 88, 379–390.  
1136 <https://doi.org/10.1007/s41064-020-00120-1>
- 1137 scikit-learn Developers, 2023. ConstantKernel [WWW Document]. URL [https://scikit-learn.org/stable/modules/generated/sklearn.gaussian\\_process.kernels.ConstantKernel.html](https://scikit-learn.org/stable/modules/generated/sklearn.gaussian_process.kernels.ConstantKernel.html)  
1138 (accessed 10.12.23).
- 1140 Sherrill, C.W., 2019. Analyzing sericea lespedeza (*lespedeza cuneata*) management practices and the  
1141 importance of forbs in the diet of cattle and bison on tallgrass prairie (Master's Thesis).  
1142 Oklahoma State University, Stillwater, OK.
- 1143 Shoko, C., Mutanga, O., Dube, T., 2016. Progress in the remote sensing of C3 and C4 grass species  
1144 aboveground biomass over time and space. *ISPRS Journal of Photogrammetry and Remote*  
1145 *Sensing* 120, 13–24. <https://doi.org/10.1016/J.ISPRSJPRS.2016.08.001>
- 1146 Si, Y., Schlerf, M., Zurita-Milla, R., Skidmore, A., Wang, T., 2012. Mapping spatio-temporal variation of  
1147 grassland quantity and quality using MERIS data and the PROSAIL model. *Remote Sens Environ*  
1148 121, 415–425. <https://doi.org/10.1016/j.rse.2012.02.011>
- 1149 Socher, S.A., Prati, D., Boch, S., Müller, J., Klaus, V.H., Hözel, N., Fischer, M., 2012. Direct and  
1150 productivity-mediated indirect effects of fertilization, mowing and grazing on grassland species  
1151 richness. *Journal of Ecology* 100, 1391–1399. <https://doi.org/10.1111/j.1365-2745.2012.02020.x>
- 1153 Stevens, A., Ramirez-Lopez, L., 2022. An introduction to the prospectr package [WWW Document].  
1154 URL <https://CRAN.R-project.org/package=prospectr>
- 1155 Tagliabue, G., Boschetti, M., Bramati, G., Candiani, G., Colombo, R., Nutini, F., Pompilio, L., Rivera-  
1156 Caicedo, J.P., Rossi, M., Rossini, M., Verrelst, J., Panigada, C., 2022. Hybrid retrieval of crop traits  
1157 from multi-temporal PRISMA hyperspectral imagery. *ISPRS Journal of Photogrammetry and*  
1158 *Remote Sensing* 187, 362–377. <https://doi.org/10.1016/j.isprsjprs.2022.03.014>
- 1159 The Nature Conservancy, 2023. Joseph H. Williams Tallgrass Prairie Preserve [WWW Document]. URL  
1160 <https://www.nature.org/en-us/get-involved/how-to-help/places-we-protect/tallgrass-prairie-preserve/> (accessed 3.29.23).
- 1162 Van Vooren, L., Reubens, B., Broekx, S., Reheul, D., Verheyen, K., 2018. Assessing the impact of  
1163 grassland management extensification in temperate areas on multiple ecosystem services and  
1164 biodiversity. *Agric Ecosyst Environ* 267, 201–212. <https://doi.org/10.1016/j.agee.2018.08.016>
- 1165 Vapnik, V., Golowich, S.E., Smola, A., 1997. Support vector method for function approximation,  
1166 regression estimation, and signal processing. *Adv Neural Inf Process Syst* 281–287.

- 1167 Verhoef, W., Jia, L., Xiao, Q., Su, Z., 2007. Unified Optical-Thermal Four-Stream Radiative Transfer  
1168 Theory for Homogeneous Vegetation Canopies. *IEEE Transactions on Geoscience and Remote*  
1169 *Sensing* 45, 1808–1822. <https://doi.org/10.1109/TGRS.2007.895844>
- 1170 Verrelst, J., Alonso, L., Rivera Caicedo, J.P., Moreno, J., Camps-Valls, G., 2013a. Gaussian Process  
1171 Retrieval of Chlorophyll Content From Imaging Spectroscopy Data. *IEEE J Sel Top Appl Earth Obs*  
1172 *Remote Sens* 6, 867–874. <https://doi.org/10.1109/JSTARS.2012.2222356>
- 1173 Verrelst, J., Camps-Valls, G., Muñoz-Marí, J., Rivera, J.P., Veroustraete, F., Clevers, J.G.P.W., Moreno,  
1174 J., 2015. Optical remote sensing and the retrieval of terrestrial vegetation bio-geophysical  
1175 properties – A review. *ISPRS Journal of Photogrammetry and Remote Sensing* 108, 273–290.  
1176 <https://doi.org/10.1016/j.isprsjprs.2015.05.005>
- 1177 Verrelst, J., Dethier, S., Rivera, J.P., Munoz-Mari, J., Camps-Valls, G., Moreno, J., 2016. Active Learning  
1178 Methods for Efficient Hybrid Biophysical Variable Retrieval. *IEEE Geoscience and Remote*  
1179 *Sensing Letters* 13, 1012–1016. <https://doi.org/10.1109/LGRS.2016.2560799>
- 1180 Verrelst, J., Halabuk, A., Atzberger, C., Hank, T., Steinhauser, S., Berger, K., 2023. A comprehensive  
1181 survey on quantifying non-photosynthetic vegetation cover and biomass from imaging  
1182 spectroscopy. *Ecol Indic* 155, 110911. <https://doi.org/10.1016/j.ecolind.2023.110911>
- 1183 Verrelst, J., Muñoz, J., Alonso, L., Delegido, J., Rivera, J.P., Camps-Valls, G., Moreno, J., 2012. Machine  
1184 learning regression algorithms for biophysical parameter retrieval: Opportunities for Sentinel-2  
1185 and -3. *Remote Sens Environ* 118, 127–139. <https://doi.org/10.1016/j.rse.2011.11.002>
- 1186 Verrelst, J., Rivera Caicedo, J., Muñoz-Marí, J., Camps-Valls, G., Moreno, J., 2017. SCOPE-Based  
1187 Emulators for Fast Generation of Synthetic Canopy Reflectance and Sun-Induced Fluorescence  
1188 Spectra. *Remote Sens (Basel)* 9, 927. <https://doi.org/10.3390/rs9090927>
- 1189 Verrelst, J., Rivera, J.P., Leonenko, G., Alonso, L., Moreno, J., 2014. Optimizing LUT-Based RTM  
1190 Inversion for Semiautomatic Mapping of Crop Biophysical Parameters from Sentinel-2 and -3  
1191 Data: Role of Cost Functions. *IEEE Transactions on Geoscience and Remote Sensing* 52, 257–  
1192 269. <https://doi.org/10.1109/TGRS.2013.2238242>
- 1193 Verrelst, J., Rivera, J.P., Moreno, J., Camps-Valls, G., 2013b. Gaussian processes uncertainty estimates  
1194 in experimental Sentinel-2 LAI and leaf chlorophyll content retrieval. *ISPRS Journal of*  
1195 *Photogrammetry and Remote Sensing* 86, 157–167.  
1196 <https://doi.org/10.1016/j.isprsjprs.2013.09.012>
- 1197 Verrelst, J., Rivera-Caicedo, J.P., Reyes-Muñoz, P., Morata, M., Amin, E., Tagliabue, G., Panigada, C.,  
1198 Hank, T., Berger, K., 2021. Mapping landscape canopy nitrogen content from space using  
1199 PRISMA data. *ISPRS Journal of Photogrammetry and Remote Sensing* 178, 382–395.  
1200 <https://doi.org/10.1016/j.isprsjprs.2021.06.017>
- 1201 Wang, G., Liu, S., Liu, T., Fu, Z., Yu, J., Xue, B., 2019. Modelling above-ground biomass based on  
1202 vegetation indexes: a modified approach for biomass estimation in semi-arid grasslands. *Int J*  
1203 *Remote Sens* 40, 3835–3854. <https://doi.org/10.1080/01431161.2018.1553319>
- 1204 Wang, Z., Féret, J.-B., Liu, N., Sun, Z., Yang, L., Geng, S., Zhang, H., Chlus, A., Kruger, E.L., Townsend,  
1205 P.A., 2023. Generality of leaf spectroscopic models for predicting key foliar functional traits  
1206 across continents: A comparison between physically- and empirically-based approaches.  
1207 *Remote Sens Environ* 293, 113614. <https://doi.org/10.1016/j.rse.2023.113614>

- 1208 Wellstein, C., Chelli, S., Campetella, G., Bartha, S., Galiè, M., Spada, F., Canullo, R., 2013. Intraspecific  
1209 phenotypic variability of plant functional traits in contrasting mountain grasslands habitats.  
1210 *Biodivers Conserv* 22, 2353–2374. <https://doi.org/10.1007/s10531-013-0484-6>
- 1211 White, R., Murray, S., Rohweder, M., 2000. Pilot Analysis of Global Ecosystems: Grassland  
1212 Ecosystems. WRI Publications, Hapden Station, Baltimore, MD.
- 1213 Woher, M., Berger, K., Verrelst, J., Hank, T., 2022. Retrieval of carbon content and biomass from  
1214 hyperspectral imagery over cultivated areas. *ISPRS Journal of Photogrammetry and Remote*  
1215 *Sensing* 193, 104–114. <https://doi.org/10.1016/j.isprsjprs.2022.09.003>
- 1216 Woodcock, C.E., 2002. Uncertainty in Remote Sensing, in: Foody, G.M., Atkinson, P.M. (Eds.),  
1217 Uncertainty in Remote Sensing and GIS. Wiley, Chichester, pp. 19–24.  
1218 <https://doi.org/10.1002/0470035269.ch2>
- 1219 Xu, D., Guo, X., Li, Z., Yang, X., Yin, H., 2014. Measuring the dead component of mixed grassland with  
1220 Landsat imagery. *Remote Sens Environ* 142, 33–43. <https://doi.org/10.1016/j.rse.2013.11.017>
- 1221 Yuan, H., Ma, R., Atzberger, C., Li, F., Loiselle, S., Luo, J., 2015. Estimating Forest fAPAR from  
1222 Multispectral Landsat-8 Data Using the Invertible Forest Reflectance Model INFORM. *Remote*  
1223 *Sens (Basel)* 7, 7425–7446. <https://doi.org/10.3390/rs70607425>
- 1224 Zeng, Y., Hao, D., Park, T., Zhu, P., Huete, A., Myneni, R., Knyazikhin, Y., Qi, J., Nemani, R.R., Li, F.,  
1225 Huang, J., Gao, Y., Li, B., Ji, F., Köhler, P., Frankenberg, C., Berry, J.A., Chen, M., 2023. Structural  
1226 complexity biases vegetation greenness measures. *Nat Ecol Evol* 7, 1790–1798.  
1227 <https://doi.org/10.1038/s41559-023-02187-6>
- 1228 Zhang, F., Bennett, J.A., Zhang, B., Zhao, T., Bai, K., Zhao, M., Han, G., 2023. Responses of grassland  
1229 productivity to mowing intensity and precipitation variability in a temperate steppe. *Oecologia*  
1230 201, 259–268. <https://doi.org/10.1007/s00442-022-05305-6>
- 1231 Zhao, Y., Liu, Z., Wu, J., 2020. Grassland ecosystem services: a systematic review of research  
1232 advances and future directions. *Landsc Ecol* 35, 793–814. <https://doi.org/10.1007/s10980-020-00980-3>
- 1234 Zupanc, A., 2017. Improving Cloud Detection with Machine Learning [WWW Document]. URL  
1235 <https://medium.com/sentinel-hub/improving-cloud-detection-with-machine-learning-c09dc5d7cf13> (accessed 9.28.21).
- 1237

1    **Appendix A**

2    **Section A.1: Pre-processing of APEX data**

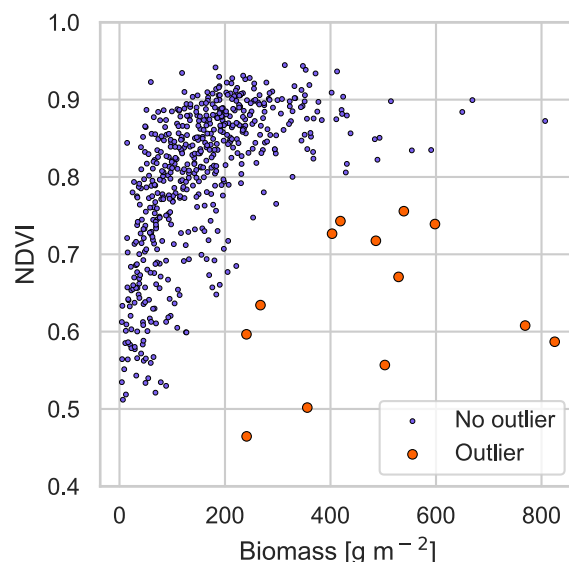
3    Remote sensing data for the 365 plots inside the Swiss National Park (SNP) were acquired on  
4    24 June 2010, 26 June 2011, 29 June 2012, and 12 July 2013 with the Airborne Prism  
5    Experiment (APEX) imaging spectrometer (Jehle et al., 2010; Schaepman et al., 2015). Of 334  
6    spectral bands in the wavelength region from 380 to 2500 nm, 285 (2011), 301 (2011), 299  
7    (2012), and 284 bands (2013) remained after noise removal. APEX data were resampled to 2  
8    m pixel size using nearest neighbor interpolation and the parametric geocoding procedure  
9    PARGE (Schläpfer and Richter, 2002) and the airborne atmospheric and topographic correction  
10   model ATCOR-4 (Richter and Schläpfer, 2002) were used for geometric and atmospheric  
11   correction, respectively (Schweiger et al., 2015). We considered the 33 plots in 2010 and 9 plots  
12   in 2011 covered by two flight strips as individual samples, resulting in 407 samples. APEX  
13   spectral reflectance was resampled to the Sentinel-2 bands (ESA, 2015) using the prospectR R  
14   package *v0.2.6* (Stevens and Ramirez-Lopez, 2022) individually for each year because of  
15   changing APEX spectral response functions.

16    **Section A.2: Outliers of ALB/HAI/SCH sites**

17    The following condition (Equation A.1) was used to determine if a sample from the  
18    ALB/HAI/SCH sites was discarded due to an unusual biomass-Normalized Difference  
19    Vegetation Index (NDVI) relation while accounting for the saturation effect of NDVI (Huete et  
20    al., 1997; Van Der Meer et al., 2001):

21                          
$$NDVI < \frac{biomass [g m^{-2}]}{400} AND NDVI < 0.8 \text{ (A.1)}$$

22    The condition was met for 13 samples of 12 different plots (Figure A.1), for which we  
23    removed all samples from 2017-2020.



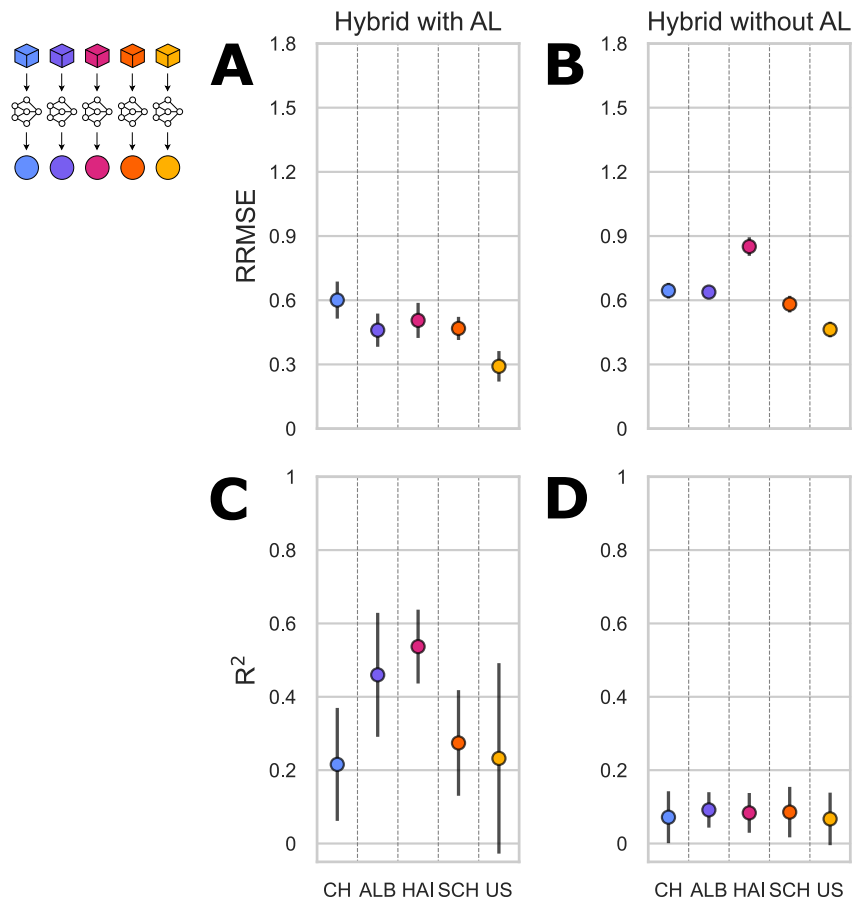
24

25    *Figure A.1: Biomass content of the ALB, HAI, and SCH samples before sample selection plotted against the Normalized  
26    Difference Vegetation Index (NDVI). ALB: Schwäbische Alb, HAI: Hainich-Dün, SCH: Schorfheide-Chorin.*

27

28 **Section A.3: Local performance of hybrid models without the use of AL**

29 Look-up tables (LUTs) generated with radiative transfer models (RTMs) such as PROSAIL are  
30 subject to inherent ill-posedness as the inversion does not necessarily lead to a unique solution  
31 (Combal et al., 2003). Additionally, such a LUT might include spectra simulated based on  
32 ecologically meaningless parameter combinations. Hence, prior knowledge can be used to  
33 subset the LUT based on correlations between plant traits (Schiefer et al., 2021). In this study,  
34 we used prior knowledge to define the value ranges and distributions of the selectable  
35 parameters, but we did not use prior information to further subset the LUT since covariances  
36 between traits might be site-specific and generating different LUTs for the study sites would  
37 have prevented any meaningful analysis of transferability. Instead, Active Learning (AL) was  
38 used to select the most informative spectra from the LUT (Verrelst et al., 2016).  
39 Correspondingly, not using AL leads to models being trained on the full LUT containing  
40 redundant and/or unrealistic information and drastically diminished model performance as  
41 illustrated in Figure A.2. Furthermore, without AL, model training is also independent of the  
42 optimization data, since no optimization of the training data takes place. Therefore, the  
43 inclusion of hybrid models without the use of AL for the systematic model comparison was  
44 waived.



45

46 *Figure A.2: Mean relative root-mean-square error (RRMSE, A, B) and coefficient of determination ( $R^2$ , C, D)  $\pm 1$  standard*  
 47 *deviation for the local hybrid models with (A, C) and without (B, D) the use of Active Learning (AL) with an initial training set*  
 48 *size of 2%. CH: Switzerland, ALB: Schwäbische Alb, HAI: Hainich-Dün, SCH: Schorfheide-Chorin, US: United States.*

49 **Section A.4: Cross-validation performance of local empirical models**

50 *Table A.1: Cross-validation performance of local empirical models. The parameters correspond to the best-performing*  
 51 *combination of parameters tested during the fivefold cross-validation. CH: Switzerland, ALB: Schwäbische Alb, HAI: Hainich-*  
 52 *Dün, SCH: Schorfheide-Chorin, US: United States, RFR: Random Forest regression, SVR: Support Vector regression, XGB:*  
 53 *Extreme Gradient Boosting regression, GPR: Gaussian Process regression, R<sup>2</sup>: coefficient of determination, RMSE: root-mean-*  
 54 *square error, RRMSE: relative root-mean-square error. Nomenclature of parameter names for RFR, SVR, and GPR according*  
 55 *to Pedregosa et al. (2012), for XGB according to Chen and Guestrin (2016).*

Site	Model	Seed	Parameters	R <sup>2</sup>	RMSE [g m <sup>-2</sup> ]	RRMSE
CH	RFR	1	'max_depth': None, 'max_features': 'sqrt', 'max_leaf_nodes': None, 'min_samples_leaf': 1, 'n_estimators': 100	0.26 2	97.383	0.567
CH	RFR	2	'max_depth': 5, 'max_features': 'sqrt', 'max_leaf_nodes': None, 'min_samples_leaf': 1, 'n_estimators': 100	0.22	97.707	0.559
CH	RFR	3	'max_depth': None, 'max_features': 10, 'max_leaf_nodes': 10, 'min_samples_leaf': 2, 'n_estimators': 100	0.18 4	104.372	0.595
CH	RFR	4	'max_depth': None, 'max_features': 10, 'max_leaf_nodes': None, 'min_samples_leaf': 2, 'n_estimators': 100	0.25	98.643	0.561
CH	RFR	5	'max_depth': 10, 'max_features': 10, 'max_leaf_nodes': None, 'min_samples_leaf': 1, 'n_estimators': 200	0.23 9	97.227	0.553
CH	RFR	6	'max_depth': 10, 'max_features': 'sqrt', 'max_leaf_nodes': None, 'min_samples_leaf': 1, 'n_estimators': 100	0.22 1	94.349	0.55
CH	RFR	7	'max_depth': None, 'max_features': 10, 'max_leaf_nodes': 10, 'min_samples_leaf': 2, 'n_estimators': 100	0.25 4	100.899	0.571
CH	RFR	8	'max_depth': 5, 'max_features': 'sqrt', 'max_leaf_nodes': 20, 'min_samples_leaf': 1, 'n_estimators': 200	0.21 7	99.517	0.578
CH	RFR	9	'max_depth': 5, 'max_features': 'sqrt', 'max_leaf_nodes': None, 'min_samples_leaf': 5, 'n_estimators': 200	0.17 2	104.461	0.593
CH	RFR	10	'max_depth': None, 'max_features': 'sqrt', 'max_leaf_nodes': None, 'min_samples_leaf': 2, 'n_estimators': 500	0.24 3	97.024	0.548
CH	SVR	1	'svr_C': 10, 'svr_epsilon': 0.01, 'svr_gamma': 'scale', 'svr_kernel': 'linear'	0.32 3	95.135	0.555
CH	SVR	2	'svr_C': 1, 'svr_epsilon': 1, 'svr_gamma': 'scale', 'svr_kernel': 'linear'	0.22	96.989	0.554
CH	SVR	3	'svr_C': 100, 'svr_epsilon': 1, 'svr_gamma': 'scale', 'svr_kernel': 'linear'	0.18 2	96.688	0.558
CH	SVR	4	'svr_C': 1, 'svr_epsilon': 1, 'svr_gamma': 'scale', 'svr_kernel': 'linear'	0.22	98.606	0.566
CH	SVR	5	'svr_C': 100, 'svr_epsilon': 0.01, 'svr_gamma': 'auto', 'svr_kernel': 'rbf'	0.29 4	93.806	0.527
CH	SVR	6	'svr_C': 10, 'svr_epsilon': 0.01, 'svr_gamma': 'scale', 'svr_kernel': 'linear'	0.22 8	96.36	0.563
CH	SVR	7	'svr_C': 100, 'svr_epsilon': 1, 'svr_gamma': 'scale', 'svr_kernel': 'linear'	0.29 6	93.581	0.531
CH	SVR	8	'svr_C': 1, 'svr_epsilon': 1, 'svr_gamma': 'scale', 'svr_kernel': 'linear'	0.25 9	96.224	0.555
CH	SVR	9	'svr_C': 10, 'svr_epsilon': 0.1, 'svr_gamma': 'scale', 'svr_kernel': 'linear'	0.22 7	96.138	0.549
CH	SVR	10	'svr_C': 1, 'svr_epsilon': 1, 'svr_gamma': 'scale', 'svr_kernel': 'linear'	0.20 5	97.674	0.555
CH	XGB	1	'xgb_colsample_bytree': 0.8, 'xgb_gamma': 0, 'xgb_learning_rate': 0.01, 'xgb_max_depth': 7, 'xgb_n_estimators': 300, 'xgb_subsample': 1.0	0.19 8	96.853	0.574
CH	XGB	2	'xgb_colsample_bytree': 0.8, 'xgb_gamma': 0, 'xgb_learning_rate': 0.1, 'xgb_max_depth': 3, 'xgb_n_estimators': 100, 'xgb_subsample': 0.8	0.21 7	99.454	0.567
CH	XGB	3	'xgb_colsample_bytree': 0.8, 'xgb_gamma': 0, 'xgb_learning_rate': 0.1, 'xgb_max_depth': 9, 'xgb_n_estimators': 100, 'xgb_subsample': 1.0	0.18 1	102.339	0.603
CH	XGB	4	'xgb_colsample_bytree': 0.8, 'xgb_gamma': 0.2, 'xgb_learning_rate': 0.2, 'xgb_max_depth': 7, 'xgb_n_estimators': 100, 'xgb_subsample': 0.8	0.24 3	98.511	0.562
CH	XGB	5	'xgb_colsample_bytree': 1.0, 'xgb_gamma': 0.2, 'xgb_learning_rate': 0.2, 'xgb_max_depth': 7, 'xgb_n_estimators': 200, 'xgb_subsample': 0.8	0.22 5	90.404	0.523
CH	XGB	6	'xgb_colsample_bytree': 0.8, 'xgb_gamma': 0.1, 'xgb_learning_rate': 0.1, 'xgb_max_depth': 7, 'xgb_n_estimators': 300, 'xgb_subsample': 0.8	0.26 6	90.79	0.529
CH	XGB	7	'xgb_colsample_bytree': 0.8, 'xgb_gamma': 0, 'xgb_learning_rate': 0.01, 'xgb_max_depth': 3, 'xgb_n_estimators': 300, 'xgb_subsample': 1.0	0.16	98.689	0.579
CH	XGB	8	'xgb_colsample_bytree': 0.8, 'xgb_gamma': 0.1, 'xgb_learning_rate': 0.1, 'xgb_max_depth': 7, 'xgb_n_estimators': 300, 'xgb_subsample': 1.0	0.22 9	93.968	0.555
CH	XGB	9	'xgb_colsample_bytree': 0.8, 'xgb_gamma': 0, 'xgb_learning_rate': 0.1, 'xgb_max_depth': 7, 'xgb_n_estimators': 100, 'xgb_subsample': 0.8	0.15 7	101.16	0.583
CH	XGB	10	'xgb_colsample_bytree': 1.0, 'xgb_gamma': 0.1, 'xgb_learning_rate': 0.1, 'xgb_max_depth': 5, 'xgb_n_estimators': 300, 'xgb_subsample': 0.8	0.24 9	97.957	0.562
CH	GPR	1	1.04**2 * RBF(length_scale=0.555)	0.03	112.276	0.669
CH	GPR	2	1.09**2 * RBF(length_scale=0.614)	0.03 4	113.143	0.66
CH	GPR	3	1.11**2 * RBF(length_scale=0.717)	0.04 6	116.921	0.679
CH	GPR	4	1.05**2 * RBF(length_scale=0.542)	0.09 1	117.013	0.691

CH	GPR	5	1.05**2 * RBF(length_scale=0.663)	0.07 1	111.359	0.644
CH	GPR	6	1.07**2 * RBF(length_scale=0.643)	0.08 9	110.957	0.655
CH	GPR	7	1.06**2 * RBF(length_scale=0.699)	0.07 5	111.392	0.646
CH	GPR	8	1.06**2 * RBF(length_scale=0.677)	0.05 4	107.571	0.631
CH	GPR	9	1.07**2 * RBF(length_scale=0.607)	0.06 3	119.623	0.693
CH	GPR	10	1.06**2 * RBF(length_scale=0.603)	0.04 3	114.67	0.672
AL B	RFR	1	'max_depth': None, 'max_features': 'sqrt', 'max_leaf_nodes': None, 'min_samples_leaf': 5, 'n_estimators': 100	0.49 2	61.884	0.447
AL B	RFR	2	'max_depth': None, 'max_features': 'sqrt', 'max_leaf_nodes': None, 'min_samples_leaf': 5, 'n_estimators': 500	0.38 9	62.498	0.463
AL B	RFR	3	'max_depth': None, 'max_features': 'sqrt', 'max_leaf_nodes': 10, 'min_samples_leaf': 5, 'n_estimators': 100	0.47	60.956	0.444
AL B	RFR	4	'max_depth': 5, 'max_features': 10, 'max_leaf_nodes': 10, 'min_samples_leaf': 5, 'n_estimators': 200	0.47 3	59.714	0.439
AL B	RFR	5	'max_depth': 5, 'max_features': 10, 'max_leaf_nodes': 10, 'min_samples_leaf': 1, 'n_estimators': 100	0.49 1	57.978	0.418
AL B	RFR	6	'max_depth': None, 'max_features': 'sqrt', 'max_leaf_nodes': 10, 'min_samples_leaf': 2, 'n_estimators': 100	0.59 8	54.306	0.388
AL B	RFR	7	'max_depth': 5, 'max_features': 'sqrt', 'max_leaf_nodes': 20, 'min_samples_leaf': 1, 'n_estimators': 100	0.59 9	54.284	0.395
AL B	RFR	8	'max_depth': None, 'max_features': 10, 'max_leaf_nodes': 10, 'min_samples_leaf': 5, 'n_estimators': 200	0.48 7	61.801	0.451
AL B	RFR	9	'max_depth': 5, 'max_features': 10, 'max_leaf_nodes': 10, 'min_samples_leaf': 5, 'n_estimators': 200	0.51 1	60.256	0.437
AL B	RFR	10	'max_depth': None, 'max_features': 10, 'max_leaf_nodes': None, 'min_samples_leaf': 5, 'n_estimators': 100	0.48 4	61.236	0.445
AL B	SVR	1	'svr_C': 10, 'svr_epsilon': 0.01, 'svr_gamma': 'scale', 'svr_kernel': 'linear'	0.52 7	60.243	0.435
AL B	SVR	2	'svr_C': 10, 'svr_epsilon': 0.5, 'svr_gamma': 'scale', 'svr_kernel': 'linear'	0.46 5	58.95	0.435
AL B	SVR	3	'svr_C': 10, 'svr_epsilon': 0.01, 'svr_gamma': 'scale', 'svr_kernel': 'linear'	0.48 8	59.269	0.431
AL B	SVR	4	'svr_C': 10, 'svr_epsilon': 1, 'svr_gamma': 'scale', 'svr_kernel': 'linear'	0.50 2	59.348	0.434
AL B	SVR	5	'svr_C': 10, 'svr_epsilon': 0.01, 'svr_gamma': 'scale', 'svr_kernel': 'linear'	0.57 2	54.454	0.393
AL B	SVR	6	'svr_C': 100, 'svr_epsilon': 1, 'svr_gamma': 1, 'svr_kernel': 'rbf'	0.6	56.361	0.406
AL B	SVR	7	'svr_C': 10, 'svr_epsilon': 1, 'svr_gamma': 'scale', 'svr_kernel': 'linear'	0.62 4	55.656	0.406
AL B	SVR	8	'svr_C': 10, 'svr_epsilon': 1, 'svr_gamma': 'scale', 'svr_kernel': 'linear'	0.51 2	63.062	0.458
AL B	SVR	9	'svr_C': 100, 'svr_epsilon': 0.01, 'svr_gamma': 'scale', 'svr_kernel': 'linear'	0.57 1	59.17	0.428
AL B	SVR	10	'svr_C': 100, 'svr_epsilon': 1, 'svr_gamma': 'scale', 'svr_kernel': 'rbf'	0.51 7	59.66	0.436
AL B	XGB	1	'xgb_colsample_bytree': 1.0, 'xgb_gamma': 0.1, 'xgb_learning_rate': 0.2, 'xgb_max_depth': 5, 'xgb_n_estimators': 100, 'xgb_subsample': 0.8	0.49 4	63.028	0.454
AL B	XGB	2	'xgb_colsample_bytree': 0.8, 'xgb_gamma': 0.2, 'xgb_learning_rate': 0.01, 'xgb_max_depth': 3, 'xgb_n_estimators': 200, 'xgb_subsample': 0.8	0.36 6	63.793	0.47
AL B	XGB	3	'xgb_colsample_bytree': 1.0, 'xgb_gamma': 0.1, 'xgb_learning_rate': 0.1, 'xgb_max_depth': 3, 'xgb_n_estimators': 100, 'xgb_subsample': 1.0	0.52 5	60.109	0.44
AL B	XGB	4	'xgb_colsample_bytree': 0.8, 'xgb_gamma': 0, 'xgb_learning_rate': 0.01, 'xgb_max_depth': 5, 'xgb_n_estimators': 200, 'xgb_subsample': 0.8	0.50 9	57.863	0.424
AL B	XGB	5	'xgb_colsample_bytree': 1.0, 'xgb_gamma': 0, 'xgb_learning_rate': 0.01, 'xgb_max_depth': 3, 'xgb_n_estimators': 300, 'xgb_subsample': 1.0	0.50 6	56.811	0.411
AL B	XGB	6	'xgb_colsample_bytree': 1.0, 'xgb_gamma': 0.2, 'xgb_learning_rate': 0.1, 'xgb_max_depth': 3, 'xgb_n_estimators': 100, 'xgb_subsample': 0.8	0.62	51.448	0.367
AL B	XGB	7	'xgb_colsample_bytree': 0.8, 'xgb_gamma': 0, 'xgb_learning_rate': 0.01, 'xgb_max_depth': 3, 'xgb_n_estimators': 300, 'xgb_subsample': 0.8	0.62 7	51.687	0.375
AL B	XGB	8	'xgb_colsample_bytree': 1.0, 'xgb_gamma': 0, 'xgb_learning_rate': 0.01, 'xgb_max_depth': 3, 'xgb_n_estimators': 300, 'xgb_subsample': 0.8	0.50 2	61.415	0.448
AL B	XGB	9	'xgb_colsample_bytree': 1.0, 'xgb_gamma': 0.1, 'xgb_learning_rate': 0.2, 'xgb_max_depth': 5, 'xgb_n_estimators': 100, 'xgb_subsample': 0.8	0.56	58.001	0.416
AL B	XGB	10	'xgb_colsample_bytree': 1.0, 'xgb_gamma': 0, 'xgb_learning_rate': 0.01, 'xgb_max_depth': 3, 'xgb_n_estimators': 200, 'xgb_subsample': 0.8	0.49 9	60.569	0.44
AL B	GPR	1	0.969**2 * RBF(length_scale=0.582)	0.36 4	70.641	0.51
AL B	GPR	2	0.988**2 * RBF(length_scale=0.571)	0.22 9	73.522	0.554
AL B	GPR	3	0.971**2 * RBF(length_scale=0.596)	0.31 2	73.961	0.551
AL B	GPR	4	1**2 * RBF(length_scale=0.602)	0.26 3	70.827	0.523
AL B	GPR	5	0.963**2 * RBF(length_scale=0.637)	0.34 6	69.188	0.506
AL B	GPR	6	0.954**2 * RBF(length_scale=0.728)	0.57 7	57.247	0.409
AL B	GPR	7	0.988**2 * RBF(length_scale=0.69)	0.41 8	66.398	0.487
AL B	GPR	8	0.96**2 * RBF(length_scale=0.603)	0.32 7	70.746	0.512
AL B	GPR	9	0.981**2 * RBF(length_scale=0.68)	0.50 3	61.572	0.445

AL B	GPR	10	0.978**2 * RBF(length_scale=0.592)	0.43 7	67.059	0.49
HA I	RFR	1	'max_depth': 10, 'max_features': 'sqrt', 'max_leaf_nodes': 20, 'min_samples_leaf': 2, 'n_estimators': 500	0.60 1	58.344	0.484
HA I	RFR	2	'max_depth': 5, 'max_features': 'sqrt', 'max_leaf_nodes': None, 'min_samples_leaf': 2, 'n_estimators': 200	0.56 7	58.231	0.481
HA I	RFR	3	'max_depth': 5, 'max_features': 'sqrt', 'max_leaf_nodes': 20, 'min_samples_leaf': 1, 'n_estimators': 200	0.49 4	60.211	0.51
HA I	RFR	4	'max_depth': 5, 'max_features': 'sqrt', 'max_leaf_nodes': None, 'min_samples_leaf': 5, 'n_estimators': 200	0.62 6	55.599	0.471
HA I	RFR	5	'max_depth': None, 'max_features': 'sqrt', 'max_leaf_nodes': 20, 'min_samples_leaf': 1, 'n_estimators': 100	0.56 3	57.184	0.48
HA I	RFR	6	'max_depth': 10, 'max_features': 'sqrt', 'max_leaf_nodes': None, 'min_samples_leaf': 1, 'n_estimators': 100	0.67 7	50.357	0.443
HA I	RFR	7	'max_depth': None, 'max_features': 'sqrt', 'max_leaf_nodes': None, 'min_samples_leaf': 5, 'n_estimators': 100	0.54 6	59.045	0.504
HA I	RFR	8	'max_depth': 5, 'max_features': 'sqrt', 'max_leaf_nodes': None, 'min_samples_leaf': 1, 'n_estimators': 500	0.59 3	56.409	0.471
HA I	RFR	9	'max_depth': 15, 'max_features': 'sqrt', 'max_leaf_nodes': None, 'min_samples_leaf': 1, 'n_estimators': 100	0.55 5	60.494	0.516
HA I	RFR	10	'max_depth': None, 'max_features': 'sqrt', 'max_leaf_nodes': None, 'min_samples_leaf': 5, 'n_estimators': 100	0.54 4	59.877	0.509
HA I	SVR	1	'svr_C': 100, 'svr_epsilon': 0.1, 'svr_gamma': 'scale', 'svr_kernel': 'linear'	0.64	55.258	0.461
HA I	SVR	2	'svr_C': 100, 'svr_epsilon': 1, 'svr_gamma': 'scale', 'svr_kernel': 'linear'	0.59 1	55.823	0.463
HA I	SVR	3	'svr_C': 100, 'svr_epsilon': 1, 'svr_gamma': 'scale', 'svr_kernel': 'linear'	0.63 7	52.765	0.447
HA I	SVR	4	'svr_C': 100, 'svr_epsilon': 0.1, 'svr_gamma': 'scale', 'svr_kernel': 'linear'	0.67	51.742	0.438
HA I	SVR	5	'svr_C': 100, 'svr_epsilon': 1, 'svr_gamma': 'scale', 'svr_kernel': 'linear'	0.57 2	55.933	0.469
HA I	SVR	6	'svr_C': 100, 'svr_epsilon': 1, 'svr_gamma': 'scale', 'svr_kernel': 'linear'	0.64 6	50.297	0.441
HA I	SVR	7	'svr_C': 100, 'svr_epsilon': 1, 'svr_gamma': 'scale', 'svr_kernel': 'linear'	0.62 4	53.9	0.458
HA I	SVR	8	'svr_C': 100, 'svr_epsilon': 1, 'svr_gamma': 'scale', 'svr_kernel': 'linear'	0.68 7	50.765	0.423
HA I	SVR	9	'svr_C': 100, 'svr_epsilon': 1, 'svr_gamma': 'scale', 'svr_kernel': 'linear'	0.57 9	59.724	0.506
HA I	SVR	10	'svr_C': 100, 'svr_epsilon': 0.5, 'svr_gamma': 'scale', 'svr_kernel': 'linear'	0.63 1	53.207	0.447
HA I	XGB	1	'xgb_colsample_bytree': 1.0, 'xgb_gamma': 0.2, 'xgb_learning_rate': 0.2, 'xgb_max_depth': 3, 'xgb_n_estimators': 300, 'xgb_subsample': 1.0	0.59 7	59.358	0.491
HA I	XGB	2	'xgb_colsample_bytree': 1.0, 'xgb_gamma': 0, 'xgb_learning_rate': 0.2, 'xgb_max_depth': 3, 'xgb_n_estimators': 100, 'xgb_subsample': 0.8	0.57 1	58.098	0.48
HA I	XGB	3	'xgb_colsample_bytree': 0.8, 'xgb_gamma': 0, 'xgb_learning_rate': 0.01, 'xgb_max_depth': 3, 'xgb_n_estimators': 300, 'xgb_subsample': 0.8	0.47 6	61.115	0.517
HA I	XGB	4	'xgb_colsample_bytree': 0.8, 'xgb_gamma': 0, 'xgb_learning_rate': 0.01, 'xgb_max_depth': 3, 'xgb_n_estimators': 300, 'xgb_subsample': 1.0	0.58 7	59.375	0.501
HA I	XGB	5	'xgb_colsample_bytree': 1.0, 'xgb_gamma': 0.1, 'xgb_learning_rate': 0.1, 'xgb_max_depth': 3, 'xgb_n_estimators': 100, 'xgb_subsample': 0.8	0.50 8	64.257	0.54
HA I	XGB	6	'xgb_colsample_bytree': 0.8, 'xgb_gamma': 0, 'xgb_learning_rate': 0.01, 'xgb_max_depth': 3, 'xgb_n_estimators': 300, 'xgb_subsample': 1.0	0.62	54.179	0.475
HA I	XGB	7	'xgb_colsample_bytree': 0.8, 'xgb_gamma': 0.1, 'xgb_learning_rate': 0.2, 'xgb_max_depth': 9, 'xgb_n_estimators': 100, 'xgb_subsample': 0.8	0.48 3	64.233	0.548
HA I	XGB	8	'xgb_colsample_bytree': 0.8, 'xgb_gamma': 0, 'xgb_learning_rate': 0.1, 'xgb_max_depth': 3, 'xgb_n_estimators': 100, 'xgb_subsample': 0.8	0.61 1	56.071	0.467
HA I	XGB	9	'xgb_colsample_bytree': 0.8, 'xgb_gamma': 0, 'xgb_learning_rate': 0.01, 'xgb_max_depth': 3, 'xgb_n_estimators': 200, 'xgb_subsample': 0.8	0.48 4	64.76	0.548
HA I	XGB	10	'xgb_colsample_bytree': 0.8, 'xgb_gamma': 0, 'xgb_learning_rate': 0.01, 'xgb_max_depth': 3, 'xgb_n_estimators': 200, 'xgb_subsample': 0.8	0.46 4	64.489	0.545
HA I	GPR	1	1.13**2 * RBF(length_scale=0.956)	0.49 1	68.263	0.569
HA I	GPR	2	1.05**2 * RBF(length_scale=0.939)	0.56 4	61.494	0.498
HA I	GPR	3	1.04**2 * RBF(length_scale=0.817)	0.44 3	65.875	0.557
HA I	GPR	4	1.01**2 * RBF(length_scale=0.866)	0.54 1	62.848	0.531
HA I	GPR	5	1.04**2 * RBF(length_scale=0.87)	0.48 9	61.989	0.516
HA I	GPR	6	0.944**2 * RBF(length_scale=0.82)	0.47 7	59.248	0.52
HA I	GPR	7	1.06**2 * RBF(length_scale=0.87)	0.46 9	66.942	0.564
HA I	GPR	8	1.03**2 * RBF(length_scale=0.835)	0.47 9	64.916	0.544
HA I	GPR	9	1.09**2 * RBF(length_scale=0.963)	0.51 2	62.062	0.53
HA I	GPR	10	1.03**2 * RBF(length_scale=0.853)	0.44 9	65.897	0.559
SC H	RFR	1	'max_depth': None, 'max_features': 'sqrt', 'max_leaf_nodes': 10, 'min_samples_leaf': 2, 'n_estimators': 200	0.35 4	95.411	0.432
SC H	RFR	2	'max_depth': 5, 'max_features': 'sqrt', 'max_leaf_nodes': 10, 'min_samples_leaf': 5, 'n_estimators': 100	0.32 8	94.618	0.427
SC H	RFR	3	'max_depth': 5, 'max_features': 'sqrt', 'max_leaf_nodes': 10, 'min_samples_leaf': 2, 'n_estimators': 100	0.43 4	90.285	0.402
SC H	RFR	4	'max_depth': 5, 'max_features': 'sqrt', 'max_leaf_nodes': None, 'min_samples_leaf': 1, 'n_estimators': 100	0.33 1	98.242	0.435

SC H	RFR	5	'max_depth': None, 'max_features': 'sqrt', 'max_leaf_nodes': 10, 'min_samples_leaf': 1, 'n_estimators': 100	0.34 3	97.047	0.445
SC H	RFR	6	'max_depth': 5, 'max_features': 10, 'max_leaf_nodes': 10, 'min_samples_leaf': 5, 'n_estimators': 100	0.39	94.588	0.421
SC H	RFR	7	'max_depth': None, 'max_features': 'sqrt', 'max_leaf_nodes': 10, 'min_samples_leaf': 2, 'n_estimators': 200	0.36 1	101.901	0.456
SC H	RFR	8	'max_depth': 10, 'max_features': 'sqrt', 'max_leaf_nodes': None, 'min_samples_leaf': 2, 'n_estimators': 100	0.40 8	94.495	0.423
SC H	RFR	9	'max_depth': 10, 'max_features': 'sqrt', 'max_leaf_nodes': None, 'min_samples_leaf': 2, 'n_estimators': 500	0.32 3	100.8	0.448
SC H	RFR	10	'max_depth': 5, 'max_features': 'sqrt', 'max_leaf_nodes': 20, 'min_samples_leaf': 2, 'n_estimators': 100	0.33 3	101.181	0.454
SC H	SVR	1	'svr_C': 100, 'svr_epsilon': 1, 'svr_gamma': 'scale', 'svr_kernel': 'rbf'	0.35 4	93.693	0.423
SC H	SVR	2	'svr_C': 100, 'svr_epsilon': 1, 'svr_gamma': 'scale', 'svr_kernel': 'linear'	0.36 1	93.28	0.418
SC H	SVR	3	'svr_C': 100, 'svr_epsilon': 1, 'svr_gamma': 'scale', 'svr_kernel': 'rbf'	0.42 1	93.033	0.413
SC H	SVR	4	'svr_C': 100, 'svr_epsilon': 0.01, 'svr_gamma': 'scale', 'svr_kernel': 'rbf'	0.42 5	91.405	0.404
SC H	SVR	5	'svr_C': 100, 'svr_epsilon': 1, 'svr_gamma': 'scale', 'svr_kernel': 'rbf'	0.36 8	92.754	0.421
SC H	SVR	6	'svr_C': 100, 'svr_epsilon': 1, 'svr_gamma': 'scale', 'svr_kernel': 'linear'	0.42 8	92.56	0.41
SC H	SVR	7	'svr_C': 100, 'svr_epsilon': 0.01, 'svr_gamma': 'scale', 'svr_kernel': 'rbf'	0.36 2	100.513	0.445
SC H	SVR	8	'svr_C': 100, 'svr_epsilon': 1, 'svr_gamma': 'scale', 'svr_kernel': 'linear'	0.47 4	94.222	0.425
SC H	SVR	9	'svr_C': 100, 'svr_epsilon': 1, 'svr_gamma': 'scale', 'svr_kernel': 'rbf'	0.40 8	95.513	0.426
SC H	SVR	10	'svr_C': 100, 'svr_epsilon': 0.01, 'svr_gamma': 'scale', 'svr_kernel': 'rbf'	0.45 4	92.601	0.416
SC H	XGB	1	'xgb_colsample_bytree': 1.0, 'xgb_gamma': 0, 'xgb_learning_rate': 0.01, 'xgb_max_depth': 3, 'xgb_n_estimators': 300, 'xgb_subsample': 1.0	0.31 3	97.182	0.439
SC H	XGB	2	'xgb_colsample_bytree': 0.8, 'xgb_gamma': 0, 'xgb_learning_rate': 0.01, 'xgb_max_depth': 3, 'xgb_n_estimators': 200, 'xgb_subsample': 0.8	0.27 1	99.375	0.451
SC H	XGB	3	'xgb_colsample_bytree': 0.8, 'xgb_gamma': 0.1, 'xgb_learning_rate': 0.01, 'xgb_max_depth': 7, 'xgb_n_estimators': 200, 'xgb_subsample': 1.0	0.42 5	92.165	0.41
SC H	XGB	4	'xgb_colsample_bytree': 0.8, 'xgb_gamma': 0, 'xgb_learning_rate': 0.01, 'xgb_max_depth': 3, 'xgb_n_estimators': 300, 'xgb_subsample': 0.8	0.30 2	98.417	0.436
SC H	XGB	5	'xgb_colsample_bytree': 1.0, 'xgb_gamma': 0, 'xgb_learning_rate': 0.01, 'xgb_max_depth': 3, 'xgb_n_estimators': 200, 'xgb_subsample': 0.8	0.30 3	97.967	0.448
SC H	XGB	6	'xgb_colsample_bytree': 0.8, 'xgb_gamma': 0, 'xgb_learning_rate': 0.01, 'xgb_max_depth': 3, 'xgb_n_estimators': 200, 'xgb_subsample': 1.0	0.41	94.208	0.42
SC H	XGB	7	'xgb_colsample_bytree': 0.8, 'xgb_gamma': 0, 'xgb_learning_rate': 0.01, 'xgb_max_depth': 3, 'xgb_n_estimators': 300, 'xgb_subsample': 0.8	0.36 3	105.444	0.473
SC H	XGB	8	'xgb_colsample_bytree': 0.8, 'xgb_gamma': 0, 'xgb_learning_rate': 0.01, 'xgb_max_depth': 3, 'xgb_n_estimators': 300, 'xgb_subsample': 0.8	0.39 2	94.985	0.422
SC H	XGB	9	'xgb_colsample_bytree': 1.0, 'xgb_gamma': 0, 'xgb_learning_rate': 0.01, 'xgb_max_depth': 3, 'xgb_n_estimators': 200, 'xgb_subsample': 0.8	0.29 1	103.28	0.459
SC H	XGB	10	'xgb_colsample_bytree': 1.0, 'xgb_gamma': 0, 'xgb_learning_rate': 0.01, 'xgb_max_depth': 3, 'xgb_n_estimators': 300, 'xgb_subsample': 0.8	0.31 4	102.488	0.461
SC H	GPR	1	1.03**2 * RBF(length_scale=0.542)	0.05 5	112.547	0.511
SC H	GPR	2	1**2 * RBF(length_scale=0.0912)	0	116.645	0.531
SC H	GPR	3	1.05**2 * RBF(length_scale=0.664)	0.02 8	116.241	0.518
SC H	GPR	4	1.05**2 * RBF(length_scale=0.624)	0.06 7	119.988	0.532
SC H	GPR	5	1.04**2 * RBF(length_scale=0.653)	0.14 6	110.328	0.505
SC H	GPR	6	1.04**2 * RBF(length_scale=0.618)	0.00 9	121.548	0.542
SC H	GPR	7	1.07**2 * RBF(length_scale=0.817)	0.14 9	119.432	0.537
SC H	GPR	8	1.04**2 * RBF(length_scale=0.679)	0.22 1	106.116	0.476
SC H	GPR	9	1.06**2 * RBF(length_scale=0.831)	0.24 5	105.753	0.473
SC H	GPR	10	1.05**2 * RBF(length_scale=0.671)	0.05 1	120.172	0.539
US	RFR	1	'max_depth': None, 'max_features': 10, 'max_leaf_nodes': 10, 'min_samples_leaf': 1, 'n_estimators': 100	0.43 3	68.608	0.267
US	RFR	2	'max_depth': 5, 'max_features': 10, 'max_leaf_nodes': 10, 'min_samples_leaf': 2, 'n_estimators': 200	0.44 4	63.617	0.25
US	RFR	3	'max_depth': None, 'max_features': 10, 'max_leaf_nodes': None, 'min_samples_leaf': 5, 'n_estimators': 500	0.37 9	67.218	0.259
US	RFR	4	'max_depth': 5, 'max_features': 10, 'max_leaf_nodes': 10, 'min_samples_leaf': 2, 'n_estimators': 200	0.46 1	70.669	0.281
US	RFR	5	'max_depth': 5, 'max_features': 10, 'max_leaf_nodes': 10, 'min_samples_leaf': 2, 'n_estimators': 100	0.45 1	66.11	0.254
US	RFR	6	'max_depth': None, 'max_features': 'sqrt', 'max_leaf_nodes': 10, 'min_samples_leaf': 2, 'n_estimators': 200	0.42 2	64.712	0.261
US	RFR	7	'max_depth': None, 'max_features': 10, 'max_leaf_nodes': 20, 'min_samples_leaf': 1, 'n_estimators': 100	0.37 7	74.124	0.29
US	RFR	8	'max_depth': None, 'max_features': 10, 'max_leaf_nodes': None, 'min_samples_leaf': 5, 'n_estimators': 100	0.39 5	67.47	0.26
US	RFR	9	'max_depth': None, 'max_features': 10, 'max_leaf_nodes': 10, 'min_samples_leaf': 1, 'n_estimators': 100	0.41 7	68.961	0.266

US	RFR	10	'max_depth': None, 'max_features': 10, 'max_leaf_nodes': None, 'min_samples_leaf': 5, 'n_estimators': 100	0.30 8	71.819	0.279
US	SVR	1	'svr_C': 100, 'svr_epsilon': 1, 'svr_gamma': 'scale', 'svr_kernel': 'linear'	0.49 4	62.487	0.24
US	SVR	2	'svr_C': 100, 'svr_epsilon': 0.01, 'svr_gamma': 'scale', 'svr_kernel': 'linear'	0.60 2	50.272	0.197
US	SVR	3	'svr_C': 100, 'svr_epsilon': 0.01, 'svr_gamma': 'scale', 'svr_kernel': 'linear'	0.49 6	61.333	0.235
US	SVR	4	'svr_C': 100, 'svr_epsilon': 1, 'svr_gamma': 'scale', 'svr_kernel': 'linear'	0.53 1	60.381	0.236
US	SVR	5	'svr_C': 100, 'svr_epsilon': 1, 'svr_gamma': 'scale', 'svr_kernel': 'linear'	0.54 7	60.469	0.232
US	SVR	6	'svr_C': 100, 'svr_epsilon': 0.5, 'svr_gamma': 'scale', 'svr_kernel': 'linear'	0.56 9	52.136	0.207
US	SVR	7	'svr_C': 100, 'svr_epsilon': 0.1, 'svr_gamma': 'scale', 'svr_kernel': 'linear'	0.56 2	60.417	0.236
US	SVR	8	'svr_C': 100, 'svr_epsilon': 1, 'svr_gamma': 'scale', 'svr_kernel': 'linear'	0.43 2	64.762	0.248
US	SVR	9	'svr_C': 100, 'svr_epsilon': 1, 'svr_gamma': 'scale', 'svr_kernel': 'linear'	0.45 5	64.825	0.247
US	SVR	10	'svr_C': 100, 'svr_epsilon': 1, 'svr_gamma': 'scale', 'svr_kernel': 'linear'	0.44 9	63.514	0.244
US	XGB	1	'xgb_colsample_bytree': 0.8, 'xgb_gamma': 0, 'xgb_learning_rate': 0.01, 'xgb_max_depth': 5, 'xgb_n_estimators': 200, 'xgb_subsample': 0.8	0.41 1	69.243	0.268
US	XGB	2	'xgb_colsample_bytree': 1.0, 'xgb_gamma': 0, 'xgb_learning_rate': 0.2, 'xgb_max_depth': 3, 'xgb_n_estimators': 100, 'xgb_subsample': 0.8	0.39 8	66.15	0.258
US	XGB	3	'xgb_colsample_bytree': 1.0, 'xgb_gamma': 0, 'xgb_learning_rate': 0.1, 'xgb_max_depth': 3, 'xgb_n_estimators': 300, 'xgb_subsample': 0.8	0.37 5	67.86	0.258
US	XGB	4	'xgb_colsample_bytree': 0.8, 'xgb_gamma': 0, 'xgb_learning_rate': 0.01, 'xgb_max_depth': 5, 'xgb_n_estimators': 200, 'xgb_subsample': 0.8	0.37 6	76.427	0.302
US	XGB	5	'xgb_colsample_bytree': 1.0, 'xgb_gamma': 0, 'xgb_learning_rate': 0.01, 'xgb_max_depth': 3, 'xgb_n_estimators': 200, 'xgb_subsample': 1.0	0.50 2	64.874	0.252
US	XGB	6	'xgb_colsample_bytree': 1.0, 'xgb_gamma': 0.2, 'xgb_learning_rate': 0.1, 'xgb_max_depth': 3, 'xgb_n_estimators': 300, 'xgb_subsample': 0.8	0.40 3	66.616	0.267
US	XGB	7	'xgb_colsample_bytree': 1.0, 'xgb_gamma': 0.2, 'xgb_learning_rate': 0.01, 'xgb_max_depth': 7, 'xgb_n_estimators': 200, 'xgb_subsample': 0.8	0.35	74.251	0.291
US	XGB	8	'xgb_colsample_bytree': 1.0, 'xgb_gamma': 0, 'xgb_learning_rate': 0.01, 'xgb_max_depth': 3, 'xgb_n_estimators': 300, 'xgb_subsample': 1.0	0.36 4	67.505	0.258
US	XGB	9	'xgb_colsample_bytree': 1.0, 'xgb_gamma': 0.1, 'xgb_learning_rate': 0.2, 'xgb_max_depth': 7, 'xgb_n_estimators': 100, 'xgb_subsample': 1.0	0.35 5	68.738	0.261
US	XGB	10	'xgb_colsample_bytree': 1.0, 'xgb_gamma': 0, 'xgb_learning_rate': 0.01, 'xgb_max_depth': 5, 'xgb_n_estimators': 200, 'xgb_subsample': 1.0	0.38 4	67.266	0.263
US	GPR	1	1.2**2 * RBF(length_scale=0.816)	0.25 5	83.361	0.323
US	GPR	2	1.06**2 * RBF(length_scale=0.696)	0.29 4	68.962	0.269
US	GPR	3	1.14**2 * RBF(length_scale=0.79)	0.21	80.838	0.31
US	GPR	4	1.12**2 * RBF(length_scale=0.725)	0.14 7	88.532	0.347
US	GPR	5	1.21**2 * RBF(length_scale=0.898)	0.20 7	85.777	0.33
US	GPR	6	1.06**2 * RBF(length_scale=0.661)	0.24 8	71.481	0.283
US	GPR	7	1.11**2 * RBF(length_scale=0.646)	0.18 2	87.213	0.341
US	GPR	8	1.1**2 * RBF(length_scale=0.744)	0.21 3	82.567	0.314
US	GPR	9	1.19**2 * RBF(length_scale=0.814)	0.16 7	82.955	0.317
US	GPR	10	1.1**2 * RBF(length_scale=0.718)	0.15 6	80.403	0.313

57 **Section A.5: Cross-validation performance of local physically-based models**

58 *Table A.2: Cross-validation performance of local physically-based models. The parameters correspond to the best-performing  
 59 combination of parameters tested during the fivefold cross-validation. CH: Switzerland, ALB: Schwäbische Alb, HAI: Hainich-  
 60 Dün, SCH: Schorfheide-Chorin, US: United States, R<sup>2</sup>: coefficient of determination, RMSE: root-mean-square error, RRMSE:  
 61 relative root-mean-square error.*

Site	Seed	Cost function	Percentage of solutions	R <sup>2</sup>	RMSE [g m <sup>-2</sup> ]	RRMSE
CH	1	min_contrast_1	1	0.221	95.683	0.556
CH	2	min_contrast_1	1	0.214	96.421	0.558
CH	3	min_contrast_1	1	0.149	107.756	0.617
CH	4	min_contrast_1	1	0.142	104.529	0.602
CH	5	min_contrast_1	1	0.207	102.279	0.589
CH	6	min_contrast_1	1	0.211	96.402	0.558
CH	7	min_contrast_1	1	0.208	101.18	0.583
CH	8	min_contrast_1	1	0.192	98.848	0.573
CH	9	min_contrast_1	1	0.23	101.751	0.583
CH	10	min_contrast_2	1	0.263	97.142	0.558
ALB	1	neyman_chi_square_divergence	1	0.419	72.6	0.521
ALB	2	neyman_chi_square_divergence	1	0.392	70.695	0.512
ALB	3	neyman_chi_square_divergence	1	0.401	73.617	0.525
ALB	4	neyman_chi_square_divergence	1	0.399	71.542	0.518
ALB	5	neyman_chi_square_divergence	1	0.491	67.975	0.491
ALB	6	neyman_chi_square_divergence	1	0.519	67.184	0.483
ALB	7	neyman_chi_square_divergence	1	0.488	68.575	0.496
ALB	8	neyman_chi_square_divergence	1	0.404	71.385	0.511
ALB	9	neyman_chi_square_divergence	1	0.424	70.498	0.505
ALB	10	neyman_chi_square_divergence	1	0.406	70.858	0.508
HAI	1	neyman_chi_square_divergence	1	0.535	76.289	0.653
HAI	2	neyman_chi_square_divergence	1	0.502	79.265	0.68
HAI	3	neyman_chi_square_divergence	1	0.488	77.544	0.67
HAI	4	neyman_chi_square_divergence	1	0.521	79.296	0.682
HAI	5	neyman_chi_square_divergence	1	0.471	79.608	0.683
HAI	6	neyman_chi_square_divergence	1	0.56	74.294	0.65
HAI	7	neyman_chi_square_divergence	1	0.496	78.714	0.679
HAI	8	neyman_chi_square_divergence	1	0.494	78.26	0.673
HAI	9	neyman_chi_square_divergence	1	0.513	79.514	0.678
HAI	10	neyman_chi_square_divergence	1	0.465	80.354	0.691
SCH	1	laplace_distribution	10	0.232	100.658	0.459
SCH	2	laplace_distribution	10	0.258	99.444	0.451
SCH	3	laplace_distribution	10	0.253	105.421	0.475
SCH	4	laplace_distribution	10	0.252	105.525	0.475
SCH	5	laplace_distribution	10	0.25	99.303	0.451
SCH	6	laplace_distribution	10	0.265	104.778	0.471

SCH	7	laplace_distribution	10	0.237	107.39	0.481
SCH	8	laplace_distribution	10	0.249	105.4	0.473
SCH	9	laplace_distribution	10	0.234	107.052	0.48
SCH	10	laplace_distribution	10	0.235	106.999	0.481
US	1	pearson_chi_square	0.01	0.11	179.487	0.684
US	2	pearson_chi_square	0.01	0.102	173.848	0.67
US	3	min_contrast_4	10	0.411	182.307	0.695
US	4	min_contrast_4	10	0.394	182.016	0.694
US	5	pearson_chi_square	0.01	0.119	176.744	0.674
US	6	pearson_chi_square	0.01	0.101	174.832	0.673
US	7	min_contrast_4	10	0.419	180.943	0.689
US	8	min_contrast_4	10	0.417	181.294	0.692
US	9	min_contrast_4	10	0.434	181.748	0.693
US	10	pearson_chi_square	0.01	0.117	175.263	0.671

62

63

64 **Section A.6: Cross-validation performance of local hybrid models**

65 *Table A.3: Cross-validation performance of local hybrid models. The parameters correspond to the best-performing  
66 combination of parameters tested during the fivefold cross-validation using Active Learning with an initial training set size of  
67 2%. CH: Switzerland, ALB: Schwäbische Alb, HAI: Hainich-Dün, SCH: Schorfheide-Chorin, US: United States, GPR: Gaussian  
68 Process regression, R<sup>2</sup>: coefficient of determination, RMSE: root-mean-square error, RRMSE: relative root-mean-square error.  
69 Nomenclature of parameter names for GPR according to Pedregosa et al. (2012).*

Site	Model	Seed	Parameters	R <sup>2</sup>	RMSE [g m <sup>-2</sup> ]	RRMSE
CH	GPR	1	2.21**2 * RBF(length_scale=1.42)	0.499	75.556	0.439
CH	GPR	2	1.38**2 * RBF(length_scale=1.19)	0.452	79.347	0.459
CH	GPR	3	2.3**2 * RBF(length_scale=1.31)	0.352	91.03	0.521
CH	GPR	4	1.65**2 * RBF(length_scale=1.54)	0.391	86.625	0.499
CH	GPR	5	1.4**2 * RBF(length_scale=1.12)	0.443	83.088	0.478
CH	GPR	6	1.35**2 * RBF(length_scale=0.905)	0.294	90.317	0.523
CH	GPR	7	2.17**2 * RBF(length_scale=1.44)	0.454	83.176	0.479
CH	GPR	8	1.86**2 * RBF(length_scale=1.39)	0.528	75.341	0.437
CH	GPR	9	2.01**2 * RBF(length_scale=1.55)	0.373	88.788	0.509
CH	GPR	10	1.88**2 * RBF(length_scale=1.51)	0.416	85.856	0.493
ALB	GPR	1	1.48**2 * RBF(length_scale=1.53)	0.598	54.526	0.391
ALB	GPR	2	1.55**2 * RBF(length_scale=1.18)	0.522	57.823	0.418
ALB	GPR	3	1.71**2 * RBF(length_scale=1.43)	0.59	55.424	0.396
ALB	GPR	4	1.23**2 * RBF(length_scale=1.06)	0.553	55.795	0.404
ALB	GPR	5	1.22**2 * RBF(length_scale=1.05)	0.651	49.486	0.357
ALB	GPR	6	1.24**2 * RBF(length_scale=0.967)	0.662	50.024	0.36
ALB	GPR	7	1.22**2 * RBF(length_scale=0.924)	0.585	54.581	0.395
ALB	GPR	8	1.46**2 * RBF(length_scale=1.77)	0.607	53.931	0.386
ALB	GPR	9	1.38**2 * RBF(length_scale=1.05)	0.605	54.212	0.388
ALB	GPR	10	1.39**2 * RBF(length_scale=1.13)	0.557	57.082	0.409
HAI	GPR	1	1.11**2 * RBF(length_scale=0.986)	0.626	55.158	0.472
HAI	GPR	2	1.61**2 * RBF(length_scale=1.39)	0.567	57.636	0.494
HAI	GPR	3	1.56**2 * RBF(length_scale=1.17)	0.558	58.089	0.502
HAI	GPR	4	1.23**2 * RBF(length_scale=1.22)	0.599	56.084	0.483
HAI	GPR	5	1.18**2 * RBF(length_scale=0.916)	0.558	58.565	0.503
HAI	GPR	6	1.34**2 * RBF(length_scale=0.889)	0.669	46.253	0.405
HAI	GPR	7	1.36**2 * RBF(length_scale=0.949)	0.551	59.404	0.512
HAI	GPR	8	1.22**2 * RBF(length_scale=1.2)	0.593	55.635	0.478
HAI	GPR	9	1.35**2 * RBF(length_scale=0.994)	0.582	58.676	0.5
HAI	GPR	10	1.07**2 * RBF(length_scale=0.729)	0.439	64.907	0.558
SCH	GPR	1	1.43**2 * RBF(length_scale=1.66)	0.42	87.105	0.397
SCH	GPR	2	2.41**2 * RBF(length_scale=1.88)	0.413	87.669	0.398
SCH	GPR	3	1.1**2 * RBF(length_scale=0.739)	0.265	103.892	0.468
SCH	GPR	4	1.67**2 * RBF(length_scale=1.46)	0.42	92.083	0.414
SCH	GPR	5	1.28**2 * RBF(length_scale=1.18)	0.419	88.073	0.4

SCH	GPR	6	1.22**2 * RBF(length_scale=0.963)	0.358	97.48	0.438
SCH	GPR	7	2.21**2 * RBF(length_scale=1.73)	0.347	98.593	0.442
SCH	GPR	8	1.87**2 * RBF(length_scale=1.72)	0.472	87.585	0.393
SCH	GPR	9	1.13**2 * RBF(length_scale=0.843)	0.313	101.202	0.454
SCH	GPR	10	1.5**2 * RBF(length_scale=1.22)	0.422	95.264	0.428
US	GPR	1	1**2 * RBF(length_scale=0.15)	0	87.721	0.334
US	GPR	2	1**2 * RBF(length_scale=0.0601)	0	78.583	0.303
US	GPR	3	1**2 * RBF(length_scale=0.107)	0	87.481	0.334
US	GPR	4	2.88**2 * RBF(length_scale=1.72)	0.522	62.153	0.237
US	GPR	5	1.73**2 * RBF(length_scale=1.58)	0.523	60.741	0.232
US	GPR	6	1**2 * RBF(length_scale=0.215)	0	78.953	0.304
US	GPR	7	2.27**2 * RBF(length_scale=1.37)	0.652	53.078	0.202
US	GPR	8	1**2 * RBF(length_scale=0.371)	0	87.852	0.335
US	GPR	9	1.67**2 * RBF(length_scale=1.35)	0.652	52.129	0.199
US	GPR	10	1**2 * RBF(length_scale=0.119)	0	85.523	0.328

70

71 **Section A.7: Cross-validation performance of global empirical models**

72 *Table A.4: Cross-validation performance of global empirical models. The parameters correspond to the best-performing*  
 73 *combination of parameters tested during the fivefold cross-validation. CH: Switzerland, ALB: Schwäbische Alb, HAI: Hainich-*  
 74 *Dün, SCH: Schorfheide-Chorin, US: United States, RFR: Random Forest regression, SVR: Support Vector regression, XGB:*  
 75 *Extreme Gradient Boosting regression, GPR: Gaussian Process regression, R<sup>2</sup>: coefficient of determination, RMSE: root-mean-*  
 76 *square error, RRMSE: relative root-mean-square error. Nomenclature of parameter names for RFR, SVR, and GPR according*  
 77 *to Pedregosa et al. (2012), for XGB according to Chen and Guestrin (2016).*

Site	Model	Parameters	R <sup>2</sup>	RMSE [g m <sup>-2</sup> ]	RRMS E
All except for CH	RFR	'max_depth': None, 'max_features': 'sqrt', 'max_leaf_nodes': None, 'min_samples_leaf': 2, 'n_estimators': 200	0.506	79.86	0.433
All except for CH	SVR	'svr_C': 100, 'svr_epsilon': 0.1, 'svr_gamma': 'scale', 'svr_kernel': 'rbf'	0.522	78.95	0.427
All except for CH	XGB	'xgb_colsample_bytree': 1.0, 'xgb_gamma': 0.1, 'xgb_learning_rate': 0.01, 'xgb_max_depth': 3, 'xgb_n_estimators': 300, 'xgb_subsample': 0.8	0.5	80.664	0.437
All except for CH	GPR	1**2 * RBF(length_scale=0.0279)	0.398	88.272	0.478
All except for ALB	RFR	'max_depth': 10, 'max_features': 'sqrt', 'max_leaf_nodes': None, 'min_samples_leaf': 1, 'n_estimators': 100	0.399	90.335	0.467
All except for ALB	SVR	'svr_C': 100, 'svr_epsilon': 1, 'svr_gamma': 'scale', 'svr_kernel': 'rbf'	0.379	92.708	0.479
All except for ALB	XGB	'xgb_colsample_bytree': 1.0, 'xgb_gamma': 0.2, 'xgb_learning_rate': 0.1, 'xgb_max_depth': 9, 'xgb_n_estimators': 100, 'xgb_subsample': 0.8	0.377	93.213	0.482
All except for ALB	GPR	1**2 * RBF(length_scale=0.0285)	0.083	109.705	0.567
All except for HAI	RFR	'max_depth': 10, 'max_features': 'sqrt', 'max_leaf_nodes': None, 'min_samples_leaf': 2, 'n_estimators': 500	0.328	91.829	0.462
All except for HAI	SVR	'svr_C': 100, 'svr_epsilon': 1, 'svr_gamma': 'scale', 'svr_kernel': 'rbf'	0.359	90.446	0.454
All except for HAI	XGB	'xgb_colsample_bytree': 1.0, 'xgb_gamma': 0, 'xgb_learning_rate': 0.01, 'xgb_max_depth': 3, 'xgb_n_estimators': 300, 'xgb_subsample': 0.8	0.294	94.275	0.474
All except for HAI	GPR	1**2 * RBF(length_scale=0.0297)	0.001	111.558	0.562
All except for SCH	RFR	'max_depth': 10, 'max_features': 10, 'max_leaf_nodes': None, 'min_samples_leaf': 1, 'n_estimators': 500	0.49	77.84	0.449
All except for SCH	SVR	'svr_C': 100, 'svr_epsilon': 1, 'svr_gamma': 'scale', 'svr_kernel': 'rbf'	0.439	82.674	0.477
All except for SCH	XGB	'xgb_colsample_bytree': 1.0, 'xgb_gamma': 0.2, 'xgb_learning_rate': 0.01, 'xgb_max_depth': 7, 'xgb_n_estimators': 300, 'xgb_subsample': 0.8	0.463	79.584	0.459
All except for SCH	GPR	1**2 * RBF(length_scale=0.0273)	0.298	90.679	0.525
All except for US	RFR	'max_depth': 15, 'max_features': 'sqrt', 'max_leaf_nodes': None, 'min_samples_leaf': 2, 'n_estimators': 200	0.349	89.073	0.547
All except for US	SVR	'svr_C': 100, 'svr_epsilon': 1, 'svr_gamma': 'auto', 'svr_kernel': 'rbf'	0.366	89.059	0.546
All except for US	XGB	'xgb_colsample_bytree': 0.8, 'xgb_gamma': 0, 'xgb_learning_rate': 0.01, 'xgb_max_depth': 3, 'xgb_n_estimators': 300, 'xgb_subsample': 0.8	0.324	90.521	0.556
All except for US	GPR	1**2 * RBF(length_scale=0.0292)	0.161	101.078	0.62

78

79    **Section A.8: Cross-validation performance of global physically-based models**

80    *Table A.5: Cross-validation performance of global physically-based models. The parameters correspond to the best-performing  
81    combination of parameters tested during the fivefold cross-validation. CH: Switzerland, ALB: Schwäbische Alb, HAI: Hainich-  
82    Dün, SCH: Schorfheide-Chorin, US: United States, R<sup>2</sup>: coefficient of determination, RMSE: root-mean-square error, RRMSE:  
83    relative root-mean-square error.*

Site	Cost function	Percentage of solutions	R <sup>2</sup>	RMSE [g m <sup>-2</sup> ]	RRMSE
All except for CH	laplace_distribution	1	0.034	120.649	0.653
All except for ALB	min_contrast_4	10	0.025	126.039	0.652
All except for HAI	min_contrast_4	10	0.025	124.348	0.625
All except for SCH	laplace_distribution	1	0.009	119.915	0.695
All except for US	min_contrast_1	1	0.266	93.696	0.576

84

85

86 **Section A.9: Cross-validation performance of global hybrid models**

87 *Table A.6: Cross-validation performance of global hybrid models. The parameters correspond to the best-performing  
 88 combination of parameters tested during the fivefold cross-validation using Active Learning with an initial training set size of  
 89 2%. CH: Switzerland, ALB: Schwäbische Alb, HAI: Hainich-Dün, SCH: Schorfheide-Chorin, US: United States, GPR: Gaussian  
 90 Process regression, R<sup>2</sup>: coefficient of determination, RMSE: root-mean-square error, RRMSE: relative root-mean-square error.*  
 91 *Nomenclature of parameter names for GPR according to Pedregosa et al. (2012).*

Site	Model	Parameters	R <sup>2</sup>	RMSE [g m <sup>-2</sup> ]	RRMSE
All except for CH	GPR	1.39**2 * RBF(length_scale=1.29)	0.427	85.269	0.462
All except for ALB	GPR	1.82**2 * RBF(length_scale=1.41)	0.31	95.682	0.495
All except for HAI	GPR	1.26**2 * RBF(length_scale=1.11)	0.237	97.987	0.492
All except for SCH	GPR	1.63**2 * RBF(length_scale=1.26)	0.368	86.338	0.5
All except for US	GPR	1.16**2 * RBF(length_scale=1.09)	0.332	89.463	0.55

92

93

94      **Section A.10: Testing performance of local and transferred empirical models: RFR**

95      *Table A.7: Testing performance of local and transferred empirical Random Forest regression (RFR) models. The parameters*  
 96      *correspond to the best-performing combination of parameters tested during the fivefold cross-validation. CH: Switzerland,*  
 97      *ALB: Schwäbische Alb, HAI: Hainich-Dün, SCH: Schorfheide-Chorin, US: United States, R<sup>2</sup>: coefficient of determination, RMSE:*  
 98      *root-mean-square error, sRMSE: systematic component of RMSE, uRMSE: unsystematic component of RMSE, RRMSE: relative*  
 99      *root-mean-square error, MBE: mean bias error.*

		Training site				
Prediction site	Metric	CH	ALB	HAI	SCH	US
CH	R <sup>2</sup>	0.30 ± 0.14	0.15 ± 0.02	0.01 ± 0.01	0.15 ± 0.02	0.01 ± 0.01
	RMSE	97.67 ± 14.48	120.81 ± 2.34	142.25 ± 6.22	112.16 ± 5.87	231.97 ± 32.68
	sRMSE	113.35 ± 9.02	127.81 ± 2.37	140.14 ± 6.24	112.57 ± 1.81	219.95 ± 26.43
	uRMSE	59.82 ± 8.76	41.61 ± 3.19	23.47 ± 6.62	29.93 ± 6.00	71.03 ± 27.47
	RRMSE	0.56 ± 0.08	0.70 ± 0.01	0.82 ± 0.04	0.65 ± 0.03	1.34 ± 0.19
	MBE	-1.62 ± 14.43	-65.16 ± 4.60	-86.25 ± 10.08	22.32 ± 9.96	189.73 ± 30.65
ALB	R <sup>2</sup>	0.28 ± 0.08	0.51 ± 0.17	0.34 ± 0.02	0.49 ± 0.03	0.30 ± 0.02
	RMSE	126.00 ± 13.26	61.60 ± 10.74	73.85 ± 1.20	104.79 ± 8.47	260.84 ± 43.11
	sRMSE	132.69 ± 11.92	85.05 ± 4.28	87.37 ± 0.61	116.88 ± 4.64	260.01 ± 38.75
	uRMSE	40.51 ± 7.35	55.77 ± 15.19	46.59 ± 2.52	50.43 ± 9.42	46.06 ± 12.45
	RRMSE	0.91 ± 0.10	0.44 ± 0.07	0.53 ± 0.01	0.75 ± 0.06	1.87 ± 0.31
	MBE	101.83 ± 15.73	3.44 ± 12.53	-22.47 ± 2.40	80.84 ± 6.72	245.55 ± 41.03
HAI	R <sup>2</sup>	0.32 ± 0.07	0.45 ± 0.02	0.64 ± 0.11	0.43 ± 0.05	0.22 ± 0.05
	RMSE	138.66 ± 14.88	63.99 ± 1.42	50.73 ± 12.60	101.03 ± 4.03	293.26 ± 41.64
	sRMSE	145.82 ± 14.20	85.35 ± 0.16	82.50 ± 9.68	114.20 ± 2.13	292.95 ± 39.55
	uRMSE	44.38 ± 6.74	56.44 ± 1.60	64.28 ± 5.88	52.93 ± 4.83	32.06 ± 12.20
	RRMSE	1.20 ± 0.13	0.55 ± 0.01	0.44 ± 0.10	0.87 ± 0.03	2.53 ± 0.36
	MBE	117.78 ± 17.85	4.41 ± 2.84	-4.10 ± 6.45	76.01 ± 3.20	279.96 ± 41.41
SCH	R <sup>2</sup>	0.19 ± 0.06	0.31 ± 0.02	0.16 ± 0.02	0.32 ± 0.09	0.09 ± 0.01
	RMSE	114.93 ± 5.97	123.22 ± 1.85	139.90 ± 1.74	103.30 ± 10.26	227.35 ± 45.71
	sRMSE	124.93 ± 5.18	138.81 ± 1.69	147.01 ± 0.98	120.49 ± 11.52	226.85 ± 41.93
	uRMSE	48.12 ± 8.52	63.90 ± 1.65	44.88 ± 4.71	60.01 ± 16.54	39.01 ± 12.37
	RRMSE	0.52 ± 0.03	0.56 ± 0.01	0.63 ± 0.01	0.46 ± 0.04	1.02 ± 0.21
	MBE	33.07 ± 20.17	-71.83 ± 3.28	-86.43 ± 1.67	0.70 ± 11.84	191.27 ± 49.71
US	R <sup>2</sup>	0.16 ± 0.14	0.32 ± 0.08	0.17 ± 0.16	0.28 ± 0.09	0.47 ± 0.16
	RMSE	173.22 ± 9.53	225.50 ± 3.77	226.10 ± 2.65	173.05 ± 8.70	64.73 ± 11.41
	sRMSE	175.60 ± 9.71	227.59 ± 3.44	226.95 ± 3.07	176.04 ± 8.23	84.35 ± 12.85
	uRMSE	26.53 ± 12.43	30.41 ± 4.20	20.87 ± 6.78	31.94 ± 3.65	51.43 ± 17.73
	RRMSE	0.66 ± 0.04	0.86 ± 0.01	0.86 ± 0.01	0.66 ± 0.03	0.25 ± 0.04
	MBE	-153.32 ± 11.21	-211.03 ± 3.71	-210.25 ± 3.37	-153.95 ± 9.37	0.12 ± 11.91

100

101

102 **Section A.11: Testing performance of local and transferred empirical models: SVR**

103 *Table A.8: Testing performance of local and transferred empirical Support Vector regression (SVR) models. The parameters*  
 104 *correspond to the best-performing combination of parameters tested during the fivefold cross-validation. CH: Switzerland,*  
 105 *ALB: Schwäbische Alb, HAI: Hainich-Dün, SCH: Schorfheide-Chorin, US: United States, R<sup>2</sup>: coefficient of determination, RMSE:*  
 106 *root-mean-square error, sRMSE: systematic component of RMSE, uRMSE: unsystematic component of RMSE, RRMSE: relative*  
 107 *root-mean-square error, MBE: mean bias error.*

		Training site				
Prediction site	Metric	CH	ALB	HAI	SCH	US
CH	R <sup>2</sup>	0.31 ± 0.12	0.26 ± 0.13	0.01 ± 0.01	0.11 ± 0.16	0.06 ± 0.04
	RMSE	96.29 ± 6.44	149.67 ± 19.71	195.16 ± 16.16	132.08 ± 27.73	293.03 ± 57.49
	sRMSE	113.92 ± 9.04	158.61 ± 23.47	185.72 ± 17.25	132.78 ± 33.06	276.07 ± 48.37
	uRMSE	58.90 ± 16.63	53.39 ± 16.13	57.92 ± 14.39	33.89 ± 17.02	94.87 ± 42.37
	RRMSE	0.55 ± 0.03	0.86 ± 0.11	1.12 ± 0.09	0.76 ± 0.16	1.69 ± 0.33
	MBE	-13.29 ± 13.09	-111.13 ± 36.03	-148.94 ± 20.88	-33.73 ± 73.95	251.96 ± 53.69
ALB	R <sup>2</sup>	0.46 ± 0.12	0.54 ± 0.21	0.47 ± 0.02	0.49 ± 0.04	0.25 ± 0.16
	RMSE	97.08 ± 16.87	59.48 ± 13.07	74.84 ± 3.45	89.75 ± 5.74	280.34 ± 30.59
	sRMSE	109.51 ± 15.79	85.21 ± 4.86	93.83 ± 2.46	106.39 ± 4.62	280.43 ± 29.37
	uRMSE	55.63 ± 2.48	59.73 ± 12.97	56.52 ± 1.47	57.02 ± 0.99	38.65 ± 18.03
	RRMSE	0.70 ± 0.12	0.43 ± 0.09	0.54 ± 0.02	0.64 ± 0.04	2.01 ± 0.22
	MBE	67.46 ± 23.94	-6.35 ± 12.74	-40.95 ± 5.37	64.65 ± 7.68	267.23 ± 30.84
HAI	R <sup>2</sup>	0.39 ± 0.04	0.49 ± 0.05	0.65 ± 0.08	0.48 ± 0.05	0.33 ± 0.15
	RMSE	107.06 ± 17.05	62.67 ± 2.62	52.62 ± 11.00	88.42 ± 5.75	281.21 ± 27.60
	sRMSE	115.94 ± 14.23	85.91 ± 0.48	83.64 ± 10.87	105.76 ± 3.62	283.83 ± 26.66
	uRMSE	51.46 ± 5.24	58.60 ± 3.47	64.67 ± 6.39	57.80 ± 2.59	42.84 ± 10.99
	RRMSE	0.92 ± 0.15	0.54 ± 0.02	0.45 ± 0.08	0.76 ± 0.05	2.42 ± 0.24
	MBE	77.08 ± 20.47	-10.15 ± 5.00	-13.82 ± 9.06	62.53 ± 6.07	270.58 ± 27.97
SCH	R <sup>2</sup>	0.33 ± 0.08	0.35 ± 0.06	0.24 ± 0.02	0.42 ± 0.15	0.18 ± 0.07
	RMSE	108.79 ± 10.83	129.53 ± 3.18	139.75 ± 2.47	94.39 ± 8.53	224.30 ± 24.65
	sRMSE	122.02 ± 2.28	146.39 ± 2.76	150.82 ± 1.61	120.78 ± 11.39	226.29 ± 23.89
	uRMSE	60.96 ± 4.19	67.90 ± 6.16	56.62 ± 2.66	73.64 ± 17.66	30.70 ± 17.05
	RRMSE	0.49 ± 0.05	0.58 ± 0.01	0.63 ± 0.01	0.42 ± 0.04	1.01 ± 0.11
	MBE	-14.42 ± 23.94	-85.56 ± 4.82	-92.86 ± 2.62	-8.22 ± 12.60	191.96 ± 28.19
US	R <sup>2</sup>	0.30 ± 0.03	0.27 ± 0.10	0.32 ± 0.05	0.23 ± 0.05	0.59 ± 0.08
	RMSE	212.61 ± 50.25	259.17 ± 42.80	272.06 ± 35.13	206.50 ± 124.22	56.89 ± 12.09
	sRMSE	216.26 ± 49.34	261.03 ± 44.64	275.78 ± 35.18	201.94 ± 127.46	84.09 ± 12.92
	uRMSE	37.24 ± 10.22	38.86 ± 11.65	44.91 ± 4.87	36.01 ± 10.46	61.61 ± 7.79
	RRMSE	0.81 ± 0.19	0.99 ± 0.16	1.04 ± 0.13	0.79 ± 0.47	0.22 ± 0.04
	MBE	-197.74 ± 53.27	-245.99 ± 48.23	-262.03 ± 37.05	-173.23 ± 140.11	5.06 ± 9.42

108

109

110 **Section A.12: Testing performance of local and transferred empirical models: XGB**

111 *Table A.9: Testing performance of local and transferred empirical Extreme Gradient Boosting (XGB) regression models. The*  
 112 *parameters correspond to the best-performing combination of parameters tested during the fivefold cross-validation. CH:*  
 113 *Switzerland, ALB: Schwäbische Alb, HAI: Hainich-Dün, SCH: Schorfheide-Chorin, US: United States, R<sup>2</sup>: coefficient of*  
 114 *determination, RMSE: root-mean-square error, sRMSE: systematic component of RMSE, uRMSE: unsystematic component of*  
 115 *RMSE, RRMSE: relative root-mean-square error, MBE: mean bias error.*

		Training site				
Prediction site	Metric	CH	ALB	HAI	SCH	US
CH	R <sup>2</sup>	0.21 ± 0.12	0.14 ± 0.04	0.03 ± 0.02	0.12 ± 0.02	0.01 ± 0.01
	RMSE	108.91 ± 14.41	120.79 ± 3.77	135.00 ± 7.13	118.44 ± 9.55	245.19 ± 28.16
	sRMSE	114.75 ± 9.07	126.57 ± 3.28	122.35 ± 8.47	115.46 ± 4.44	226.56 ± 20.67
	uRMSE	45.54 ± 17.66	36.60 ± 9.39	55.24 ± 13.55	32.39 ± 14.39	92.17 ± 25.75
	RRMSE	0.62 ± 0.08	0.70 ± 0.02	0.78 ± 0.04	0.68 ± 0.05	1.41 ± 0.16
	MBE	-4.43 ± 22.19	-62.52 ± 6.61	-50.27 ± 19.49	32.21 ± 15.07	197.58 ± 23.88
ALB	R <sup>2</sup>	0.26 ± 0.08	0.52 ± 0.14	0.27 ± 0.04	0.43 ± 0.05	0.29 ± 0.04
	RMSE	160.89 ± 25.32	62.46 ± 9.74	80.56 ± 5.19	110.64 ± 11.96	276.58 ± 47.77
	sRMSE	160.00 ± 25.02	85.18 ± 4.05	85.99 ± 1.05	119.77 ± 6.70	271.73 ± 40.69
	uRMSE	30.33 ± 12.62	55.91 ± 12.22	31.39 ± 11.26	44.40 ± 11.66	48.92 ± 35.67
	RRMSE	1.16 ± 0.18	0.45 ± 0.07	0.58 ± 0.04	0.79 ± 0.09	1.99 ± 0.34
	MBE	134.91 ± 29.78	5.48 ± 12.68	-15.09 ± 5.91	84.81 ± 9.27	257.94 ± 42.81
HAI	R <sup>2</sup>	0.28 ± 0.10	0.42 ± 0.03	0.60 ± 0.12	0.39 ± 0.07	0.21 ± 0.07
	RMSE	171.69 ± 29.31	66.22 ± 2.31	54.35 ± 12.33	104.55 ± 5.87	309.70 ± 49.19
	sRMSE	170.75 ± 27.39	85.31 ± 0.16	82.40 ± 9.71	115.71 ± 2.53	305.52 ± 44.89
	uRMSE	29.35 ± 16.82	53.67 ± 2.76	60.99 ± 7.58	48.62 ± 8.13	48.84 ± 29.02
	RRMSE	1.48 ± 0.25	0.57 ± 0.02	0.47 ± 0.09	0.90 ± 0.05	2.67 ± 0.42
	MBE	146.87 ± 32.43	1.04 ± 4.03	-1.05 ± 6.02	78.21 ± 3.66	293.04 ± 46.78
SCH	R <sup>2</sup>	0.15 ± 0.05	0.30 ± 0.03	0.16 ± 0.03	0.28 ± 0.11	0.08 ± 0.02
	RMSE	143.38 ± 24.47	122.21 ± 1.83	138.84 ± 3.83	105.79 ± 10.74	245.25 ± 54.24
	sRMSE	144.35 ± 18.33	137.27 ± 1.59	145.15 ± 3.27	120.40 ± 11.45	240.77 ± 50.72
	uRMSE	41.01 ± 15.05	62.41 ± 3.65	42.00 ± 4.92	54.61 ± 18.41	42.26 ± 27.55
	RRMSE	0.65 ± 0.11	0.55 ± 0.01	0.63 ± 0.02	0.48 ± 0.04	1.11 ± 0.24
	MBE	73.97 ± 39.45	-68.78 ± 3.22	-83.11 ± 5.78	1.31 ± 10.30	207.36 ± 58.12
US	R <sup>2</sup>	0.11 ± 0.07	0.01 ± 0.01	0.09 ± 0.11	0.20 ± 0.10	0.48 ± 0.14
	RMSE	188.78 ± 15.31	230.54 ± 10.24	218.55 ± 8.05	161.57 ± 10.24	70.77 ± 16.44
	sRMSE	190.10 ± 14.80	229.73 ± 9.88	218.53 ± 8.71	164.25 ± 9.59	85.74 ± 12.11
	uRMSE	28.13 ± 7.24	18.67 ± 5.59	25.85 ± 6.50	27.59 ± 10.06	57.22 ± 15.89
	RRMSE	0.72 ± 0.06	0.88 ± 0.04	0.84 ± 0.03	0.62 ± 0.04	0.27 ± 0.06
	MBE	-169.64 ± 16.38	-213.05 ± 10.63	-201.01 ± 9.52	-140.22 ± 11.11	8.79 ± 16.87

116

117

118 **Section A.13: Testing performance of local and transferred empirical models: GPR**

119 *Table A.10: Testing performance of local and transferred empirical Gaussian Process regression (GPR) models. The parameters*  
 120 *correspond to the best-performing combination of parameters tested during the fivefold cross-validation. CH: Switzerland,*  
 121 *ALB: Schwäbische Alb, HAI: Hainich-Dün, SCH: Schorfheide-Chorin, US: United States, R<sup>2</sup>: coefficient of determination, RMSE:*  
 122 *root-mean-square error, sRMSE: systematic component of RMSE, uRMSE: unsystematic component of RMSE, RRMSE: relative*  
 123 *root-mean-square error, MBE: mean bias error.*

		Training site				
Prediction site	Metric	CH	ALB	HAI	SCH	US
CH	R <sup>2</sup>	0.08 ± 0.05	0.04 ± 0.02	0.00 ± 0.01	0.01 ± 0.01	0.01 ± 0.00
	RMSE	111.15 ± 11.89	119.06 ± 0.86	127.48 ± 0.77	120.40 ± 0.54	141.09 ± 0.68
	sRMSE	112.90 ± 8.85	116.71 ± 0.31	126.56 ± 0.30	119.92 ± 0.44	141.15 ± 0.67
	uRMSE	29.83 ± 7.91	23.29 ± 3.44	14.59 ± 4.63	10.04 ± 6.02	4.10 ± 0.51
	RRMSE	0.64 ± 0.06	0.69 ± 0.00	0.73 ± 0.00	0.69 ± 0.00	0.81 ± 0.00
	MBE	-2.56 ± 6.57	-37.63 ± 0.98	-62.02 ± 0.58	47.10 ± 1.32	87.98 ± 1.09
ALB	R <sup>2</sup>	0.08 ± 0.05	0.40 ± 0.17	0.30 ± 0.03	0.16 ± 0.06	0.03 ± 0.01
	RMSE	120.96 ± 8.61	68.44 ± 10.35	73.29 ± 2.35	117.93 ± 3.14	149.15 ± 0.93
	sRMSE	106.10 ± 4.70	84.25 ± 4.60	85.62 ± 0.56	121.40 ± 3.34	149.21 ± 0.91
	uRMSE	57.35 ± 11.71	49.63 ± 11.75	44.02 ± 4.02	27.76 ± 8.15	4.34 ± 1.28
	RRMSE	0.87 ± 0.06	0.49 ± 0.07	0.53 ± 0.02	0.85 ± 0.02	1.07 ± 0.01
	MBE	62.85 ± 7.90	3.40 ± 3.12	-13.74 ± 3.73	87.03 ± 4.69	122.53 ± 1.11
HAI	R <sup>2</sup>	0.10 ± 0.02	0.31 ± 0.02	0.54 ± 0.17	0.18 ± 0.08	0.02 ± 0.00
	RMSE	139.71 ± 10.59	72.53 ± 1.41	58.39 ± 15.42	119.74 ± 6.59	169.59 ± 1.21
	sRMSE	124.83 ± 6.69	85.96 ± 0.43	83.06 ± 9.53	124.76 ± 4.28	169.53 ± 1.13
	uRMSE	62.36 ± 10.70	46.09 ± 1.54	57.05 ± 9.37	32.59 ± 11.80	4.80 ± 2.47
	RRMSE	1.20 ± 0.09	0.63 ± 0.01	0.50 ± 0.12	1.03 ± 0.06	1.46 ± 0.01
	MBE	90.08 ± 9.29	9.95 ± 3.68	-3.37 ± 11.12	90.80 ± 5.68	146.09 ± 1.31
SCH	R <sup>2</sup>	0.03 ± 0.04	0.13 ± 0.01	0.16 ± 0.04	0.16 ± 0.11	0.01 ± 0.00
	RMSE	130.30 ± 5.04	132.47 ± 1.17	139.77 ± 3.58	114.35 ± 13.95	125.86 ± 0.39
	sRMSE	122.19 ± 1.57	138.90 ± 1.49	147.30 ± 2.73	120.78 ± 11.53	125.90 ± 0.36
	uRMSE	41.31 ± 19.05	41.74 ± 2.03	46.04 ± 6.08	42.75 ± 15.76	3.52 ± 1.53
	RRMSE	0.59 ± 0.02	0.60 ± 0.01	0.63 ± 0.02	0.51 ± 0.05	0.57 ± 0.00
	MBE	-24.84 ± 7.79	-71.68 ± 2.96	-86.85 ± 4.66	0.83 ± 12.62	39.83 ± 1.14
US	R <sup>2</sup>	0.08 ± 0.05	0.04 ± 0.02	0.16 ± 0.04	0.09 ± 0.03	0.35 ± 0.07
	RMSE	124.71 ± 1.27	150.08 ± 0.78	170.72 ± 0.70	94.63 ± 0.49	71.05 ± 13.37
	sRMSE	123.64 ± 0.65	150.07 ± 0.70	170.33 ± 0.57	94.82 ± 0.49	84.52 ± 12.87
	uRMSE	14.83 ± 6.96	4.60 ± 1.81	11.10 ± 3.36	5.57 ± 2.35	45.13 ± 6.76
	RRMSE	0.48 ± 0.00	0.57 ± 0.00	0.65 ± 0.00	0.36 ± 0.00	0.27 ± 0.05
	MBE	-88.80 ± 0.88	-123.02 ± 0.86	-146.93 ± 0.65	-39.81 ± 1.23	2.37 ± 12.21

125 **Section A.14: Testing performance of local and transferred physically-based models**

126 *Table A.11: Testing performance of local and transferred physically-based models. The parameters correspond to the best-*  
 127 *performing combination of parameters tested during the fivefold cross-validation. CH: Switzerland, ALB: Schwäbische Alb,*  
 128 *HAI: Hainich-Dün, SCH: Schorfheide-Chorin, US: United States, R<sup>2</sup>: coefficient of determination, RMSE: root-mean-square error,*  
 129 *sRMSE: systematic component of RMSE, uRMSE: unsystematic component of RMSE, RRMSE: relative root-mean-square error,*  
 130 *MBE: mean bias error.*

		Calibration site				
Prediction site	Metric	CH	ALB	HAI	SCH	US
CH	R <sup>2</sup>	0.26 ± 0.17	0.14 ± 0.00	0.14 ± 0.00	0.12 ± 0.00	0.13 ± 0.00
	RMSE	102.57 ± 16.64	105.26 ± 0.00	105.26 ± 0.00	104.55 ± 0.00	111.23 ± 6.82
	sRMSE	115.97 ± 11.28	112.62 ± 0.00	112.62 ± 0.00	109.99 ± 0.00	111.71 ± 1.21
	uRMSE	56.88 ± 12.05	40.06 ± 0.00	40.06 ± 0.00	34.17 ± 0.00	35.29 ± 0.87
	RRMSE	0.59 ± 0.09	0.61 ± 0.00	0.61 ± 0.00	0.60 ± 0.00	0.64 ± 0.04
	MBE	-24.33 ± 15.87	-24.61 ± 0.00	-24.61 ± 0.00	-3.44 ± 0.00	-18.58 ± 7.28
ALB	R <sup>2</sup>	0.41 ± 0.00	0.43 ± 0.17	0.43 ± 0.00	0.45 ± 0.00	0.22 ± 0.21
	RMSE	74.27 ± 0.25	73.17 ± 7.39	71.13 ± 0.00	87.55 ± 0.00	95.30 ± 9.71
	sRMSE	91.30 ± 0.15	90.63 ± 4.41	89.28 ± 0.00	103.76 ± 0.00	94.25 ± 7.34
	uRMSE	53.10 ± 0.09	51.44 ± 13.34	53.95 ± 0.00	55.69 ± 0.00	56.83 ± 2.11
	RRMSE	0.53 ± 0.00	0.52 ± 0.05	0.51 ± 0.00	0.63 ± 0.00	0.68 ± 0.07
	MBE	34.97 ± 0.37	32.34 ± 9.65	29.33 ± 0.00	60.49 ± 0.00	19.05 ± 37.63
HAI	R <sup>2</sup>	0.53 ± 0.00	0.53 ± 0.00	0.66 ± 0.10	0.50 ± 0.00	0.26 ± 0.23
	RMSE	80.00 ± 0.20	76.46 ± 0.00	68.05 ± 7.50	98.54 ± 0.00	97.42 ± 2.45
	sRMSE	99.66 ± 0.12	96.69 ± 0.00	93.07 ± 7.16	115.10 ± 0.00	99.09 ± 12.78
	uRMSE	59.42 ± 0.06	59.18 ± 0.00	63.13 ± 6.46	59.47 ± 0.00	54.68 ± 4.44
	RRMSE	0.69 ± 0.00	0.66 ± 0.00	0.59 ± 0.05	0.85 ± 0.00	0.84 ± 0.02
	MBE	51.81 ± 0.23	45.83 ± 0.00	42.64 ± 7.51	77.44 ± 0.00	41.44 ± 31.11
SCH	R <sup>2</sup>	0.21 ± 0.00	0.20 ± 0.00	0.20 ± 0.00	0.30 ± 0.04	0.12 ± 0.12
	RMSE	114.19 ± 0.09	116.67 ± 0.00	116.67 ± 0.00	103.95 ± 11.54	133.47 ± 27.96
	sRMSE	125.42 ± 0.08	127.32 ± 0.00	127.32 ± 0.00	120.51 ± 11.65	130.78 ± 11.16
	uRMSE	51.87 ± 0.01	50.98 ± 0.00	50.98 ± 0.00	60.75 ± 5.32	66.61 ± 10.26
	RRMSE	0.51 ± 0.00	0.53 ± 0.00	0.53 ± 0.00	0.47 ± 0.04	0.60 ± 0.13
	MBE	-40.07 ± 0.25	-45.64 ± 0.00	-45.64 ± 0.00	-9.99 ± 6.58	-45.40 ± 31.62
US	R <sup>2</sup>	0.45 ± 0.00	0.44 ± 0.00	0.44 ± 0.00	0.43 ± 0.00	0.30 ± 0.24
	RMSE	196.60 ± 1.42	196.25 ± 0.00	196.25 ± 0.00	184.59 ± 0.00	185.01 ± 11.81
	sRMSE	201.31 ± 1.51	201.00 ± 0.00	201.00 ± 0.00	190.55 ± 0.00	187.33 ± 10.73
	uRMSE	43.27 ± 0.53	43.42 ± 0.00	43.42 ± 0.00	47.29 ± 0.00	36.63 ± 5.86
	RRMSE	0.75 ± 0.01	0.75 ± 0.00	0.75 ± 0.00	0.71 ± 0.00	0.71 ± 0.04
	MBE	-182.43 ± 1.66	-182.09 ± 0.00	-182.09 ± 0.00	-170.48 ± 0.00	-167.32 ± 6.38

132 **Section A.15: Testing performance of local and transferred hybrid models**

133 *Table A.12: Testing performance of local and transferred hybrid models. The parameters correspond to the best-performing  
 134 combination of parameters tested during the fivefold cross-validation using Active Learning with an initial training set size of  
 135 2%. CH: Switzerland, ALB: Schwäbische Alb, HAI: Hainich-Dün, SCH: Schorfheide-Chorin, US: United States, R<sup>2</sup>: coefficient of  
 136 determination, RMSE: root-mean-square error, sRMSE: systematic component of RMSE, uRMSE: unsystematic component of  
 137 RMSE, RRMSE: relative root-mean-square error, MBE: mean bias error.*

		Calibration site				
Prediction site	Metric	CH	ALB	HAI	SCH	US
CH	R <sup>2</sup>	0.23 ± 0.14	0.02 ± 0.02	0.02 ± 0.03	0.03 ± 0.03	0.01 ± 0.01
	RMSE	112.22 ± 31.13	127.07 ± 7.94	125.43 ± 9.89	136.69 ± 13.00	164.02 ± 35.27
	sRMSE	113.87 ± 9.18	116.51 ± 7.64	117.34 ± 6.45	125.35 ± 13.19	146.02 ± 14.56
	uRMSE	54.73 ± 39.46	49.79 ± 13.76	44.33 ± 15.06	53.38 ± 17.36	58.53 ± 64.41
	RRMSE	0.64 ± 0.18	0.73 ± 0.05	0.72 ± 0.06	0.79 ± 0.07	0.94 ± 0.20
	MBE	-3.46 ± 17.01	-31.66 ± 21.59	-36.42 ± 18.12	36.96 ± 48.54	93.61 ± 20.14
ALB	R <sup>2</sup>	0.07 ± 0.07	0.46 ± 0.18	0.34 ± 0.07	0.41 ± 0.09	0.03 ± 0.02
	RMSE	122.05 ± 8.44	64.39 ± 11.93	72.30 ± 4.12	107.21 ± 8.09	158.60 ± 28.14
	sRMSE	103.03 ± 10.46	84.85 ± 4.76	86.83 ± 1.25	118.81 ± 4.89	147.49 ± 33.86
	uRMSE	61.51 ± 21.43	54.13 ± 12.30	47.60 ± 5.58	50.35 ± 6.74	42.55 ± 41.87
	RRMSE	0.88 ± 0.06	0.46 ± 0.08	0.52 ± 0.03	0.77 ± 0.06	1.14 ± 0.20
	MBE	55.91 ± 19.27	-0.37 ± 11.47	-19.74 ± 5.34	83.55 ± 6.82	117.33 ± 42.37
HAI	R <sup>2</sup>	0.03 ± 0.03	0.32 ± 0.04	0.54 ± 0.11	0.25 ± 0.06	0.02 ± 0.03
	RMSE	131.67 ± 12.72	72.81 ± 1.65	58.51 ± 11.47	110.02 ± 5.09	179.92 ± 31.30
	sRMSE	112.79 ± 15.17	86.15 ± 0.83	83.22 ± 9.76	115.72 ± 4.17	171.60 ± 35.17
	uRMSE	65.35 ± 16.62	45.90 ± 3.40	58.49 ± 6.67	35.08 ± 7.02	40.01 ± 41.06
	RRMSE	1.13 ± 0.11	0.63 ± 0.01	0.51 ± 0.09	0.95 ± 0.04	1.55 ± 0.27
	MBE	70.71 ± 24.06	0.42 ± 12.18	-9.55 ± 8.77	78.01 ± 6.21	146.89 ± 38.34
SCH	R <sup>2</sup>	0.02 ± 0.02	0.23 ± 0.04	0.17 ± 0.07	0.27 ± 0.15	0.02 ± 0.03
	RMSE	142.90 ± 12.30	129.56 ± 8.21	144.81 ± 6.85	104.35 ± 14.22	144.01 ± 25.57
	sRMSE	129.70 ± 11.57	141.33 ± 6.42	152.09 ± 3.38	120.30 ± 11.46	132.76 ± 16.64
	uRMSE	58.91 ± 12.09	56.03 ± 4.71	44.91 ± 12.62	56.42 ± 18.15	46.69 ± 44.79
	RRMSE	0.64 ± 0.06	0.58 ± 0.04	0.65 ± 0.03	0.47 ± 0.06	0.65 ± 0.12
	MBE	-44.35 ± 27.74	-75.77 ± 12.38	-94.74 ± 5.45	-0.14 ± 8.90	39.24 ± 43.46
US	R <sup>2</sup>	0.13 ± 0.10	0.12 ± 0.10	0.14 ± 0.11	0.19 ± 0.05	0.23 ± 0.26
	RMSE	184.27 ± 27.00	161.10 ± 38.01	155.40 ± 9.64	118.22 ± 23.46	76.40 ± 20.77
	sRMSE	171.80 ± 24.72	159.96 ± 38.99	148.05 ± 10.26	106.73 ± 19.36	84.04 ± 13.67
	uRMSE	63.41 ± 27.27	33.24 ± 13.22	45.41 ± 12.44	52.36 ± 23.27	22.45 ± 24.84
	RRMSE	0.70 ± 0.10	0.62 ± 0.15	0.59 ± 0.04	0.45 ± 0.09	0.29 ± 0.07
	MBE	-148.09 ± 28.52	-132.65 ± 46.57	-120.22 ± 12.54	-48.41 ± 44.96	0.49 ± 7.92

139 **Section A.16: Testing performance of global models**

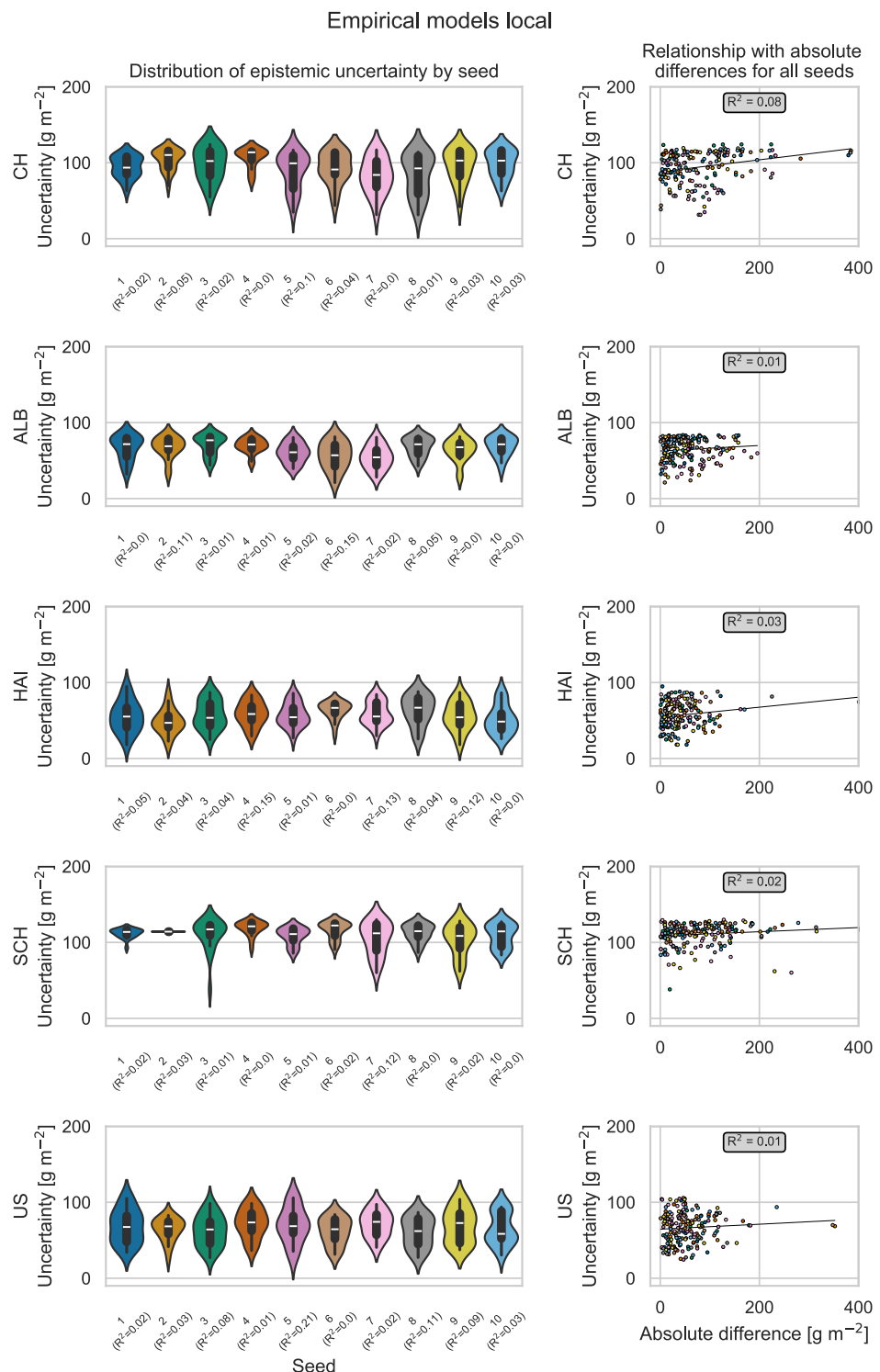
140 *Table A.13: Testing performance of global models. RFR: Random Forest regression, SVR: Support Vector regression, XGB:*  
 141 *Extreme Gradient Boosting regression, GPR: Gaussian process regression, CH: Switzerland, ALB: Schwäbische Alb, HAI: Hainich-*  
 142 *Dün, SCH: Schorfheide-Chorin, US: United States, R<sup>2</sup>: coefficient of determination, RMSE: root-mean-square error, sRMSE:*  
 143 *systematic component of RMSE, uRMSE: unsystematic component of RMSE, RRMSE: relative root-mean-square error, MBE:*  
 144 *mean bias error.*

		Model type					
Prediction site	Metric	Empirical RFR	Empirical SVR	Empirical XGB	Empirical GPR	Physically-based	Hybrid
CH	R <sup>2</sup>	0	0.02	0	0	0.08	0
	RMSE	120.76	130.09	127.31	110.83	108.31	124.45
	sRMSE	110.28	111.77	110.95	110.83	110.73	112.64
	uRMSE	49.22	66.56	62.43	0	23.04	52.92
	RRMSE	0.7	0.75	0.73	0.64	0.62	0.72
	MBE	-2.51	-17.25	11.75	11	-12.76	22.71
ALB	R <sup>2</sup>	0.41	0.49	0.42	0	0.43	0.43
	RMSE	82.9	68.51	83.38	100.75	85.6	74.31
	sRMSE	96.33	89.08	94.89	100.74	101.59	92.2
	uRMSE	49.06	56.93	45.28	1.41	54.72	54.58
	RRMSE	0.6	0.49	0.6	0.72	0.61	0.53
	MBE	46.55	28.87	43.51	54.13	56.67	37.3
HAI	R <sup>2</sup>	0.44	0.43	0.34	0	0.49	0.42
	RMSE	85.81	76.13	93.5	119.47	94.98	73.71
	sRMSE	102.59	94.17	105.47	119.47	111.87	91.89
	uRMSE	56.22	55.43	48.81	0	59.12	54.87
	RRMSE	0.74	0.66	0.81	1.03	0.82	0.64
	MBE	57.15	40.11	62.07	83.08	72.55	34.41
SCH	R <sup>2</sup>	0.28	0.27	0.29	0	0.22	0.18
	RMSE	117.09	127.69	116.49	129.1	111.52	134.26
	sRMSE	132.45	141.13	132.16	129.1	124.09	143.04
	uRMSE	61.9	60.12	62.42	0	54.43	49.34
	RRMSE	0.53	0.58	0.52	0.58	0.5	0.6
	MBE	-58.6	-76.21	-57.97	-49.32	-35.71	-79.54
US	R <sup>2</sup>	0.28	0.05	0.2	0	0.45	0.25
	RMSE	211.53	224.32	211.52	130.9	197.08	136.03
	sRMSE	214.28	221.48	213.6	0	201.81	127.12
	uRMSE	34.21	35.59	29.74	0	43.45	48.43
	RRMSE	0.81	0.86	0.81	0.5	0.75	0.52
	MBE	-196.59	-204.11	-195.82	-98.89	-182.99	-93.37

145

146

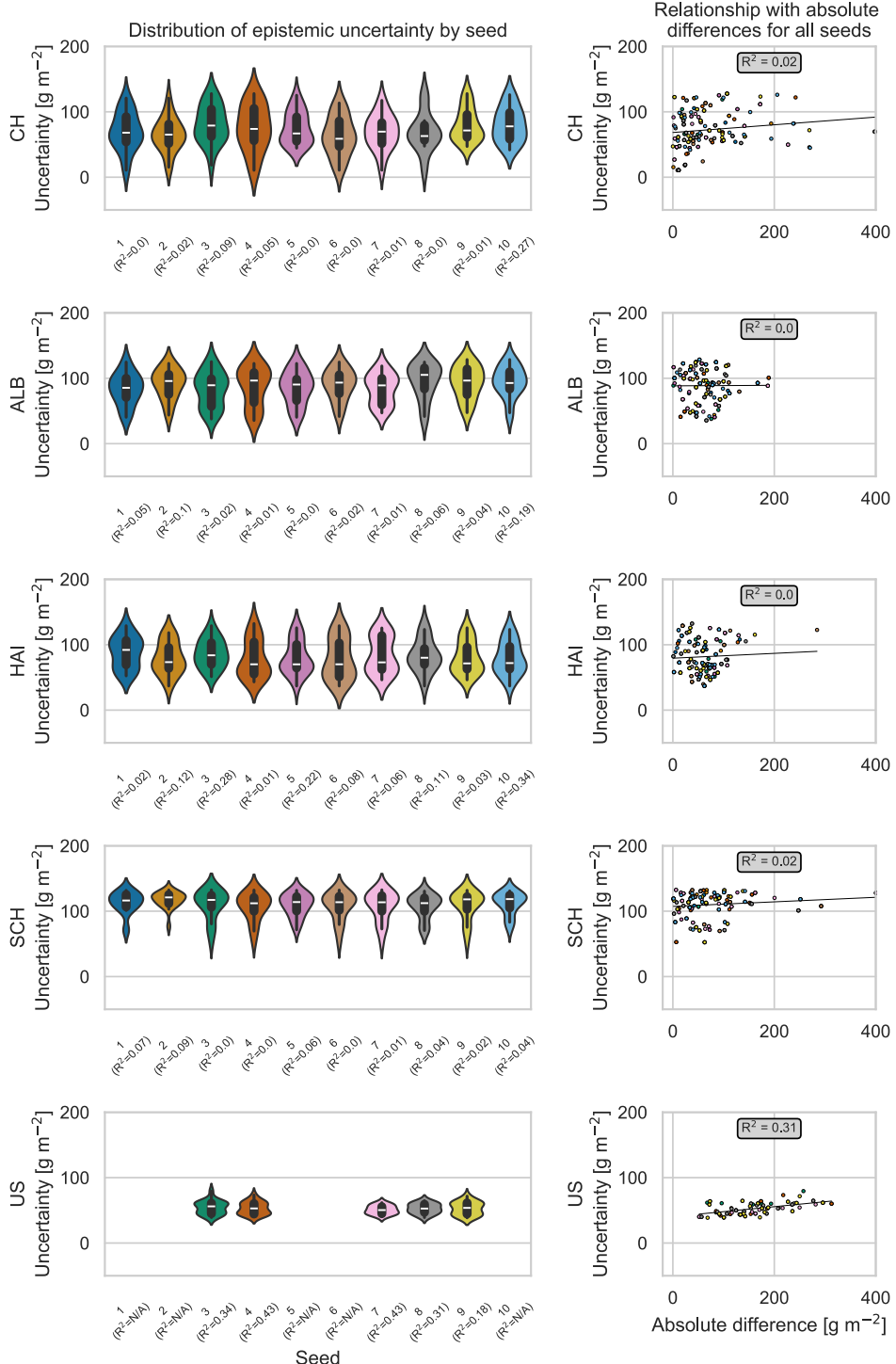
147    Section A.17: Epistemic uncertainty



148

149    Figure A.3: Epistemic uncertainty of local empirical Gaussian process regression models. Absolute differences correspond to  
 150    the absolute difference between measured and predicted biomass value. In case a model predicted a straight line (e.g., the  
 151    prediction is constant), the calculation of the coefficient of determination ( $R^2$ ) was not possible. The corresponding  
 152    predictions were omitted for the calculation of the overall  $R^2$  showed in the textbox in the right column. CH: Switzerland,  
 153    ALB: Schwäbische Alb, HAI: Hainich-Dün, SCH: Schorfheide-Chorin, US: United States.

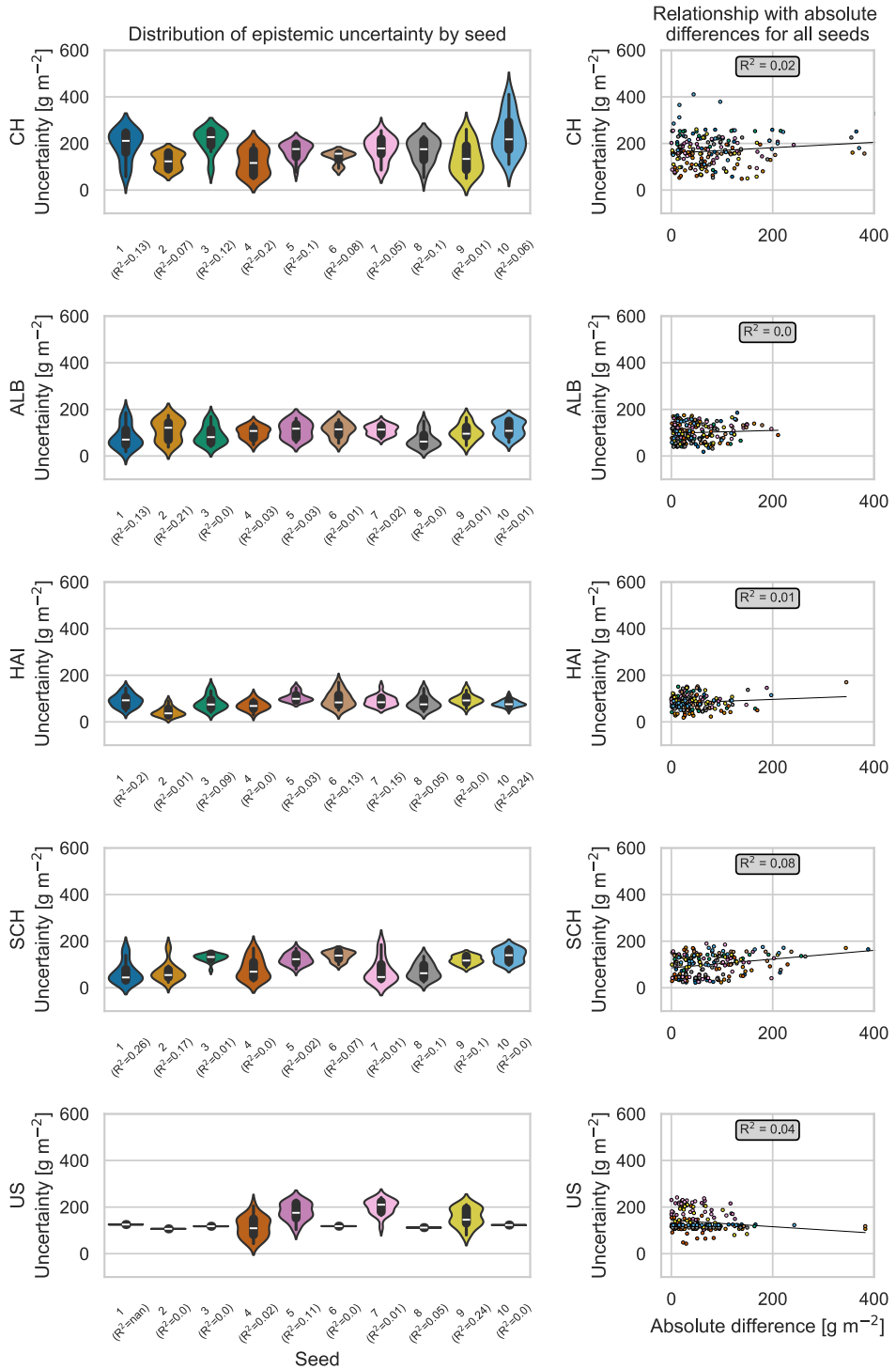
### Physically-based models local



154

155      *Figure A.4: Epistemic uncertainty of local physically-based models. Absolute differences correspond to the absolute*  
 156 *difference between measured and predicted biomass value. If the percentage of solutions was equal to 0.01% (e.g., only 1*  
 157 *sample), no standard deviation and  $R^2$  could be calculated. The corresponding predictions were omitted for the calculation*  
 158 *of the overall  $R^2$  showed in the textbox in the right column. CH: Switzerland, ALB: Schwäbische Alb, HAI: Hainich-Dün, SCH:*  
 159 *Schorfheide-Chorin, US: United States.*

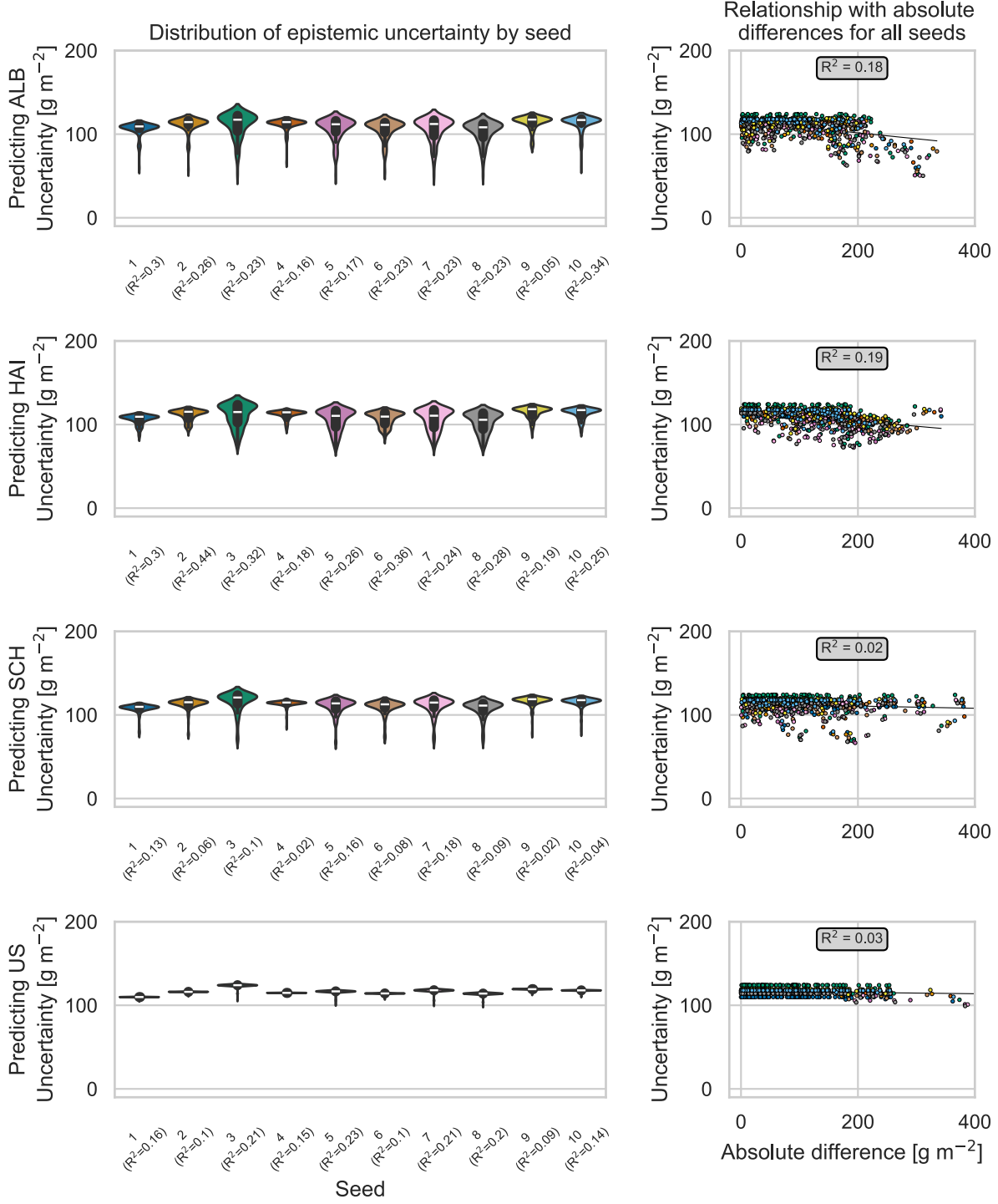
### Hybrid models local



160

161 *Figure A.5: Epistemic uncertainty of local hybrid models. Absolute differences correspond to the absolute difference between*  
 162 *measured and predicted biomass value. In case a model predicted a straight line (e.g., the prediction is constant), the*  
 163 *calculation of the coefficient of determination ( $R^2$ ) was not possible. The corresponding predictions were omitted for the*  
 164 *calculation of the overall  $R^2$  showed in the textbox in the right column. CH: Switzerland, ALB: Schwäbische Alb, HAI:*  
 165 *Dün, SCH: Schorfheide-Chorin, US: United States.*

## Empirical models transferred CH model



166

167

Figure A.6: Epistemic uncertainty of transferred empirical Gaussian process regression models for the CH site. Absolute differences correspond to the absolute difference between measured and predicted biomass value. In case a model predicted a straight line (e.g., the prediction is constant), the calculation of the coefficient of determination ( $R^2$ ) was not possible. The corresponding predictions were omitted for the calculation of the overall  $R^2$  showed in the textbox in the right column. CH: Switzerland, ALB: Schwäbische Alb, HAI: Hainich-Dün, SCH: Schorfheide-Chorin, US: United States.

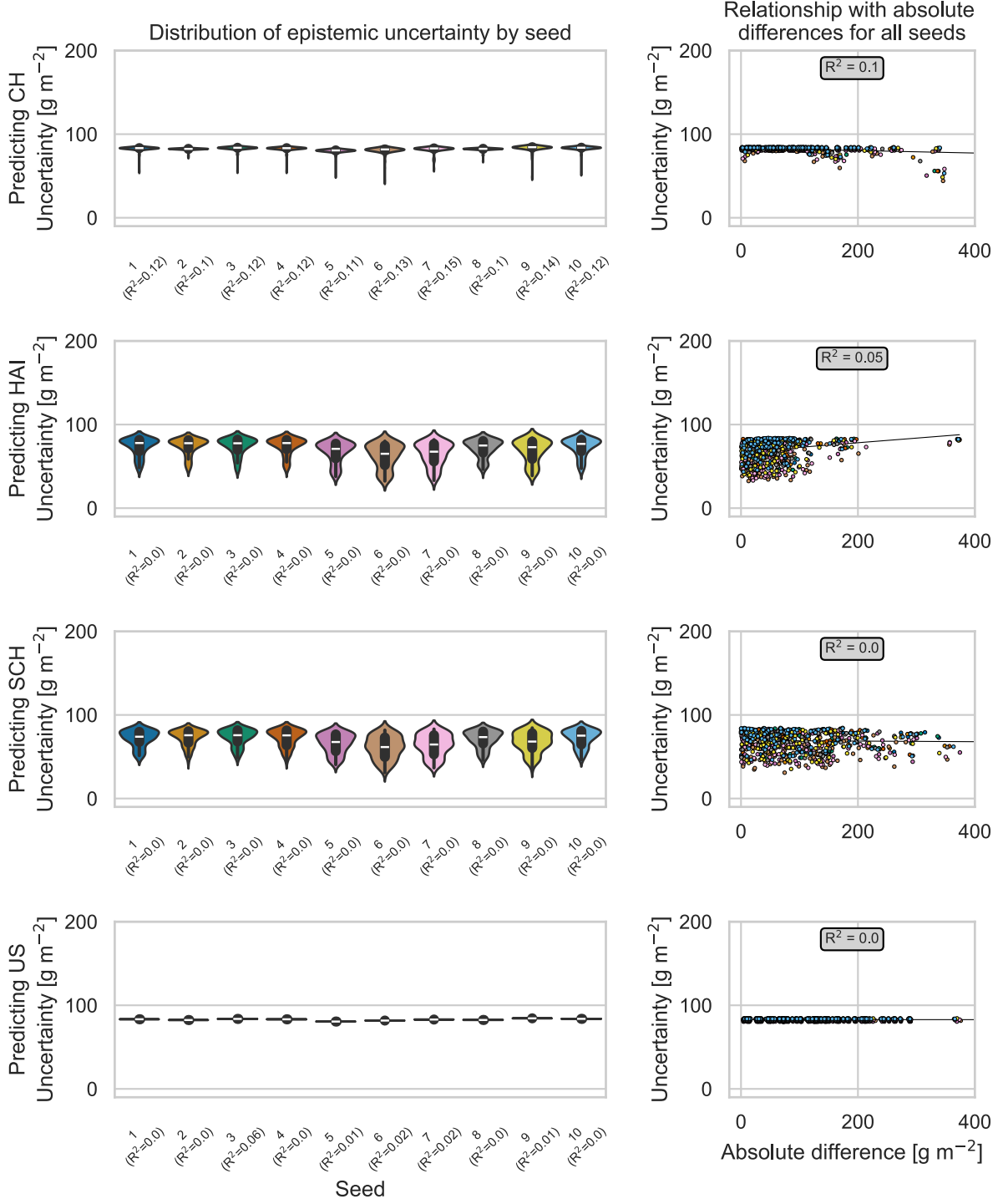
168

169

170

171

## Empirical models transferred ALB model



172

173

Figure A.7: Epistemic uncertainty of transferred empirical Gaussian process regression models for the ALB site. Absolute differences correspond to the absolute difference between measured and predicted biomass value. In case a model predicted a straight line (e.g., the prediction is constant), the calculation of the coefficient of determination ( $R^2$ ) was not possible. The corresponding predictions were omitted for the calculation of the overall  $R^2$  showed in the textbox in the right column. CH: Switzerland, ALB: Schwäbische Alb, HAI: Hainich-Dün, SCH: Schorfheide-Chorin, US: United States.

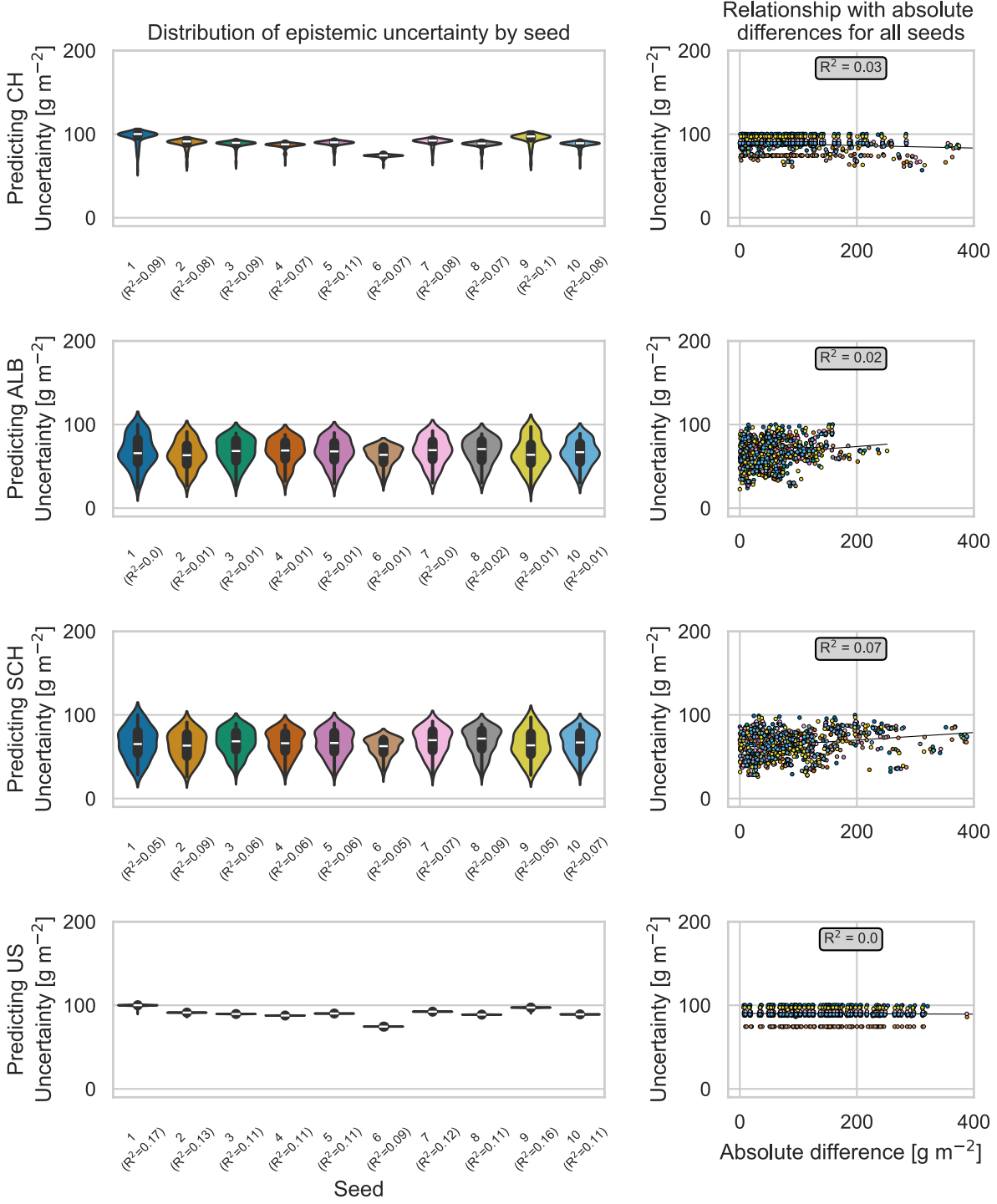
174

175

176

177

## Empirical models transferred HAI model



178

179

180

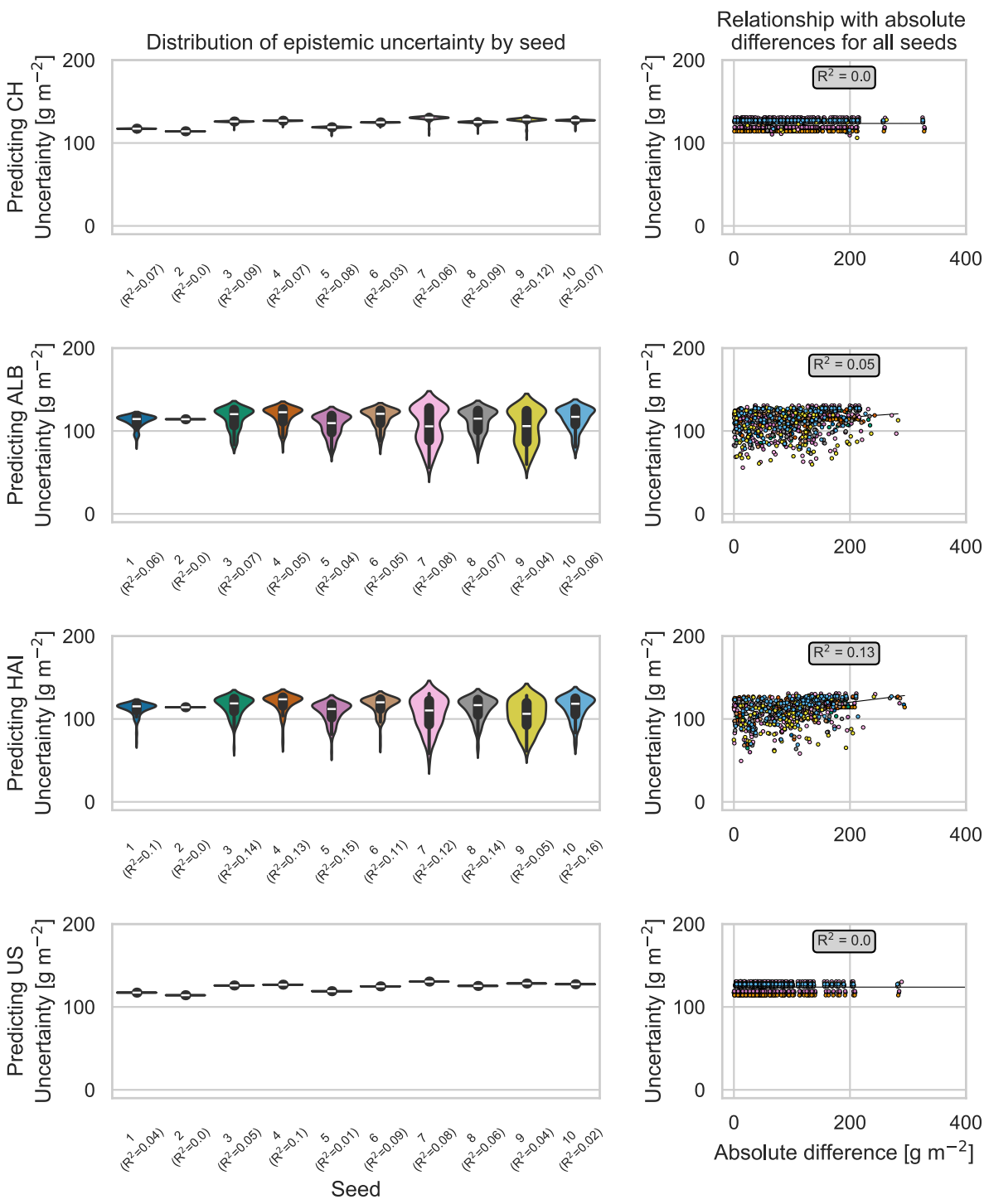
181

182

183

Figure A.8: Epistemic uncertainty of transferred empirical Gaussian process regression models for the HAI site. Absolute differences correspond to the absolute difference between measured and predicted biomass value. In case a model predicted a straight line (e.g., the prediction is constant), the calculation of the coefficient of determination ( $R^2$ ) was not possible. The corresponding predictions were omitted for the calculation of the overall  $R^2$  showed in the textbox in the right column. CH: Switzerland, ALB: Schwäbische Alb, HAI: Hainich-Dün, SCH: Schorfheide-Chorin, US: United States.

### Empirical models transferred SCH model

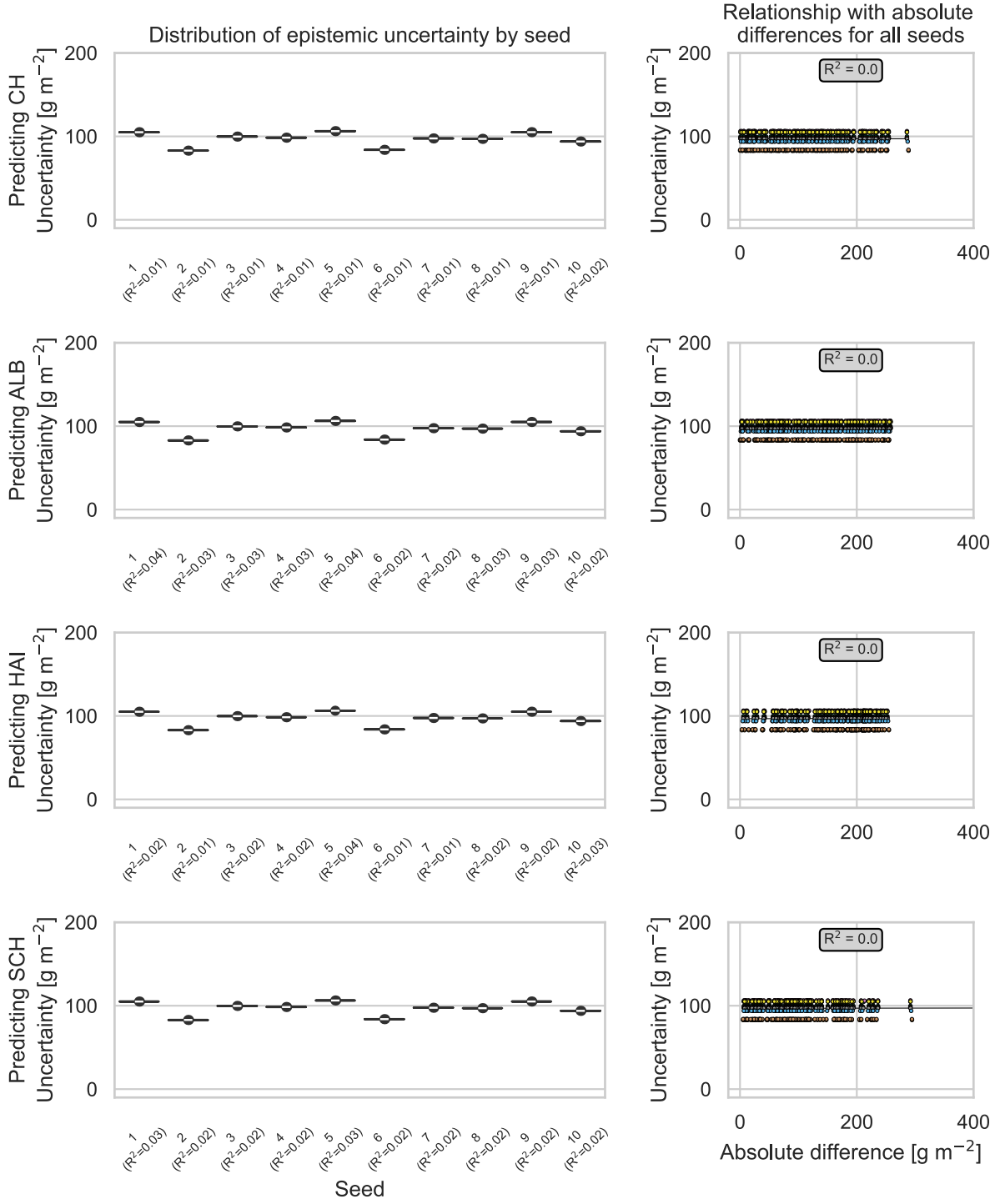


184

185

Figure A.9: Epistemic uncertainty of transferred empirical Gaussian process regression models for the SCH site. Absolute differences correspond to the absolute difference between measured and predicted biomass value. In case a model predicted a straight line (e.g., the prediction is constant), the calculation of the coefficient of determination ( $R^2$ ) was not possible. The corresponding predictions were omitted for the calculation of the overall  $R^2$  showed in the textbox in the right column. CH: Switzerland, ALB: Schwäbische Alb, HAI: Hainich-Dün, SCH: Schorfheide-Chorin, US: United States.

## Empirical models transferred US model



190

191

192

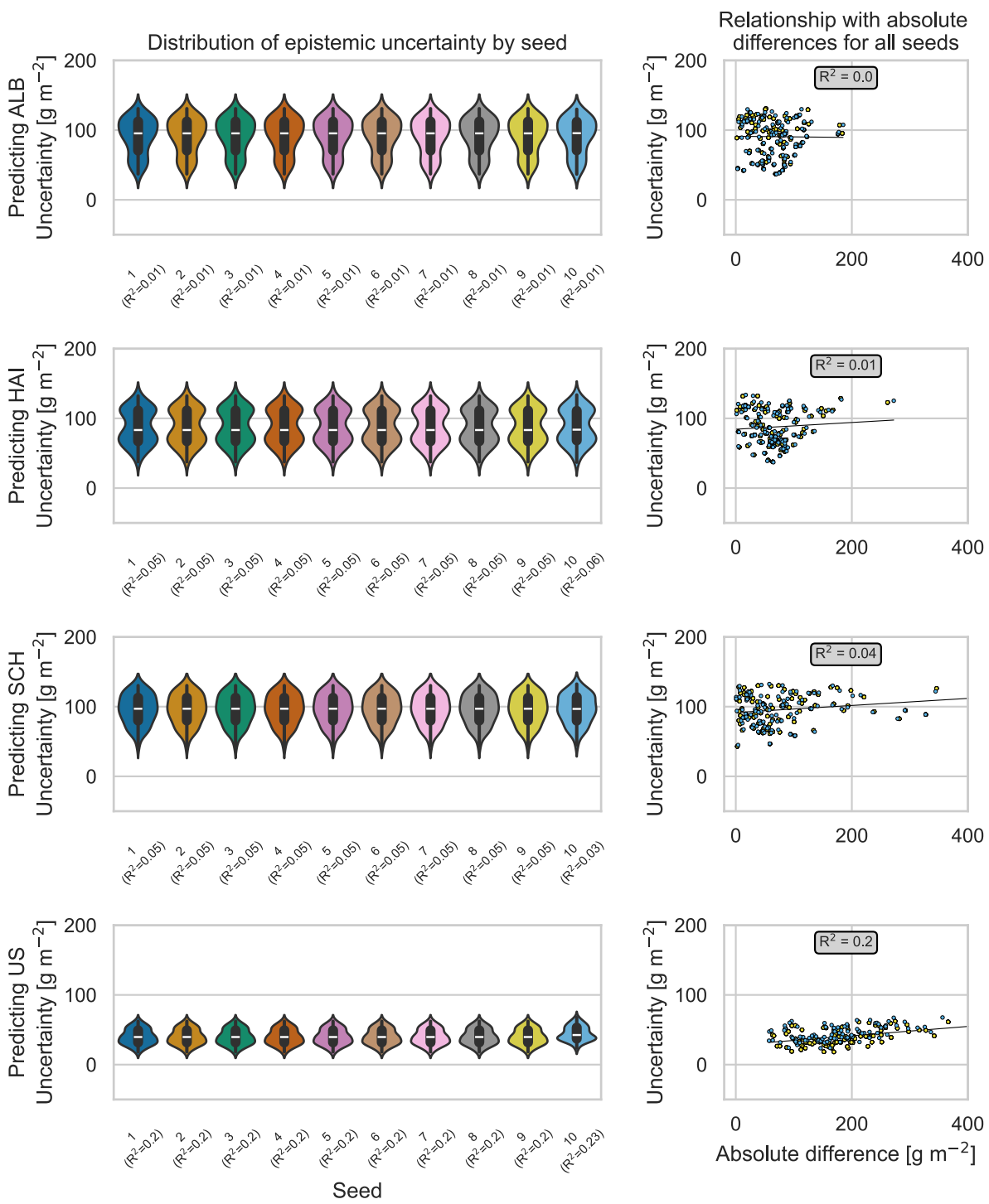
193

194

195

Figure A.10: Epistemic uncertainty of transferred empirical Gaussian process regression models for the US site. Absolute differences correspond to the absolute difference between measured and predicted biomass value. In case a model predicted a straight line (e.g., the prediction is constant), the calculation of the coefficient of determination ( $R^2$ ) was not possible. The corresponding predictions were omitted for the calculation of the overall  $R^2$  showed in the textbox in the right column. CH: Switzerland, ALB: Schwäbische Alb, HAI: Hainich-Dün, SCH: Schorfheide-Chorin, US: United States.

## Physically-based models transferred CH model

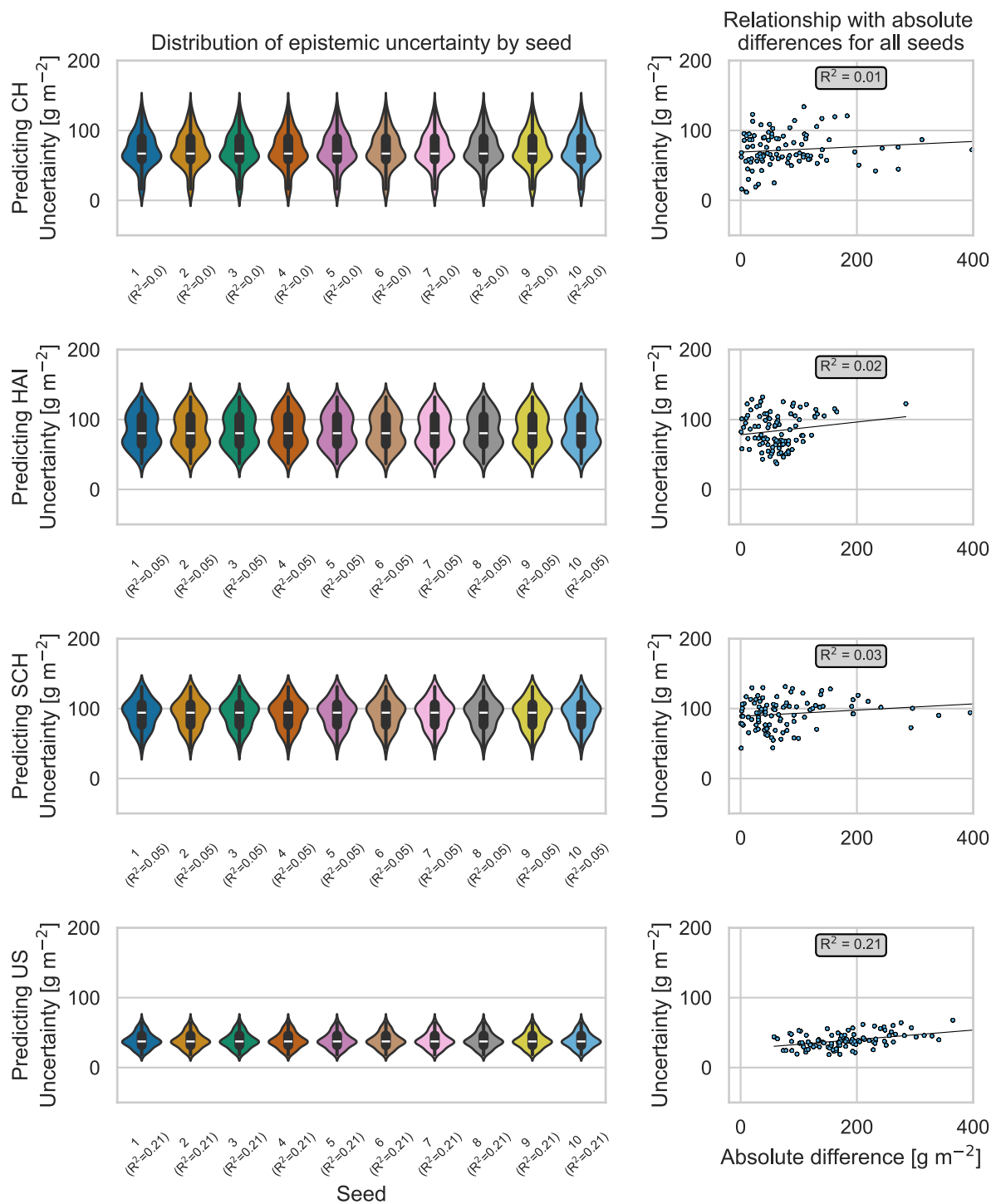


196

197

Figure A.11: Epistemic uncertainty of transferred physically-based models for the CH site. Absolute differences correspond to the absolute difference between measured and predicted biomass value. If the percentage of solutions was equal to 0.01% (e.g., only 1 sample), no standard deviation and  $R^2$  could be calculated. The corresponding predictions were omitted for the calculation of the overall  $R^2$  showed in the textbox in the right column. CH: Switzerland, ALB: Schwäbische Alb, HAI: Hainich-Dün, SCH: Schorfheide-Chorin, US: United States.

### Physically-based models transferred ALB model



202

203

Figure A.12: Epistemic uncertainty of transferred physically-based models for the ALB site. Absolute differences correspond

204

to the absolute difference between measured and predicted biomass value. If the percentage of solutions was equal to

205

0.01% (e.g., only 1 sample), no standard deviation and R<sup>2</sup> could be calculated. The corresponding predictions were omitted

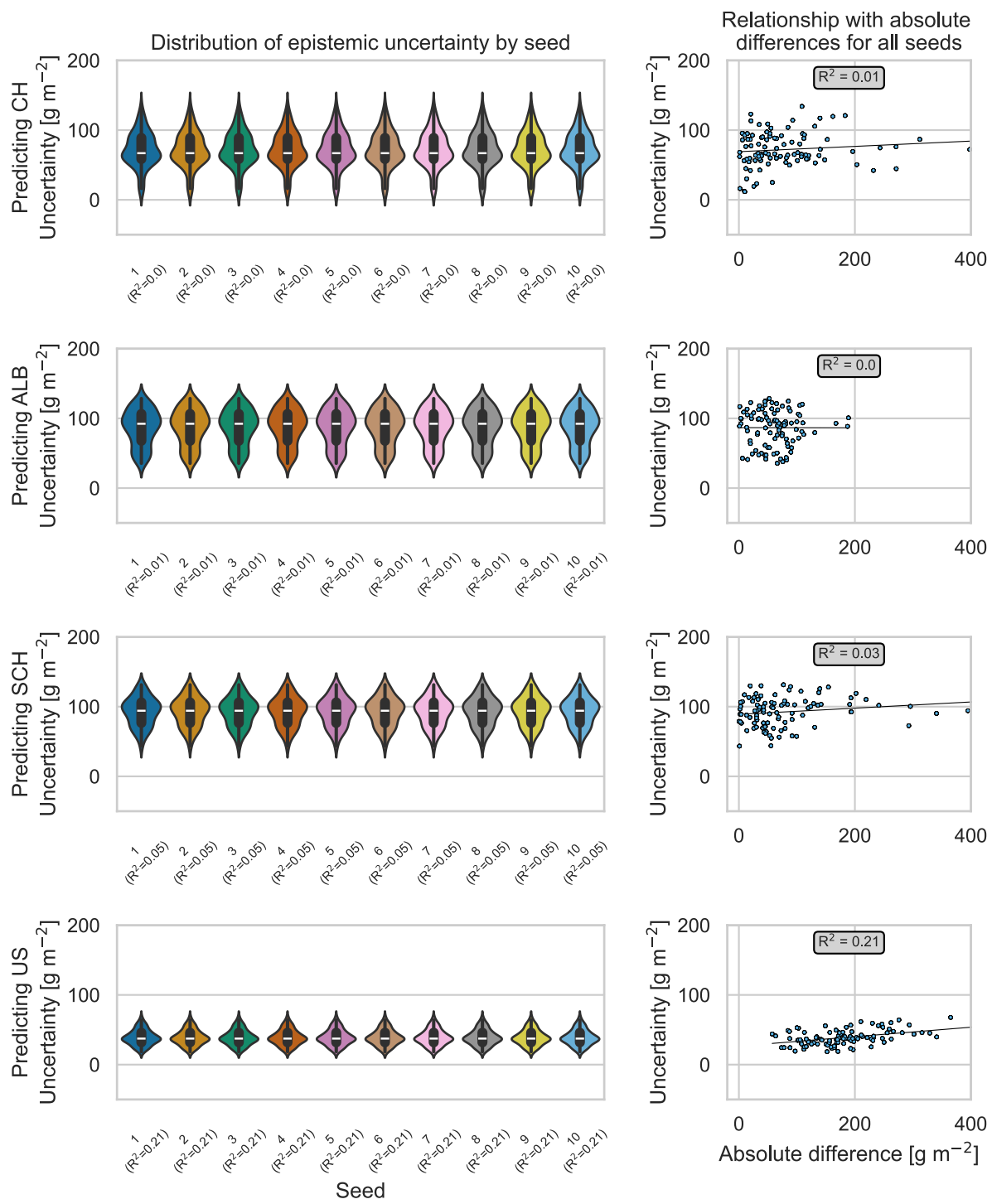
206

for the calculation of the overall R<sup>2</sup> showed in the textbox in the right column. CH: Switzerland, ALB: Schwäbische Alb, HAI:

207

Hainich-Dün, SCH: Schorfheide-Chorin, US: United States.

### Physically-based models transferred HAI model



208

209

210

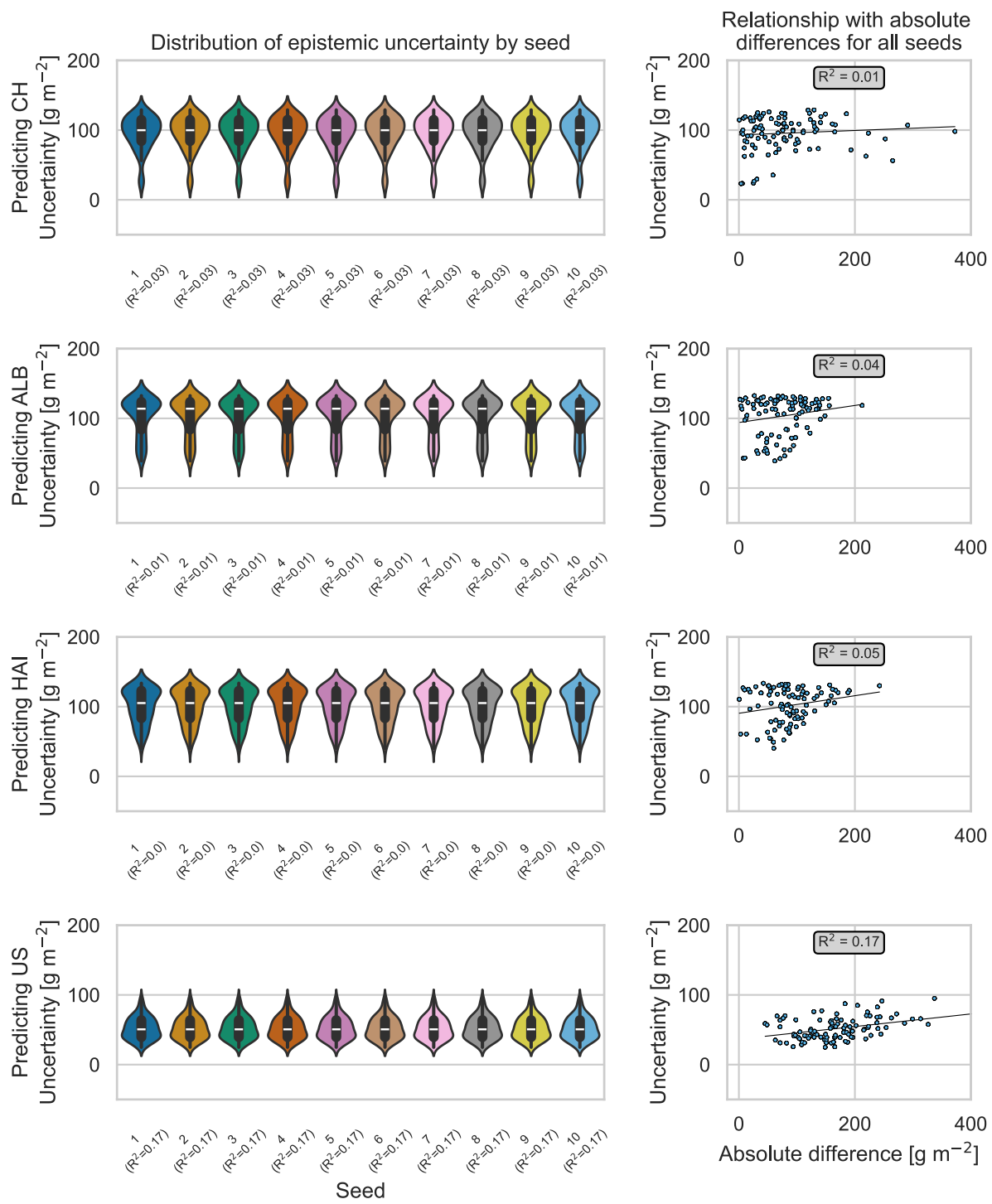
211

212

213

Figure A.13: Epistemic uncertainty of transferred physically-based models for the HAI site. Absolute differences correspond to the absolute difference between measured and predicted biomass value. If the percentage of solutions was equal to 0.01% (e.g., only 1 sample), no standard deviation and  $R^2$  could be calculated. The corresponding predictions were omitted for the calculation of the overall  $R^2$  showed in the textbox in the right column. CH: Switzerland, ALB: Schwäbische Alb, HAI: Hainich-Dün, SCH: Schorfheide-Chorin, US: United States.

### Physically-based models transferred SCH model



214

215

216

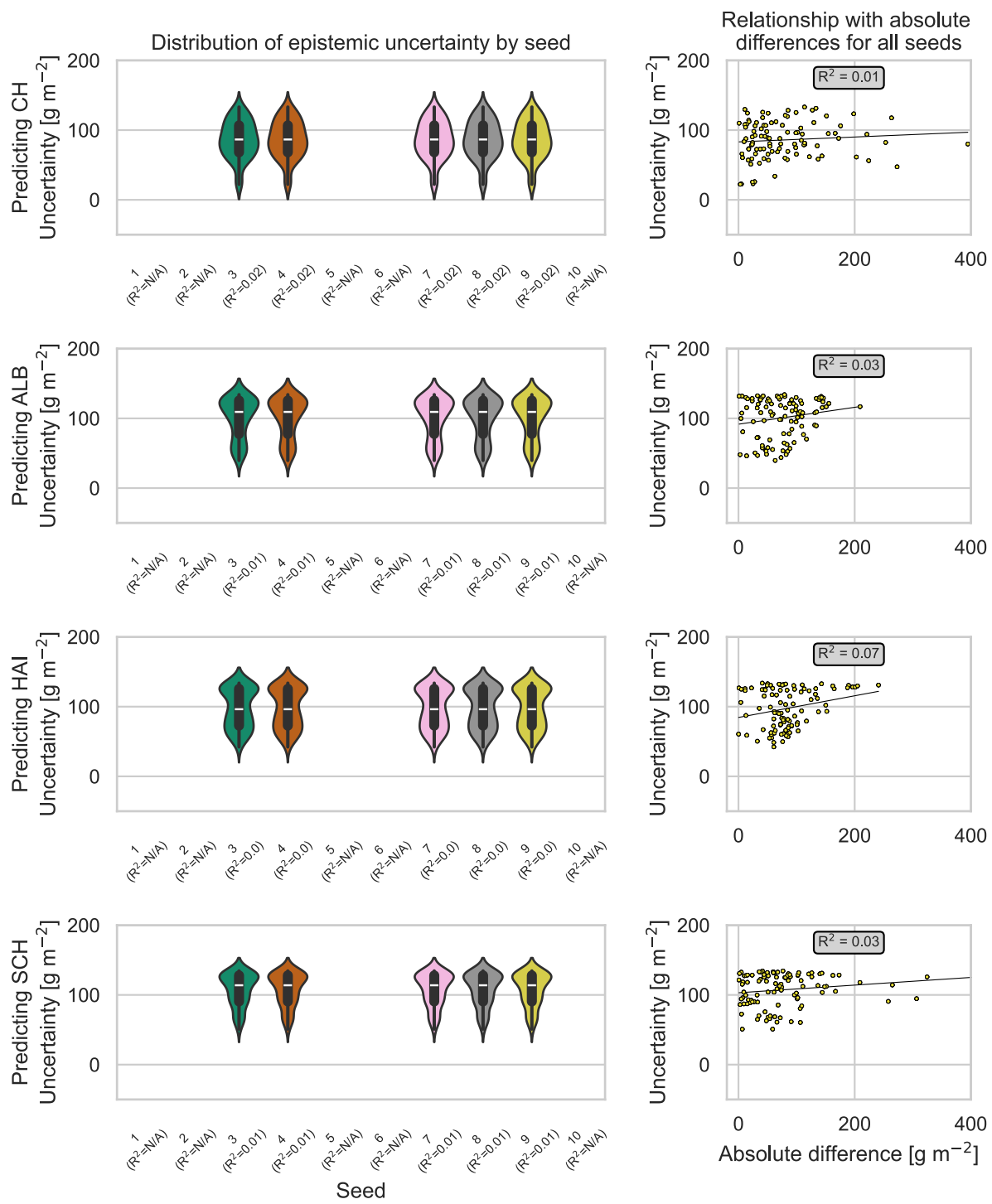
217

218

219

Figure A.14: Epistemic uncertainty of transferred physically-based models for the SCH site. Absolute differences correspond to the absolute difference between measured and predicted biomass value. If the percentage of solutions was equal to 0.01% (e.g., only 1 sample), no standard deviation and  $R^2$  could be calculated. The corresponding predictions were omitted for the calculation of the overall  $R^2$  showed in the textbox in the right column. CH: Switzerland, ALB: Schwäbische Alb, HAI: Hainich-Dün, SCH: Schorfheide-Chorin, US: United States.

### Physically-based models transferred US model



220

221

Figure A.15: Epistemic uncertainty of transferred physically-based models for the US site. Absolute differences correspond to the absolute difference between measured and predicted biomass value. If the percentage of solutions was equal to 0.01% (e.g., only 1 sample), no standard deviation and  $R^2$  could be calculated. The corresponding predictions were omitted for the calculation of the overall  $R^2$  showed in the textbox in the right column. CH: Switzerland, ALB: Schwäbische Alb, HAI: Hainich-Dün, SCH: Schorfheide-Chorin, US: United States.

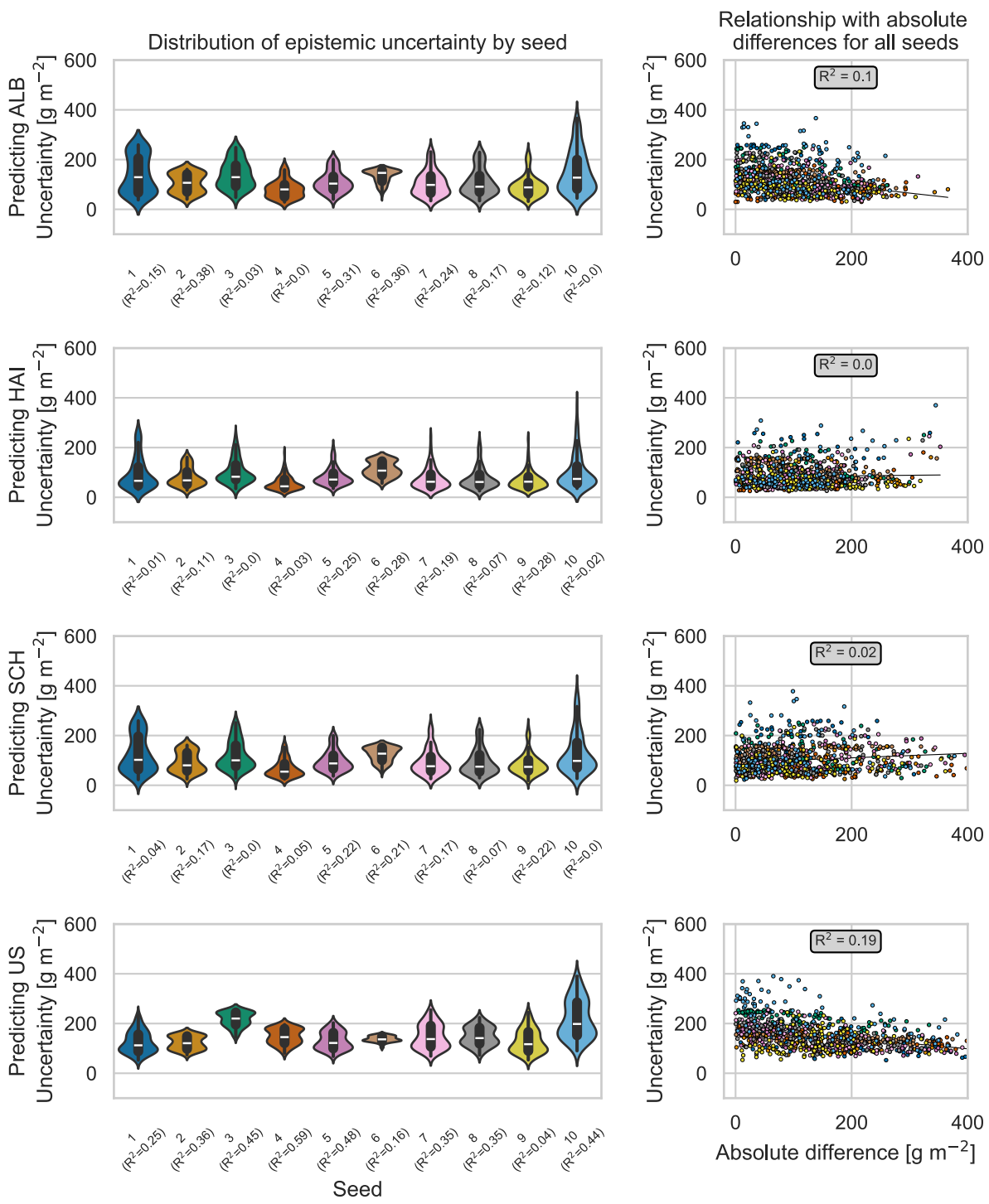
222

223

224

225

## Hybrid models transferred CH model



226

227

228

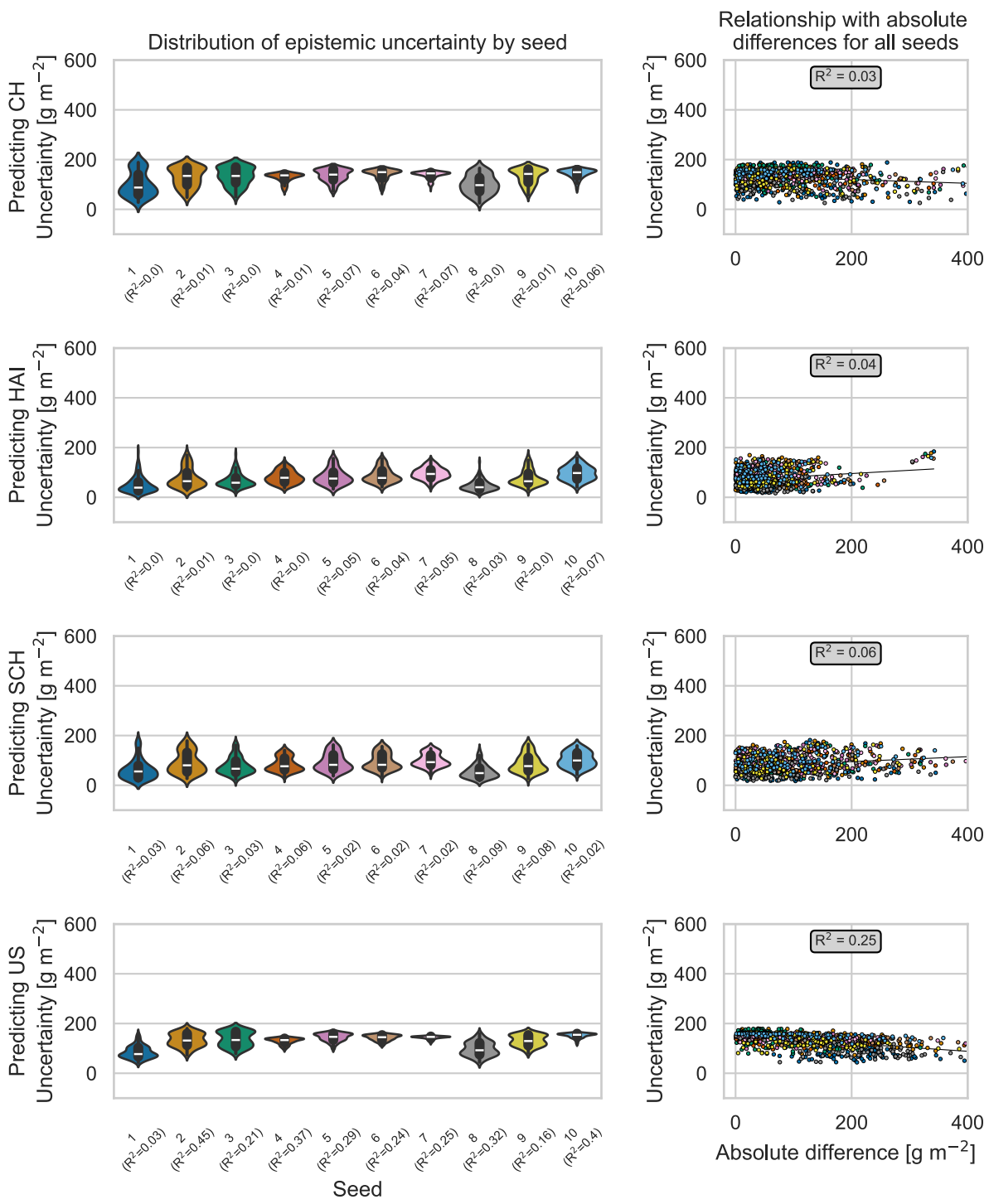
229

230

231

Figure A.16: Epistemic uncertainty of transferred hybrid models for the CH site. Absolute differences correspond to the absolute difference between measured and predicted biomass value. In case a model predicted a straight line (e.g., the prediction is constant), the calculation of the coefficient of determination ( $R^2$ ) was not possible. The corresponding predictions were omitted for the calculation of the overall  $R^2$  showed in the textbox in the right column. CH: Switzerland, ALB: Schwäbische Alb, HAI: Hainich-Dün, SCH: Schorfheide-Chorin, US: United States.

## Hybrid models transferred ALB model



232

233 *Figure A.17: Epistemic uncertainty of transferred hybrid models for the ALB site. Absolute differences correspond to the*

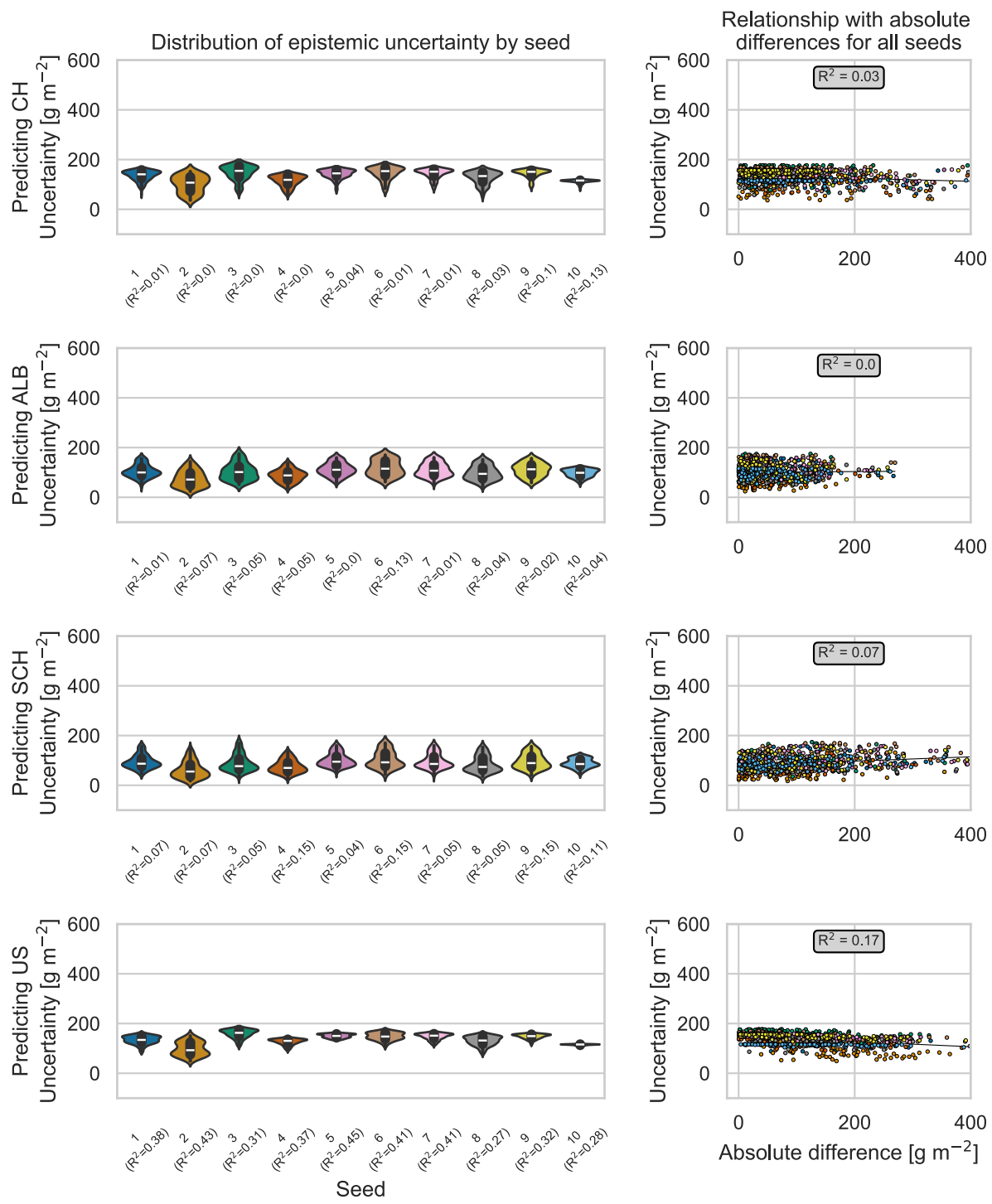
234 *absolute difference between measured and predicted biomass value. In case a model predicted a straight line (e.g., the*

235 *prediction is constant), the calculation of the coefficient of determination ( $R^2$ ) was not possible. The corresponding*

236 *predictions were omitted for the calculation of the overall  $R^2$  showed in the textbox in the right column. CH: Switzerland,*

237 *ALB: Schwäbische Alb, HAI: Hainich-Dün, SCH: Schorfheide-Chorin, US: United States.*

### Hybrid models transferred HAI model



238

239

240

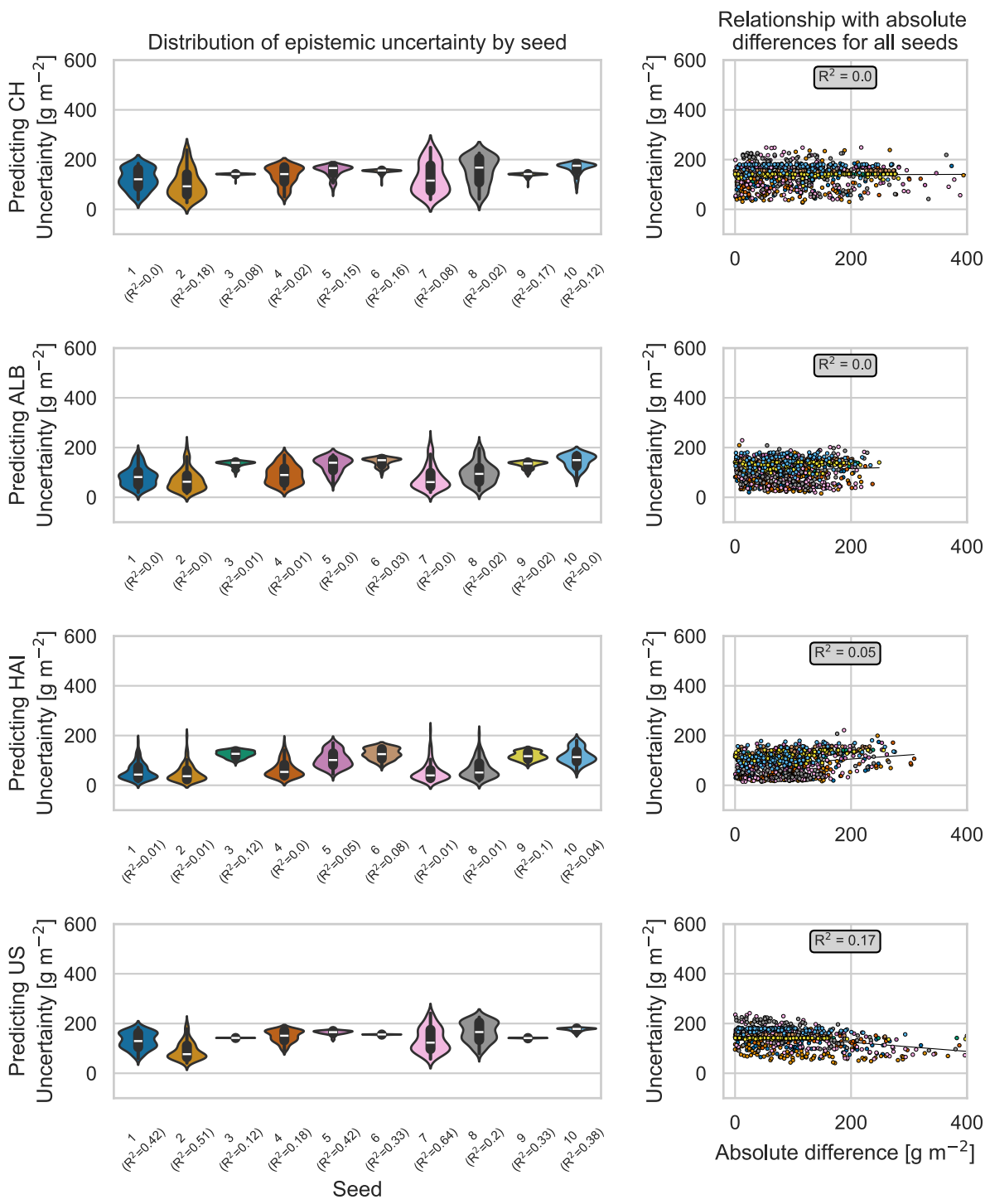
241

242

243

Figure A.18: Epistemic uncertainty of transferred hybrid models for the HAI site. Absolute differences correspond to the absolute difference between measured and predicted biomass value. In case a model predicted a straight line (e.g., the prediction is constant), the calculation of the coefficient of determination ( $R^2$ ) was not possible. The corresponding predictions were omitted for the calculation of the overall  $R^2$  showed in the textbox in the right column. CH: Switzerland, ALB: Schwäbische Alb, HAI: Hainich-Dün, SCH: Schorfheide-Chorin, US: United States.

### Hybrid models transferred SCH model

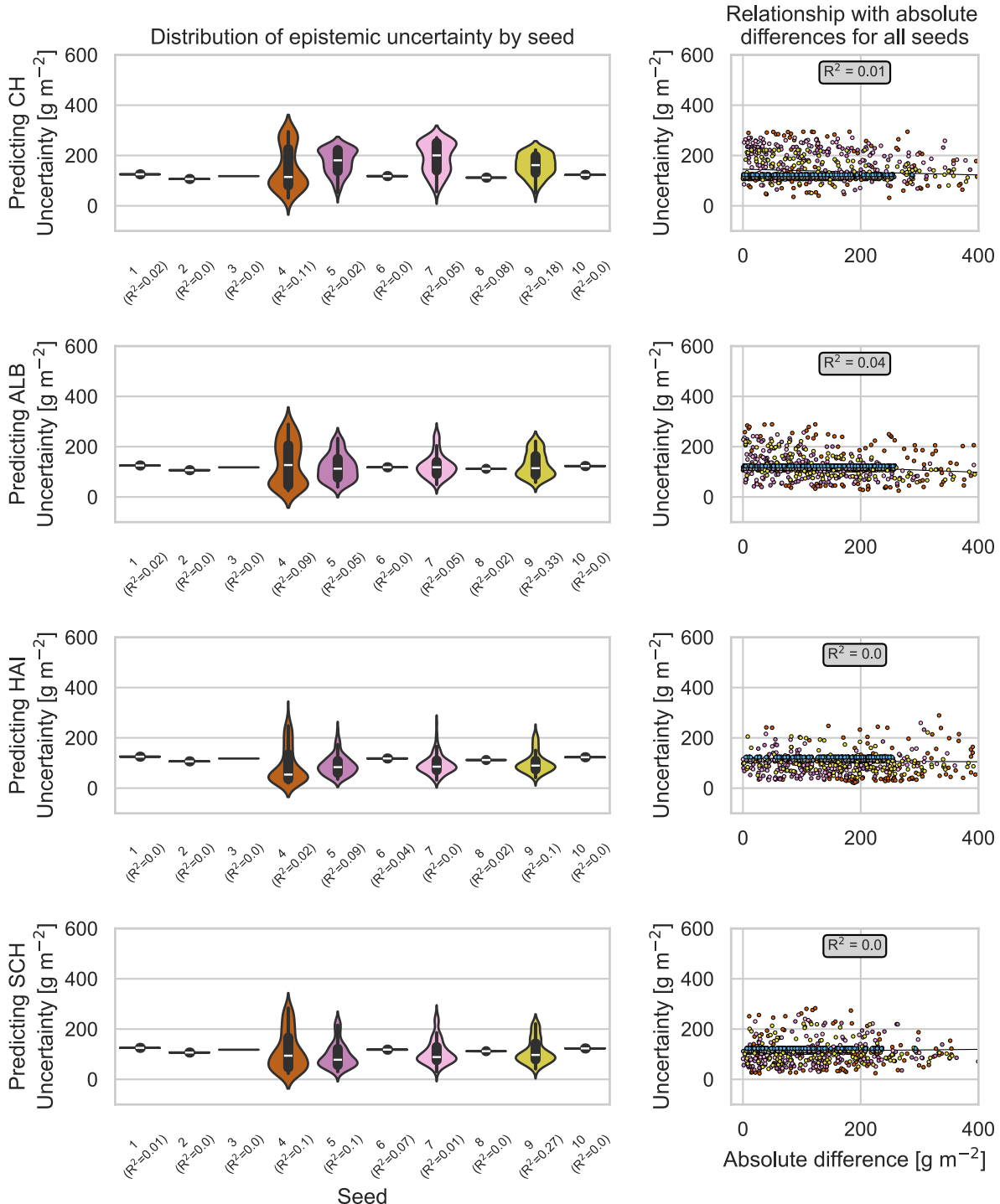


244

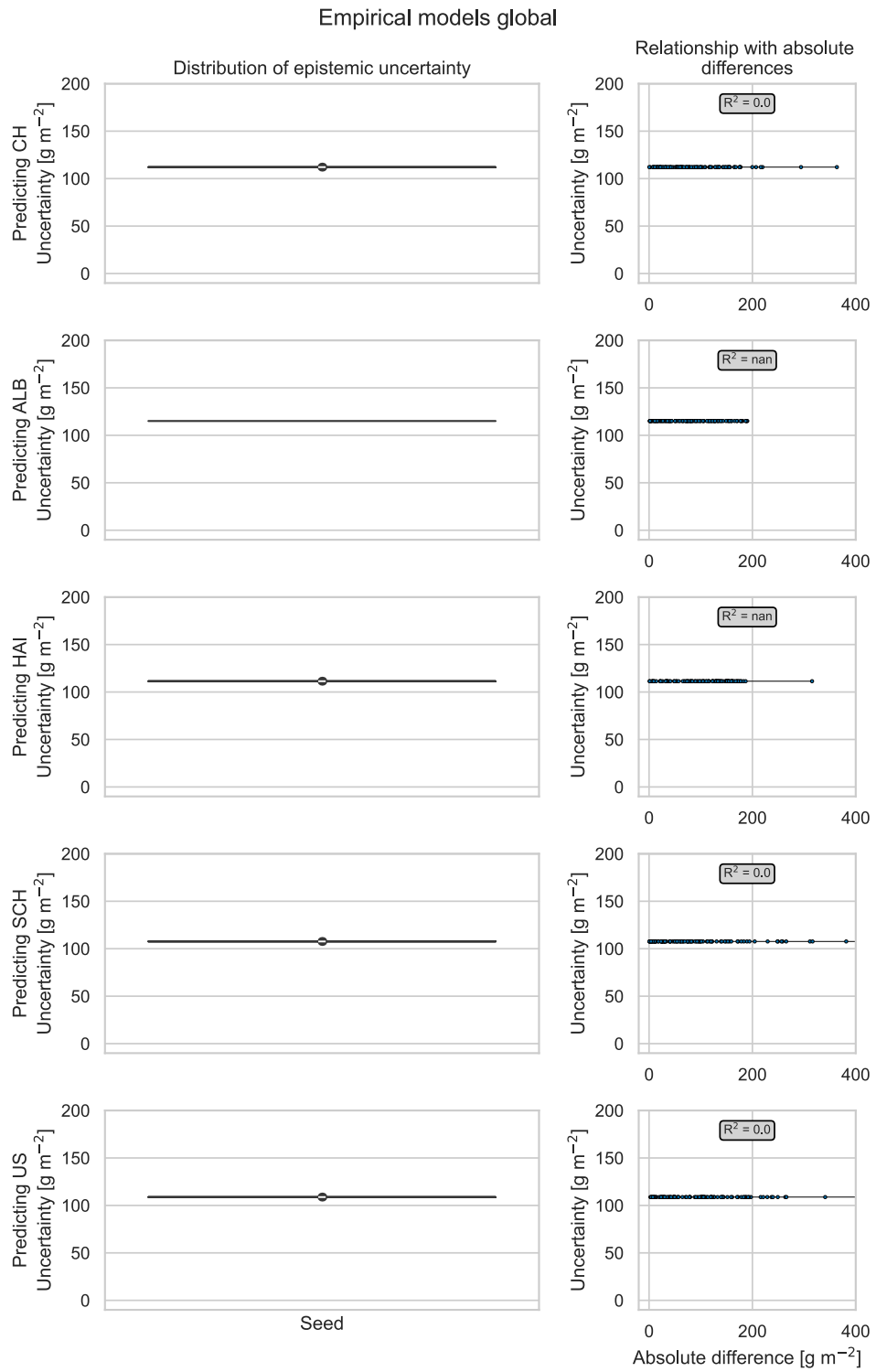
245

Figure A.19: Epistemic uncertainty of transferred hybrid models for the SCH site. Absolute differences correspond to the  
246 absolute difference between measured and predicted biomass value. In case a model predicted a straight line (e.g., the  
247 prediction is constant), the calculation of the coefficient of determination ( $R^2$ ) was not possible. The corresponding  
248 predictions were omitted for the calculation of the overall  $R^2$  showed in the textbox in the right column. CH: Switzerland,  
249 ALB: Schwäbische Alb, HAI: Hainich-Dün, SCH: Schorfheide-Chorin, US: United States.

## Hybrid models transferred US model



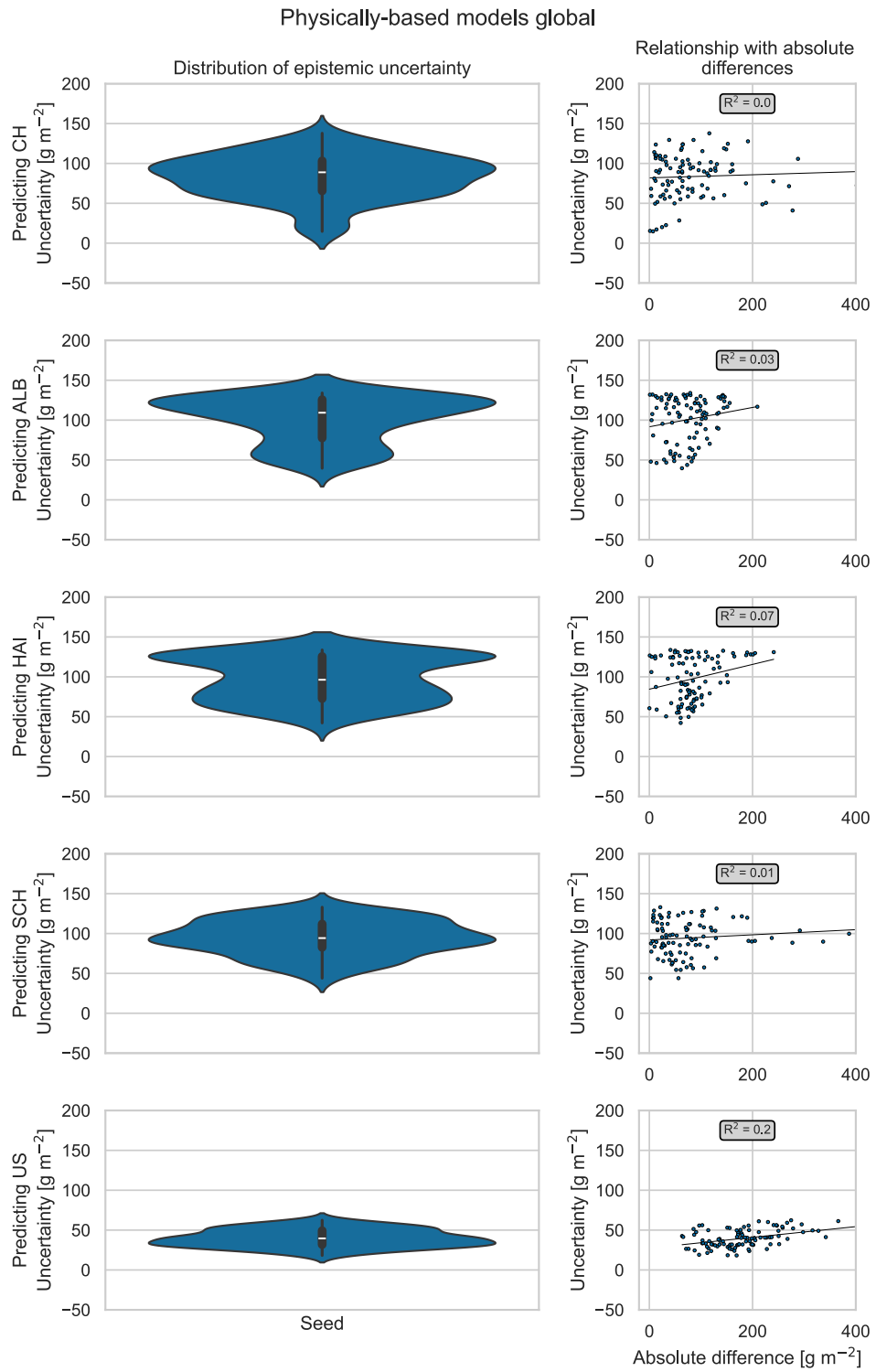
**Figure A.20: Epistemic uncertainty of transferred hybrid models for the US site.** Absolute differences correspond to the absolute difference between measured and predicted biomass value. In case a model predicted a straight line (e.g., the prediction is constant), the calculation of the coefficient of determination ( $R^2$ ) was not possible. The corresponding predictions were omitted for the calculation of the overall  $R^2$  showed in the textbox in the right column. CH: Switzerland, ALB: Schwäbische Alb, HAI: Hainich-Dün, SCH: Schorfheide-Chorin, US: United States.



256

257 *Figure A.21: Epistemic uncertainty of global empirical models. Absolute differences correspond to the absolute difference*  
 258 *between measured and predicted biomass value. In case a model predicted a straight line (e.g., the prediction is constant),*  
 259 *the calculation of the coefficient of determination ( $R^2$ ) was not possible. The corresponding predictions were omitted for the*  
 260 *calculation of the overall  $R^2$  showed in the textbox in the right column. CH: Switzerland, ALB: Schwäbische Alb, HAI:*  
 261 *Hainich-Dün, SCH: Schorfheide-Chorin, US: United States.*

262

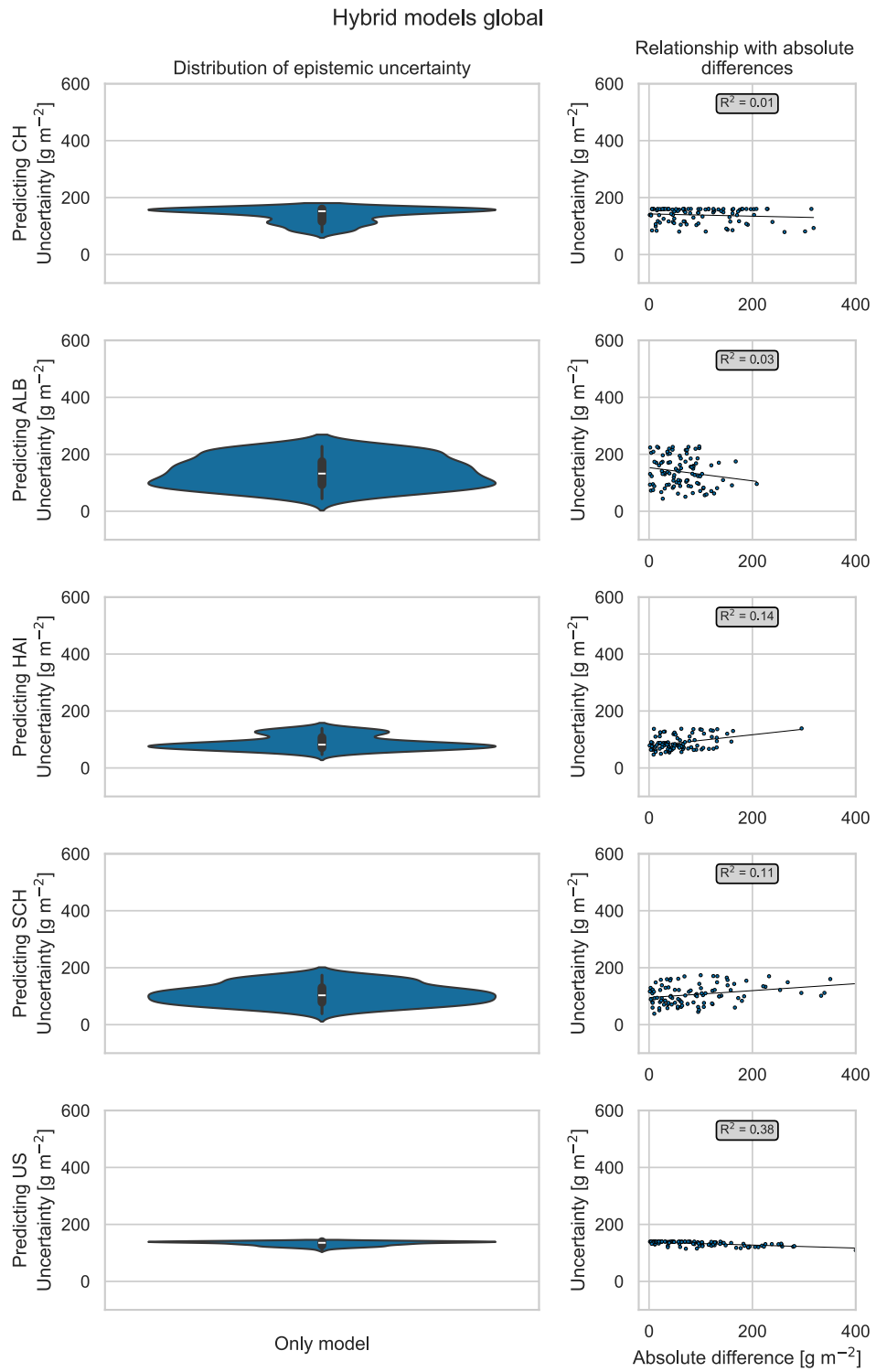


263

264

Figure A.22: Epistemic uncertainty of global physically-based models. Absolute differences correspond to the absolute difference between measured and predicted biomass value. If the percentage of solutions was equal to 0.01% (e.g., only 1 sample), no standard deviation and  $R^2$  could be calculated. The corresponding predictions were omitted for the calculation of the overall  $R^2$  showed in the textbox in the right column. CH: Switzerland, ALB: Schwäbische Alb, HAI: Hainich-Dün, SCH: Schorfheide-Chorin, US: United States.

269



270

271

272

273

274

275

Figure A.23: Epistemic uncertainty of global hybrid models. Absolute differences correspond to the absolute difference between measured and predicted biomass value. In case a model predicted a straight line (e.g., the prediction is constant), the calculation of the coefficient of determination ( $R^2$ ) was not possible. The corresponding predictions were omitted for the calculation of the overall  $R^2$  showed in the textbox in the right column. CH: Switzerland, ALB: Schwäbische Alb, HAI: Hainich-Dün, SCH: Schorfheide-Chorin, US: United States.

276 **Section A.18: Biomass and spectral variability by site**

277 *Table A.14: Properties of biomass (range and coefficient of variation (CV), calculated by dividing the variance by the mean)*  
 278 *and the spectral bands (CV) by site, and mean relative root-mean-square error (RRMSE) and coefficient of determination ( $R^2$ )*  
 279 *of best local empirical, physically-based, and hybrid models. For the empirical models, only the best-performing model in terms*  
 280 *of lowest RRMSE is shown with the model specified in brackets. A missing  $R^2$  indicates that its calculation was not possible due*  
 281 *to predictions of constant values (=horizontal line). CH: Switzerland, ALB: Schwäbische Alb, HAI: Hainich-Dün, SCH:*  
 282 *Schorfheide-Chorin, US: United States, RFR: Random Forest regression, SVR: Support Vector regression, XGB: Extreme Gradient*  
 283 *Boosting regression, GPR: Gaussian Process regression.*

Property	Site				
	CH	ALB	HAI	SCH	US
Biomass range [ $\text{g m}^{-2}$ ]	540.49	379.00	502.37	643.00	518.60
Biomass CV [ $\text{g m}^{-2}$ ]	70.73	52.40	64.18	64.78	28.41
490 nm band CV * 100	0.94	0.37	0.36	0.24	0.49
560 nm band CV * 100	0.56	0.20	0.18	0.15	0.08
665 nm band CV * 100	1.25	1.02	0.75	0.57	0.09
705 nm band CV * 100	0.60	0.40	0.34	0.24	0.23
740 nm band CV * 100	1.72	0.71	0.57	0.56	0.19
783 nm band CV * 100	2.15	1.24	1.03	1.01	0.26
842 nm band CV * 100	2.06	1.23	1.05	0.90	0.27
865 nm band CV * 100	2.14	1.09	0.92	0.89	0.27
1610 nm band CV * 100	0.98	1.00	0.78	0.65	0.37
2190 nm band CV * 100	0.99	1.09	0.84	0.61	0.46
Mean CV of all bands * 100	1.34	0.84	0.68	0.58	0.27
Mean RRMSE of best local empirical models	0.55 (SVR)	0.43 (SVR)	0.44 (RFR)	0.42 (SVR)	0.22 (SVR)
Mean $R^2$ of best local empirical models	0.31 (SVR)	0.54 (SVR)	0.64 (RFR)	0.42 (SVR)	0.59 (SVR)
Mean RRMSE of best local physically-based models	0.59	0.52	0.59	0.47	0.71
Mean $R^2$ of best local physically-based models	0.26	0.43	0.66	0.30	0.30
Mean RRMSE of best local hybrid models	0.64	0.46	0.51	0.47	0.29
Mean $R^2$ of best local hybrid models	0.23	0.46	0.54	0.27	0.23

285 **Section A.19: Performances of local physically-based models with US-tailored LUT**

286 *Table A.15: Value ranges and distributions of PROSAIL input parameters when adjusting the upper bound of LMA to the  
 287 conditions of the study site in the United States.*

Parameter	Variable	Unit	Minimum value	Maximum value	Distribution
Leaf structure parameter	N	[ $\cdot$ ]	1.5	1.9	uniform
Chlorophyll content	CHL	[ $\mu\text{g cm}^{-2}$ ]	5	75	uniform
Carotenoid content	CAR	[ $\mu\text{g cm}^{-2}$ ]	2	60	uniform
Anthocyanin content	ANT	[ $\mu\text{g cm}^{-2}$ ]	0	2	uniform
Brown pigment content	BROWN	[ $\cdot$ ]	0	1	uniform
Equivalent water thickness	EWT	[cm]	0.001	0.04	uniform
Leaf mass per area	LMA	[ $\text{g cm}^{-2}$ ]	0.002	0.03	uniform
Angle for incident light at leaf surface	alpha	[ $^\circ$ ]	40	40	fixed
Leaf inclination distribution function	TypeLidf	[ $\cdot$ ]	2	2	fixed
Average leaf angle	LIDFa	[ $^\circ$ ]	40	70	uniform
Leaf area index	LAI	[ $\cdot$ ]	0.1	4	uniform
Hot spot parameter	q	[ $\cdot$ ]	0.01	0.1	uniform
Sun zenith angle	tts	[ $^\circ$ ]	25	75	uniform
Observer zenith angle	tto	[ $^\circ$ ]	0	0	fixed
Relative azimuth angle	psi	[ $^\circ$ ]	50	180	uniform
Dry/wet soil factor	psoil	[ $\cdot$ ]	0	1	uniform

288

289

290 *Table A.16: Cost function, percentage of solutions, coefficient of determination ( $R^2$ ), root-mean-square error (RMSE), and*  
 291 *relative root-mean-square error (RRMSE) of best performing local physically-based models with US-tailored look-up table*  
 292 *(LUT) and the LUT used in this study. The last columns show the difference for the three metrics.CH: Switzerland, ALB:*  
 293 *Schwäbische Alb, HAI: Hainich-Dün, SCH: Schorfheide-Chorin, US: United States.*

		US-tailored LUT					LUT used in this study					Difference		
Site	Seen	Cost function	Percent age of solution s	$R^2$	RMSE [g m <sup>-2</sup> ]	RRM SE	Cost function	Percent age of solution s	$R^2$	RMSE [g m <sup>-2</sup> ]	RRM SE	$R^2$	RMSE [g m <sup>-2</sup> ]	RRM SE
CH	1	min_contrast_1	10 46	0.1 77	183.9 77	1.06 9	min_contrast_1	1 21	0.2 3	95.68 3	0.55 6	- 0.0 75	88.29 4	0.51 3
CH	2	min_contrast_1	10 29	0.1 67	192.0 1	1.11 1	min_contrast_1	1 14	0.2 1	96.42 1	0.55 8	- 0.0 85	95.64 6	0.55 3
CH	3	min_contrast_1	10 89	0.0 82	182.8 82	1.04 7	min_contrast_1	1 49	0.1 56	107.7 7	0.61 7	- 0.0 6	75.12 6	0.43
CH	4	min_contrast_1	10 04	0.1 59	187.0 7	1.07 7	min_contrast_1	1 42	0.1 29	104.5 2	0.60 2	- 0.0 38	82.53 5	0.47 5
CH	5	min_contrast_1	10 52	0.1 47	176.0 47	1.01 4	min_contrast_1	1 07	0.2 79	102.2 9	0.58 9	- 0.0 55	73.76 8	0.42 5
CH	6	min_contrast_1	10 2	0.1 01	189.1 5	1.09 5	min_contrast_1	1 11	0.2 2	96.40 8	0.55 8	- 0.0 91	92.69 9	0.53 7
CH	7	min_contrast_1	10 38	0.1 92	187.2 92	1.07 9	min_contrast_1	1 08	0.2 8	101.1 3	0.58 7	- 0.0 7	86.11 2	0.49 6
CH	8	min_contrast_1	10 23	0.1 73	189.0 6	1.09 6	min_contrast_1	1 92	0.1 8	98.84 3	0.57 3	- 0.0 69	90.22 5	0.52 3
CH	9	min_contrast_1	10 5	0.1 83	183.1 83	1.05 1	min_contrast_1	1 3	0.2 51	101.7 3	0.58 8	- 0.0 8	81.43 2	0.46 7
CH	10	min_contrast_1	10 68	0.1 39	185.0 3	1.06 3	min_contrast_2	1 63	0.2 2	97.14 8	0.55 8	- 0.0 95	87.89 7	0.50 5
ALB	1	min_contrast_1	0.01 04	0.0 98	175.4 8	1.25 8	neyman_chi_square_di vergence	1 19	0.4 1	72.6 1	0.52 1	- 0.4 15	102.8 98	0.73 7
ALB	2	min_contrast_1	0.01 0	0 04	169.2 5	1.22 5	neyman_chi_square_di vergence	1 92	0.3 5	70.69 2	0.51 2	- 0.3 92	98.50 9	0.71 3
ALB	3	min_contrast_1	0.01 -0.0 01	- 0.0 01	174.7 03	1.24 7	neyman_chi_square_di vergence	1 01	0.4 7	73.61 5	0.52 5	- 0.4 02	101.0 86	0.72 2
ALB	4	min_contrast_1	0.01 0	0 25	179.9 3	1.30 3	neyman_chi_square_di vergence	1 99	0.3 2	71.54 8	0.51 8	- 0.3 99	108.3 83	0.78 5
ALB	5	min_contrast_4	0.01 -0.0 02	- 0.0 02	166.6 53	1.20 3	neyman_chi_square_di vergence	1 91	0.4 5	67.97 1	0.49 1	- 0.4 93	98.67 8	0.71 2
ALB	6	min_contrast_1	0.01 -0.0 01	- 0.0 01	178.3 91	1.28 3	neyman_chi_square_di vergence	1 19	0.5 4	67.18 3	0.48 3	- 0.5 2	111.2 07	0.8
ALB	7	min_contrast_1	0.01 0	0 14	183.3 5	1.32 5	neyman_chi_square_di vergence	1 88	0.4 5	68.57 6	0.49 6	- 0.4 88	114.7 39	0.82 9
ALB	8	min_contrast_1	0.01 -0.0 01	- 0.0 01	175.7 28	1.25 8	neyman_chi_square_di vergence	1 04	0.4 5	71.38 1	0.51 1	- 0.4 05	104.3 43	0.74 7
ALB	9	min_contrast_1	0.01 0.03	0.0 69	165.6 7	1.18 7	neyman_chi_square_di vergence	1 24	0.4 8	70.49 5	0.50 5	- 0.4 21	95.17 1	0.68 2
ALB	10	min_contrast_1	0.01 -0.0 03	- 0.0 03	168.6 71	1.20 9	neyman_chi_square_di vergence	1 06	0.4 8	70.85 8	0.50 8	- 0.4 09	97.81 3	0.70 1
HAI	1	min_contrast_4	1 48	0.2 48	201.9 64	1.73 7	neyman_chi_square_di vergence	1 35	0.5 9	76.28 3	0.65 3	- 0.2 87	125.6 75	1.07 7
HAI	2	min_contrast_4	1 21	0.2 21	203.5 9	1.74 7	neyman_chi_square_di vergence	1 02	0.5 5	79.26 4	0.68 8	- 0.2 81	124.3 25	1.06 7
HAI	3	min_contrast_4	1 55	0.2 51	197.6 7	1.70 7	neyman_chi_square_di vergence	1 88	0.4 4	77.54 3	0.67 3	- 0.2 33	120.1 07	1.03 7
HAI	4	min_contrast_4	1 62	0.2 88	206.5 88	1.77 7	neyman_chi_square_di vergence	1 21	0.5 6	79.29 2	0.68 2	- 0.2 59	127.2 92	1.09 5
HAI	5	min_contrast_3	1 58	0.2 56	204.6 7	1.75 7	neyman_chi_square_di vergence	1 71	0.4 8	79.60 3	0.68 3	- 0.2 13	125.0 48	1.07 4

H AI	6	min_contrast_4	1	0.2 9	209.1 37	1.83 1	neyman_chi_square_di vergence	1	0.5 6	74.29 4	0.65	- 0.2 7	134.8 43	1.18 1
H AI	7	min_contrast_3	1	0.2 42	202.9 82	1.75	neyman_chi_square_di vergence	1	0.4 96	78.71 4	0.67 9	- 0.2 54	124.2 68	1.07 1
H AI	8	min_contrast_4	1	0.2 79	199.7 8	1.71 8	neyman_chi_square_di vergence	1	0.4 94	78.26	0.67 3	- 0.2 15	121.5 2	1.04 5
H AI	9	min_contrast_4	1	0.2 15	205.1 01	1.74 8	neyman_chi_square_di vergence	1	0.5 13	79.51 4	0.67 8	- 0.2 98	125.5 87	1.07
H AI	10	min_contrast_2	1	0.2 05	206.1 58	1.77 3	neyman_chi_square_di vergence	1	0.4 65	80.35 4	0.69 1	- 0.2 6	125.8 04	1.08 2
SC H	1	neyman_chi_square_di vergence	1	0.0 77	152.8 4	0.69 6	laplace_distribution	10	0.2 32	100.6 58	0.45 9	- 0.1 55	52.18 2	0.23 7
SC H	2	neyman_chi_square_di vergence	1	0.0 81	151.2 54	0.68 6	laplace_distribution	10	0.2 58	99.44 4	0.45 1	- 0.1 77	51.81	0.23 5
SC H	3	neyman_chi_square_di vergence	1	0.0 58	157.6 18	0.71	laplace_distribution	10	0.2 53	105.4 21	0.47 5	- 0.1 95	52.19 7	0.23 5
SC H	4	neyman_chi_square_di vergence	1	0.0 81	156.8 51	0.70	laplace_distribution	10	0.2 52	105.5 25	0.47 5	- 0.1 71	51.32	0.23
SC H	5	neyman_chi_square_di vergence	1	0.0 96	150.8 07	0.68 5	laplace_distribution	10	0.2 5	99.30 3	0.45 1	- 0.1 54	51.50 4	0.23 4
SC H	6	neyman_chi_square_di vergence	1	0.1 47	154.5 5	0.69	laplace_distribution	10	0.2 65	104.7 78	0.47 1	- 0.1 65	49.76 9	0.22 4
SC H	7	neyman_chi_square_di vergence	1	0.0 58	156.7 55	0.70 3	laplace_distribution	10	0.2 37	107.3 9	0.48 1	- 0.1 79	49.36 5	0.22 2
SC H	8	neyman_chi_square_di vergence	1	0.0 81	156.4 81	0.70 2	laplace_distribution	10	0.2 49	105.4 3	0.47 3	- 0.1 68	51.08 1	0.22 9
SC H	9	neyman_chi_square_di vergence	1	0.0 78	157.0 69	0.70 5	laplace_distribution	10	0.2 34	107.0 52	0.48 1	- 0.1 56	50.01 7	0.22 5
SC H	10	neyman_chi_square_di vergence	1	0.0 75	152.0 34	0.68 3	laplace_distribution	10	0.2 35	106.9 99	0.48 1	- 0.1 6	45.03 5	0.20 2
US	1	min_contrast_4	10	0.4 46	90.50 1	0.34 5	pearson_chi_square	0.01	0.1 1	179.4 87	0.68 4	0.3 36	- 88.98 6	- 0.33 9
US	2	min_contrast_4	10	0.4 63	83.10 6	0.32	pearson_chi_square	0.01	0.1 02	173.8 48	0.67	0.3 61	- 90.74 2	-0.35
US	3	min_contrast_4	10	0.4 24	93.41 5	0.35 6	min_contrast_4	10	0.4 11	182.3 07	0.69 5	0.0 13	- 88.89 2	- 0.33 9
US	4	min_contrast_4	10	0.4 08	93.22 5	0.35 5	min_contrast_4	10	0.3 94	182.0 16	0.69 4	0.0 14	- 88.79 6	- 0.33 9
US	5	min_contrast_4	10	0.4 6	93.35 2	0.35 6	pearson_chi_square	0.01	0.1 19	176.7 44	0.67 4	0.3 41	- 83.39 2	- 0.31 8
US	6	min_contrast_4	10	0.4 8	84.64 2	0.32 6	pearson_chi_square	0.01	0.1 01	174.8 32	0.67 3	0.3 79	- 90.19	- 0.34 7
US	7	min_contrast_4	10	0.4 34	90.61 6	0.34 5	min_contrast_4	10	0.4 19	180.9 43	0.68 9	0.0 15	- 90.32 7	- 0.34 4
US	8	min_contrast_4	10	0.4 26	91.64 7	0.35	min_contrast_4	10	0.4 17	181.2 94	0.69 2	0.0 09	- 89.64 7	- 0.34 2
US	9	min_contrast_4	10	0.4 46	92.04 4	0.35 1	min_contrast_4	10	0.4 34	181.7 48	0.69 3	0.0 12	- 89.70 4	- 0.34 2
US	10	min_contrast_4	10	0.3 56	93.23 6	0.35 7	pearson_chi_square	0.01	0.1 17	175.2 63	0.67 1	0.2 39	- 82.02 7	- 0.31 4

296 *Table A.17: Testing performance of local and transferred physically-based models with US-tailored look-up table (LUT). The*  
 297 *parameters correspond to the best-performing combination of parameters tested during the fivefold cross-validation. CH:*  
 298 *Switzerland, ALB: Schwäbische Alb, HAI: Hainich-Dün, SCH: Schorfheide-Chorin, US: United States, R<sup>2</sup>: coefficient of*  
 299 *determination, RMSE: root-mean-square error, sRMSE: systematic component of RMSE, uRMSE: unsystematic component of*  
 300 *RMSE, RRMSE: relative root-mean-square error, MBE: mean bias error.*

		Calibration site				
Prediction site	Metric	CH	ALB	HAI	SCH	US
CH	R <sup>2</sup>	0.19 ± 0.13	0.00 ± 0.00	0.04 ± 0.01	0.08 ± 0.00	0.08 ± 0.00
CH	RMSE	178.67 ± 17.06	243.85 ± 1.43	205.20 ± 3.28	191.83 ± 0.00	209.39 ± 0.00
CH	sRMSE	174.39 ± 16.33	190.96 ± 1.14	192.41 ± 1.93	184.07 ± 0.00	197.37 ± 0.00
CH	uRMSE	50.21 ± 16.79	151.61 ± 3.64	71.24 ± 4.32	54.00 ± 0.00	69.92 ± 0.00
CH	RRMSE	1.02 ± 0.11	1.40 ± 0.01	1.18 ± 0.02	1.10 ± 0.00	1.21 ± 0.00
CH	MBE	131.38 ± 26.00	155.84 ± 1.40	157.81 ± 2.34	147.59 ± 0.00	163.87 ± 0.00
ALB	R <sup>2</sup>	0.39 ± 0.00	0.03 ± 0.06	0.23 ± 0.00	0.28 ± 0.00	0.38 ± 0.00
ALB	RMSE	247.91 ± 0.00	184.72 ± 26.81	194.44 ± 0.70	200.32 ± 0.00	256.10 ± 0.00
ALB	sRMSE	247.01 ± 0.00	119.67 ± 19.71	195.75 ± 0.76	202.49 ± 0.00	255.04 ± 0.00
ALB	uRMSE	21.15 ± 0.00	140.06 ± 22.64	22.58 ± 0.61	29.60 ± 0.00	23.24 ± 0.00
ALB	RRMSE	1.78 ± 0.00	1.32 ± 0.19	1.40 ± 0.01	1.44 ± 0.00	1.84 ± 0.00
ALB	MBE	232.16 ± 0.00	82.11 ± 27.44	176.57 ± 0.85	184.05 ± 0.00	240.69 ± 0.00
HAI	R <sup>2</sup>	0.48 ± 0.00	0.02 ± 0.00	0.31 ± 0.11	0.41 ± 0.00	0.46 ± 0.00
HAI	RMSE	251.88 ± 0.00	223.38 ± 0.41	195.40 ± 13.23	206.53 ± 0.00	258.13 ± 0.00
HAI	sRMSE	255.37 ± 0.00	146.79 ± 0.46	199.40 ± 11.86	213.06 ± 0.00	261.40 ± 0.00
HAI	uRMSE	42.12 ± 0.00	168.38 ± 0.15	36.22 ± 15.28	52.33 ± 0.00	41.20 ± 0.00
HAI	RRMSE	2.17 ± 0.00	1.93 ± 0.00	1.70 ± 0.13	1.78 ± 0.00	2.22 ± 0.00
HAI	MBE	240.75 ± 0.00	118.96 ± 0.56	180.96 ± 16.51	195.27 ± 0.00	247.13 ± 0.00
SCH	R <sup>2</sup>	0.16 ± 0.00	0.01 ± 0.00	0.02 ± 0.00	0.12 ± 0.06	0.15 ± 0.00
SCH	RMSE	202.61 ± 0.00	171.44 ± 0.78	160.21 ± 0.80	153.17 ± 10.08	209.93 ± 0.00
SCH	sRMSE	204.89 ± 0.00	121.59 ± 0.04	155.64 ± 0.39	156.26 ± 10.45	211.96 ± 0.00
SCH	uRMSE	30.48 ± 0.00	120.86 ± 1.08	37.93 ± 1.77	33.74 ± 13.43	29.31 ± 0.00
SCH	RRMSE	0.91 ± 0.00	0.77 ± 0.00	0.72 ± 0.00	0.69 ± 0.04	0.95 ± 0.00
SCH	MBE	166.86 ± 0.00	-23.08 ± 0.08	100.12 ± 0.59	99.35 ± 9.47	175.46 ± 0.00
US	R <sup>2</sup>	0.42 ± 0.00	0.24 ± 0.04	0.44 ± 0.00	0.44 ± 0.00	0.51 ± 0.12
US	RMSE	110.88 ± 0.00	125.92 ± 2.43	92.36 ± 1.66	100.72 ± 0.00	87.52 ± 13.13
US	sRMSE	123.50 ± 0.00	127.06 ± 0.43	107.97 ± 1.56	115.29 ± 0.00	104.15 ± 13.18
US	uRMSE	54.39 ± 0.00	11.22 ± 12.61	55.91 ± 0.30	56.10 ± 0.00	55.88 ± 8.20
US	RRMSE	0.42 ± 0.00	0.48 ± 0.01	0.35 ± 0.01	0.39 ± 0.00	0.33 ± 0.05
US	MBE	-89.48 ± 0.00	-94.19 ± 0.62	-66.41 ± 2.51	-77.77 ± 0.00	-61.92 ± 7.33

301

302

303    **Section A.20: Precipitation at US site**

304    *Table A.1818: Summarized precipitation data in millimeters [mm] at the Norman (OK) weather station as provided by Mesonet*  
 305    *(2024) for the summer months (June to August) from 2004-2023. \* denotes the months in which the field measurements used*  
 306    *in this study were conducted.*

Year	Monthly precipitation [mm]			Cumulative precipitation
	June	July	August	
2004	8.11	4.37	3.55	16.03
2005	3.51	2.60	4.92	11.03
2006	2.63	2.05	2.15	6.83
2007	10.82	8.08	6.09	24.99
2008	5.90	0.76	10.26	16.92
2009	1.27	3.56	4.59	9.42
2010	4.03	5.55	0.72	10.30
2011	2.35	0.34	2.06	4.75
2012	0.82	0.02	3.14	3.98
2013	4.16	9.56	2.73	16.45
2014	4.58	3.76	1.34	9.68
2015	5.95	7.46	1.74	15.15
2016	2.93	6.48	0.51	9.92
2017	0.66	2.43	8.43	11.52
2018	6.55	2.28	6.87	15.70
2019	5.67	0.18	6.61	12.46
2020	2.19	2.65	5.15	9.99
2021	6.54	2.70	1.46	10.70
2022	5.39	<b>1.19 *</b>	<b>0.84 *</b>	7.42
2023	5.13	7.62	0.59	13.34
Average	4.46	3.68	3.69	11.83

307

308

309 **Section A.21: C3 and C4 species per study site**

310 Information about the photosynthetic pathway of the species in the study sites investigated in  
311 this study were estimated from the TRY database (Cornelissen, 1996; Cornelissen et al., 2004;  
312 Cornwell et al., 2017, 2008; Craine et al., 2005; Diaz et al., 2004; Fitter and Peat, 1994; Flowers  
313 et al., 2023, 2017; Iversen et al., 2017; Kapralov et al., 2012; Kattge et al., 2020, 2009; Laughlin  
314 et al., 2011, 2010; Lin et al., 2015; Meir et al., 2002; Munroe et al., 2021; Poschlod et al., 2003;  
315 Quested et al., 2003; Reich et al., 2009, 2008; Smith and Dukes, 2017; Wang et al., 2017;  
316 Wright et al., 2004). We point out that the percentages indicated in Table A.19 relate to species  
317 occurrence and not species abundance. In fact, the abundance of C4 species was considerably  
318 higher for the US site. However, species abundance data was not available for all sites which is  
319 why we did not add a separate column.

320 *Table A.19: Number of C3 and C4 species, and relative share of C4 species per study site. CH: Switzerland, ALB: Schwäbische  
321 Alb, HAI: Hainich-Dün, SCH: Schorfheide-Chorin, US: United States.*

Study site	Number of C3 species	Number of C4 species	Relative share of C4 species [%]
CH	152	4	2.56
ALB	42	0	0.00
HAI	80	1	1.23
SCH	174	8	4.40
US	156	23	12.85

322

323 **Section A.22: Transferability of local hybrid models with varying initial training set size**

324 *Table A.20: Testing performance of local and transferred hybrid models. The parameters correspond to the best-performing*  
 325 *combination of parameters tested during the fivefold cross-validation using Active Learning with an initial training set size of*  
 326 *1%. CH: Switzerland, ALB: Schwäbische Alb, HAI: Hainich-Dün, SCH: Schorfheide-Chorin, US: United States, R<sup>2</sup>: coefficient of*  
 327 *determination, RMSE: root-mean-square error, sRMSE: systematic component of RMSE, uRMSE: unsystematic component of*  
 328 *RMSE, RRMSE: relative root-mean-square error, MBE: mean bias error.*

Initial training set size = 1%		Calibration site				
Prediction site	Metric	CH	ALB	HAI	SCH	US
CH	R <sup>2</sup>	0.25 ± 0.19	0.03 ± 0.02	0.06 ± 0.06	0.02 ± 0.02	0.01 ± 0.02
CH	RMSE	103.69 ± 18.85	129.44 ± 8.99	134.83 ± 21.99	142.12 ± 9.30	191.62 ± 63.09
CH	sRMSE	113.31 ± 9.08	119.74 ± 9.18	122.02 ± 12.26	121.00 ± 9.74	171.73 ± 52.16
CH	uRMSE	47.11 ± 27.93	45.47 ± 18.60	52.98 ± 38.71	72.81 ± 15.75	71.14 ± 58.50
CH	RRMSE	0.59 ± 0.10	0.75 ± 0.05	0.78 ± 0.13	0.82 ± 0.05	1.10 ± 0.36
CH	MBE	-2.72 ± 13.49	-41.46 ± 23.45	-40.36 ± 35.62	5.02 ± 50.57	126.33 ± 63.89
ALB	R <sup>2</sup>	0.08 ± 0.10	0.49 ± 0.17	0.32 ± 0.10	0.40 ± 0.07	0.06 ± 0.06
ALB	RMSE	126.21 ± 16.94	62.87 ± 10.57	74.22 ± 7.02	111.74 ± 12.28	162.29 ± 23.31
ALB	sRMSE	108.82 ± 16.12	85.15 ± 4.63	85.61 ± 0.94	120.57 ± 8.51	143.02 ± 14.02
ALB	uRMSE	59.38 ± 24.24	54.70 ± 14.70	41.52 ± 11.89	43.36 ± 9.64	61.41 ± 49.65
ALB	RRMSE	0.91 ± 0.12	0.45 ± 0.07	0.53 ± 0.05	0.80 ± 0.09	1.17 ± 0.17
ALB	MBE	65.03 ± 25.47	0.44 ± 13.69	-12.72 ± 6.51	85.76 ± 11.92	114.26 ± 18.83
HAI	R <sup>2</sup>	0.06 ± 0.06	0.37 ± 0.10	0.51 ± 0.13	0.26 ± 0.08	0.08 ± 0.09
HAI	RMSE	135.73 ± 8.34	70.17 ± 7.51	60.93 ± 11.56	112.65 ± 10.12	188.68 ± 31.60
HAI	sRMSE	118.33 ± 13.62	86.30 ± 0.99	82.65 ± 9.90	116.60 ± 4.41	167.83 ± 26.43
HAI	uRMSE	62.44 ± 20.15	48.49 ± 10.83	54.56 ± 10.28	36.40 ± 12.60	70.53 ± 52.63
HAI	RRMSE	1.17 ± 0.07	0.60 ± 0.06	0.53 ± 0.09	0.97 ± 0.09	1.63 ± 0.27
HAI	MBE	79.76 ± 21.29	1.45 ± 13.36	-5.70 ± 6.34	79.31 ± 6.29	143.04 ± 31.57
SCH	R <sup>2</sup>	0.04 ± 0.06	0.25 ± 0.05	0.17 ± 0.07	0.29 ± 0.12	0.07 ± 0.08
SCH	RMSE	139.32 ± 13.87	128.55 ± 9.52	143.68 ± 8.58	108.25 ± 12.61	151.20 ± 25.32
SCH	sRMSE	127.16 ± 10.54	141.13 ± 6.90	150.62 ± 4.83	120.60 ± 11.47	125.22 ± 2.90
SCH	uRMSE	54.08 ± 19.89	57.44 ± 6.97	42.75 ± 15.06	58.95 ± 11.45	69.11 ± 55.27
SCH	RRMSE	0.63 ± 0.06	0.58 ± 0.04	0.65 ± 0.04	0.49 ± 0.05	0.68 ± 0.11
SCH	MBE	-33.08 ± 31.21	-75.39 ± 12.86	-92.23 ± 8.13	0.41 ± 12.44	24.95 ± 28.13
US	R <sup>2</sup>	0.11 ± 0.12	0.10 ± 0.08	0.18 ± 0.13	0.19 ± 0.10	0.30 ± 0.25
US	RMSE	226.44 ± 69.67	204.36 ± 51.18	197.08 ± 52.07	148.20 ± 37.87	72.09 ± 14.27
US	sRMSE	210.86 ± 61.49	200.61 ± 51.46	185.05 ± 60.75	125.16 ± 38.69	84.44 ± 12.64
US	uRMSE	76.37 ± 45.34	37.57 ± 20.66	58.73 ± 27.86	72.22 ± 36.25	34.16 ± 27.01
US	RRMSE	0.87 ± 0.27	0.78 ± 0.20	0.75 ± 0.20	0.57 ± 0.14	0.28 ± 0.05
US	MBE	-190.17 ± 68.45	-179.42 ± 57.72	-159.16 ± 72.14	-79.48 ± 58.63	1.16 ± 10.21

329

330

331 *Table A.21: Testing performance of local and transferred hybrid models. The parameters correspond to the best-performing*  
 332 *combination of parameters tested during the fivefold cross-validation using Active Learning with an initial training set size of*  
 333 *2%. CH: Switzerland, ALB: Schwäbische Alb, HAI: Hainich-Dün, SCH: Schorfheide-Chorin, US: United States, R<sup>2</sup>: coefficient of*  
 334 *determination, RMSE: root-mean-square error, sRMSE: systematic component of RMSE, uRMSE: unsystematic component of*  
 335 *RMSE, RRMSE: relative root-mean-square error, MBE: mean bias error.*

Initial training set size = 2%		Calibration site				
Prediction site	Metric	CH	ALB	HAI	SCH	US
CH	R <sup>2</sup>	0.23 ± 0.14	0.02 ± 0.02	0.02 ± 0.03	0.03 ± 0.03	0.01 ± 0.01
CH	RMSE	112.22 ± 31.13	127.07 ± 7.94	125.43 ± 9.89	136.69 ± 13.00	164.02 ± 35.27
CH	sRMSE	113.87 ± 9.18	116.51 ± 7.64	117.34 ± 6.45	125.35 ± 13.19	146.02 ± 14.56
CH	uRMSE	54.73 ± 39.46	49.79 ± 13.76	44.33 ± 15.06	53.38 ± 17.36	58.53 ± 64.41
CH	RRMSE	0.64 ± 0.18	0.73 ± 0.05	0.72 ± 0.06	0.79 ± 0.07	0.94 ± 0.20
CH	MBE	-3.46 ± 17.01	-31.66 ± 21.59	-36.42 ± 18.12	36.96 ± 48.54	93.61 ± 20.14
ALB	R <sup>2</sup>	0.07 ± 0.07	0.46 ± 0.18	0.34 ± 0.07	0.41 ± 0.09	0.03 ± 0.02
ALB	RMSE	122.05 ± 8.44	64.39 ± 11.93	72.30 ± 4.12	107.21 ± 8.09	158.60 ± 28.14
ALB	sRMSE	103.03 ± 10.46	84.85 ± 4.76	86.83 ± 1.25	118.81 ± 4.89	147.49 ± 33.86
ALB	uRMSE	61.51 ± 21.43	54.13 ± 12.30	47.60 ± 5.58	50.35 ± 6.74	42.55 ± 41.87
ALB	RRMSE	0.88 ± 0.06	0.46 ± 0.08	0.52 ± 0.03	0.77 ± 0.06	1.14 ± 0.20
ALB	MBE	55.91 ± 19.27	-0.37 ± 11.47	-19.74 ± 5.34	83.55 ± 6.82	117.33 ± 42.37
HAI	R <sup>2</sup>	0.03 ± 0.03	0.32 ± 0.04	0.54 ± 0.11	0.25 ± 0.06	0.02 ± 0.03
HAI	RMSE	131.67 ± 12.72	72.81 ± 1.65	58.51 ± 11.47	110.02 ± 5.09	179.92 ± 31.30
HAI	sRMSE	112.79 ± 15.17	86.15 ± 0.83	83.22 ± 9.76	115.72 ± 4.17	171.60 ± 35.17
HAI	uRMSE	65.35 ± 16.62	45.90 ± 3.40	58.49 ± 6.67	35.08 ± 7.02	40.01 ± 41.06
HAI	RRMSE	1.13 ± 0.11	0.63 ± 0.01	0.51 ± 0.09	0.95 ± 0.04	1.55 ± 0.27
HAI	MBE	70.71 ± 24.06	0.42 ± 12.18	-9.55 ± 8.77	78.01 ± 6.21	146.89 ± 38.34
SCH	R <sup>2</sup>	0.02 ± 0.02	0.23 ± 0.04	0.17 ± 0.07	0.27 ± 0.15	0.02 ± 0.03
SCH	RMSE	142.90 ± 12.30	129.56 ± 8.21	144.81 ± 6.85	104.35 ± 14.22	144.01 ± 25.57
SCH	sRMSE	129.70 ± 11.57	141.33 ± 6.42	152.09 ± 3.38	120.30 ± 11.46	132.76 ± 16.64
SCH	uRMSE	58.91 ± 12.09	56.03 ± 4.71	44.91 ± 12.62	56.42 ± 18.15	46.69 ± 44.79
SCH	RRMSE	0.64 ± 0.06	0.58 ± 0.04	0.65 ± 0.03	0.47 ± 0.06	0.65 ± 0.12
SCH	MBE	-44.35 ± 27.74	-75.77 ± 12.38	-94.74 ± 5.45	-0.14 ± 8.90	39.24 ± 43.46
US	R <sup>2</sup>	0.13 ± 0.10	0.12 ± 0.10	0.14 ± 0.11	0.19 ± 0.05	0.23 ± 0.26
US	RMSE	184.27 ± 27.00	161.10 ± 38.01	155.40 ± 9.64	118.22 ± 23.46	76.40 ± 20.77
US	sRMSE	171.80 ± 24.72	159.96 ± 38.99	148.05 ± 10.26	106.73 ± 19.36	84.04 ± 13.67
US	uRMSE	63.41 ± 27.27	33.24 ± 13.22	45.41 ± 12.44	52.36 ± 23.27	22.45 ± 24.84
US	RRMSE	0.70 ± 0.10	0.62 ± 0.15	0.59 ± 0.04	0.45 ± 0.09	0.29 ± 0.07
US	MBE	-148.09 ± 28.52	-132.65 ± 46.57	-120.22 ± 12.54	-48.41 ± 44.96	0.49 ± 7.92

336

337

338 *Table A.22: Testing performance of local and transferred hybrid models. The parameters correspond to the best-performing*  
 339 *combination of parameters tested during the fivefold cross-validation using Active Learning with an initial training set size of*  
 340 *5%. CH: Switzerland, ALB: Schwäbische Alb, HAI: Hainich-Dün, SCH: Schorfheide-Chorin, US: United States, R<sup>2</sup>: coefficient of*  
 341 *determination, RMSE: root-mean-square error, sRMSE: systematic component of RMSE, uRMSE: unsystematic component of*  
 342 *RMSE, RRMSE: relative root-mean-square error, MBE: mean bias error.*

Initial training set size = 5%		Calibration site				
Prediction site	Metric	CH	ALB	HAI	SCH	US
CH	R <sup>2</sup>	0.15 ± 0.15	0.02 ± 0.02	0.01 ± 0.01	0.02 ± 0.02	0.01 ± 0.01
CH	RMSE	111.07 ± 19.79	120.25 ± 4.85	120.99 ± 5.25	140.38 ± 6.01	143.60 ± 7.80
CH	sRMSE	114.20 ± 9.45	112.32 ± 1.75	115.70 ± 2.65	134.66 ± 4.40	141.40 ± 1.41
CH	uRMSE	44.88 ± 23.47	39.92 ± 16.58	31.77 ± 16.23	37.52 ± 13.52	10.75 ± 24.04
CH	RRMSE	0.63 ± 0.11	0.69 ± 0.03	0.70 ± 0.03	0.81 ± 0.03	0.83 ± 0.04
CH	MBE	-13.64 ± 13.37	-18.65 ± 10.31	-34.13 ± 8.57	76.89 ± 7.50	88.51 ± 2.21
ALB	R <sup>2</sup>	0.04 ± 0.04	0.44 ± 0.16	0.30 ± 0.08	0.37 ± 0.09	0.02 ± 0.04
ALB	RMSE	113.02 ± 16.52	64.96 ± 10.37	73.35 ± 4.82	106.73 ± 8.13	152.55 ± 10.94
ALB	sRMSE	97.54 ± 10.32	84.72 ± 4.70	86.16 ± 1.01	118.23 ± 5.02	144.84 ± 12.28
ALB	uRMSE	53.11 ± 24.62	55.35 ± 8.69	44.39 ± 7.09	50.06 ± 6.30	16.82 ± 44.59
ALB	RRMSE	0.81 ± 0.12	0.46 ± 0.07	0.53 ± 0.03	0.77 ± 0.06	1.10 ± 0.08
ALB	MBE	44.89 ± 19.52	1.22 ± 10.29	-16.04 ± 6.17	82.66 ± 7.32	116.72 ± 16.84
HAI	R <sup>2</sup>	0.05 ± 0.06	0.26 ± 0.08	0.46 ± 0.13	0.22 ± 0.07	0.02 ± 0.02
HAI	RMSE	125.35 ± 18.84	76.21 ± 4.91	63.10 ± 11.90	107.83 ± 7.36	171.78 ± 8.86
HAI	sRMSE	106.93 ± 9.33	85.54 ± 0.22	83.12 ± 9.67	113.64 ± 5.75	166.19 ± 8.06
HAI	uRMSE	61.60 ± 28.97	37.05 ± 10.57	52.57 ± 10.79	33.82 ± 11.05	16.02 ± 40.76
HAI	RRMSE	1.08 ± 0.16	0.66 ± 0.04	0.55 ± 0.09	0.93 ± 0.06	1.48 ± 0.08
HAI	MBE	62.55 ± 15.42	1.85 ± 5.40	-4.17 ± 11.12	74.69 ± 8.72	142.14 ± 9.74
SCH	R <sup>2</sup>	0.02 ± 0.03	0.19 ± 0.05	0.13 ± 0.04	0.22 ± 0.08	0.01 ± 0.01
SCH	RMSE	142.94 ± 9.99	134.32 ± 4.59	147.07 ± 5.50	108.28 ± 11.79	131.14 ± 16.47
SCH	sRMSE	130.85 ± 5.26	143.28 ± 3.57	152.39 ± 3.78	121.01 ± 11.26	125.12 ± 1.57
SCH	uRMSE	54.97 ± 22.31	49.01 ± 8.91	38.37 ± 10.96	52.54 ± 12.04	15.61 ± 39.65
SCH	RRMSE	0.64 ± 0.05	0.61 ± 0.02	0.66 ± 0.02	0.49 ± 0.04	0.59 ± 0.07
SCH	MBE	-51.63 ± 16.42	-79.81 ± 6.50	-95.12 ± 6.11	-5.58 ± 14.29	34.03 ± 16.48
US	R <sup>2</sup>	0.09 ± 0.09	0.18 ± 0.06	0.20 ± 0.05	0.19 ± 0.03	0.11 ± 0.17
US	RMSE	147.63 ± 26.06	163.08 ± 11.32	152.60 ± 7.63	102.45 ± 8.77	82.00 ± 16.11
US	sRMSE	142.80 ± 19.56	151.49 ± 11.25	145.50 ± 7.02	89.77 ± 5.75	82.40 ± 10.50
US	uRMSE	43.32 ± 20.47	59.97 ± 7.16	45.30 ± 8.60	48.85 ± 9.79	10.56 ± 16.63
US	RRMSE	0.56 ± 0.10	0.62 ± 0.04	0.58 ± 0.03	0.39 ± 0.03	0.31 ± 0.06
US	MBE	-113.41 ± 23.40	-124.34 ± 13.64	-117.09 ± 8.69	-18.94 ± 17.36	-1.07 ± 5.78

343

344 *Table A.23: Testing performance of local and transferred hybrid models. The parameters correspond to the best-performing*  
 345 *combination of parameters tested during the fivefold cross-validation using Active Learning with an initial training set size of*  
 346 *10%. CH: Switzerland, ALB: Schwäbische Alb, HAI: Hainich-Dün, SCH: Schorfheide-Chorin, US: United States, R<sup>2</sup>: coefficient of*  
 347 *determination, RMSE: root-mean-square error, sRMSE: systematic component of RMSE, uRMSE: unsystematic component of*  
 348 *RMSE, RRMSE: relative root-mean-square error, MBE: mean bias error.*

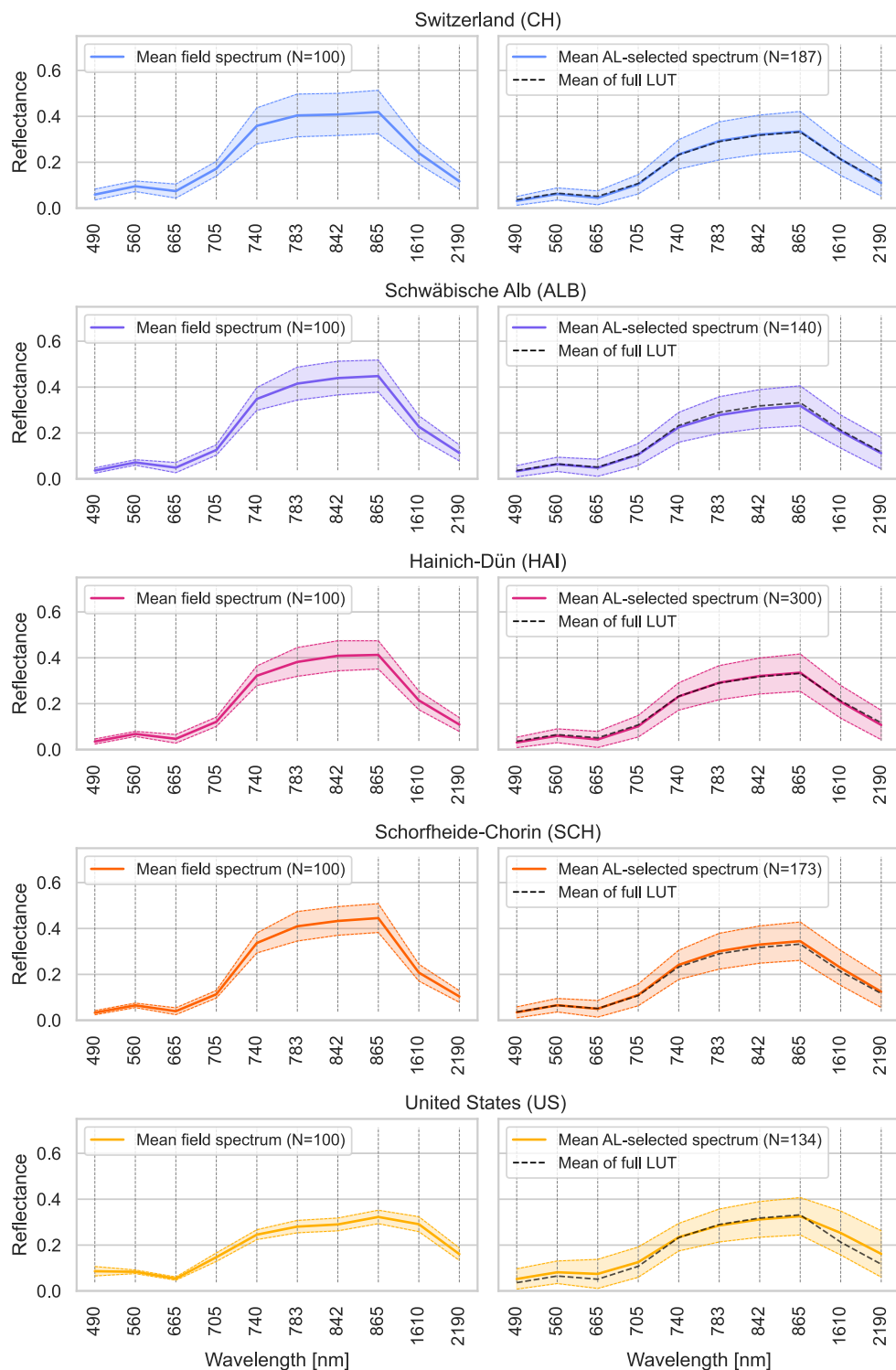
Initial training set size = 10%		Calibration site				
Prediction site	Metric	CH	ALB	HAI	SCH	US
CH	R <sup>2</sup>	0.17 ± 0.17	0.02 ± 0.01	0.02 ± 0.03	0.01 ± 0.02	0.01 ± 0.03
CH	RMSE	104.26 ± 15.57	117.78 ± 3.98	118.99 ± 2.31	138.46 ± 3.69	141.06 ± 0.68
CH	sRMSE	113.18 ± 8.79	111.64 ± 0.99	115.54 ± 2.58	135.89 ± 4.20	140.93 ± 0.76
CH	uRMSE	34.21 ± 26.09	35.90 ± 13.64	26.58 ± 11.38	25.48 ± 7.16	0.89 ± 2.34
CH	RRMSE	0.60 ± 0.08	0.68 ± 0.02	0.69 ± 0.01	0.80 ± 0.02	0.81 ± 0.00
CH	MBE	-4.20 ± 10.30	-17.59 ± 9.13	-33.37 ± 8.68	79.04 ± 7.44	87.96 ± 1.08
ALB	R <sup>2</sup>	0.03 ± 0.04	0.32 ± 0.21	0.27 ± 0.09	0.29 ± 0.10	0.00 ± 0.00
ALB	RMSE	102.02 ± 10.17	71.02 ± 12.27	74.43 ± 3.86	110.90 ± 5.44	149.05 ± 0.90
ALB	sRMSE	94.03 ± 5.34	84.82 ± 4.60	85.93 ± 0.66	119.22 ± 3.30	148.91 ± 0.95
ALB	uRMSE	34.53 ± 24.13	41.66 ± 20.56	41.94 ± 8.43	42.80 ± 7.97	0.08 ± 0.20
ALB	RRMSE	0.73 ± 0.07	0.51 ± 0.08	0.53 ± 0.03	0.80 ± 0.04	1.07 ± 0.01
ALB	MBE	38.65 ± 12.74	1.15 ± 9.86	-15.28 ± 4.10	84.09 ± 4.60	122.46 ± 1.10
HAI	R <sup>2</sup>	0.04 ± 0.06	0.19 ± 0.07	0.39 ± 0.15	0.18 ± 0.07	0.00 ± 0.01
HAI	RMSE	119.38 ± 14.55	81.05 ± 4.65	67.97 ± 13.90	111.40 ± 5.62	169.02 ± 0.99
HAI	sRMSE	105.85 ± 9.46	85.95 ± 0.67	82.95 ± 9.52	115.88 ± 3.43	168.84 ± 1.10
HAI	uRMSE	45.78 ± 32.95	29.93 ± 9.05	45.05 ± 11.36	29.84 ± 11.23	1.37 ± 2.93
HAI	RRMSE	1.03 ± 0.13	0.70 ± 0.04	0.59 ± 0.11	0.96 ± 0.05	1.46 ± 0.01
HAI	MBE	60.19 ± 17.35	1.81 ± 11.26	-4.00 ± 9.09	78.19 ± 5.01	145.55 ± 1.23
SCH	R <sup>2</sup>	0.01 ± 0.01	0.18 ± 0.06	0.10 ± 0.04	0.19 ± 0.12	0.00 ± 0.01
SCH	RMSE	138.26 ± 10.83	139.34 ± 4.02	149.11 ± 4.27	110.25 ± 11.89	125.74 ± 0.36
SCH	sRMSE	130.54 ± 9.74	147.00 ± 3.88	153.22 ± 2.61	120.60 ± 11.67	125.65 ± 0.38
SCH	uRMSE	40.52 ± 21.39	47.67 ± 11.13	33.54 ± 10.32	45.77 ± 18.46	1.70 ± 2.33
SCH	RRMSE	0.62 ± 0.05	0.63 ± 0.02	0.67 ± 0.02	0.50 ± 0.05	0.57 ± 0.00
SCH	MBE	-47.97 ± 24.76	-86.04 ± 6.35	-96.47 ± 4.13	-7.42 ± 8.90	39.67 ± 1.17
US	R <sup>2</sup>	0.05 ± 0.04	0.18 ± 0.06	0.15 ± 0.07	0.17 ± 0.04	0.08 ± 0.20
US	RMSE	142.09 ± 13.04	156.92 ± 11.19	158.49 ± 7.94	94.97 ± 3.44	84.34 ± 12.95
US	sRMSE	140.19 ± 10.94	148.43 ± 9.00	153.74 ± 8.54	87.67 ± 1.33	82.16 ± 10.98
US	uRMSE	24.30 ± 16.72	51.18 ± 16.01	37.17 ± 9.65	35.88 ± 7.41	1.63 ± 4.32
US	RRMSE	0.54 ± 0.05	0.60 ± 0.04	0.61 ± 0.03	0.36 ± 0.01	0.32 ± 0.04
US	MBE	-110.53 ± 13.95	-120.95 ± 10.53	-127.21 ± 10.27	-13.80 ± 8.37	0.28 ± 5.41

350 *Table A.24: Testing performance of local and transferred hybrid models. The parameters correspond to the best-performing*  
 351 *combination of parameters tested during the fivefold cross-validation using Active Learning with an initial training set size of*  
 352 *100% (= no Active Learning). CH: Switzerland, ALB: Schwäbische Alb, HAI: Hainich-Dün, SCH: Schorfheide-Chorin, US: United*  
 353 *States, R<sup>2</sup>: coefficient of determination, RMSE: root-mean-square error, sRMSE: systematic component of RMSE, uRMSE:*  
 354 *unsystematic component of RMSE, RRMSE: relative root-mean-square error, MBE: mean bias error.*

Initial training set size = 100% (= no Active Learning)		Calibration site				
Prediction site	Metric	CH	ALB	HAI	SCH	US
CH	R <sup>2</sup>	0.07 ± 0.07	0.03 ± 0.00	0.03 ± 0.00	0.03 ± 0.00	0.03 ± 0.00
CH	RMSE	112.71 ± 8.67	109.87 ± 0.00	109.87 ± 0.00	109.87 ± 0.00	109.87 ± 0.00
CH	sRMSE	112.96 ± 8.67	110.10 ± 0.00	110.10 ± 0.00	110.10 ± 0.00	110.10 ± 0.00
CH	uRMSE	7.59 ± 4.63	7.18 ± 0.00	7.18 ± 0.00	7.18 ± 0.00	7.18 ± 0.00
CH	RRMSE	0.64 ± 0.04	0.63 ± 0.00	0.63 ± 0.00	0.63 ± 0.00	0.63 ± 0.00
CH	MBE	0.07 ± 3.45	0.99 ± 0.00	0.99 ± 0.00	0.99 ± 0.00	0.99 ± 0.00
ALB	R <sup>2</sup>	0.06 ± 0.00	0.09 ± 0.05	0.06 ± 0.00	0.06 ± 0.00	0.06 ± 0.00
ALB	RMSE	89.47 ± 0.00	89.24 ± 3.93	89.47 ± 0.00	89.47 ± 0.00	89.47 ± 0.00
ALB	sRMSE	90.72 ± 0.00	90.41 ± 3.59	90.72 ± 0.00	90.72 ± 0.00	90.72 ± 0.00
ALB	uRMSE	14.99 ± 0.00	13.53 ± 5.02	14.99 ± 0.00	14.99 ± 0.00	14.99 ± 0.00
ALB	RRMSE	0.64 ± 0.00	0.64 ± 0.02	0.64 ± 0.00	0.64 ± 0.00	0.64 ± 0.00
ALB	MBE	32.42 ± 0.00	32.03 ± 2.86	32.42 ± 0.00	32.42 ± 0.00	32.42 ± 0.00
HAI	R <sup>2</sup>	0.03 ± 0.00	0.03 ± 0.00	0.08 ± 0.06	0.03 ± 0.00	0.03 ± 0.00
HAI	RMSE	100.17 ± 0.00	100.17 ± 0.00	98.26 ± 7.91	100.17 ± 0.00	100.17 ± 0.00
HAI	sRMSE	100.91 ± 0.00	100.91 ± 0.00	99.17 ± 7.33	100.91 ± 0.00	100.91 ± 0.00
HAI	uRMSE	12.20 ± 0.00	12.20 ± 0.00	14.74 ± 2.59	12.20 ± 0.00	12.20 ± 0.00
HAI	RRMSE	0.86 ± 0.00	0.86 ± 0.00	0.85 ± 0.05	0.86 ± 0.00	0.86 ± 0.00
HAI	MBE	53.30 ± 0.00	53.30 ± 0.00	54.24 ± 2.70	53.30 ± 0.00	53.30 ± 0.00
SCH	R <sup>2</sup>	0.08 ± 0.00	0.08 ± 0.00	0.08 ± 0.00	0.09 ± 0.07	0.08 ± 0.00
SCH	RMSE	128.15 ± 0.00	128.15 ± 0.00	128.15 ± 0.00	129.58 ± 12.06	128.15 ± 0.00
SCH	sRMSE	130.20 ± 0.00	130.20 ± 0.00	130.20 ± 0.00	131.46 ± 12.23	130.20 ± 0.00
SCH	uRMSE	23.03 ± 0.00	23.03 ± 0.00	23.03 ± 0.00	20.49 ± 8.84	23.03 ± 0.00
SCH	RRMSE	0.58 ± 0.00	0.58 ± 0.00	0.58 ± 0.00	0.58 ± 0.04	0.58 ± 0.00
SCH	MBE	-52.78 ± 0.00	-52.78 ± 0.00	-52.78 ± 0.00	-53.14 ± 5.05	-52.78 ± 0.00
US	R <sup>2</sup>	0.02 ± 0.00	0.02 ± 0.00	0.02 ± 0.00	0.02 ± 0.00	0.07 ± 0.08
US	RMSE	122.36 ± 0.00	122.36 ± 0.00	122.36 ± 0.00	122.36 ± 0.00	121.22 ± 12.12
US	sRMSE	122.41 ± 0.00	122.41 ± 0.00	122.41 ± 0.00	122.41 ± 0.00	121.32 ± 12.08
US	uRMSE	3.69 ± 0.00	3.69 ± 0.00	3.69 ± 0.00	3.69 ± 0.00	4.87 ± 1.51
US	RRMSE	0.47 ± 0.00	0.47 ± 0.00	0.47 ± 0.00	0.47 ± 0.00	0.46 ± 0.04
US	MBE	-87.21 ± 0.00	-87.21 ± 0.00	-87.21 ± 0.00	-87.21 ± 0.00	-86.97 ± 4.31

355

356    **Section A.23: Mean field spectrum and AL-selected spectra by site**



357

358    *Figure A.24: Line plots of selected field spectra (left columns) and Active Learning (AL) selected training spectra of the look-up  
 359    table (LUT) of the best performing local hybrid model with an initial training set size of 2% in terms of lowest relative root-  
 360    mean-square error (right column) by study site. Bold lines represent mean spectra and colored areas represent the mean  
 361    spectra ± 1 standard deviation.*

362 **References**

- 363 Chen, T., Guestrin, C., 2016. XGBoost: A scalable tree boosting system. Proceedings of the ACM  
364 SIGKDD International Conference on Knowledge Discovery and Data Mining 13-17-August-2016,  
365 785–794. <https://doi.org/10.1145/2939672.2939785>
- 366 Combal, B., Baret, F., Weiss, M., Trubuil, A., Macé, D., Pragnère, A., Myneni, R., Knyazikhin, Y., Wang,  
367 L., 2003. Retrieval of canopy biophysical variables from bidirectional reflectance. *Remote Sens  
368 Environ* 84, 1–15. [https://doi.org/10.1016/S0034-4257\(02\)00035-4](https://doi.org/10.1016/S0034-4257(02)00035-4)
- 369 Cornelissen, J.H.C., 1996. An Experimental Comparison of Leaf Decomposition Rates in a Wide Range  
370 of Temperate Plant Species and Types. *J Ecol* 84, 573–582. <https://doi.org/10.2307/2261479>
- 371 Cornelissen, J.H.C., Quested, H.M., Gwynn-Jones, D., Van Logtestijn, R.S.P., De Beus, M.A.H.,  
372 Kondratchuk, A., Callaghan, T. V., Aerts, R., 2004. Leaf Digestibility and Litter Decomposability  
373 Are Related in a Wide Range of Subarctic Plant Species and Types. *Funct Ecol* 18, 779–786.
- 374 Cornwell, W.K., Cornelissen, J.H.C., Amatangelo, K., Dorrepaal, E., Eviner, V.T., Godoy, O., Hobbie,  
375 S.E., Hoorens, B., Kurokawa, H., Pérez-Harguindeguy, N., Quested, H.M., Santiago, L.S., Wardle,  
376 D.A., Wright, I.J., Aerts, R., Allison, S.D., Van Bodegom, P., Brovkin, V., Chatain, A., Callaghan, T.  
377 V., Díaz, S., Garnier, E., Gurvich, D.E., Kazakou, E., Klein, J.A., Read, J., Reich, P.B., Soudzilovskaia,  
378 N.A., Vaieretti, M.V., Westoby, M., 2008. Plant species traits are the predominant control on  
379 litter decomposition rates within biomes worldwide. *Ecol Lett* 11, 1065–1071.  
380 <https://doi.org/10.1111/j.1461-0248.2008.01219.x>
- 381 Cornwell, W.K., Wright, I., Turner, J., Maire, V., Barbour, M., Cernusak, L., Dawson, T., Ellsworth, D.,  
382 Farquhar, G., Griffiths, H., Keitel, C., Knohl, A., Reich, P., Williams, D., Bhaskar, R., Cornelissen,  
383 J.H.C., Richards, A., Schmidt, S., Valladares, F., Körner, C., Schulze, E., Buchmann, N., Santiago,  
384 L., 2017. A global dataset of leaf D13 C values.
- 385 Craine, J.M., Lee, W.G., Bond, W.J., Williams, R.J., Johnson, L.C., 2005. Environmental constraints on a  
386 global relationship among leaf and root traits of grasses. *Ecology* 86, 12–19.  
387 <https://doi.org/10.1890/04-1075>
- 388 Diaz, S., Hodgson, J.G., Thompson, K., Cabido, M., Cornelissen, J.H.C., Jalili, A., Montserrat-Martí, G.,  
389 Grime, J.P., Zarrinkamar, F., Asri, Y., Band, S.R., Basconcelo, S., Castro-Díez, P., Funes, G.,  
390 Hamzehee, B., Khoshnevi, M., Pérez-Harguindeguy, N., Pérez-Rontomé, M.C., Shirvany, F.A.,  
391 Vendramini, F., Yazdani, S., Abbas-Azimi, R., Bogaard, A., Boustani, S., Charles, M., Dehghan, M.,  
392 de Torres-Espuny, L., Falcuk, V., Guerrero-Campo, J., Hynd, A., Jones, G., Kowsary, E., Kazemi-  
393 Saeed, F., Maestro-Martínez, M., Romo-Díez, A., Shaw, S., Siavash, B., Villar-Salvador, P., Zak,  
394 M.R., 2004. The plant traits that drive ecosystems: Evidence from three continents. *Journal of  
395 Vegetation Science* 15, 295–304. <https://doi.org/10.1111/j.1654-1103.2004.tb02266.x>
- 396 ESA, 2015. Sentinel-2 User Handbook Issue 1 Revision 2. Noordwijk.
- 397 Fitter, A.H., Peat, H.J., 1994. The Ecological Flora Database. *J Ecol* 82, 415–425.  
398 <https://doi.org/10.2307/2261309>
- 399 Flowers, T., Santos, J., Jahns, M., Warburton, B., Reed, P., 2023. eHALOPH - Halophytes Database  
400 (version 3.11) [WWW Document]. URL <http://www.sussex.ac.uk/affiliates/halophytes>,  
401 (accessed 11.28.23).

- 402 Flowers, T., Santos, J., Jahns, M., Warburton, B., Reed, P., 2017. eHALOPH - Halophytes Database  
403 (version 3.11) [WWW Document]. URL <http://www.sussex.ac.uk/affiliates/halophytes>,  
404 (accessed 1.1.17).
- 405 Huete, A.R., Liu, H., van Leeuwen, W.J.D., 1997. The use of vegetation indices in forested regions:  
406 issues of linearity and saturation, in: IGARSS'97. 1997 IEEE International Geoscience and  
407 Remote Sensing Symposium Proceedings. Remote Sensing - A Scientific Vision for Sustainable  
408 Development. IEEE, pp. 1966–1968. <https://doi.org/10.1109/IGARSS.1997.609169>
- 409 Iversen, C.M., McCormack, M.L., Powell, A.S., Blackwood, C.B., Freschet, G.T., Kattge, J., Roumet, C.,  
410 Stover, D.B., Soudzilovskaia, N.A., Valverde-Barrantes, O.J., van Bodegom, P.M., Violle, C., 2017.  
411 A global Fine-Root Ecology Database to address below-ground challenges in plant ecology. New  
412 Phytologist 215, 15–26. <https://doi.org/10.1111/nph.14486>
- 413 Jehle, M., Hueni, A., Damm, A., D'Odorico, P., Weyermann, J., Kneubühler, M., Schlapfer, D.,  
414 Schaeppman, M.E., Meuleman, K., 2010. APEX - current status, performance and validation  
415 concept, in: 2010 IEEE Sensors. IEEE, pp. 533–537.  
416 <https://doi.org/10.1109/ICSENS.2010.5690122>
- 417 Kapralov, M. V., Smith, J.A.C., Filatov, D.A., 2012. Rubisco Evolution in C4 Eudicots: An Analysis of  
418 Amaranthaceae Sensu Lato. PLoS One 7, e52974.  
419 <https://doi.org/10.1371/journal.pone.0052974>
- 420 Kattge, J., Bönisch, G., Díaz, S., Lavorel, S., Prentice, I.C., Leadley, P., Tautenhahn, S., Werner, G.D.A.,  
421 Aakala, T., Abedi, M., Acosta, A.T.R., Adamidis, G.C., Adamson, K., Aiba, M., Albert, C.H.,  
422 Alcántara, J.M., Alcázar C, C., Aleixo, I., Ali, H., Amiaud, B., Ammer, C., Amoroso, M.M., Anand,  
423 M., Anderson, C., Anten, N., Antos, J., Apgaua, D.M.G., Ashman, T., Asmara, D.H., Asner, G.P.,  
424 Aspinwall, M., Atkin, O., Aubin, I., Bastrup-Spohr, L., Bahalkeh, K., Bahn, M., Baker, T., Baker,  
425 W.J., Bakker, J.P., Baldocchi, D., Baltzer, J., Banerjee, A., Baranger, A., Barlow, J., Barneche, D.R.,  
426 Baruch, Z., Bastianelli, D., Battles, J., Bauerle, W., Bauters, M., Bazzato, E., Beckmann, M.,  
427 Beeckman, H., Beierkuhnlein, C., Bekker, R., Belfry, G., Belluau, M., Belouli, M., Benavides, R.,  
428 Benomar, L., Berdugo-Lattke, M.L., Berenguer, E., Bergamin, R., Bergmann, J., Bergmann  
429 Carlucci, M., Berner, L., Bernhardt-Römermann, M., Bigler, C., Bjorkman, A.D., Blackman, C.,  
430 Blanco, C., Blonder, B., Blumenthal, D., Bocanegra-González, K.T., Boeckx, P., Bohlman, S.,  
431 Böhning-Gaese, K., Boisvert-Marsh, L., Bond, W., Bond-Lamberty, B., Boom, A., Boonman,  
432 C.C.F., Bordin, K., Boughton, E.H., Boukili, V., Bowman, D.M.J.S., Bravo, S., Brendel, M.R.,  
433 Broadley, M.R., Brown, K.A., Bruelheide, H., Brunnich, F., Bruun, H.H., Bruylants, D., Buchanan, S.W.,  
434 Bucher, S.F., Buchmann, N., Buitenhof, R., Bunker, D.E., Bürger, J., Burrascano, S., Burslem,  
435 D.F.R.P., Butterfield, B.J., Byun, C., Marques, M., Scalon, M.C., Caccianiga, M., Cadotte, M.,  
436 Cailleret, M., Camac, J., Camarero, J.J., Campany, C., Campetella, G., Campos, J.A., Cano-  
437 Arboleda, L., Canullo, R., Carbognani, M., Carvalho, F., Casanoves, F., Castagnérol, B., Catford,  
438 J.A., Cavender-Bares, J., Cerabolini, B.E.L., Cervellini, M., Chacón-Madrigal, E., Chapin, K.,  
439 Chapin, F.S., Chelli, S., Chen, S., Chen, A., Cherubini, P., Chianucci, F., Choat, B., Chung, K.,  
440 Chytrý, M., Ciccarelli, D., Coll, L., Collins, C.G., Conti, L., Coomes, D., Cornelissen, J.H.C.,  
441 Cornwell, W.K., Corona, P., Coyea, M., Craine, J., Craven, D., Cromsigt, J.P.G.M., Csecserits, A.,  
442 Cufar, K., Cuntz, M., da Silva, A.C., Dahlin, K.M., Dainese, M., Dalke, I., Dalle Fratte, M., Dang-Le,  
443 A.T., Danihelka, J., Dannoura, M., Dawson, S., de Beer, A.J., De Frutos, A., De Long, J.R., Dechant,  
444 B., Delagrange, S., Delpierre, N., Derroire, G., Dias, A.S., Diaz-Toribio, M.H., Dimitrakopoulos,  
445 P.G., Dobrowolski, M., Doktor, D., Dřevojan, P., Dong, N., Dransfield, J., Dressler, S., Duarte, L.,  
446 Ducouret, E., Dullinger, S., Durka, W., Duursma, R., Dymova, O., E-Vojtkó, A., Eckstein, R.L.,  
447 Ejtehadi, H., Elser, J., Emilio, T., Engemann, K., Erfanian, M.B., Erfmeier, A., Esquivel-Muelbert,

448 A., Esser, G., Estiarte, M., Domingues, T.F., Fagan, W.F., Fagúndez, J., Falster, D.S., Fan, Y., Fang,  
449 J., Farris, E., Fazlioglu, F., Feng, Y., Fernandez-Mendez, F., Ferrara, C., Ferreira, J., Fidelis, A.,  
450 Finegan, B., Firn, J., Flowers, T.J., Flynn, D.F.B., Fontana, V., Forey, E., Forgiarini, C., François, L.,  
451 Frangipani, M., Frank, D., Frenette-Dussault, C., Freschet, G.T., Fry, E.L., Fyllas, N.M.,  
452 Mazzochini, G.G., Gachet, S., Gallagher, R., Ganade, G., Ganga, F., García-Palacios, P.,  
453 Gargaglione, V., Garnier, E., Garrido, J.L., de Gasper, A.L., Gea-Izquierdo, G., Gibson, D., Gillison,  
454 A.N., Giroldo, A., Glasenhardt, M., Gleason, S., Gliesch, M., Goldberg, E., Göldel, B., Gonzalez-  
455 Akre, E., Gonzalez-Andujar, J.L., González-Melo, A., González-Robles, A., Graae, B.J., Granda, E.,  
456 Graves, S., Green, W.A., Gregor, T., Gross, N., Guerin, G.R., Günther, A., Gutiérrez, A.G.,  
457 Haddock, L., Haines, A., Hall, J., Hambuckers, A., Han, W., Harrison, S.P., Hattingh, W., Hawes,  
458 J.E., He, T., He, P., Heberling, J.M., Helm, A., Hempel, S., Hentschel, J., Hérault, B., Hereş, A.,  
459 Herz, K., Heuertz, M., Hickler, T., Hietz, P., Higuchi, P., Hipp, A.L., Hirons, A., Hock, M., Hogan,  
460 J.A., Holl, K., Honnay, O., Hornstein, D., Hou, E., Hough-Snee, N., Hovstad, K.A., Ichie, T., Igić, B.,  
461 Illa, E., Isaac, M., Ishihara, M., Ivanov, L., Ivanova, L., Iversen, C.M., Izquierdo, J., Jackson, R.B.,  
462 Jackson, B., Jactel, H., Jagodzinski, A.M., Jandt, U., Jansen, S., Jenkins, T., Jentsch, A., Jespersen,  
463 J.R.P., Jiang, G., Johansen, J.L., Johnson, D., Jokela, E.J., Joly, C.A., Jordan, G.J., Joseph, G.S.,  
464 Junaedi, D., Junker, R.R., Justes, E., Kabzems, R., Kane, J., Kaplan, Z., Kattenborn, T., Kavelenova,  
465 L., Kearsley, E., Kempel, A., Kenzo, T., Kerkhoff, A., Khalil, M.I., Kinlock, N.L., Kissling, W.D.,  
466 Kitajima, K., Kitzberger, T., Kjøller, R., Klein, T., Kleyer, M., Klimešová, J., Klipel, J., Kloepel, B.,  
467 Klotz, S., Knops, J.M.H., Kohyama, T., Koike, F., Kollmann, J., Komac, B., Komatsu, K., König, C.,  
468 Kraft, N.J.B., Kramer, K., Kreft, H., Kühn, I., Kumarathunge, D., Kuppler, J., Kurokawa, H.,  
469 Kurosawa, Y., Kuyah, S., Laclau, J., Lafleur, B., Lallai, E., Lamb, E., Lamprecht, A., Larkin, D.J.,  
470 Laughlin, D., Le Bagousse-Pinguet, Y., le Maire, G., le Roux, P.C., le Roux, E., Lee, T., Lens, F.,  
471 Lewis, S.L., Lhotsky, B., Li, Y., Li, X., Lichstein, J.W., Liebergesell, M., Lim, J.Y., Lin, Y., Linares, J.C.,  
472 Liu, C., Liu, D., Liu, U., Livingstone, S., Llusià, J., Lohbeck, M., López-García, Á., Lopez-Gonzalez,  
473 G., Lososová, Z., Louault, F., Lukács, B.A., Lukeš, P., Luo, Y., Lussu, M., Ma, S., Maciel Rabelo  
474 Pereira, C., Mack, M., Maire, V., Mäkelä, A., Mäkinen, H., Malhado, A.C.M., Mallik, A., Manning,  
475 P., Manzoni, S., Marchetti, Z., Marchino, L., Marcilio-Silva, V., Marcon, E., Marignani, M.,  
476 Markesteijn, L., Martin, A., Martínez-Garza, C., Martínez-Vilalta, J., Mašková, T., Mason, K.,  
477 Mason, N., Massad, T.J., Masse, J., Mayrose, I., McCarthy, J., McCormack, M.L., McCulloh, K.,  
478 McFadden, I.R., McGill, B.J., McPartland, M.Y., Medeiros, J.S., Medlyn, B., Meerts, P., Mehrabi,  
479 Z., Meir, P., Melo, F.P.L., Mencuccini, M., Meredieu, C., Messier, J., Mészáros, I., Metsaranta, J.,  
480 Michaletz, S.T., Michelaki, C., Migalina, S., Milla, R., Miller, J.E.D., Minden, V., Ming, R., Mokany,  
481 K., Moles, A.T., Molnár, A., Molofsky, J., Molz, M., Montgomery, R.A., Monty, A., Moravcová, L.,  
482 Moreno-Martínez, A., Moretti, M., Mori, A.S., Mori, S., Morris, D., Morrison, J., Mucina, L.,  
483 Mueller, S., Muir, C.D., Müller, S.C., Munoz, F., Myers-Smith, I.H., Myster, R.W., Nagano, M.,  
484 Naidu, S., Narayanan, A., Natesan, B., Negoita, L., Nelson, A.S., Neuschulz, E.L., Ni, J., Niedrist,  
485 G., Nieto, J., Niinemets, Ü., Nolan, R., Nottebrock, H., Nouvellon, Y., Novakovskiy, A., Nystuen,  
486 K.O., O'Grady, A., O'Hara, K., O'Reilly-Nugent, A., Oakley, S., Oberhuber, W., Ohtsuka, T.,  
487 Oliveira, R., Öllerer, K., Olson, M.E., Onipchenko, V., Onoda, Y., Onstein, R.E., Ordonez, J.C.,  
488 Osada, N., Ostonen, I., Ottaviani, G., Otto, S., Overbeck, G.E., Ozinga, W.A., Pahl, A.T., Paine,  
489 C.E.T., Pakeman, R.J., Papageorgiou, A.C., Parfionova, E., Pärtel, M., Patacca, M., Paula, S.,  
490 Paule, J., Pauli, H., Pausas, J.G., Peco, B., Penuelas, J., Perea, A., Peri, P.L., Petisco-Souza, A.C.,  
491 Petraglia, A., Petritan, A.M., Phillips, O.L., Pierce, S., Pillar, V.D., Pisek, J., Pomogaybin, A.,  
492 Poorter, H., Portsmouth, A., Poschlod, P., Potvin, C., Pounds, D., Powell, A.S., Power, S.A.,  
493 Prinzing, A., Puglielli, G., Pyšek, P., Raever, V., Rammig, A., Ransijn, J., Ray, C.A., Reich, P.B.,  
494 Reichstein, M., Reid, D.E.B., Réjou-Méchain, M., de Dios, V.R., Ribeiro, S., Richardson, S., Riibak,  
495 K., Rillig, M.C., Riviera, F., Robert, E.M.R., Roberts, S., Robroek, B., Roddy, A., Rodrigues, A.V.,

- 496 Rogers, A., Rollinson, E., Rolo, V., Römermann, C., Ronzhina, D., Roscher, C., Rosell, J.A.,  
 497 Rosenfield, M.F., Rossi, C., Roy, D.B., Royer-Tardif, S., Rüger, N., Ruiz-Peinado, R., Rumpf, S.B.,  
 498 Rusch, G.M., Ryo, M., Sack, L., Saldaña, A., Salgado-Negret, B., Salguero-Gomez, R., Santa-  
 499 Regina, I., Santacruz-García, A.C., Santos, J., Sardans, J., Schamp, B., Scherer-Lorenzen, M.,  
 500 Schleuning, M., Schmid, B., Schmidt, M., Schmitt, S., Schneider, J. V., Schowanek, S.D., Schrader,  
 501 J., Schrodt, F., Schuldt, B., Schurr, F., Selaya Garvizu, G., Semchenko, M., Seymour, C., Sfair, J.C.,  
 502 Sharpe, J.M., Sheppard, C.S., Sheremetiev, S., Shiodera, S., Shipley, B., Shovon, T.A., Siebenkäs,  
 503 A., Sierra, C., Silva, V., Silva, M., Sitzia, T., Sjöman, H., Slot, M., Smith, N.G., Sodhi, D., Soltis, P.,  
 504 Soltis, D., Somers, B., Sonnier, G., Sørensen, M.V., Sosinski, E.E., Soudzilovskaia, N.A., Souza,  
 505 A.F., Spasojevic, M., Sperandii, M.G., Stan, A.B., Stegen, J., Steinbauer, K., Stephan, J.G., Sterck,  
 506 F., Stojanovic, D.B., Strydom, T., Suarez, M.L., Svenning, J., Svitková, I., Svitok, M., Svoboda, M.,  
 507 Swaine, E., Swenson, N., Tabarelli, M., Takagi, K., Tappeiner, U., Tarifa, R., Tauugourdeau, S.,  
 508 Tavsanoglu, C., te Beest, M., Tedersoo, L., Thiffault, N., Thom, D., Thomas, E., Thompson, K.,  
 509 Thornton, P.E., Thuiller, W., Tichý, L., Tissue, D., Tjoelker, M.G., Tng, D.Y.P., Tobias, J., Török, P.,  
 510 Tarin, T., Torres-Ruiz, J.M., Tóthmérész, B., Treurnicht, M., Trivellone, V., Trolliet, F., Trotsiuk, V.,  
 511 Tsakalos, J.L., Tsiripidis, I., Tysklind, N., Umehara, T., Usoltsev, V., Vadeboncoeur, M., Vaezi, J.,  
 512 Valladares, F., Vamosi, J., van Bodegom, P.M., van Breugel, M., Van Cleemput, E., van de Weg,  
 513 M., van der Merwe, S., van der Plas, F., van der Sande, M.T., van Kleunen, M., Van Meerbeek,  
 514 K., Vanderwel, M., Vanselow, K.A., Vårhammar, A., Varone, L., Vasquez Valderrama, M.Y.,  
 515 Vassilev, K., Vellend, M., Veneklaas, E.J., Verbeeck, H., Verheyen, K., Vibrans, A., Vieira, I.,  
 516 Villacís, J., Violle, C., Vivek, P., Wagner, K., Waldram, M., Waldron, A., Walker, A.P., Waller, M.,  
 517 Walther, G., Wang, H., Wang, F., Wang, W., Watkins, H., Watkins, J., Weber, U., Weedon, J.T.,  
 518 Wei, L., Weigelt, P., Weiher, E., Wells, A.W., Wellstein, C., Wenk, E., Westoby, M., Westwood,  
 519 A., White, P.J., Whitten, M., Williams, M., Winkler, D.E., Winter, K., Womack, C., Wright, I.J.,  
 520 Wright, S.J., Wright, J., Pinho, B.X., Ximenes, F., Yamada, T., Yamaji, K., Yanai, R., Yankov, N.,  
 521 Yguel, B., Zanini, K.J., Zanne, A.E., Zelený, D., Zhao, Y., Zheng, Jingming, Zheng, Ji, Ziemińska, K.,  
 522 Zirbel, C.R., Zizka, G., Zo-Bi, I.C., Zottz, G., Wirth, C., 2020. TRY plant trait database – enhanced  
 523 coverage and open access. *Glob Chang Biol* 26, 119–188. <https://doi.org/10.1111/gcb.14904>  
 524 Kattge, J., Knorr, W., Raddatz, T., Wirth, C., 2009. Quantifying photosynthetic capacity and its  
 525 relationship to leaf nitrogen content for global-scale terrestrial biosphere models. *Glob Chang  
 526 Biol* 15, 976–991. <https://doi.org/10.1111/j.1365-2486.2008.01744.x>  
 527 Laughlin, D.C., Fulé, P.Z., Huffman, D.W., Crouse, J., Laliberté, E., 2011. Climatic constraints on trait-  
 528 based forest assembly. *Journal of Ecology* 99, 1489–1499. [https://doi.org/10.1111/j.1365-2745.2011.01885.x](https://doi.org/10.1111/j.1365-<br/>
    529 2745.2011.01885.x)  
 530 Laughlin, D.C., Leppert, J.J., Moore, M.M., Sieg, C.H., 2010. A multi-trait test of the leaf-height-seed  
 531 plant strategy scheme with 133 species from a pine forest flora. *Funct Ecol* 24, 493–501.  
 532 <https://doi.org/10.1111/j.1365-2435.2009.01672.x>  
 533 Lin, Y.-S., Medlyn, B.E., Duursma, R.A., Prentice, I.C., Wang, H., Baig, S., Eamus, D., de Dios, V.R.,  
 534 Mitchell, P., Ellsworth, D.S., de Beeck, M.O., Wallin, G., Uddling, J., Tarvainen, L., Linderson, M.-  
 535 L., Cernusak, L.A., Nippert, J.B., Ocheltree, T.W., Tissue, D.T., Martin-StPaul, N.K., Rogers, A.,  
 536 Warren, J.M., De Angelis, P., Hikosaka, K., Han, Q., Onoda, Y., Gimeno, T.E., Barton, C.V.M.,  
 537 Bennie, J., Bonal, D., Bosc, A., Löw, M., Macinins-Ng, C., Rey, A., Rowland, L., Setterfield, S.A.,  
 538 Tausz-Posch, S., Zaragoza-Castells, J., Broadmeadow, M.S.J., Drake, J.E., Freeman, M.,  
 539 Ghannoum, O., Hutley, L.B., Kelly, J.W., Kikuzawa, K., Kolari, P., Koyama, K., Limousin, J.-M.,  
 540 Meir, P., Lola da Costa, A.C., Mikkelsen, T.N., Salinas, N., Sun, W., Wingate, L., 2015. Optimal

- 541 stomatal behaviour around the world. *Nat Clim Chang* 5, 459–464.  
542 <https://doi.org/10.1038/nclimate2550>
- 543 Meir, P., Kruijt, B., Broadmeadow, M., Barbosa, E., Kull, O., Carswell, F., Nobre, A., Jarvis, P.G., 2002.  
544 Acclimation of photosynthetic capacity to irradiance in tree canopies in relation to leaf nitrogen  
545 concentration and leaf mass per unit area. *Plant Cell Environ* 25, 343–357.  
546 <https://doi.org/10.1046/j.0016-8025.2001.00811.x>
- 547 Mesonet, 2024. Monthly Rainfall Table: Norman (NRMN) Monthly Actual Oklahoma Mesonet Rainfall  
548 Table (in inches) [WWW Document]. URL <https://www.mesonet.org/weather/rainfall/monthly-rainfall-table?ref=1210> (accessed 1.4.24).
- 549
- 550 Munroe, S.E.M., McInerney, F.A., Andrae, J., Welti, N., Guerin, G.R., Leitch, E., Hall, T., Szarvas, S.,  
551 Atkins, R., Caddy-Retalic, S., Sparrow, B., 2021. The photosynthetic pathways of plant species  
552 surveyed in Australia's national terrestrial monitoring network. *Sci Data* 8, 97.  
553 <https://doi.org/10.1038/s41597-021-00877-z>
- 554 Pedregosa, F., Varoquaux, G., Gramfort, A., Michel, V., Thirion, B., Grisel, O., Blondel, M., Müller, A.,  
555 Nothman, J., Louppe, G., Prettenhofer, P., Weiss, R., Dubourg, V., Vanderplas, J., Passos, A.,  
556 Cournapeau, D., Brucher, M., Perrot, M., Duchesnay, É., 2012. Scikit-learn: Machine Learning in  
557 Python. *Journal of Machine Learning Research* 12, 2825–2830.
- 558 Poschlod, P., Kleyer, M., Jackel, A.-K., Dannemann, A., Tackenberg, O., 2003. BIOPOP — A database of  
559 plant traits and internet application for nature conservation. *Folia Geobot* 38, 263–271.  
560 <https://doi.org/10.1007/BF02803198>
- 561 Quested, H.M., Cornelissen, J.H.C., Press, M.C., Callaghan, T. V., Aerts, R., Trosien, F., Riemann, P.,  
562 Gwynn-Jones, D., Kondratchuk, A., Jonasson, S.E., 2003. Decomposition of sub-arctic plants with  
563 differing nitrogen economies: A functional role for hemiparasites. *Ecology* 84, 3209–3221.  
564 <https://doi.org/10.1890/02-0426>
- 565 Reich, P.B., Oleksyn, J., Wright, I.J., 2009. Leaf phosphorus influences the photosynthesis–nitrogen  
566 relation: a cross-biome analysis of 314 species. *Oecologia* 160, 207–212.  
567 <https://doi.org/10.1007/s00442-009-1291-3>
- 568 Reich, P.B., Tjoelker, M.G., Pregitzer, K.S., Wright, I.J., Oleksyn, J., Machado, J., 2008. Scaling of  
569 respiration to nitrogen in leaves, stems and roots of higher land plants. *Ecol Lett* 11, 793–801.  
570 <https://doi.org/10.1111/j.1461-0248.2008.01185.x>
- 571 Richter, R., Schläpfer, D., 2002. Geo-atmospheric processing of airborne imaging spectrometry data.  
572 Part 2: Atmospheric/topographic correction. *Int J Remote Sens* 23, 2631–2649.  
573 <https://doi.org/10.1080/01431160110115834>
- 574 Schaepman, M.E., Jehle, M., Hueni, A., D'Odorico, P., Damm, A., Weyermann, J., Schneider, F.D.,  
575 Laurent, V., Popp, C., Seidel, F.C., Lenhard, K., Gege, P., Küchler, C., Brazile, J., Kohler, P., De Vos,  
576 L., Meuleman, K., Meynard, R., Schläpfer, D., Kneubühler, M., Itten, K.I., 2015. Advanced  
577 radiometry measurements and Earth science applications with the Airborne Prism Experiment  
578 (APEX). *Remote Sens Environ* 158, 207–219. <https://doi.org/10.1016/j.rse.2014.11.014>
- 579 Schiefer, F., Schmidlein, S., Kattenborn, T., 2021. The retrieval of plant functional traits from canopy  
580 spectra through RTM-inversions and statistical models are both critically affected by plant  
581 phenology. *Ecol Indic* 121, 107062. <https://doi.org/10.1016/j.ecolind.2020.107062>

- 582 Schläpfer, D., Richter, R., 2002. Geo-atmospheric processing of airborne imaging spectrometry data.  
583 Part 1: Parametric orthorectification. *Int J Remote Sens* 23, 2609–2630.  
584 <https://doi.org/10.1080/01431160110115825>
- 585 Schweiger, A.K., Schütz, M., Anderwald, P., Schaepman, M.E., Kneubühler, M., Haller, R., Risch, A.C.,  
586 2015. Foraging ecology of three sympatric ungulate species – Behavioural and resource maps  
587 indicate differences between chamois, ibex and red deer. *Mov Ecol* 3, 6.  
588 <https://doi.org/10.1186/s40462-015-0033-x>
- 589 Smith, N.G., Dukes, J.S., 2017. LCE: leaf carbon exchange data set for tropical, temperate, and boreal  
590 species of North and Central America. *Ecology* 98, 2978–2978.  
591 <https://doi.org/10.1002/ecy.1992>
- 592 Stevens, A., Ramirez-Lopez, L., 2022. An introduction to the prospectr package [WWW Document].  
593 URL <https://CRAN.R-project.org/package=prospectr>
- 594 Van Der Meer, F., Bakker, W., Scholte, K., Skidmore, A., De Jong, S., Clevers, J., Addink, E., Epema, G.,  
595 2001. Spatial scale variations in vegetation indices and above-ground biomass estimates:  
596 Implications for MERIS. *Int J Remote Sens* 22, 3381–3396.  
597 <https://doi.org/10.1080/01431160152609227>
- 598 Verrelst, J., Dethier, S., Rivera, J.P., Munoz-Mari, J., Camps-Valls, G., Moreno, J., 2016. Active Learning  
599 Methods for Efficient Hybrid Biophysical Variable Retrieval. *IEEE Geoscience and Remote  
600 Sensing Letters* 13, 1012–1016. <https://doi.org/10.1109/LGRS.2016.2560799>
- 601 Wang, H., Harrison, S.P., Prentice, I.C., Yang, Y., Bai, F., Furstenau Togashi, H., Wang, M., Zhou, S., Ni,  
602 J., 2017. The China Plant Trait Database.
- 603 Wright, I.J., Reich, P.B., Westoby, M., Ackerly, D.D., Baruch, Z., Bongers, F., Cavender-Bares, J.,  
604 Chapin, T., Cornelissen, J.H.C., Diemer, M., Flexas, J., Garnier, E., Groom, P.K., Gulias, J.,  
605 Hikosaka, K., Lamont, B.B., Lee, T., Lee, W., Lusk, C., Midgley, J.J., Navas, M.-L., Niinemets, Ü.,  
606 Oleksyn, J., Osada, N., Poorter, H., Poot, P., Prior, L., Pyankov, V.I., Roumet, C., Thomas, S.C.,  
607 Tjoelker, M.G., Veneklaas, E.J., Villar, R., 2004. The worldwide leaf economics spectrum. *Nature*  
608 428, 821–827. <https://doi.org/10.1038/nature02403>
- 609